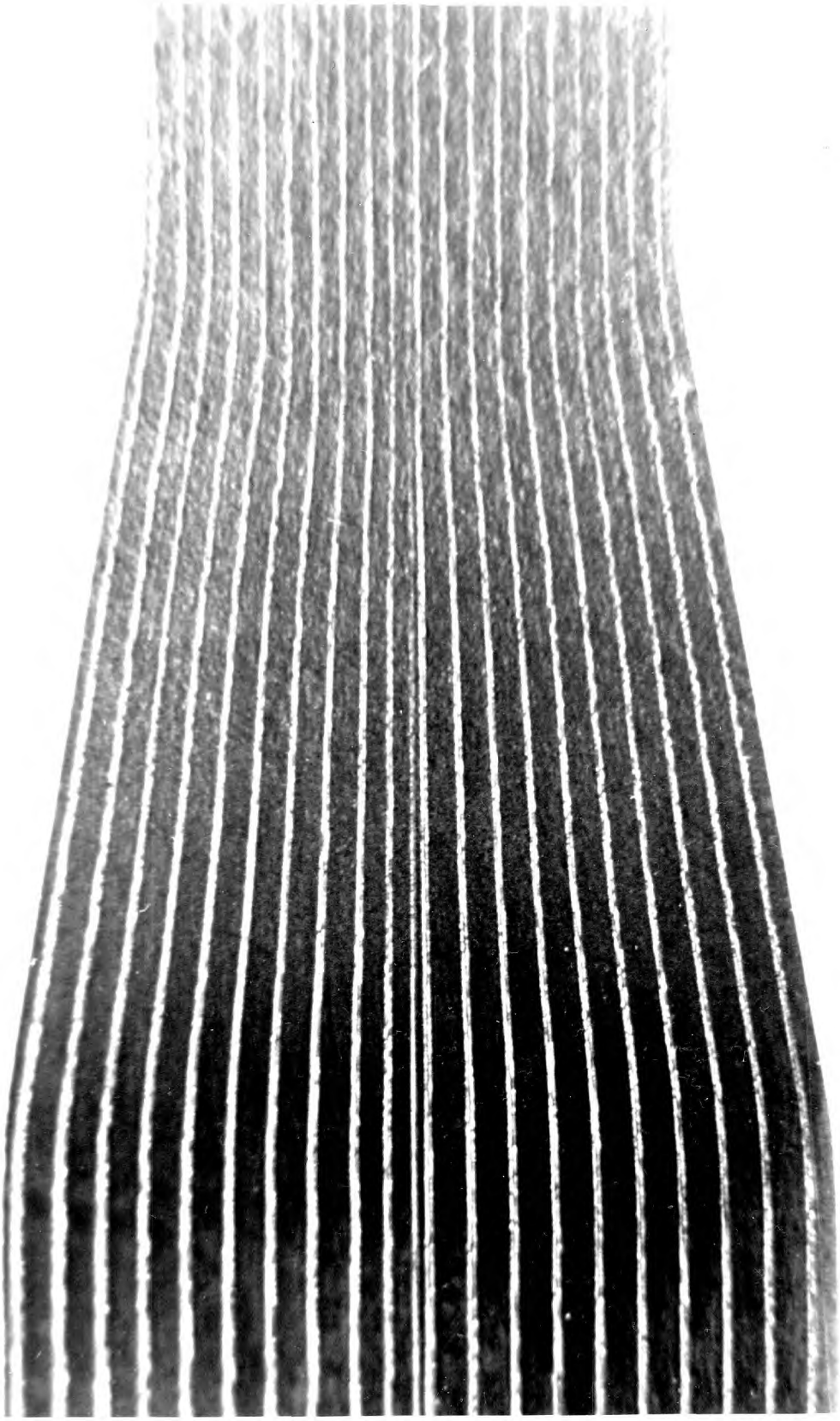

LUBRICATION IN

HYDROSTATIC EXTRUSION

PETER DUNN B.Sc.(Eng.), A.C.G.I.

A thesis submitted for the
degree of
DOCTOR OF PHILOSOPHY
of the University of London
and also for the
DIPLOMA OF IMPERIAL COLLEGE

Department of Mechanical Engineering
Imperial College of Science and Technology
London S.W.7.

SUMMARY

The literature is reviewed to decide on the best method of approach to develop tests for the evaluation of lubricants in cold working, with particular reference to hydrostatic extrusion.

An apparatus for performing hydrostatic extrusion with product augmentation under conditions of constant speed and constant extrusion pressure is described. The preparation and extrusion of split and gridded billets for this apparatus is also detailed. The design of a falling weight viscometer for the measurement of viscosity and compressibility of fluids under pressures of up to 30 kbar is given, along with preliminary results at low pressure.

Visioplasticity theory is used to analyse the results of the extrusion experiments. The computer program given here is shown to be capable of detecting changes in the flow due to changes of frictional conditions. This analysis is used to show the variation of lubrication conditions with speed, extrusion stress-drawing stress ratio and fluid or lubricant used.

It is found that low coefficients of friction are favoured by high speed, ~~low~~ high extrusion stress-drawing stress ratio and the use of a lubricant such as molybdenum disulphide.

CONTENTS

LIST OF FIGURES

LIST OF TABLES

NOTATION

Subscripts which are not defined below are explained as they are used in the text.

A	area of contact
A,B,C	constants
a,b,c	
A,B,E,F	functions defined in section 3.3.1
a	reference point in deformation zone
D	diameter of cylinder
D_A	diameter of parallel portion of sinker
D_B	diameter of bore hole in sinker
D_I	diameter of inlet face of sinker
D_O	diameter of outlet face of sinker
d	capillary diameter
E	Young's modulus
F	frictional force
F	axial assembly force
f(α)	function in Avitzur's theory
g	acceleration due to gravity
G	bulk modulus
h	film thickness
h_o	minimum film thickness for hydrodynamic lubrication
K_f	shear strength of lubricant film
KC	array defining non-zero coefficients
K_m	mean shear yield stress
K	diameter ratio of cylinder
K_C	diameter ratio of elastic-plastic interface
k	shear yield stress
k	theoretical viscometer constant

k'	experimental viscometer constant
L	length of die land
ℓ	length of cylinder
ℓ	length of capillary
ℓ_A	length of parallel portion of sinker
ℓ_B	length of bore hole in sinker
ℓ_I	length of inlet portion of sinker
ℓ_O	length of outlet portion of sinker
ℓ_T	length of timed fall of sinker
m	mass of sinker
m	constant between 0 and 1
m	outside diameter/diameter
$\dot{m}$	lubricant mass flow rate
N	number of experimental data points
p	extrusion or fluid pressure
p	fluid film pressure in hydrodynamic lubrication
p	hydrostatic stress
p_1	pressure above sinker
p_2	pressure below sinker
δp	$(p_2 - p_1)$ or change of pressure
Δp	pressure drop across capillary
Q	flow through capillary or past sinker
Q_A	flow through annular gap
Q_B	flow through bore of sinker
q	flow per unit circumference
q	die pressure
R	reduction ratio
R_ℓ	radius of flow line in rigid billet
R,Z	radial and axial coordinates

r_A	radius of parallel portion of sinker
r_B	radius of bore hole in sinker
r_I	radius of inlet face of sinker
r_O	radius of outlet face of sinker
r_T	radius of viscometer tube
r_i	internal radius of vessel
r_p	product radius
S	sum of squares of deviations
S_S	shear force on sinker surface
S_A	shear force on annular surface
S_B	shear force on bore hole surface
T	temperature
T_o	ambient temperature
t	time or time of fall of sinker
t*	corrected fall time of sinker
$t_{\ell K}$	time to reach section K on flow line ℓ
U	sliding velocity
U,V	axial and radial velocities
U_C	billet velocity for initiation of fluid film
U_S	steady state billet velocity for hydrodynamic lubrication
U_f	fluid velocity in hydrodynamic theory
U_s	surface velocity or fluid velocity in viscometer theory
V_b	billet velocity
V,v	terminal velocity of sinker
W	normal force
x	independent variable
x,y	coordinate directions for fluid film calculations
x_i, y_i	experimental points
Y	flow stress

Y_m	mean yield stress
y	dependent variable
α	die semi-angle or half angle of taper
α	temperature coefficient of expansion
α_K	angle of billet surface to axis at K section
γ	pressure coefficient of viscosity
δ	relative interference
δ_C	change of relative interference
ε	natural strain
$\varepsilon_1, \varepsilon_2, \varepsilon_3, \varepsilon_C$	strains as defined in the text
ε_θ	hoop strain
$\dot{\varepsilon}_{RR}, \dot{\varepsilon}_{\theta\theta}, \dot{\varepsilon}_{ZZ}$	strain rates in the radial, hoop and axial directions
$\dot{\varepsilon}_{RZ}$	shear strain rate on RZ plane
$\bar{\dot{\varepsilon}}$	mean effective strain rate
$\bar{\varepsilon}$	mean effective strain
η	fluid viscosity
θ	angle between axis of billet and axis of measuring machine
$\dot{\lambda}$	constant in Levy-Mises flow rule
μ	coefficient of friction
ν	Poisson's ratio
ρ, ρ_f	fluid density
ρ_S	sinker density
σ_r, σ_{RR}	radial stress
$\sigma_\theta, \sigma_{\theta\theta}$	hoop stress
σ_z, σ_{ZZ}	axial stress
σ_{RZ}	shear stress on RZ plane
$\bar{\sigma}$	mean effective stress
σ_S	surface shear stress
σ_N	normal stress on surface
τ	shear stress

ψ	flow function
ψ_{ℓ}	flow function on flow line ℓ

Symbols used in the Computer Program

CR(L,N), CZ(L,N)	input data coordinates
CR1, CZ1	transformed data coordinates
CPSI	flow function
DBIL	diameter of billet
DPROD	diameter of product
ETRR, ETHH, ETZZ	strain rates in the radial, hoop and axial directions
ETRZ	shear strain rate on RZ plane
EFFST	mean effective strain rate
PRESS	hydrostatic stress
I,K	mesh parameters in radial and axial directions
IMAX(K), KMIN(I)	reference arrays characterising the mesh
L	flow line reference number
NI, NK	no. of mesh points in radial and axial directions
R,Z	radial and axial coordinates of point (I,K)
RREF, ZREF	reference points for input data
RPSI(L,K)	radius of flow line L at section K
SSEF	mean effective stress
SSRR, SSHH, SSZZ	stresses in the radial, hoop and axial directions
SSRZ	shear stress on the RZ plane
TEFFST	total effective strain
TEMP	temperature
TIME(L,K)	time to reach section K along line L
UF	axial component of velocity on line L
U,V	axial and radial velocities

VBIL	billet velocity
VPROD	product velocity
XKDIV	step length in axial direction

ACKNOWLEDGEMENTS

My sincere thanks go to Dr. B. Lengyel for his advice and encouragement while supervising this work.

The assistance given by all the members of the staff and students of the Metalworking Laboratory is also gratefully acknowledged. In particular I wish to thank Mr. M.G. Gutteridge for help in assembling the apparatus, Mr. S.C. Pridham for preparation of the split billets and other technical assistance and Mr. J.W.C. Bentley for the design of the viscometer timing circuit.

P.D.

August 1971.

CHAPTER 1 - INTRODUCTION

1.1 Critical Review of Friction and Lubrication in Hydrostatic Extrusion

1.1.1 Introduction

Although metal working processes have been in use for several thousand years, it is only in this century that tools have been available for the systematic experimental and theoretical study of the parameters involved. Even so, the study of friction has had to wait until the last two decades for two main reasons. The first is that its study cuts across established disciplines such as metallurgy, mechanical engineering and surface chemistry. The second is that the effects of friction are often inseparable from those of the other parameters involved.

The importance of lubrication and its effect on forming loads, die wear and product properties has long been recognised. Indeed, it proved impossible to cold extrude steels economically until suitable lubricants were found (1).

Recently efforts have been made to bring together specialists in the various fields and this has produced two works of note (2,3). The latter is a general review of the whole field of lubrication in metal working, while the former consists of several papers specialising on topics within the field.

In practice the use of lubricants can have wide ranging effects on the economics of the process. For instance the useful life of tooling in extrusion and drawing can be greatly increased by extreme pressure lubricants which prevent pickup on the die and reduce wear. The lubricant may also have a profound effect on the properties of the product and the temperatures involved in the deformation.

In studying friction in hydrostatic extrusion the problem again occurs of separating the effect of friction from other effects. A comparison with conventional cold extrusion shows that hydrostatic extrusion has the advantage that there is no friction between the billet and the container and that there is a ready supply of fluid to lubricate the billet die interface. A general review of hydrostatic extrusion is given by Krönberger (4).

In an industrial process, control of the product velocity would be achieved in most cases by augmenting with a load either on the billet or product, although one free extrusion press has been designed and built (5) which has very high product speeds associated with its operation. Thus a wide range of lubrication conditions are likely to be met, ranging from extrusion to drawing orientated processes, low to high speeds, reductions and die angles and many different product geometries and materials.

1.1.2 Regimes of Friction and Associated Governing Laws

Frictional effects can, in general, be divided into three regimes, namely, boundary, mixed or quasi-hydrodynamic and hydrodynamic lubrication.

In boundary lubrication, which covers the vast majority of cases in metal forming, the surfaces are lubricated either by molecular layers adsorbed onto the surfaces or by surface films formed by chemical reaction with the surface (extreme pressure lubrication).

The laws governing boundary lubrication, especially in contact between elastic bodies, have received attention since they were first suggested by Leonardo da Vinci. They were rediscovered by Amontons in 1699 and verified by Coulomb in 1781, who distinguished between static and dynamic friction. More recently theories have been proposed and tested which attempt to predict the value of the coefficient of friction from the properties of the materials and the lubricant film.

A theory proposed by Bowden and Tabor (6) suggests that the surface asperities deform to make junctions until the real area of contact is just sufficient to support the load at the mean yield stress, Y_m. If the mean shear yield stress of the junction is K_m, then we have

$$F = A.K_m = \frac{W}{Y_m} . K_m$$

and $$\mu = \frac{F}{W} = \frac{K_m}{Y_m} .$$

This theory was improved both by recognising that in plastic flow the shear stress and the normal stress are related to a flow stress by a yield criterion and by accounting for the lubricant film present. However, for usual lubricant films, where the shear strength of the film, K_f, is much lower than that of the metal, this may be approximated by $\mu = \frac{K_f}{Y_m}$. This is satisfactory for $\mu < 0.17$.

Under the very high pressures which may exist in metalworking, the surface film of lubricant is often insufficient to prevent metallic contact. In these circumstances junction growth leading to metallic pickup on the tools can take place. Avoidance of this metal transfer is, in practice, often more important than the precise value of the coefficient of friction, as it results in rapid tool wear and poor surface finish of the product. Unfortunately, no theory can satisfactorily predict when this will occur.

Recently it has been realised that hydrodynamic films could exist in certain metalworking processes. The governing laws of hydrodynamic lubrication are well documented and apply when one of the bodies is plastically deforming. The basic Navier-Stokes equations are simplified (7) to give the well known Reynold's equation.

For many metalworking geometries, for instance rolling and wire drawing, the one dimensional form of this equation is suitable, as there is no flow in the cross or hoop directions. For drawing, or extrusion, the flow, q, per unit circumference is given by

$$q = \frac{Uh}{2} - \frac{h^3}{\eta} \cdot \frac{dp}{dx} \quad .$$

This equation must be solved, along with the equilibrium equations, boundary conditions, yield criterion and associated flow rate, to give a complete solution. This cannot generally be done without severe simplification.

The transition region between boundary and full film lubrication is less well understood and difficult to examine theoretically. As yet, no theories have been proposed for this region but many workers have tried to predict the onset of full film lubrication. Usually a constant coefficient of friction is assumed if the film thickness, calculated from Reynold's equation, is insufficient to maintain complete separation of the surfaces.

1.1.3 Measurement of Lubricant Properties

In the different regimes of lubrication, different properties are predominant in determining the effectiveness of a lubricant.

For hydrodynamic lubrication the single most important property is the viscosity of the lubricant. In metalworking where contact pressures between the tool and workpiece are large, the variation of viscosity with pressure may be of paramount importance. Further, in the high speed processes where hydrodynamic lubrication is most likely, high strain rates can give rise to high temperatures being generated. As viscosity is extremely sensitive to temperature, this effect must also be considered.

Under the pressures used in hydrostatic extrusion it is also necessary to account for the change of density of the pressurising fluid. Of the many works on variation of viscosity and density of lubricants with pressure and temperature, the A.S.M.E. report (8) would seem the most comprehensive to date. Chu and Cameron (9) have published empirical fits to the data given in this report which can be used in analytical work.

Although many other works are available in this field, either the pressures used are too low to be of interest here, or else, as in Bridgman's work (10,11), the fluids studied are not usually used as lubricants. The data up to 1952 was collected by Hersey and Hopkins (12) and presented in anuniform manner. The work from 1952 to 1966 has been reviewed by Hersey (13). One other recent work by Wilson (14) is of interest as castor oil is studied up to 14 kbar and this fluid is often used in hydrostatic extrusion.

Further evidence on the suitability of a fluid as an hydrodynamic lubricant could be produced by performing drawing experiments with a pressure tube to produce a 'viscosity pump'. The pressure tube has a diameter only slightly larger than the wire and is filled with oil. This was originally suggested by MacLellan and Cameron (5) and extended by Christopherson and Naylor (16). Their apparatus could be used to grade fluids by performing drawing experiments with different fluids and noting the speed at which the onset of full film lubrication occurred.

This type of experiment has been carried out in rolling by Dromgold and Rodman (17) who used the percentage reduction of a strip to indicate the effectiveness of a fluid in lubrication. If roll speed, load and entry thickness are held constant, then the greater the reduction, the more effective has been the lubricant.

However experiments of this kind can do no more than grade the fluids in order of suitability. Pressure-temperature-viscosity characteristics

are necessary if a full theoretical solution of the problem is to be attempted.

In boundary lubrication situations the alternative of grading by tests or measuring lubricant properties does not exist. It has not yet proved possible to measure, say, the shear strength of the lubricant film and put this into a theory of boundary lubrication. The best that has been achieved is performing experiments on simple geometries, which can be solved theoretically and calculating coefficients of friction.

Unfortunately, the validity of using a coefficient of friction found, say, in a forging operation in some other geometry, for example extrusion, is questionable. Therefore a different approach is often adopted. In this a simplified solution is assumed and experiments performed to measure forming loads or pressures. The coefficient of friction can then be calculated. The problem here is that experimental errors and errors due to assumptions in the theory are all incorporated in the result.

For the former method of tackling the problem, forging has been most extensively used. Schroeder and Webster (18) forged thin discs of aluminium and magnesium alloys between overhanging platens with different lubricants. Their results show that the coefficient of friction is influenced by the lubricant and, within experimental error, is independent of the mean pressure or material. Van Rooyen and Backofen (19) performed similar experiments but measured the normal and shear forces directly by inserting strain gauged pins in the platens.

A qualitative method of grading lubricants was suggested by Kunogi (20) and was developed by Male and Cockcroft (21). This involves forging a ring and measuring the internal diameter after deformation. This parameter is very sensitive to changes in coefficient of friction. For low coefficients the internal diameter increases whereas for higher values the diameter decreases. They found coefficients of friction by calibrating against the method of Schroeder and Webster. Upper bound

solutions for this geometry have been found by Kobayashi (22), Kudo (23) and Avitzur (24).

Further studies using this method by Male (25) show that it is possible for thick films to be present. With graphite as lubricant, press speed has no effect on the coefficient of friction; with lanolin, however, there is a sudden change of slope in the curve of percentage reduction of internal diameter against percentage deformation, corresponding to a change in frictional coefficient. The change varies in position with press speed. Male attributes this to breakdown of full film lubrication. Further evidence of this can be gleaned from the surface finish of the ring.

Guminski and Willis (26) used the plane strain compression test, described by Watts and Ford (27), to grade fluids by observing the reduction after indenting at a certain load. Alexander (28) solved the plane strain indentation problem for two different breadth to thickness ratios with Coulomb friction acting. This solution is used by Takahasi and Alexander (29). Their results show that the coefficient of friction is greatly influenced by the build up of detritus. With brass the accumulation of debris in the fluid could reduce the coefficient by a factor of four.

Of the other processes which can be used to study coefficients, drawing is probably the best understood, both theoretically and experimentally. Indeed, many experimental studies have been carried out solely to evaluate coefficients of friction. It is likely that the values found will also be applicable in hydrostatic extrusion as the geometries are essentially the same. In theoretical treatments, the same approach is often applied to both processes, although the assumption that redundant work can be neglected, which is often applicable in wire drawing, cannot be made for large die angles used for large reductions in hydrostatic extrusion. The field of lubrication in drawing is reviewed by Shaw, Stableford and

Sansome (30).

Wistreich (31) used the 'split die' technique suggested by MacLellan (32) to investigate the mean coefficient of friction and die pressure in drawing, without recourse to theory. While giving excellent results, this method was difficult to use and could not be used with liquid lubricants. The method was improved by Yang (33), who used a strain gauged dynamometer to measure the separating force. Majors (34) used a strain gauged die, calibrated by fluid pressure to measure die pressure and hence calculated coefficient of friction.

The plug drawing process (Blazynski and Cole (35) and Lancaster and Rowe (36)) can also be used to advantage, as the geometry is simple. By measuring the separating force on the dies and the tension in the plug bar, a mean coefficient of friction can be calculated without recourse to drawing theory. In their paper, Lancaster and Rowe also measured the throughput of lubricant by a radiotracer technique.

Finally, the visioplasticity method has been used in extrusion to give detailed information on the strain rates, total strain and state of stress throughout the deformation zone. This method was first suggested by Thomsen and Lapsley (37) and Thomsen, Yang and Bierbower (38). However, it did not become really feasible until digital computers with large core storage were available and the calculations could be programmed, for instance by Shabaik, Lee and Kobayashi (39) and Shabaik and Kobayashi (40).

In this method, an experiment must be performed on a billet which has been split and gridded on its mid-plane. The steady state coordinates of the flow lines are then read off and a flow function defined which is constant along a flow line. By numerical differentiation the velocities and then the strain rates can be found at mesh points defined to cover the deformation zone. These strain rates can then be integrated to give

total strains and used with the equilibrium equation, written in integral form, to give the complete stress field where plastic flow is taking place. Elastic stresses are ignored throughout, as is usually the case in problems of large plastic flow.

The method was also further extended to give temperatures in the deformation zone by Altan and Kobayashi (41) and the friction conditions at the die billet interface by Shabaik and Thomsen (42). They found the variation of normal stress and coefficient of friction along the die billet interface. While doubts exist about the accuracy of their method, especially near the surface, their results show that there is considerable variation of the coefficient of friction over the deformation boundary. Doubts are therefore cast on the validity of assuming a constant coefficient of friction.

Thus it can be seen from this limited survey of other processes, much information is available on the lubricated contact between an extending and a non-extending surface. The majority of this information has been given in the form of average coefficients of friction, although the assumption of either a constant coefficient or constant shear stress is unlikely to be correct in actual deformations.

1.1.4 Theoretical Studies of Hydrostatic Extrusion

One method of studying friction in hydrostatic extrusion is to attempt to analyse the deformation theoretically. The analysis can then be used, as mentioned previously for other processes, along with experimental data to give a coefficient of friction. In this section theoretical solutions are considered which are applicable to this procedure.

Firstly, solutions which have been obtained for conventional extrusion can easily be modified by neglecting billet-container friction. Empirical formulae in this field are usually of the form

$$\frac{p}{Y_m} = a + b \ln R$$

Equations of this type are used successfully to fit experimental results. While they are useful in predicting extrusion pressures experimentally, they do not help in understanding the friction process. To do this a more sophisticated theory must be developed.

For wire drawing Pomp, Siebel and Houdrement (43) make the assumption that the mean die pressure, q_m, is equal to the mean yield stress of the material. They derive the equation

$$p = (1 + \frac{\mu}{\alpha}) \ Y_m \ \ln R$$

Siebel (44) later attempted to account for redundant work and produced the equation $p = (1 + \frac{\mu}{\alpha}) \ Y_m \ \ln R + \frac{2}{3} \ \alpha \ Y_m$. This is on the assumption that redundant shearing takes place at entry to and exit from the die. Deformation is assumed to take place with radial flow, that is towards the apex of the cone of the die surface in the manner assumed by Shield (45).

The frictional term derived in this manner has been criticised as it leads to an overestimate of the stress. The redundant work term produces a stress curve parallel with the homogeneous work curve, as it does not depend on the reduction ratio. As Hill and Tupper (46) point out, this does not agree with plane strain theory; neither does it agree with Wistreich's (31) experimental results. Further the frictional term does not depend on the redundant work, which in fact increases frictional forces. Duffill and Mellor (47) suggest the following modification to overcome this

$$p = (1 + \frac{\mu}{\alpha}) \int_0^{\varepsilon_c} Y \, d\varepsilon \quad \text{where} \quad \varepsilon_c = \frac{2}{3} \alpha + \ln R \quad .$$

Although this theory is much criticised it does predict an optimum die angle for a given reduction and coefficient of friction.

Sachs and van Horn (48) assumed that the mean die pressure is independent of the presence of friction and deduced

$$p = Y_m (1 + \mu \cot \alpha) \ln R .$$

Green (49) shows this is applicable only for very low reductions and coefficients of friction.

Duffill and Mellor (47) and Parsons, Bretherton and Cole (50), for the more general case of extrusion drawing, derived the extrusion pressure by Sach's (51) slab method. This is the first theory considered here which is capable of predicting different driving stresses for extrusion and drawing in the same conditions of friction, die angle and reduction. They obtain the equation,

$$p = Y_m \left(\frac{1 + \mu \cot \alpha}{\mu \cot \alpha} \right) (R^{\mu \cot \alpha} - 1)$$

The assumptions inherent in this formula are that plane sections remain plane and that the Tresca yield criterion can be written $\sigma_z + q = Y$. In fact $\sigma_r = q (1 - \mu \tan \alpha)$ so this amounts to assuming $\mu \tan\alpha << 1$.

A different approach to the problem is to use limit analysis, suggested by Hill (52) and Drucker, Greenberg and Prager (53). The upper bound approach is used as it is easier to visualise kinematically admissible velocity fields than statically admissible stress fields. After choosing a velocity field which satisfies the incompressibility, continuity and boundary conditions, the forces required to make it operate are calculated. By trying different velocity fields a minimum load is found and this is taken as the approximation of the driving stress.

Pugh (54), in his upper bound approach, assumes the work can be split into three parts, namely the homogeneous work, p_H, redundant work, p_R, and friction work, p_F.

To calculate the redundant work, Pugh tried three different types of boundaries to the deformation zone. These were of plane transverse, conical and spherical form.

In the case of the conical boundary only the optimum, which gives the lowest rate of working is considered. All three boundaries produce redundant work terms which closely approximate that given by Siebel (44) originally suggested by Eichinger and Leug (55) for small die angles. Of the three the conical boundary gives a lower pressure estimate; however, Pugh chooses to use the spherical boundary.

Friction is taken into account by calculating the mean die pressure from quasi-equilibrium considerations and assuming this is not affected by superposing frictional effects. This gives

$$p_F = \frac{\mu R \ln {}^{2R} Y_m}{\sin \alpha (R - 1)}$$

or more generally

$$p_F = \frac{\mu R \ln R}{\sin \alpha (R - 1)} \int_{\varepsilon_1}^{\varepsilon_2} Y \, d\varepsilon$$

The total extrusion pressure can now be expressed as

$$p = \int_0^{\varepsilon_1} Y \, d\varepsilon + \int_{\varepsilon_1}^{\varepsilon_2} Y \, d\varepsilon + \frac{\mu R \ln R}{\sin \alpha (R - 1)} \int_{\varepsilon_1}^{\varepsilon_2} Y \, d\varepsilon + \int_{\varepsilon_2}^{\varepsilon_3} Y \, d\varepsilon$$

$$\text{or } p = \int_0^{\varepsilon_3} Y \, d\varepsilon + \frac{\mu R \ln R}{\sin \alpha (R - 1)} \int_{\varepsilon_1}^{\varepsilon_2} Y \, d\varepsilon$$

where $\varepsilon_1 = \frac{1}{2} \left(\frac{\alpha}{\sin^2 \alpha} + \cot \alpha\right)$, $\varepsilon_2 = \varepsilon_1 + \ln R$ and $\varepsilon_3 = \varepsilon_1 + \varepsilon_2$

Assuming a mean yield stress,

$$p = Y_m \ln R + Y_m \left(\frac{\alpha}{\sin^2\alpha} - \cot\alpha\right) + \frac{\mu R \ln^2 R}{\sin\alpha\,(R-1)} \cdot Y_m$$

The value of 0.5 in ε_1 is obtained on the Tresca yield criterion. Pugh found a better correlation with his experimental redundant strains by adjusting this to 0.462.

Another solution, along similar lines was obtained by Avitzur (56, 57) for drawing and extrusion again assuming conical boundaries. The latter work was later extended to hydrostatic extrusion (58). His solution proceeds by equating power consumption of the external forces to the internal power dissipation. This, of course, yields the same expression for the redundant component as Pugh's theory above, with the factor 0.5 changed to $1/\sqrt{3}$ as Avitzur uses the von Mises yield criterion. He also assumes a mean yield stress throughout.

In the deformation zone Avitzur again assumes the von Mises yield criterion and, on the assumption of radial flow, calculates the effective strain rate as a function of position in terms of spherical polar co-ordinates. By integrating to find the internal rate of power dissipation and equating this to the rate of working of the external forces, he finds that the contribution to the extrusion pressure is $f(\alpha).\ln R$ where

$$f(\alpha) = \frac{1}{\sin^2\alpha}\left\{1 - \sqrt{\left[1 - \frac{11}{12}\sin^2\alpha\right]}\cos\alpha + \frac{1}{\sqrt{11\times12}}\ln\left[\frac{1+\sqrt{\frac{11}{12}}}{\sqrt{\frac{11}{12}}\cos\alpha + \sqrt{\left[1-\frac{11}{12}\sin^2\alpha\right]}}\right]\right\}$$

The frictional component is calculated on two different assumptions; firstly, of Coulomb friction and secondly, of constant shear stress. Further the die pressure is taken as that given by Sachs' method, which gives a die pressure falling towards the exit, contrasting Pugh's assumption of constant die pressure. Finally, a term is added to account for die land friction, giving, for simple hydrostatic extrusion, the following expression,

$$p = f(\alpha) \cdot Y_m \cdot \ln R + \frac{2Y_m}{\sqrt{3}} \left(\frac{\alpha}{\sin^2\alpha} - \cot\alpha\right) +$$

$$2Y_m \mu \left\{ \cot\alpha \left[1 + \frac{1}{2} \ln R\right] \frac{\ln R}{2} + \frac{L}{r_p} \right\}$$

or, if a constant shear stress $\tau = mK_m = m\frac{2}{\sqrt{3}} Y_m$ is assumed

$$p = f(\alpha) \cdot Y_m \cdot \ln R + \frac{2Y_m}{\sqrt{3}} \left(\frac{\alpha}{\sin^2\alpha} - \cot\alpha\right) +$$

$$m Y_m \left(\frac{\cot\alpha . \ln R}{2} + \frac{L}{r_p} \right)$$

The frictional term in Pugh's equation is $\frac{\mu}{\sin\alpha} \cdot \frac{R(\ln R)^2}{R-1} \cdot Y_m$ and in Avitzur's, neglecting die land friction and putting $f(\alpha) = 1$, is $\mu \cot\alpha (1 + \frac{1}{2} \ln R) \ln R \, Y_m$.

The factors $\frac{\mu}{\sin\alpha}$ and $\mu \cot\alpha$ are approximately equal for small die angles but, as shown by Table 1.1, the factors $\frac{R(\ln R)^2}{R-1}$ and $(1 + \frac{1}{2} \ln R) \ln R$ are quite different.

Table 1.1

R	1	10	100	1000
$\frac{R}{R-1}(\ln R)^2$	0	5.873	21.43	47.79
$(1 + \frac{1}{2}.\ln R)\ln R$	0	4.955	15.22	30.78

Both of the theories outlined above predict optimum die angles, dependent on other process variables. Avitzur has further used his theory to investigate dead zone formation (58), flow characteristics (59), central bursting defects (60), and, with Evans, die design (61) and friction (62). In a later paper a more general set of boundaries is assumed by Zimerman and Avitzur (63).

Upper bounds have been obtained by a numerical method, using a digital computer, by Lambert and Kobayashi (64,65). This overcomes the difficulty of velocity discontinuities by superposing a very large number of basic flow patterns. Their comparison of forming pressures predicted by this method with those of other authors (64) is reproduced in Table 1.2. These apply to frictionless conventional extrusion, $\alpha = 45^{\circ}$, $R = 4$ and show a considerable improvement on previous attempts. However this method has not yet been applied to the smaller die angles and deformation zones commonly met in hydrostatic extrusion.

Other theoretical work of interest, although it has not been directly applied to hydrostatic extrusion, is that of Richmond and Devenpeck (69,70). They designed a sigmoidal profile die for plane strain drawing which, in the frictionless case, would deform the billet without redundant work. This work was later extended by Richmond and Morrison (71), Hill (72) and Sortais and Kobayashi (73). They use the

Table 1.2

Data Source	P/Y_m
Avitzur	2.08
Kobayashi (66)	1.90
Halling and Mitchell (67)	2.08
Pierce (68)	2.08
Lambert and Kobayashi	1.69
Lower bound	1.39

method of characteristics to solve axisymmetric problems in the ideal case where the principal stress directions are tangents to the streamlines throughout the deformation zone. This means the die surface must be a streamline and, to be a principal stress direction, it must be frictionless.

Of these solutions, Richmond and Morrison found a die profile which gave perfect efficiency without having zero entrance and exit angles as in a sigmoidal die. These dies are very close to conical dies apart from the entrance region, which is contoured. The deformation in hydrostatic extrusion often takes place in this manner without contouring the die, as pressure can be built up before the die by the hydrodynamic action of the fluid or lubricant.

Several theories have been proposed in which hydrodynamic lubrication is postulated over the whole die surface, that is full film lubrication. The work of Christopherson and Naylor (16), in which hydrodynamic lubrication was promoted in drawing by a pressure tube, has been mentioned. This was extended both theoretically and experimentally by Tattersall (74) and Osterle and Dixon (75).

Rozner and Faupel (76) first considered full film lubrication in hydrostatic extrusion by assuming linear decay of film thickness and parabolic decay of pressure. Hillier (77) attempts a comprehensive analysis, based on Avitzur's theory. Both of these papers neglect the pressure build up in the zone before deformation and the large change of viscosity with pressure. Hillier defines a modified Sommerfeld number and states that hydrodynamic lubrication will exist above a certain, critical value of this number.

The build up of pressure due to the hydrodynamic wedge is considered by Iyengar and Rice (78) although they also neglect the effect of pressure on viscosity. Assuming hydrodynamic lubrication exists if the fluid film at exit was greater than h_o, they found the steady state speed U_s to be:

$$U_s = \frac{Y_m \cdot h_o \cdot \tan \alpha}{6\eta} \cdot 2\sqrt{R} \quad .$$

As long as the speed is greater than this value a film will exist all over the die. They also estimated the speed, U_c, at which the film would start to build up. This was

$$U_c = \frac{Y_m \cdot h_o \cdot \tan \alpha}{6\eta}$$

As this is $2\sqrt{R}$ smaller than the value for a film over the whole die, it follows that at intermediate speeds the film will extend part of the way down the die. Their experiments with wax extrusions (79), designed to test this theory, will be described later.

A complete theory was first suggested by Wilson and Walowit (80). They assume the product goes rigid before the plane of the die exit and there is an 'outlet zone'. The film thickness at the start of the work

zone is found by solving Reynold's equation for the hydrodynamic wedge in the inlet zone and the yield criterion along the edge of the work zone.

In the work zone Reynold's equation is solved along with the equilibrium equation and the yield criterion. Assumptions are constant flow stress and incompressible flow. The outlet zone is also analysed, although it has very little effect on the film thickness. Finally they arrive at the following equation for free hydrostatic extrusion.

$$\frac{p}{Y_m} = 1 - \frac{1}{\gamma Y_m} \ln \left[\frac{2}{3} \frac{(1 - e^{-\gamma Y_m})(R^{-3/2} - R^{-\gamma Y_m})}{(3 - 2\gamma Y_m)} + R^{-\gamma Y_m} \right]$$

It is interesting to note that the addition of a drawing stress to the left hand side of this equation would not affect the analysis, unlike in other theories which assume Coulomb friction. Further, as the theory assumes uniform deformation, the pressure is found to be independent of die angle. The theory would break down if applied to large die angles but full film lubrication is, in any case, less likely in these conditions.

This theory has been developed by Thiruvarudchelvan and Alexander (81) to allow for deformation of the billet in the inlet zone and for a work hardening material.

It can be seen, therefore, that a great number of theories are available for the prediction of conditions in hydrostatic extrusion. For the estimation of extrusion pressure only, it is rarely necessary to use a more complicated equation than

$$p = a + b \ln R$$

—However, to gain insight into the mechanism of deformation and the operative frictional conditions it is necessary to use a much more sophisticated approach.

1.1.5 Experimental Studies of Hydrostatic Extrusion

Although hydrostatic extrusion was first suggested by Robertson (82), it was not carried out until the late 1940's by Bridgman (83). He notes some difficulties with the process, namely stick-slip extrusion, high speed of emergence of the product and cracked products.

More detailed studies of the process and development work was started by Beresnev, Vereshchagin, Riabinen and Livshits (84) in Russia and by Pugh (85,86,87). These references contain summaries of their work and also reference to earlier work by them. Many other workers have taken an interest in hydrostatic extrusion, including Randall, Davis, Sievgiej and Lowestein (88), Fiorentino, Sabroff and Boulger (89), Bobrowsky (90), Rozner and Faupel (76), Green (91) and Alexander and Lengyel (92, 93). Interest continued to grow and by 1967, at a High Pressure Engineering conference organised by the Institution of Mechanical Engineers, seven papers relate specifically to hydrostatic extrusion. Also, several papers in this field were given at the C.I.R.P. conference in Nottingham and the M.T.D.R. conference in Birmingham, both in September 1968.

In all these works, the effect of the pressure transmitting fluid and lubricant has received only limited attention. The major difficulty involved is that the change of extrusion pressure due to a change of fluid is often of the same order as the reproducibility of the results. This is shown in Pugh's results (85) for rolled mild steel bar extruded through a 45° die at a ratio of 2. Using different fluids (glycerine, glycerine and glycol, castor oil with and without 10% methylated spirits,

DTD 585 oil with and without E.P. additive) and with MoS_2 grease as lubricant the maximum variation in pressure is only 5%. Using Dag 724 as fluid and six different lubricants or none at all the variation is 6%. In similar conditions with glycerine and glycol as the fluid, 10% variation is found.

The lubricants tried in these experiments were sprayed PTFE, fused PTFE, sprayed IFC (fluorocarbon compound), sprayed ADF (MoS_2 in epoxy resin base), evostik and methyl ethyl ketone and zinc phosphate and stearate. However the combination of glycerine and glycol fluid with evostik lubricant gives 25% higher pressure and much poorer surface finish than when either fluid or lubricant is used in other combinations.

Fiorentino, Sabroff and Boulger (94,95) conducted the most extensive study on the effect of pressure transmitting fluid, by extruding AISI 4340 steel, titanium (Ti-6Al-4V) alloy, annealed, commercially pure 1100-0 and a 7075-0 aluminium through a 45° die. Table 1.3 shows their results for maximum and run out pressures for AISI steel at an extrusion ratio of 2. The lubrication is zinc phosphate and sodium stearate with 10% MoS_2 in all liquids. Again it can be seen that this method can only be used to identify fluids which are definitely unsuitable. With the paraffinic oil 167 with 10 W/o MoS_2 in suspension, they also tried the following lubricants; lithium soap grease with 10% MoS_2, calcium soap grease with lead naphthanate and with either silver chloride or calcium iodide, an E.P. grease and no lubricant at all. They could discern no change in either run out or peak pressures, however. The only effect which the viscosity of the fluid has is that there is increased tendency to stick-slip with decrease in viscosity. Similar results were obtained with aluminium and titanium alloy.

Bobrowsky and Stack (96) and Beresnev et al. (84) have shown that large pressure differences can occur due solely to the fluid used. For

Table 1.3

Effect of fluid on the pressure for the extrusion of AISI 4340 steel

Hydrostatic fluid	Kinematic viscosity at 100°F, ‡ (centistokes)	Average fluid pressure (10^3 lb/in^2) p_{max}	$p_{run\ out}$	Difference
Paraffinic oil 514*	514	108.2	102.0	6.2
Paraffinic oil 167	167	108.4	104.0	4.4
Paraffinic 55	55	109.6	105.1	4.5
Spindle oil	3	107.5	102.4	5.1
Naphthenic oil 146*	146	c. 135†	-	-
Naphthenic oil 55	55	c. 130†	-	-
Diester	13	108.4	102.7	5.7
Polyalkylene glycol	37	110.7	104.1	6.6
Palm oil	105	102.8	99.2	3.6

* Trials with these fluids were made at a plunger speed of 6 in./min. All other fluids were evaluated at 1 in./min.
† Trials discontinued at these pressures with no breakthrough.
‡ Values at atmosphiric pressure.

instance Beresnev et al. found that in extruding 99.5% aluminium at a ratio of 4.4 through an 80^{o} die, the pressure varied from 100,000 p.s.i. for petrol to 55,000 p.s.i. for an Hypoid lubricant. This is certainly due to the very poor lubrication properties of the petrol. Bobrowsky and Stack found a variation of up to $3^{1}/3$ times in extruding steel, presumably for the same reason.

Further results have been obtained by Lowe and Goold (97). They tested their fluids for freezing by monitoring punch load and the output from a manganin coil in the fluid. Above a certain pressure these begin to diverge, showing the fluid has started to freeze. Some of their extrusion results, namely for copper at a reduction of 9.5 and titanium at a reduction of 2, through 45^{o} dies, are given in Table 1.4. This shows there is no difference at all in run-out pressures, even when there is a very large difference in the peak pressure.

From the above discussion, it is apparent that the extrusion pressure cannot be used to grade suitable lubricants but only to reject those which are unsuitable.

An alternative method is to use the strain gauged die approach to find a mean die pressure and a mean coefficient of friction. This has been carried out by Parsons, Bretherton and Cole (50,98). They have not used this method to evaluate different fluids as they were primarily interested in studying the extrusion drawing process. However, they have found values of coefficient of friction in extruding copper in the as received condition from Shell Tellus 27 with a concentration of 2% Dag Dispersion 724. Their results for the coefficient of friction with percentage reduction, for various die angles, show a variation in the range 0.01 - 0.07. Interesting also is the variation of friction coefficient with extrusion stress-drawing stress ratio. As this ratio increases from 1 to 12 the friction coefficient increases from 0.06 to 0.12, rapidly at first, then more slowly. Thus the coefficient is

Table 1.4

Effects of various billet coatings and pressure-transmitting fluids

Billet material	Billet coating	Fluid	Extrusion pressure, tonf/in^2		Remarks on run-out pressure	Product finish
			Breakthrough	Initial run-out		
Titanium 130	Trilac 45	DTD.585	54	48	Oscillatory	Arrest marks
Titanium 130	Trilac 45	Glycerine 80 v/o Ethylene Glycol 20 v/o	52	48	Oscillatory	Arrest marks
Titanium 130	Trilac 45	Tellus 27	53	48	Constant	Good
Titanium 130	Trilac 45	Castor oil	52	48	Constant	Good
Titanium 130	None	Castor oil	69	48	Rising	Scored, poor
Titanium 130	Anodized	Castor oil	52	48	Rising	Fair
Titanium 130	Dry film graphite	Castor oil	52	48	Rising	Fair
Titanium 130	Graphite grease	Castor oil	52	48	Constant	Good
Copper	None	Castor oil	66	58	Constant	Good
Copper	None	Tellus 27	66	58	Constant	Good
Copper	None	DTD. 585	67	58	Constant	Good
Copper	None	Glycerine 80 v/o Ethylene Glycol 20 v/o	66	58	Constant	Good
Copper	Trilac 45	Castor oil	70	58	Constant	Good
Copper	Graphite grease	Castor oil	74	58	Constant	Good

smaller for drawing biased operation.

The strain gauged die technique has been further refined by Alexander and Kamyab (99). They have used long, narrow strain gauges to measure the circumferential strain at sections along the die during a copper extrusion. By this method they have determined the die pressure distribution by assuming it to be polynomial and using a finite element method to match the strains produced by the pressure distribution to the experimental ones. The coefficients in the polynomial are adjusted until the sum of the squared deviations of the calculated and experimental strains is a minimum. In the calculations they assumed a constant coefficient of friction. For their experiments, with castor oil as fluid and MoS_2 grease as lubricant, this was found to be 0.03.

Coefficients of friction determined by assuming a given theory to be correct and finding a value which gives the closest fit to experimental results have been quoted. This is not entirely satisfactory, especially as most of the theories are of the upper bound type. It might be expected that coefficients found in this way would be too low, as the theory itself tends to give an overestimate of the extrusion pressure.

As far as hydrodynamic lubrication is concerned, the experimental evidence of steady state full film lubrication is very limited. That it exists in the high speed part of stick-slip extrusions can be seen from the 'bamboo' effect which is typical of the product in this case. In the areas of high speed extrusion, the surface finish is much worse and the diameter is smaller than the 'stick' portions of the extrusion. This corresponds to the build up of a full film when the billet moves at high speed. The film cannot be sustained as the pressure falls off, resulting in a short portion of slow speed extrusion as the pressure rises again.

Rice and Iyengar (79) carried out extrusion experiments on wax, designed to test their theory of hydrodynamic lubrication. They also

found a stick-slip type of extrusion and, on removing the billet from the die, found bands of fluid, separated by dry bands along the cone. Full film lubrication was achieved, but not in the steady state; extrusion gradually reverted to boundary lubrication.

Finally, Wilson and Walowit (80) give a comparison of their theory with extrusion-drawing results by Sabroff and Fiorentino. Although they quote no experimental evidence of hydrodynamic films, the agreement obtained with their theory is good. Further, their theory predicts thick films even for slow extrusion speeds associated with augmented extrusion processes.

1.2 Aims of the Present Work

The basic aim of the work described in this thesis is to establish a method of evaluating fluids and lubricants for use in metalforming, with particular reference to hydrostatic extrusion.

It will be clear from the literature survey that the properties which are of primary importance are the viscosity, compressibility and boundary lubrication properties of the fluid. Therefore, these are the properties which must be measured in comparing different fluids.

Apparatus was therefore built to measure the viscosity and compressibility of the fluids directly and the change of these properties with pressure.

However, the boundary lubricant properties are more difficult to establish and will, in general, depend on factors such as workpiece material. These were evaluated in hydrostatic extrusion-drawing apparatus, using the visioplasticity approach. This apparatus could also be used to study other parameters, for instance the effect of speed or the effect of extrusion stress, drawing stress ratio. Further, the more general form of the mesh used in the visioplasticity programs would enable them to be used for more complicated geometries, such as rolling,

than has been possible before in computer methods.

CHAPTER 2 - EXPERIMENTAL APPARATUS

2.1 Description of Extrusion-Drawing Apparatus

2.1.1 Introduction

The extrusion-drawing process, or product augmented hydrostatic extrusion process, is shown schematically in Fig. 2.1. In designing apparatus for experiments on this process, the single most important feature is that pressure should be held constant in the high pressure chamber as the experiment proceeds. On the other hand, the drawing side can be designed so that the experiment is either load or speed orientated.

For the experiments which were to be carried out, it was decided to design on the latter criterion. Thus a pressure would be applied to the billet and a pull to the product at a constant speed, load settling down to a steady state value.

This method was thought to be more likely to produce constant frictional conditions than the alternative method of setting a constant load and building up to a pressure sufficient to cause extrusion.

2.1.2 Drawbench Design

2.1.21 Driving Mechanism

To obtain the constant speed drawing force a screw jack, 1, Fig. 2.2, was used. This was of standard design and manufactured by Messrs. Duff-Norton & Co. Ltd. The maximum permissible pulling force was 5 tons.

This was driven by a $1\frac{1}{2}$ h.p. induction motor, via a Kopp variator and reduction gear box, 2, in Fig. 2.2, and an Autogard torque limiting device, 3, Fig. 2.2. The speed variation of the motor between zero and full load was only 3% and as the fluctuations in load during the extrusion were much smaller in range, it was not possible to measure any

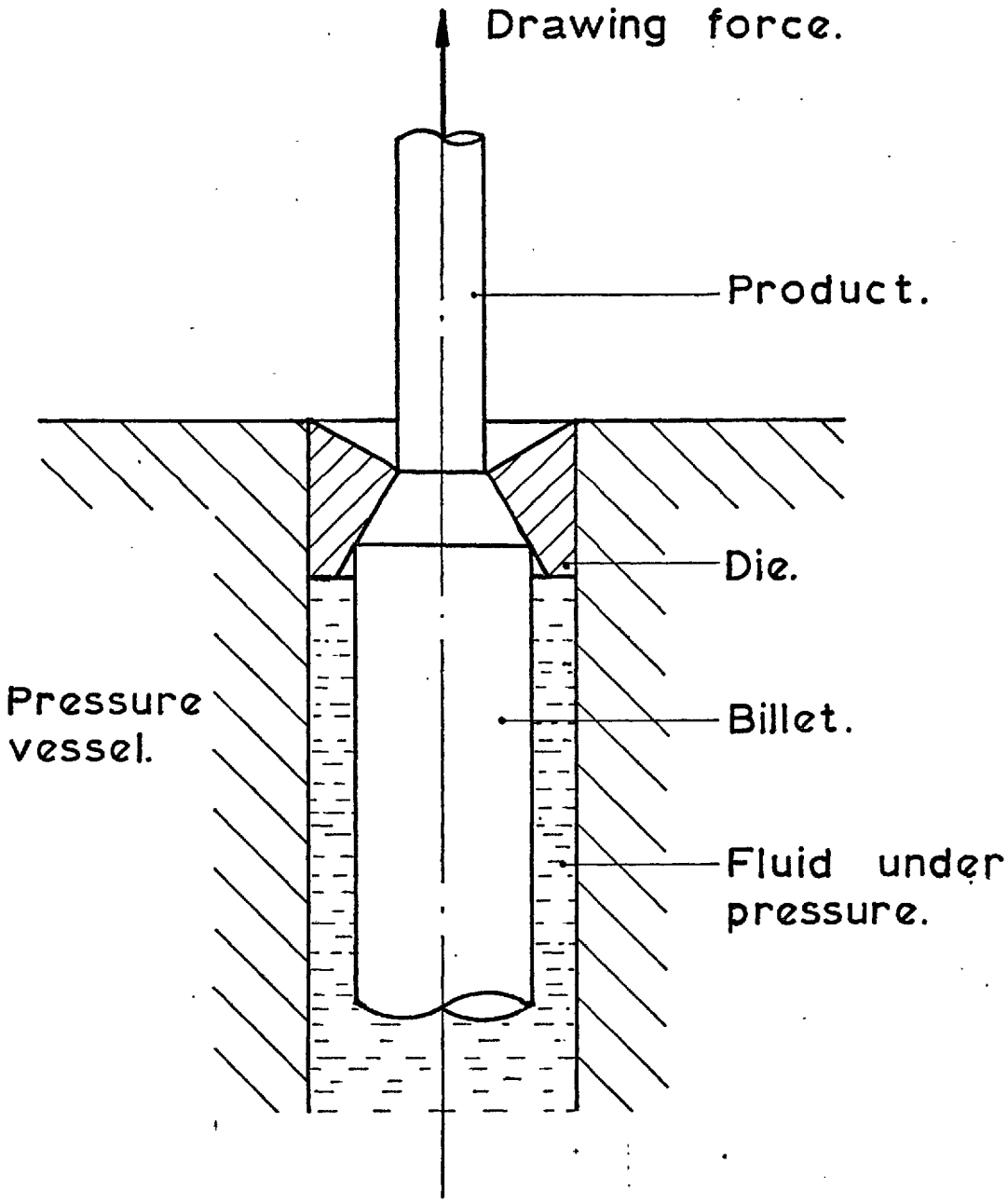

Fig. 2.1. Schematic of extrusion-drawing.

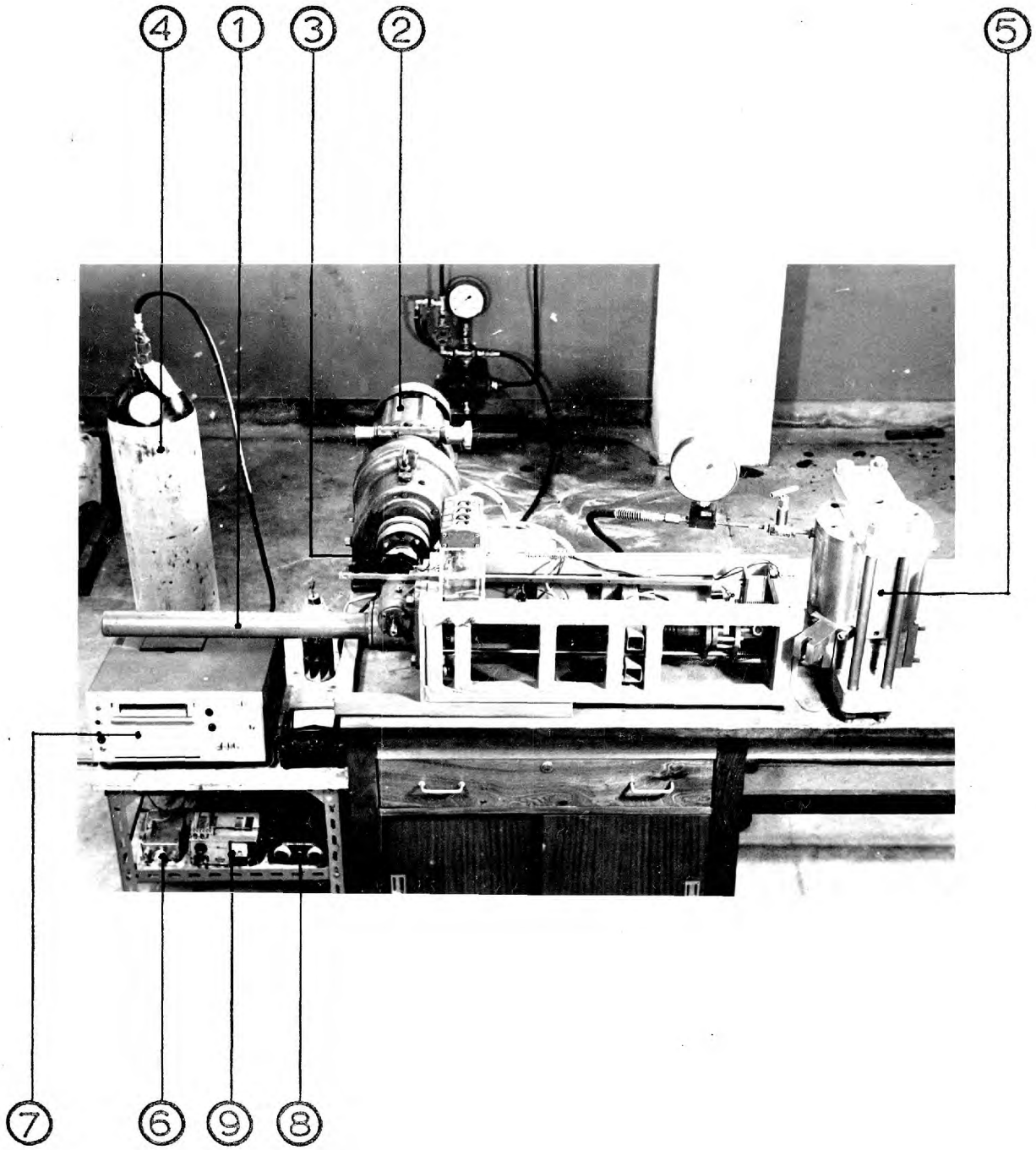

Fig. 2.2. The extrusion-drawing apparatus.

speed fluctuations during a test.

Use of the Kopp variator enabled the pulling speed, that is the product velocity, to be varied in the range 0.15 cm/sec to 1.3 cm/sec. The billet velocity, of course, depends on the extrusion ratio.

The torque limiting device served two purposes. The first was to ensure that the load applied to the product was not great enough to cause it to fracture. If the pressure had not been set high enough, or if it fell during the experiment for any reason, the load on the product would rise until the torque into the jack reached the value at which the limiter was set. The drive would then be disconnected, protecting the product. This device was especially useful in protecting split billets, for use in the visioplasticity program, from damage as they were difficult and expensive to manufacture.

The other purpose of the limiter was to allow the extrusion to be ended abruptly. This was to ensure that the flow pattern found was that for steady state deformation and not a function of the deceleration of the billet which would occur, due to the inertia of the jack, if the extrusion were stopped by switching off the motor. Extrusion was ended by the pulling head hitting a stop; the load on the jack then built up until the torque limiter dropped out.

2.1.22 Drawing Head

The drawing head was designed to be able to take the maximum force which the jack could exert but also so that load cells of different sensitivities could be attached. Thus it is necessary to have some idea of the load to be expected in the experiment before it is carried out. This is not a serious limitation, however, as on the assumption that the sum of the drawing stress and the extrusion pressure is constant, the drawing stress, and hence the load, can be roughly calculated for a given pressure.

The head is shown in Fig. 2.3. As well as taking different load cells, it also allows a run up so that the motor is not started on load. Its final purpose is to stop the jack from rotating. If it were free to rotate it would do so and load could not be transmitted. The torque tending to rotate the jack, due to friction between the worm and the screw, is transmitted via guides, 1, Fig.2.3, to the main frame on which the drawbench is mounted. This frame bears up against an end plate of the high pressure assembly.

Load cells, 2, Fig. 2.3, are of simple construction comprising a flange, drilled to take six $\frac{1}{4}$" B.S.F. bolts, and a shaft onto which strain gauges are cemented. The shaft can be bored out to increase the sensitivity of the cell. The load cell is bolted to a shaft which slides into a sleeve, 3, Fig. 2.3, bolted to the drawing head. This shaft and sleeve are drilled, at right angles to their axes, to accept a pin, 4, Fig.2.3, which takes the load. The other end of the load cell is threaded to take either a chuck or a threaded coupling, 5, Fig. 2.3, to connect to the product.

2.1.3 Extrusion Apparatus

2.1.31 Low Pressure Side

An existing pressure supply was adapted for use to generate the high pressure needed for extrusion. This consisted of a 500 litre air bottle and a 55 litre air-oil piston type accumulator. Oil from the accumulator was fed to the system via a pressure reducing valve. It was hoped that as extrusion proceeded the pressure reducing valve would feed more oil to the intensifier, thus maintaining constant pressure in the extrusion chamber. However, as the flow required was very much lower than that for which the valve was designed, it did not operate satisfactorily and pressure fell off.

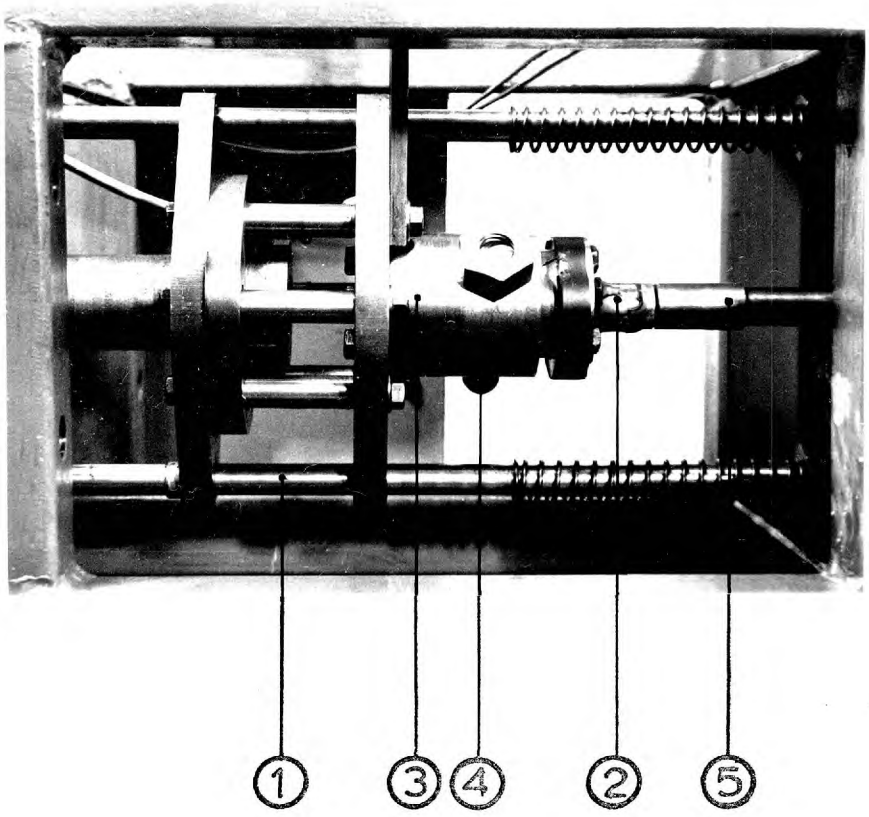

Fig. 2.3. Drawing head.

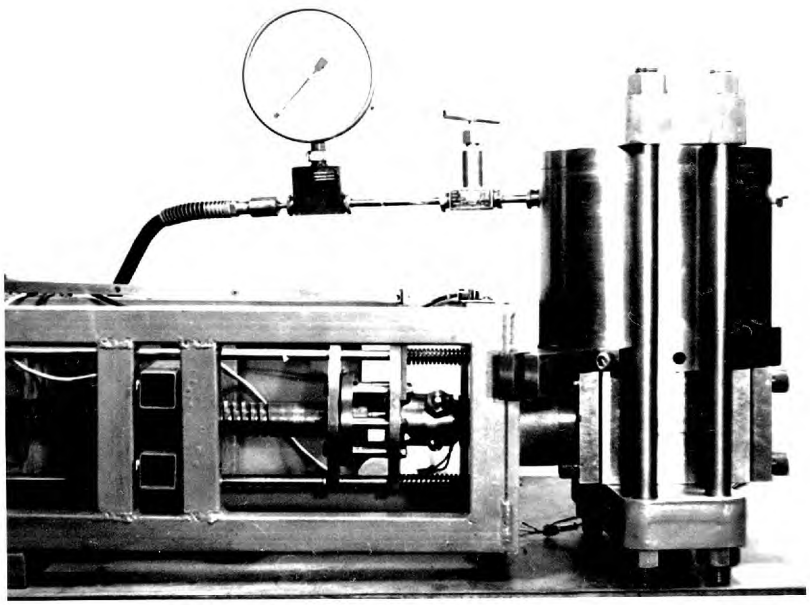

Fig. 2.4. High pressure subpress.

An alternative system was therefore used in which a smaller, 29 litre, air-oil accumulator was connected directly to the low pressure intensifier, 5, Fig. 2.2. This was charged with nitrogen from a bottle, 4, Fig. 2.2, to about four-fifths of the required pressure on one side of the floating piston. The side of the accumulator connected to the intensifier was then charged with oil to the required value by the system described above and this was then disconnected by a stop valve. Pressure was therefore maintained throughout an extrusion solely by an accumulator. The maximum fall in pressure at the high pressure side during an extrusion was about 40 bars.

The low pressure intensifier which was used will be described later in conjunction with the viscosity apparatus. Here it was only used to around 140 bars, much lower than its design pressure.

2.1.32 High Pressure Side

The low pressure system was originally designed for use with the large pressure vessel built for viscosity measurements. However, for the low pressure extrusions contemplated, it was decided to use the low pressure system with an existing subpress, described elsewhere (92), as this was more convenient. This subpress is shown in Fig. 2.4.

Two recesses, one at each end of the main bore, accommodate a die and a plug. The plug has four insulated terminals so that measurements of temperature and pressure can be taken inside the vessel.

To pressurise the fluid, a plunger is depressed into a cross bore. This is done by the piston of the low pressure intensifier, the end load being simply taken by two end plates and four tie bars.

2.1.4 Billet Design

2.1.41 Types of Billet

A certain number of solid billets were manufactured for testing the apparatus. These were used to establish free extrusion pressures and also to test the drawing rig and find the limits of augmentation.

No unusual features were incorporated but care was taken to ensure conditions which were as nearly constant as possible. After machining to a fine, turned finish and annealing, the billets were cleaned with 600 emery paper and then degreased with carbon tetrachloride. The surface roughness of the billets was then approximately 20-30μ C.L.A.

Further, for all tests, the billet was nosed to an angle of 2° less than the die angle. In addition, a tag was machined on the billet and threaded for attaching to the drawing head. This procedure was used throughout for billets of aluminium and copper.

For the visioplasticity experiments billets of the same design were required but split on their mid-plane along their longitudinal axis.

2.1.42 Manufacture of Split Billets

Several different methods were tried before a satisfactory approach was formulated. The final method, described below, resulted in specimens with the split on their mid-plane to within 0.0015 cm and no tendency for the two halves to bow apart.

Firstly, two rectangular pieces of material were fly-cut until they were accurately of the same thickness. These were then cemented together with Araldite while held in a vice. The composite bar was then held in a four-jaw chuck and clocked up so a centre could be accurately drilled in each end.

On first attempts to turn the bar between centres, it was found there was a tendency for the centre to separate the two halves. Therefore, jubilee clips were used at each end of the billet and only the central

portion was turned. The billet was then transferred to a collet where the ends were turned down. This was sufficiently accurate for the end portions, as no measurements are actually taken in these regions.

After machining the billets had to be annealed. During annealing the billets were again clamped together by jubilee clips, the billet surface being protected by copper sheet. Thus no bowing could take place during stress relieving.

One further requirement was realised, after carrying out some experiments. This was that the billet should be guided and the two halves held together while the container was filled with fluid. It was fulfilled by drilling a hole through the billet, perpendicular to the split. A piece of silver steel was then pushed through this hole and holes in a collar which was a sliding fit both on the billet and in the container bore. Longitudinal grooves were cut in the collar, for pressure equilisation.

Two split billets, one assembled, are shown in Fig. 2.5.

2.1.43 Grid Preparation and Measurement

During the annealing process the Araldite bonding the two halves of the billet was burnt and it could easily be separated into its two halves. The surfaces were then cleaned by abrasion on 600 grade wet and dry paper. They were then polished with 6μ diamond paste on a flat polishing table. After this treatment the surface was highly reflective.

Full grids were not drawn on all specimens as only flow lines were needed as input data for the computer program. These lines were scribed on the surface using a Société Genevoise Universal Measuring Machine. Grid lines as thin as 0.01 mm could be discerned after extrusion but only with difficulty. It was more practical to use lines about 0.04 mm thick. The accuracy of measurement was still greater than this figure as the centre of the line could be estimated under the microscope.

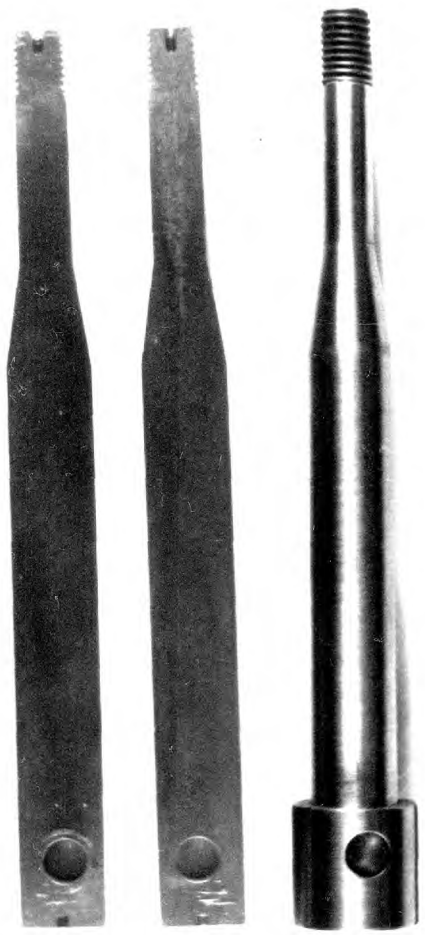

Fig. 2.5. Split billets.

Two different measuring techniques were tried to find the coordinates of the lines after extrusion. The first method was to look at the lines through an Optical Projector and the second was to use the measuring instrument again. The former was less fatiguing than looking through the microscope but, because of difficulties with illumination, the measurement was less accurate and repeatability was worse. Therefore, the measuring machine was used throughout.

To estimate the accuracy of measurement several points were measured repeatedly, approaching them from different directions. The coordinates never varied by more than 0.004 mm for any one point, so this can be taken to be the measuring error. As this was much less than the thickness of the line attempts at more accurate reading would not be meaningful.

Although other methods of putting the lines on the specimens, such as the photo-resist method, were considered, it was thought none were likely to give as high an accuracy as was obtained by the method used.

2.1.5 Die Design

2.1.51 Original Design

The first die design which was used was intended for aluminium billets. As the bore of the container was only 1.91 cm the dies were designed so that the largest possible billet could be used, that is about 1.52 cm diameter. This resulted in the rather unusual design shown in Fig. 2.6 in which part of the die is fluid supported.

For aluminium, the product augmentation which can be applied is small, as its tensile strength is low. Hence a fluid supported design is feasible as the reduction in pressure due to augmentation will be small. However, this design proved too fragile in practice, one die actually fractured during assembly.

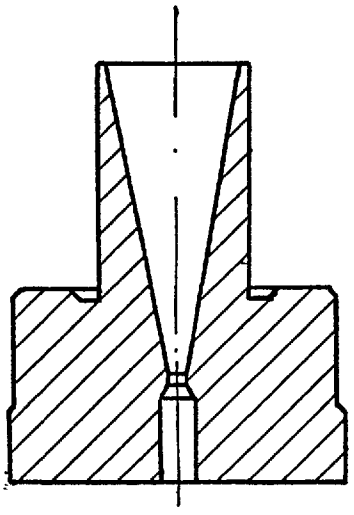

Original die design.

Full size.

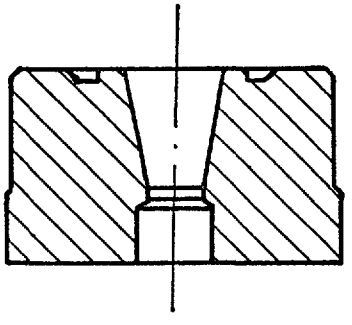

Final die design
for copper billets.

Fig. 2.6. Original and final die designs.

2.1.52 Final Design

For the extrusion of copper it was not possible to use a fluid supported die for extrusion drawing in this assembly, as it would still have had to be thick walled. The billet size was therefore reduced to 1.25 cm diameter so the usual type of thick walled die could be used. This is shown in Fig. 2.6.

Also, this die was made of high tensile steel, EN30B, as opposed to the tool steel used for the previous design. The only disadvantage is the lower hardness, and consequently greater wear of the die, but this is more than offset by the greater fracture toughness and ductility, especially as relatively few experiments were contemplated.

Die geometries, that is angles and reduction ratios, will be discussed later.

2.1.6 Instrumentation

2.1.61 Load Measurement

A tensile load cell was used and the mechanical construction has been described in section 2.1.22. The two, 120Ω strain gauges were attached diametrically opposed and connected in series so that any effects due to bending were automatically eliminated.

The strain gauges were of the self-temperature compensating type when used on steel; that is, the material is chosen such that the change of resistance due to temperature change is equal and opposite to the change in resistance the temperature induced strain produces.

Continuous monitoring of the load is carried out by feeding the output from a D.C. bridge, 6, Fig. 2.2, to an Ultra-Violet Recorder, S.E. Labs type 3006, 7, Fig. 2.2.

The load cell was calibrated in a Tinius-Olsun testing machine which is itself capable of holding and recording load to better than 1%,

the accuracy claimed for the galvanometer of the recorder. Thus no appreciable errors should have been introduced by this method. The calibration of the load cell gave a straight line graph, with no discernible hysteresis on unloading and is therefore not included here.

2.1.62 Pressure Measurement

Pressure is sensed inside the vessel by monitoring the resistance of a manganin coil of approximately 100Ω resistance. This was wound on a plastic former from 42 S.W.G. manganin, diamel insulated.

After winding the coil was stress relieved by heating to 140°C for 10 hrs in a neutral atmosphere. It was then pressure seasoned by pressurising it to 16 kbar five or six times. After this treatment there was no drift in resistance at ambient pressure and temperature over the period of the experiments.

Calibration of the coil was obtained by using an Harwood Dead-Weight Pressure Gauge. This was capable of much greater accuracy than the ancillary equipment, namely a D.C. bridge, 8, Fig. 2.2, and a U.V. recorder, so it was not necessary to calculate all the corrections. The full calibration procedure is described in section 2.3.7.

Unlike the load bridge, which is always set up with a six volt supply from the power pack, 9, Fig. 2.2, and used as calibrated, the pressure bridge has a 'set calibration' resistor. From the calibration graph, given in Fig. 2.7, it can be seen that this resistor corresponds to a certain pressure. Using this resistor and a potentiometeter, the galvanometer can be set so this pressure will cause any convenient deflection. This, of course, introduces a multiplying factor when using the calibration graph.

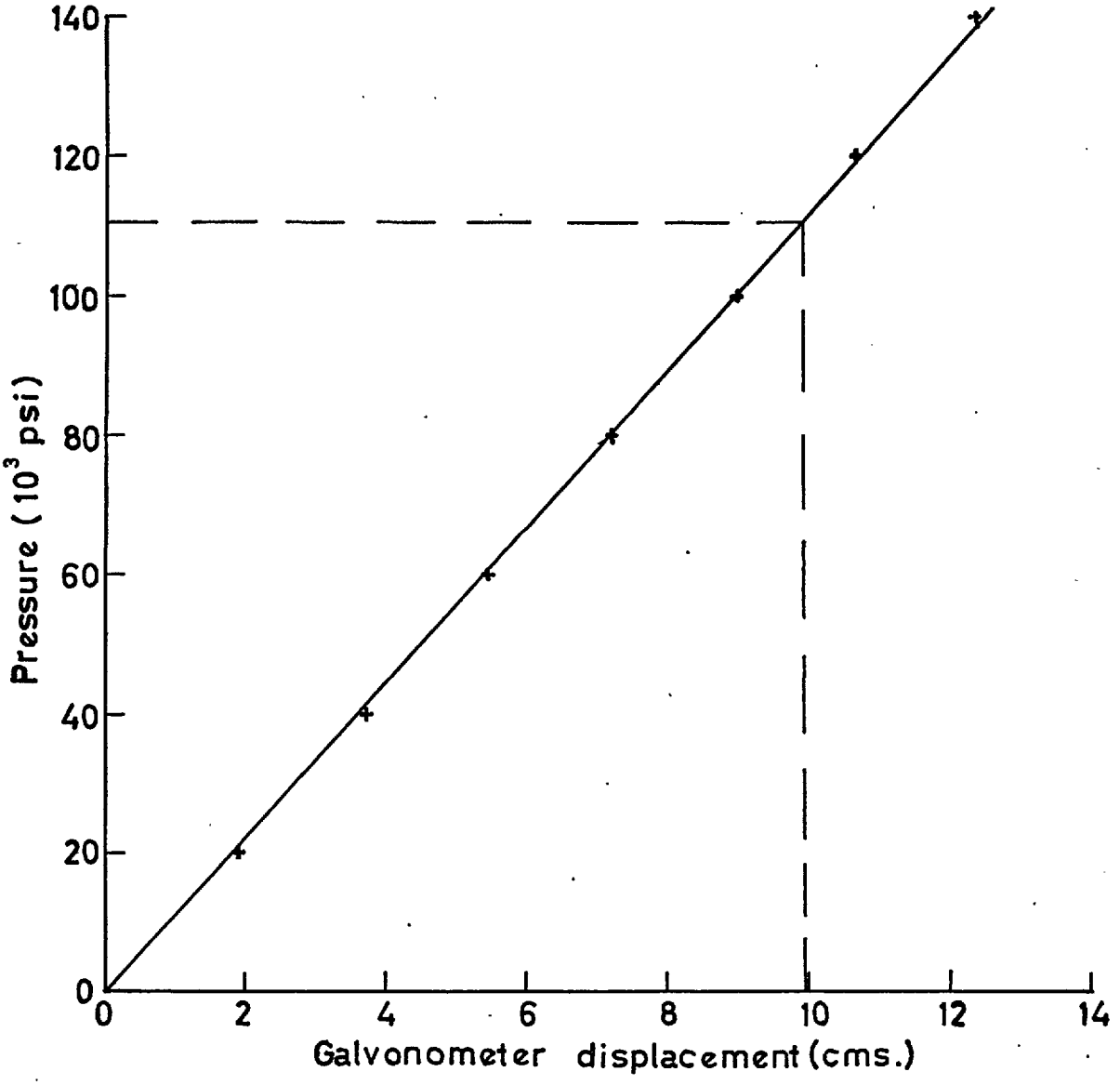

Set calibration resistor corresponds to 7.633 kbar (110,700 psi)

Galvonometer type A.100. Serial no. 8-2557.

U.V. Recorder channel 2.

Fig. 2.7. Pressure cell calibration.

2.1.63 Temperature Measurement

Temperature of the fluid was sensed by using a chromel-alumel thermocouple. The cold junction was held at $0^{o}C$ in a 'Thermos' flask of ice and water and the hot junction was in the high pressure fluid.

Electrical leads were taken from the vessel using a standard arrangement of a cone of metal, insulated from the plug by a conical, ceramic insulator. In the case of the thermocouple the metallic conductors were made of chromel and alumel, hence eliminating any spurious e.m.f.'s which might otherwise have been generated.

The output from the thermocouple was connected directly across the galvanometer. Whilst this is not an ideal arrangement, as current is drawn, it was capable of giving results of accuracy comparable with the other measurements.

Calibration was carried out at two points only, namely $0^{o}C$ and $100^{o}C$.

2.1.64 Displacement Measurement

In order that the extrusion velocity could be calculated, the displacement of the drawing head was recorded. This was done by attaching a rack to the head, operating a pinion, which turned a standard, multi-turn potentiometer.

As previously described, a D.C. bridge was used with a potentiometer in series with the supply. This enabled the scale to be set to any convenient value for the extrusion being carried out.

Timing marks were put on the U.V. recording paper by the recorder, hence no further information was necessary. With the instrumentation described all the extrusion drawing parameters were continuously recorded against time throughout the experiment.

2.2 The Viscometer

2.2.1 Introduction

Since the first attempts to measure viscosities at high pressures by Warburg and Babo (100) and Roentgen (101) many different viscometers have been constructed for use at high pressures. The summaries by Hersey and Hopkins (12) and Hersey (13) were mentioned earlier.

The various methods which have been used are described below, in the order in which they were first attempted.

2.2.11 Capillary Flow

This was the method which was used by the early experimenters in this field (100, 101, 102, 103, 104). A column of mercury was used to drive a sample of fluid through the capillary, but only one reading was obtained from each set up. The viscosity was calculated from Poiseuille's equation -

$$Q = \frac{\pi d^4 \Delta p}{128 \eta \ell} \qquad 2.1$$

Rankine's method (105) of measuring the viscosities of small quantities of a gas suggested a convenient form of appratus for measuring viscosities under pressure and was used by Phillips (106). In this the capillary is vertical and is one arm of a closed loop. The other vertical arm, of larger diameter, contains a slug of mercury. Gas under test is introduced to the closed loop and then driven through the capillary by inverting the whole assembly. To obtain absolute measurements different lengths of mercury slug must be used so the reduction in pressure difference due to surface tension can be calculated. This method was later extended to higher pressures by Nasini and Pastonesi (107) and Comings and Egly (108, 109).

Another closed circuit system, capable of repetitive measurements, was devised by Hyde (110). In this the capillary is horizontal and is connected at each end to two, large bore vertical tubes which are in turn connected by a large bore tube. Mercury is contained in the bottom half of the system, while the top half is filled with pressurised fluid under test, the whole assembly being mounted on a pivot. A head of mercury is produced in one vertical tube and the system rebalanced about the pivot, with the aid of a spring. By careful arrangement of the spring geometry, the head is kept constant. The fall of the frame, about the pivot, is then a measure of the fluid which has been displaced. Similar systems have been used more recently by Eakin and Ellington (111) and Parisot and Johnson (112).

The method of producing a head used by Michels and Gibson (113) was to rely on the compressibility of the gas and the restriction provided by the capillary. Rapid pressurisation caused mercury to rise faster in a large bore tube than a capillary tube which were joined at the top but with their ends open in a bath of mercury. The head then drove the gas through the capillary.

Swearingen and Redding (114) built an apparatus consisting of a glass capillary with a reservoir at one end and a stop cock at the other. Pressure was transmitted to a fluid under test by a gas and the reservoir was filled by inverting the vessel. Flow was started by opening the cock with a shaft through the wall of the vessel and timed visually, windows being provided in the vessel.

A continuous discharge method, in which fluid is discharged from a reservoir, through a capillary into a reservoir at a lower pressure, was first suggested by Dane and Birch (115) for molten glass. More recently, it has also been used by Mayinger (116) and Novak and Winer (117) who studied non-Newtonian effects at high shear rates.

Recent work by Barnett and Bosco (118) has shown the capillary viscometer can be used to measure viscosities at pressures of up to 60 kbar. Their apparatus consists of a vessel vented by a capillary, with manganin coils inside and outside the vessel, the whole assembly mounted inside a hexahedral press. Pumping up the pressure caused a pressure difference to develop between the inside and outside of the vessel. When pumping stopped, the pressure equalised over a period of time.

2.2.12 Rolling Ball Viscometers

A viscometer in which the time of a ball rolling down an inclined tube is used to measure viscosity was first suggested by Flowers (119). It has been utilised as a high pressure viscometer by many workers, among them Hersey (120), Hersey and Shore (121), Dow (122, 123), Sage, Lacey and Yale (124), Bicher and Katz (125), Hubbard and Brown (126), Webb, Griest and Schliessler (127) and Carmichael and Sage (128).

If the system is to be used at high pressures, then it must be built in the form of a tube, containing the ball, which is inserted in a high pressure environment. Otherwise the dilation of the tube due to internal pressure will cause unacceptable errors. The inclination used in the above works was around 15° to the horizontal, although larger angles have been used of the order of 80°.

2.2.13 Falling Body Viscometers

In this type of instrument a spherical or cylindrical body falls vertically in a tube containing the fluid under test at the required pressure. If it can be arranged that the diameter of the tube is large in comparison with that of the body then Stoke's Law, with wall corrections, can be applied to give absolute measurements.

The first falling body instrument used under pressure was that designed by Bridgman (10) and used up to 12 kbar. This consisted of a cylindrical weight with hemispherical ends falling in a tube with small clearance. The fall was guided and timing started before the viscometer was vertical, that is before steady state conditions had been reached. The same instrument was used later by Kleinschmidt (129) and Dow (122, 130) and later by the A.S.M.E (8) in producing their pressure viscosity report. In all these works guides were used on the sinkers to keep eccentricity of fall within small limits.

Mason (131) suggested a method of overcoming the difficulty of assessing electrical contact at the end of fall. He put a small magnet in the sinker and detected this by measuring the voltage induced as it fell through four coils. Cappi (132) used guided sinkers in his measurements to 15 kbar. His timing system relied on a magnetic sinker upsetting the balance of an A.C. bridge. The out of balance voltage triggered a timing circuit automatically.

Unguided sinkers were first used by Hawkins, Solberg and Potter (133), who, at about the same time as Mason, detected the passage of the sinker by coils. They used a pair of coils at each end and wired them into an A.C. bridge. As the sinker passed the bridge was unbalanced and the output fed to a recording millivoltmeter. Von Wijk, Van der Veen, Brinkman and Seeder (134) and Boelhouwer and Toneman (135) used needle shaped bodies falling in fine bore tubes. The former authors again used coils to detect the sinker but used a varying capacitance method. Jobling and Lawrence (136) also used unguided sinkers but provided an initial section with very small clearance to steady the sinker and ensure it was concentric with the tube.

Measurements to 30 kbar were made by Bridgman (11) in an apparatus which timed a vane swinging through an angle of about 60° but this was not capable of great accuracy.

An absolute method of measuring viscosity was devised by Suge (137). He timed the fall of balls, by a variable capacitance method, in a tube with large clearance. This method has since been used by other workers, the most recent being Rowe (138). Further absolute measurements have been made by a new method by Wilson (14), using a suggestion by Nadai (139). This involves timing the fall of a circular plate onto another flat surface by a capacitance method.

2.2.14 Rotating Cylinder Method

Although this system has been used extensively at atmospheric pressure, high pressure application has been limited to use by Thomas, Horn and Dow (140) and Dow (123). As the motor is inside the pressure vessel care must be taken to ensure it does not heat the fluid. In all accuracy is not good owing to difficulties in measuring torque on the cylinder which is not being rotated and also in ensuring concentricity between the two cylinders.

2.2.15 Oscillatory Viscometers

Measurement of viscosity by measuring the period of oscillation of a disc immersed in the fluid was first suggested by Maxwell (141). It has been used at pressures above atmospheric by Mason and Maas (142), Gonikberg and Vereshchagin (143) and Moszynski (144). Spheres and cylinders have been used as the oscillating bodies.

Although the system gives absolute measurements, it is limited to use with gases and low viscosity fluids. With high viscosities the period of oscillation would be long and consequently more difficult to measure. Further, it is difficult to estimate the effect of a high pressure environment on the suspension characteristics.

2.2.16 High Frequency Methods

The final method considered here is to immerse a crystal in the fluid and oscillate it electrically. A measure of the viscosity of the fluid can then be obtained by measuring the absorption of the sound wave produced, as by Litowitz and Carnevale (145), Tait (146), Richardson and Tait (147) and Eden and Richardson (148). Alternatively the viscosity can be deduced by measuring the electrical properties and resonant frequency of the crystal itself, as by Barlow, Harrison, Richter, Sequin and Lamb (149).

These methods are essentially high shear rate methods and are not applicable in the range normally met in mechanical situations.

2.2.17 Selection of Viscometer

Before choosing the type of viscometer for use in this study, a decision had to be taken on the pressure range for which the instrument was to be designed.

It is preferable that the instrument should be able to cover the whole range of pressures which have been used, or are likely to be used, in hydrostatic extrusion. To date, experimental rigs have been used to pressures of 30 kbar and commercial design of cylinders to 22 kbar has been considered by Lengyel, Prasad and Burns (150) and to 30 kbar by Hornmark (151) and Pennell (152). It is therefore desirable that a viscometer should be able to operate up to 30 kbar, which in any case is approaching the limit of pressure for which pressure vessels can be designed with present day materials.

The only viscometers which have been used up to this pressure are those of Bridgman (11) and Barnett and Bosco (118). The former was not capable of great accuracy, while the latter was only expected 'to determine appropriate relaxation times and limits of hydrostatic behaviour when using

particular liquids' rather than a precise study of viscosity.

Two other important factors must be considered in selecting a method. The first is that valves, tubing and fittings cannot be used at the pressures which are of interest here. Pressure generation must be on the 'one-shot' intensifier principle. The second is that the bore diameter of the vessel should be kept as small as possible, as large diameter ratios are necessary to contain 30 kbar. With these considerations in mind, the viscometers described above can now be studied for suitability.

Rotating cylinder instruments were ruled out because of bulk and lack of accuracy. Oscillatory body viscometers were rejected because of the high viscosities of lubricating oils at high pressures and high frequency methods because the results are not applicable at low shear rates.

While it would be possible to design a capillary viscometer of the type used by Novak and Winer (117) this would be difficult without the aid of fittings. At high pressures the expansion of the capillary would have to be taken into account, unless it were fluid supported. Further it would be much more difficult to control temperature and to hold the two pressures constant in a system designed for 30 kbar.

Thus we are left with falling or rolling body viscometers. Absolute measurements were eliminated because of the difficulty in timing fall without putting coils near the fall path. A radio-tracer technique first used by Heiks and Orban (153) and later by Rowe (138) is of questionable accuracy. The falling plate method requires a fairly bulky instrument as the end corrections would be large for a small diameter plate.

In designing an instrument it is relatively easy to arrange it so that it could be used for all the different types of viscometer left, namely rolling ball or falling sinker, either guided or unguided. It was therefore decided to design an instrument of this type and, in the first instance, to use it with either unguided sinkers, if they could be

made to cover a sufficient range of viscosities, or else with guided sinkers.

Flow past the sinker tends to centralise it but if this is very slow it is overcome by the tendency for the sinker to yaw over. At high flow speeds surface irregularities can cause the sinker to oscillate about the axis of the tube as the flow is not completely uniform. Both of these effects lead to erratic fall times and so the range of use of a sinker without guide pins is likely to be much smaller than one with them. On the other hand unguided sinkers are preferable, if they give repeatable results, as they introduce less turbulence than ones with guide pins. Both have advantages over the rolling ball method in that they are easier to correct for compressibility and are not subject to the possible error of the ball slipping instead of rolling.

A further advantage of the falling weight method is that it can also be used to give density measurements by timing two sinkers of different densities. These measurements will not be as accurate as the viscosity measurements as they depend on the difference between the fall times. However, they will be sufficiently accurate for density correction terms in the viscosity expression.

Finally, a means of retrieval must be chosen from either inversion or magnetic methods. The former is chosen as the latter method causes heating of the fluid and needs more leads into the vessel. The inversion method complicates the pressure system but has the advantage that readings can be taken from both ends.

2.2.2 Design of Viscometer

For reasons given above, it was decided to use a falling weight viscometer of the type originally described by Bridgman (10). Several improvements have been suggested by later workers and these are incorporated in the present design. In particular, the method used by Cappi (132) of

accommodating two sinkers is included.

A drawing and photograph of the assembled viscometer are given in Fig. 2.8. The central part of the viscometer, 1, contains the bore in which the timed fall of the sinker takes place. This is made from a non-magnetic, austenitic stainless steel, EN58JM. The bore is straight to within 0.01 mm, round to within 0.0025 mm and does not vary from its nominal diameter of 7.933 mm by more than 0.005 mm. The surface finish of the bore is better than 1μ C.L.A.

At each end of the main tube two grooves are machined in which the coils are wound for the timing system. The central portion is also turned down to enable plugs to be attached here, if necessary.

The two end caps, 2 and 3, contain bores at 15° to the main axis which are 7.93 mm diameter by 20 mm deep. One of the end caps, 3, screws directly onto the main tube while the other is attached by a locking collar, 4. This arrangement enables the two angled bores to be aligned so they are both in the same plane. It is then possible to select for fall either of two sinkers by rotating the viscometer in the correct direction. The sinker which is not required is then lodged in the angled bore to prevent it from falling.

One end cap, 2, is attached to a piston, 5, and cylinder 6. The piston is free floating and strokes forward during pressurisation, to take up the compressibility of the fluid.

The other end cap, 3, has a closure, 7, with a 2 B.A. threaded hole in the end. This is used for filling the viscometer, under vacuum, when a connection is screwed in and sealed by P.T.F.E. tape. In use it is sealed by a plug, 8, which is also used for inserting the viscometer and lifting it from the high pressure vessel. There is also a bursting disc, 9, which would fail in the event of a high pressure seal leak causing sudden depressurisation. This greatly diminishes the risk of damage to the viscometer. The disc is of 0.1 mm thick copper foil,

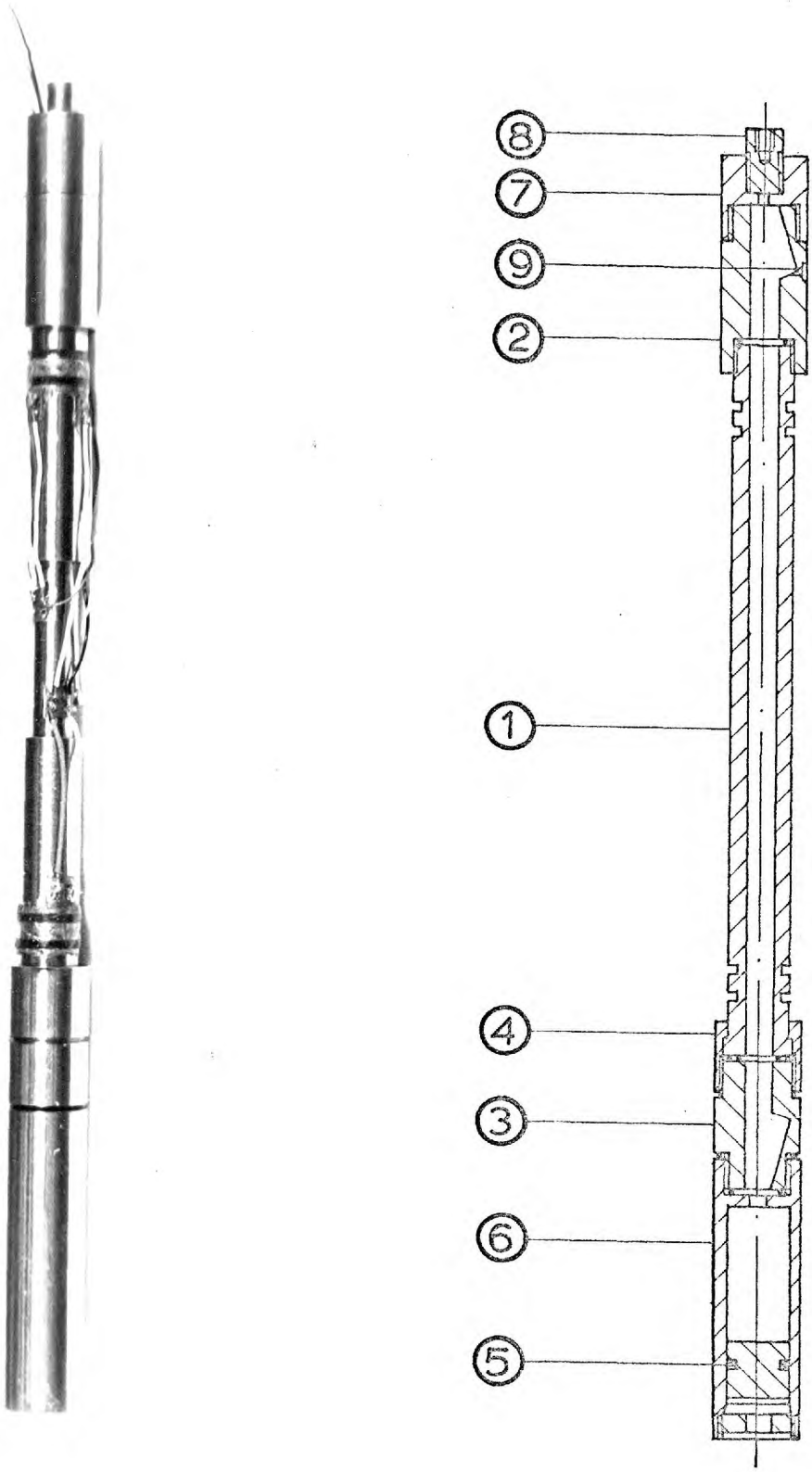

Half full size.

Fig. 2.8 The viscometer.

soldered in place by stainless steel solder.

When unguided sinkers are in use guides can be provided to steady the sinker and ensure it is concentric with the bore of the viscometer tube immediately before triggering. The sinker is thrown to one side of the tube by the sudden deceleration as the viscometer comes to rest in its stop and may not have settled down to concentric travel by the start of timing if these guides were absent.

Sealing of the viscometer was originally intended to be by thin copper gasket seals. However, it was found to be easier in practice to use O-rings of suitable size. The viscometer was tested with an internal air pressure of 5 bars to test the seals. In fact, the same fluid was used outside the viscometer as was being tested to reduce the possibility of contamination of the test fluid. The sealing simply made it possible to fill the viscometer under vacuum, with a carefully filtered sample of fluid.

2.2.3 Design of Sinkers

The design of sinkers is governed, to a certain extent, by the requirements of the timing system. It was necessary to have a soft iron core in the sinker of at least 0.5 cm in diameter by 1 cm long. To make sinkers of different densities they had to be of composite construction.

Originally they were designed and made so that, when assembled over a core, they were cylinders with hemispherical ends. Guidance was obtained by inserting four pins in holes drilled at each end of the parallel portion and were thus in the region of highest velocity of fluid flow. This is undesirable as they are most likely to cause disturbance of the flow in this position. Further,it proved difficult to machine the hemispherical ends so that the sinker was symmetrical. This resulted in different fall times in different directions.

Two different designs were therefore considered which are geometrically very similar, except that one has guide pins. Photographs and drawings of sinkers with guide pins are given in Fig. 2.9, while those without pins are shown in Fig. 2.10. In this design the guided sinkers have pins which are in a region where the radial clearance is much larger and therefore where the flow velocity is lower. Thus they are less likely to cause turbulence in the flow.

Two examples of each type were made, one with the main body of EN58JM stainless steel and the other of an aluminium alloy. Thus the two composites had different densities.

Adjustment of the fall time to suit given fluids can be made either by decreasing the diameter of the cylindrical portion of the sinker or by increasing the diameter of the central hole. A range of sinkers were tried and the most suitable chosen for the tests described later.

It is worthwhile noting that great care was taken in manufacturing these sinkers. The soft iron core was machined first, with a pilot hole, slightly smaller than the finished size required, drilled through. Two end shells were then machined, again with pilot holes, and one was left on the bar. The sinker was then assembled, with Araldite, and the hole reamed out. If pins are to be used the holes are drilled before the sinker is parted off. Final machining and polishing was carried out with the sinker on a mandrel to ensure concentricity and pins, if necessary, are then Araldited in place and turned down to the required diameter. The last step was to polish the ends and the central hole.

As can be seen from Fig. 2.9 a lead-in angle was also machined on the pins. This served two purposes. The first is that it helped to prevent the sinker from sticking at the joints between the end caps and the main bore. Secondly, the lead-in would help the build up of a thin film between the end of the pin and the wall of the tube.

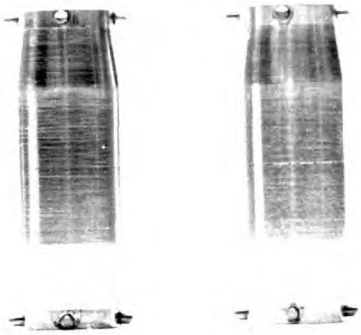

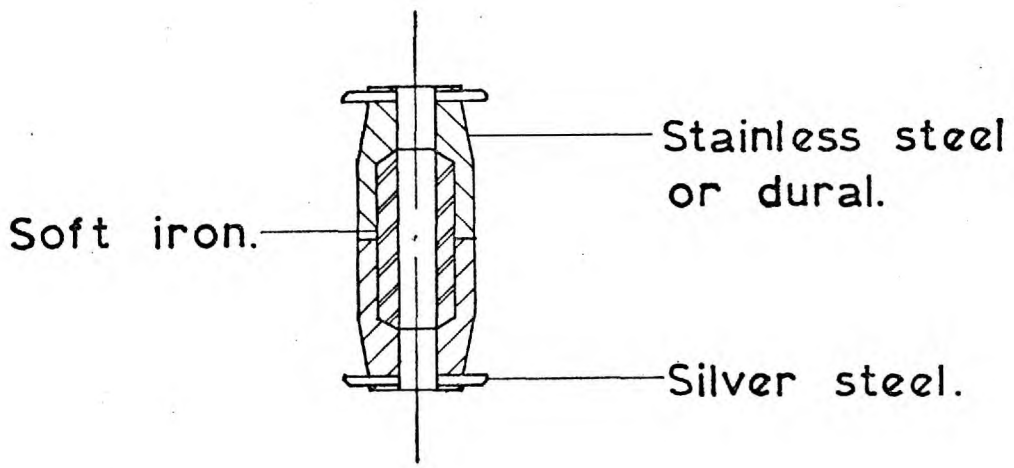

Twice full size.

Fig. 2.9. Sinkers with guide pins.

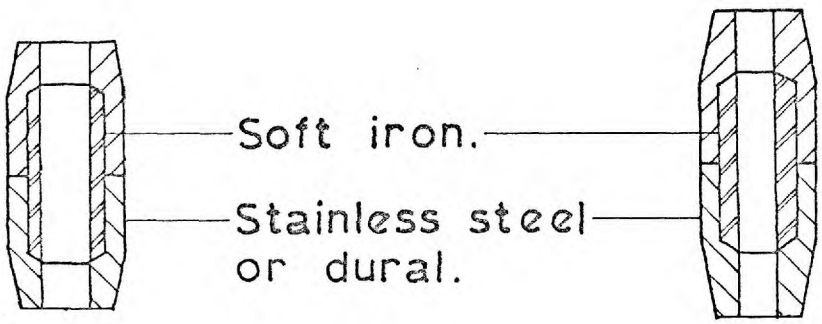

Twice full size.

Fig. 2.10. Sinkers without guide pins.

Manufacture in this way ensured the sinkers were as symmetrical as possible and that the surface finish was very good. Hence the fall times will be as nearly independent of direction of fall as possible and also that the sinkers will be usable over a wide range of viscosities.

2.2.4 Timing System

The only method of timing which is likely to produce results of the same accuracy as the rest of the equipment is an electrical method which automatically triggers a counter. Previous designs of this type have depended on the sinker upsetting the balance of two coils, in opposing arms of an A.C. bridge, as it passes through them.

As bridge circuits are liable to be upset by stray capacitance and other spurious effects, it was decided that a different system, relying on mutual inductance between two coils, would be used. One coil of each pair is fed with A.C. from an oscillator, at 500 Hz. As a sinker passes through a pair of coils, a voltage is induced in the second coil.

The signal from this coil is fed through two stage amplification with a voltage gain of 30 in each amplifier, to a trigger circuit. One such circuit starts an Advance counter, type TC1, while a second one stops it when the sinker passes through the second pair of coils. The counter counts pulses from a 1,000 Hz pulse generator. A reversing switch is situated between the amplifiers and the trigger so that either pair of coils can be used to start timing. In other words fall can be timed in either direction. The voltage supply, at 25 V, is from a stabilised power pack.

Coils on the viscometer are wound from diamel coated copper wire of 42 S.W.G. 500 turns are wound into each groove, the total resistance then being about 50 ohms for each coil. To guard the coils against damage in the case of sudden depressurisation the coils are wound in a matrix of polystyrene dissolved in toluene. This allows pressure to be

transmitted to the coil but prevents fluid entering. Otherwise the coils might be damaged if the high pressure suddenly dropped to zero.

A full circuit diagram of the timing system is given in Fig. 2.11. Here all transistors are type 2N2926, unless otherwise specified.

By adjusting the voltage at which the triggers operated and careful shielding of the leads to avoid pickup and interference, the system could be set up so that the stop and start circuits did not trigger off randomly when the viscometer was not in the pressure vessel. At first it was thought that the situation would be much more satisfactory with the viscometer in the vessel, on the assumption that, as the vessel was well earthed, it would operate as a further shield. In practice pickup caused both triggers to go off as soon as the circuit was reset. Presumably the vessel and other high pressure apparatus was acting as an aerial and voltages being induced in the leads by capacitance effects.

Tuned filter circuits were therefore incorporated before the input to the amplifiers so that only a narrow pass band, in the region of 500 Hz, was allowed to reach the amplifiers.

2.2.5 Filling System

The filling system is shown in Fig. 2.12. It is connected to the viscometer by the filling port, as described earlier, and to a rotary pump to evacuate the whole system. When this has been carried out the valve between the viscometer and the absorption trap is shut and the valve at the bottom of the funnel opened. The liquid which is to be tested then runs into the viscometer. After a charge of fluid has been let in, not necessarily enough to fill the viscometer, the funnel valve is shut and the fluid is subjected to vacuum. This ensures that the fluid is deaerated.

While still under vacuum the piston at the end of the viscometer is moved up and down and the viscometer tilted to dislodge any air bubbles

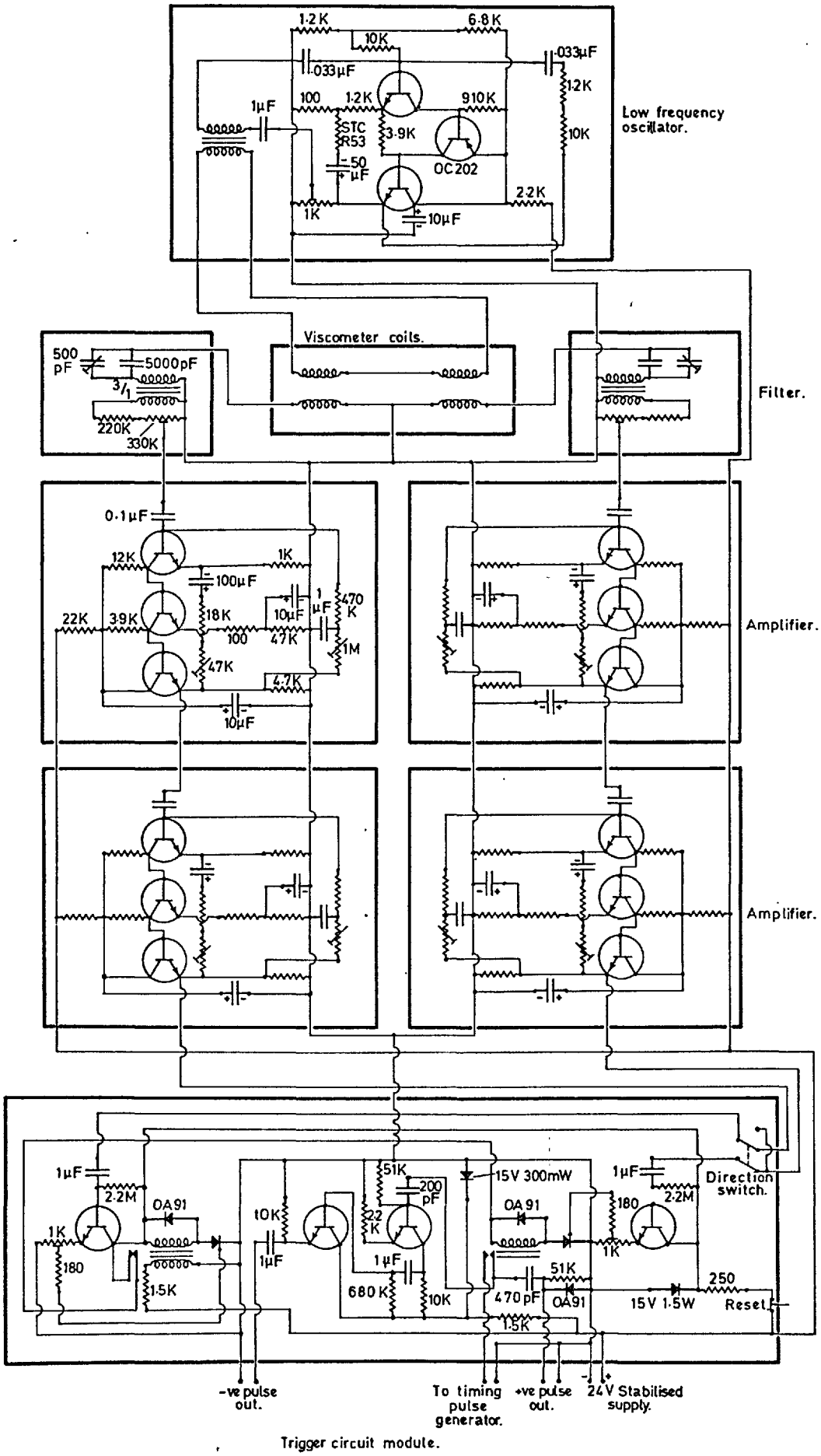

Trigger circuit module.

Fig.2.11. Timing circuit diagram.

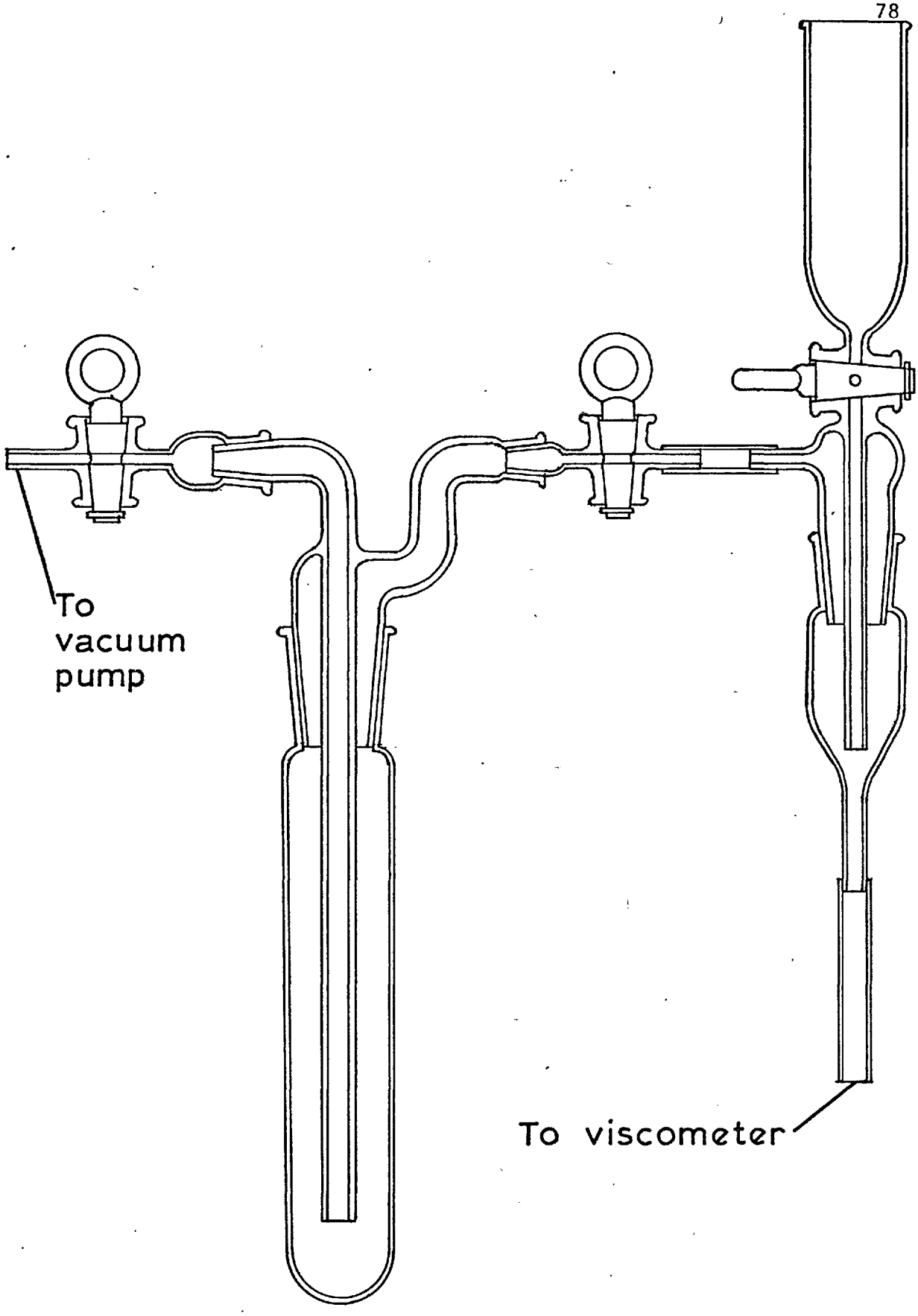

Fig. 2.12. Viscometer filling system.

which might otherwise be trapped. This process is continued and further charges of fluid are let in until the viscometer is full of fluid and no further bubbles come from it. Although somewhat time consuming this method ensures the viscometer is completely full of de-aerated fluid and no other method could do this.

2.3 Description of High Pressure Apparatus

2.3.1 Design Requirements

Two of the most important design requirements have already been mentioned, namely that the system should be capable of developing and containing pressures in the region of 30 kbar and of inverting for sinker retrieval in the viscometer.

It has also been mentioned that as valves and fittings are not possible at this pressure, the system must work on the 'one-shot' intensifier principle. The viscometer itself is 36 cm long and with space for leads and pressure coil the working length of the vessel must be 41 cm long by 2.54 cm diameter. The length of stroke on a single piston to produce 30 kbar would be too great and so two pistons must be used, one at each end of the bore.

This results in the set up shown in Figs. 2.13 and 2.14. The pressure vessel is 76 cm long with a bore diameter of 2.54 cm. Detailed description of the design and function of the constituent parts is given below.

2.3.2 Pressure Vessel Design

2.3.21 Preliminary Considerations

Several different designs of pressure vessel have been suggested and used over the pressure range of interest here. Firstly, it is important to note that fatigue was not considered in the design. This is acceptable

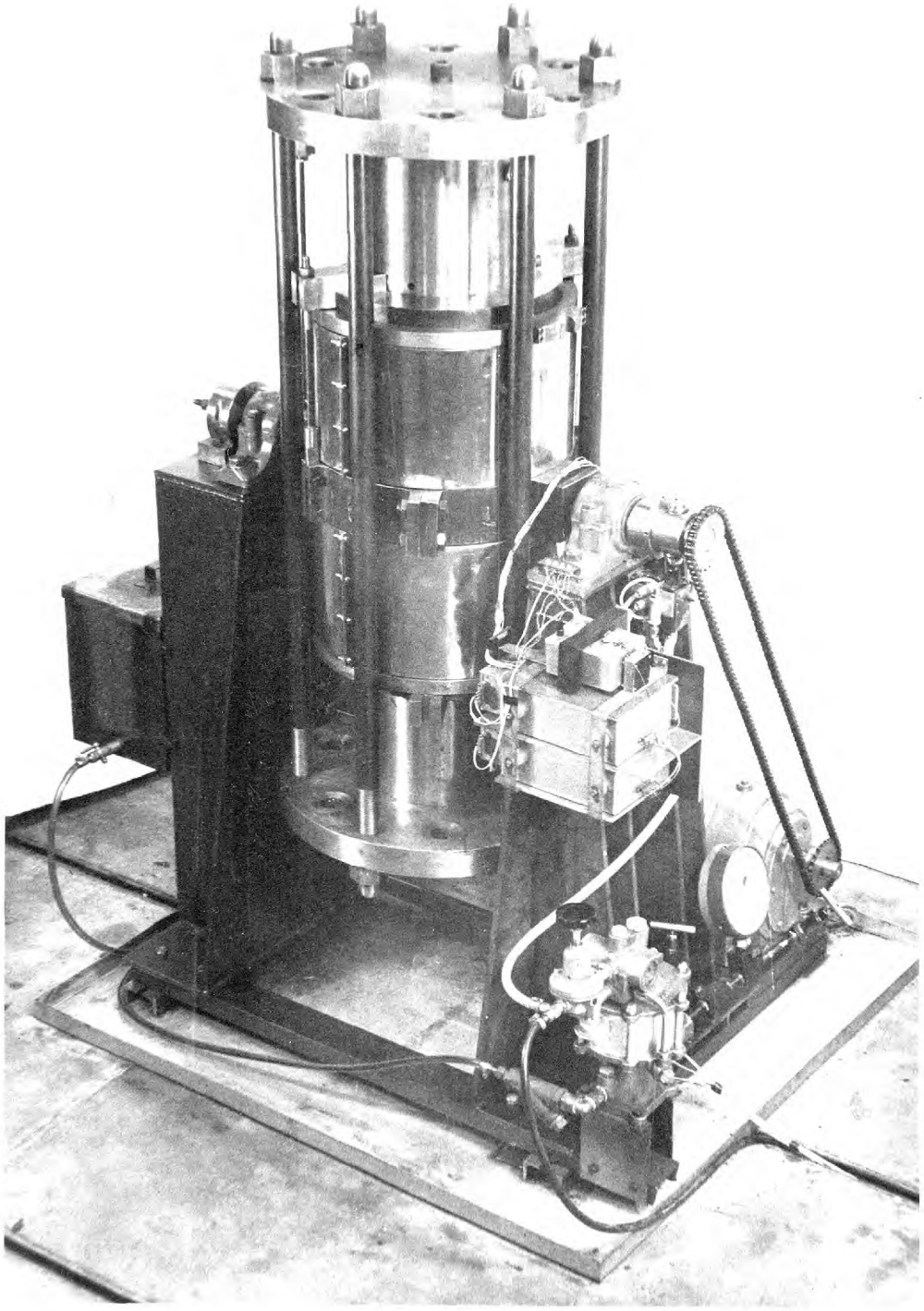

Fig. 2.13. Assembled high pressure apparatus.

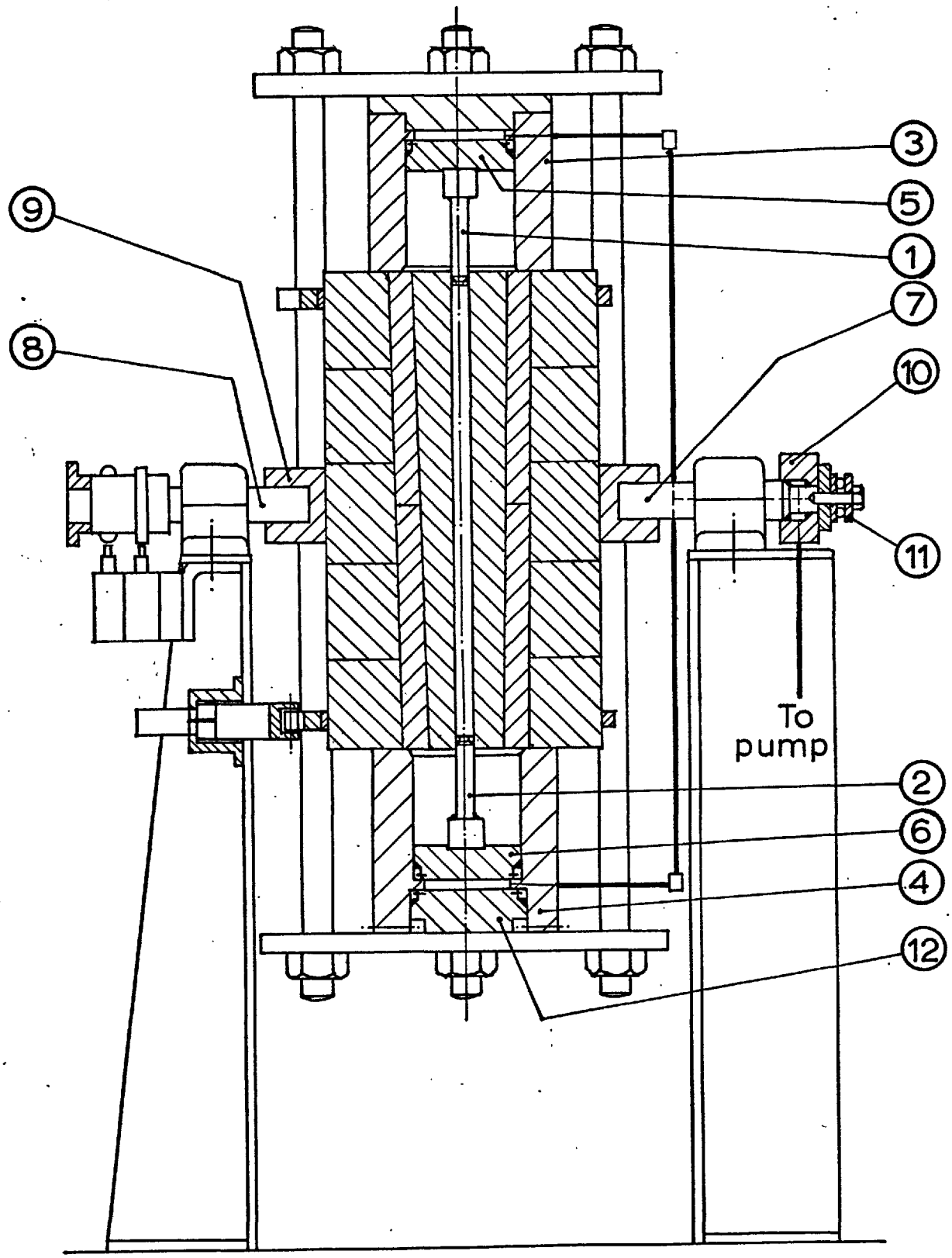

Fig. 2.14. Schematic of high pressure apparatus.

in laboratory equipment as the number of experiments to be carried out, especially at the highest pressures, was small.

Exotic designs, such as those based on sectors of tungsten carbide, were first ruled out because the expense of manufacture could not be justified. These are only likely to be economic when long life is essential. Fluid support was not considered either as it would make the apparatus more complicated, especially as the vessel must be inverted for sinker retrieval.

Dynamic support designs, in which the liner is supported by movement into a large angle of taper, were also eliminated. The force required to push the liner can be supplied either externally or by having a stepped bore in the container. The former system would again make the system complicated while the latter could not be used with the design envisaged in Fig. 2.14 where two balanced punches are necessary.

Thus we are left with monobloc cylinders, either elastic or autofrettaged, or designs in which the liner is prestressed in compression by multicomponent design. Assuming the Tresca yield criterion, the maximum pressure for an elastic monobloc cylinder, with infinite diameter ratio, is half the yield stress of the material. For high tensile steels, such as the maraging variety, the yield stress is around 17 kbar, hence an elastic monobloc design would be limited to 8.5 kbar.

Autofrettage to give prestress to the point of reverse yield doubles the pressure range, to give maximum pressures of 17 kbar. With large diameter ratios it is possible to use the monobloc cylinder to higher pressures, allowing the bore to yield in compression when the pressure is removed. This will lead to a very short fatigue life, of the order of a few hundred cycles but the main objection in the present circumstances was that it is not possible to harden conventional high tensile steels in the required section. A maraging steel would therefore have to be used and this would be very expensive, approximately £1,600 for the pressure vessel

required.

Prestressing the bore by wire-winding was considered next, as it obviates accurately machining interferences. However, it is not suitable for the small bore container required as the spring steel normally used in this process would be greatly weakened by the bending involved in winding on a small diameter.

For all the designs considered in detail, a diameter ratio of 15 was chosen as this produces a cylinder which is not excessively large but has an adequate safety factor on burst. With designs containing tool steel inner components it is difficult to assess the burst pressure accurately as the inner member is likely to fail with low tensile hoop stress in the bore. However, this is not likely to result in catastrophic failure of the outer members as pressure would be lost by leakage and, in any case, with an overall diameter ratio of 15, the burst pressure of the outer member would be over 22 kbar. Further, with the present design, any fragments of liner which were ejected parallel with the longitudinal axis would be shrouded by the low pressure intensifiers. This type of design should therefore be safe.

2.3.22 Thick-Walled Liner with One Support Ring

The first design which was considered in detail consisted of a thick-walled tool steel liner supported by an autofrettaged cylinder of EN30B. After consideration of different geometries the optimum was found to be a diameter ratio of 3 for the liner and 5 for the support ring. Detailed stress calculations and the assumptions inherent in these are given in Appendix I. Fig. 2.15 shows the radial, hoop and shear stresses in the cylinder, both residual and under load.

As can be seen from Fig. 2.15 this design is limited to 23 kbar. This is because the inner cylinder must be stressed so that the liner is

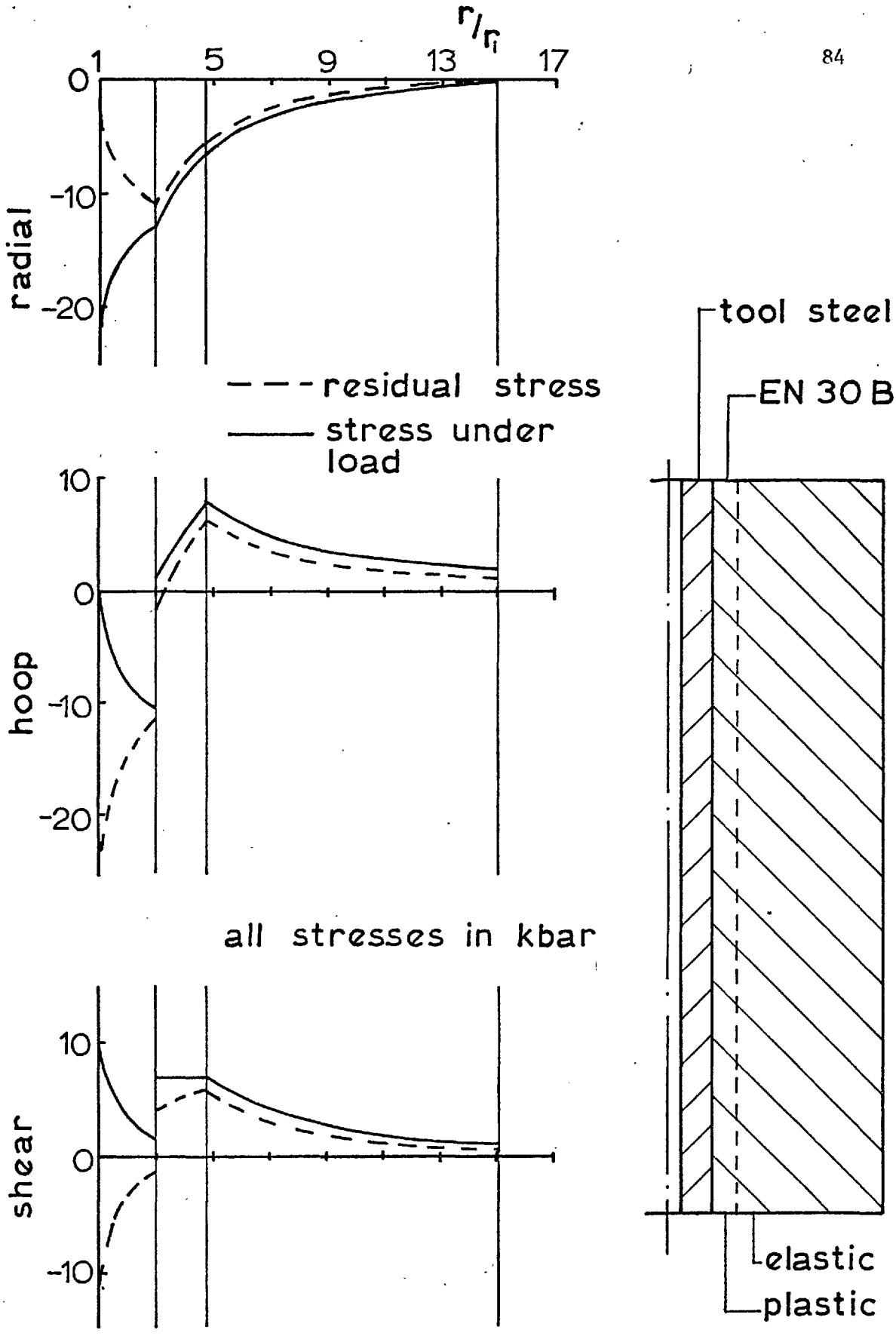

Fig. 2.15. Stresses in first cylinder design.

always in hoop compression and the outer cylinder could not be autofrettaged to withstand a higher pressure as it would go into reversed yield. This design was rejected as it would not cover the full pressure range required and also because of practical difficulties in autofrettaging the support ring.

2.3.23 Elastic Multi-Component Design

The next design considered was one in which all the components remain elastic. Designing for 30 kbar, a diameter ratio of 15 and so that diametral interference is less than 0.006 cm/cm results in a design consisting of four rings. The inner two rings would be made of a high speed tool steel, A.I.S.I. specification M2 (Jessop-Saville J34) while the outer two cylinders would be of EN30B (Jessop-Saville G.1. Special).

Again detailed stress calculations are given in Appendix I but the stress distribution is shown in Fig. 2.16. The tensile hoop stress in the inner two members is limited to 3 kbar. This should be satisfactory as the second cylinder would have to withstand greater tensile hoop stress during assembly.

It can also be seen from Fig. 2.16 that the outer cylinders are not solid but split up into sleeves or rings. This construction has two advantages. The first is that it is easier to manufacture; indeed the first support cylinder could not be ground on its internal diameter, if it were in one piece, as the length to diameter ratio would be too great. Secondly, the force required to assemble the cylinder by push fit is reduced by this method. The largest capacity press easily available for the assembly of the vessel was of 2.99 meganewtons (300 tons). Although not important here, with larger vessels thick-walled cylinders which would be eliminated because of ruling section considerations could be manufactured in rings.

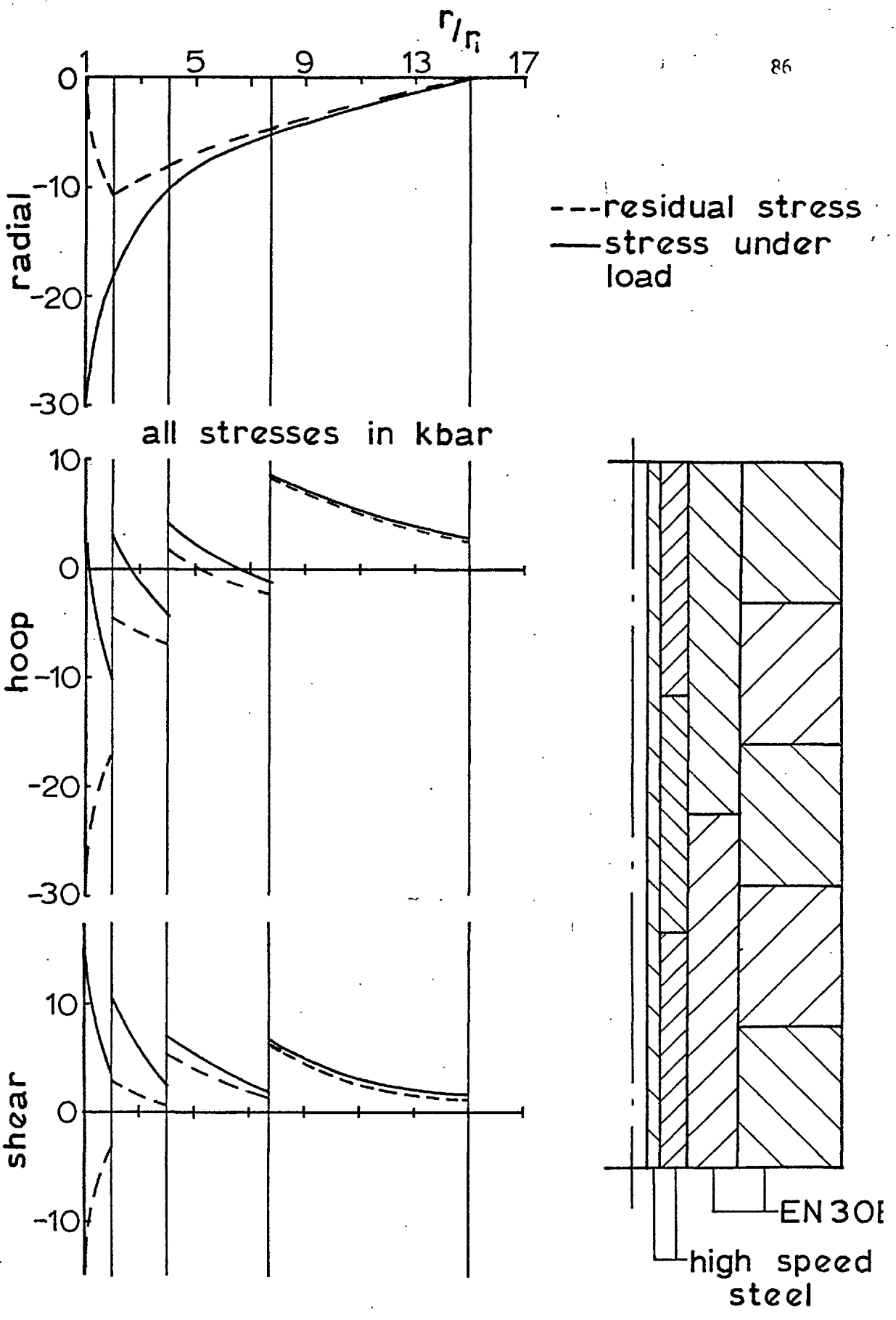

Fig. 2.16. Stresses in second cylinder design.

The major difficulty in designing pressure vessels of this type is in calculating the interferences which should be used when assembling the vessel. Free state interferences, that is the difference in hoop strains between components when the vessel is assembled, can easily be calculated from

$$\delta = \frac{1}{E_2}(\sigma_{\theta_{2i}} - \sigma_{r_{2i}}.\nu_2) - \frac{1}{E}(\sigma_{\theta_{10}} - \sigma_{r_{10}}.\nu_1) \qquad 2.2$$

Subscripts 1 and 2 refer to the number of the ring while subscripts i and 0 refer to bore and outside diameter respectively. It should be noted that the residual stresses must be used in this formula if the two rings have different elastic constants.

Becker and Mollick (154) have shown that for two cylinders of the same materials, assembled with interference, this interference is not changed by the application of internal or external pressure. When a composite vessel is made from materials with different elastic constants, however, the interference is changed by pressure as shown in Appendix II. This must be taken into account when calculating the actual interferences used during assembly. Becker and Mollick have also shown that the strain at the outside diameter of a subassembly must be added to the free state interference when assembling a further component to give the correct interface pressures.

The procedure which must be followed in calculating the interferences used during assembly is given below for the vessel described previously, with the two inner members of one material and the two outer members of a different material.

1. The stresses under load are calculated and from these the residual stresses, taking into account the change of interference at the interface between two different materials.

2. The free state interferences are calculated from equation 2.2.

3. The inner members are ground and assembled with the free state interference as they are of the same material. Application of external pressure will not alter the interference, therefore.

4. Pressure at the interface between these two members is calculated, and the strain this will cause at the external radius, ε_{20}.

5. When the fourth cylinder is assembled over the other three, the interface pressure must equal the residual radial pressure. As shown in Appendix II, this pressure causes a change of the relative interference by, say, ε_c at the interface between the second and third cylinders.

6. The external diameter of the subassembly and the internal diameter of the third cylinder is now ground to give a relative interference of the free state value + ε_{20} + ε_c.

7. The interface pressure between the second and third cylinders and the strain this causes at the external diameter, ε_{30}, is calculated.

8. Finally, the outside diameter of the subassembly and the inside diameter of the fourth ring are ground with the free state interference + ε_{30} and assembled.

This procedure was started but unfortunately, during assembly, the tensile hoop stress in the second cylinder proved to be too great. It has been calculated to be 6.6 kbar and as the high speed steel used had good fracture toughness when used in forged bar form, it was thought it would be able to withstand this stress. Also, this is far below the ultimate tensile stress for this steel, quoted by the manufacturers as being of the order of 15 kbar. Difficulties had been encountered in heat treatment, however, and the sleeve had to be heat treated twice. This could have resulted in grain growth with consequent reduction in tensile strength.

2.3.24 Plastic Liner with Elastic Support Cylinders

The cylinder which fractured, in the design above, could have been replaced by one of maraging steel, with only slight reduction of working pressure, but it was decided instead to use a different type of design. In this the two outer cylinders, as manufactured for the previous design in the form of sleeves and rings, would be used with a thick-walled liner of maraging steel. They would be assembled with an interference sufficient simply to hold them together. Thus the design is similar to a monobloc vessel but it has two important advantages. Firstly, the cost is less than for a monobloc vessel of the same size made from maraging steel, in spite of the fact that it is more complicated to manufacture. Secondly, when it fails only the liner need be replaced and not the whole vessel.

As stated in section 2.3.21 the vessel will go into reversed yield at the bore if it is autofrettaged to 30 kbar. An approximate stress distribution for an internal pressure of 30 kbar and the residual stress after releasing this pressure is given in Fig. 2.17. This was calculated on the following assumptions: the Tresca yield criterion applies, the deformations are small and do not affect the geometry, the material is perfectly plastic with a constant yield stress and no Bauschinger effect exists. While these assumptions introduce unknown errors, the calculations show that the plastic region is confined to the liner and that reversed yield occurs to a depth of 0.61 cm approximately.

The burst pressure was calculated on the method given by Manning (155). This is a numerical method of evaluating the stress and strain history of a thick-walled cylinder of work-hardening material on the von Mises criterion. The method proceeds by assuming a bore strain and calculating the pressure necessary to cause this by numerical integration. If a large number of bore strains are considered, it is found there is a

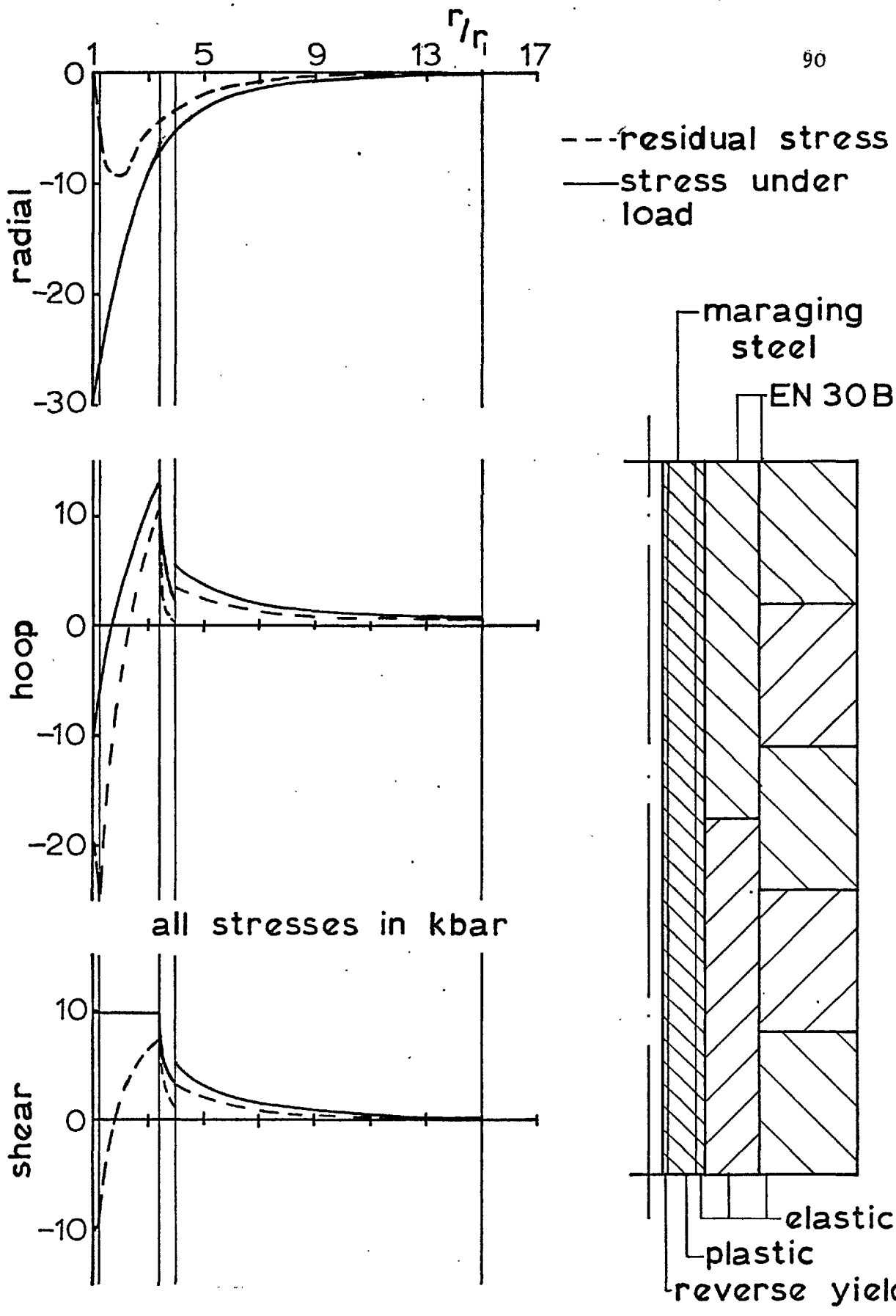

Fig. 2.17. Stresses in final cylinder design.

maximum in the pressure-bore strain curve and this is taken as the burst pressure. Calculated in this way, the burst pressure for the compound cylinder is 40.2 kbar.

2.3.3 Low Pressure Apparatus

As two high pressure plungers, 1, 2, Fig. 2.14, had to be used, this necessitated mounting a low pressure cylinder, 3, 4, Fig. 2.14, on each end of the high pressure vessel. The low pressure pistons, 5, 6, had a diameter of 13.1 cms, giving an area ratio between the low and high pressure sides of 31. Thus, allowing for seal friction, the low pressure side had to be designed for a pressure of just over 1 kbar.

The most convenient method, in this situation, of producing this pressure was to use an air-hydro pump. Air pressure can then be set to a certain value and the pump delivers fluid until it is in the stalled condition. If there is a slight leak in the low pressure side the pump will hold pressure and keep it constant. As the pressure vessel must be able to rotate, flexible hose was first considered to connect the pump to the intensifer. However, it would be difficult to arrange for the vessel to rotate continuously, in one direction, with flexible hose so this was abandoned in favour of the system shown in Fig. 2.14.

Stub axles, 7, 8, inserted in a strap, 9, are used with self-aligning roller bearings in plummer blocks to mount the high pressure assembly on trunnions. One of these stub axles, 7, is also used with a pressure connector, 10, for the transmission of low pressure fluid. The load on the pressure connector is transferred to the stub axle, via a thrust bearing, 11.

The low pressure cylinders are held in position, and located on the outer diameter of the vessel, by two clamps and rods, which are in turn connected to the strap which holds the pressure vessel. These are simply to take the weight of the low pressure cylinders during assembly. The end

force produced by the cylinders is taken by end plates and six tie bars. To ensure that both low pressure cylinders remain in contact with the pressure vessel, and also to obviate pretensioning the tie bars, a tensioning piston, 12, is included. This is of slightly larger diameter than the low pressure pistons so the tension in the tie bars is always greater than the end force.

Heaters are provided around the vessel and controlled by a 'Variac' variable transformer. These enable the temperature of the vessel to be raised to about 100°C.

2.3.4 Turning and Locking Mechanism

Inversion of the pressure vessel and low pressure intensifier assembly to start the fall of the sinker is carried out by means of an air motor. This drives, via a triple reduction gear box, chain and sprockets, onto one of the stub axles. The motor and reduction gear box are a Globe RM 100BG/372 assembly.

A pneumatic circuit diagram of the control system is given in Fig. 2.18.

The speed of the air motor is controlled by a modular spool valve, operated by a cam. The exhaust from the motor is fed to the inlet of the valve and the cam operates it, selecting either of two exhausts, both fitted with muffler valves. By choking down the exhaust, the speed of the motor can be reduced. With this system the starting torque is limited by reducing the acceleration from rest. After rotation through 20°, the cam allows the valve to operate and the assembly accelerates to the higher speed setting. When the assembly is within 20° of the vertical, the valve is again operated, selecting the slower speed, thus ensuring minimum inertia loading on the detent locking mechanism as it operates. The detent is a roller mounted on the end of a piston which slides in a DU bush.

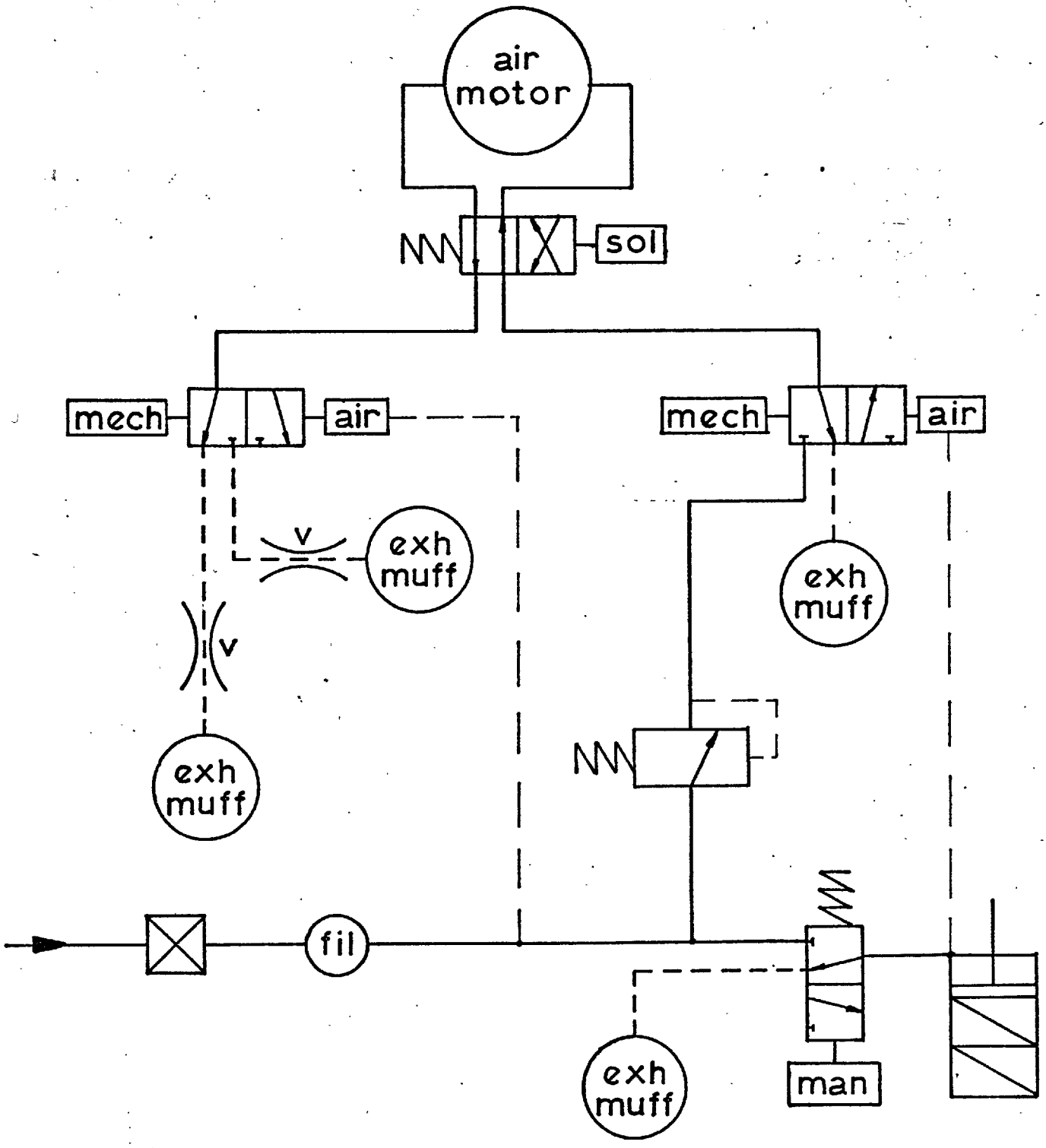

Fig. 2.18. Pneumatic circuit for the turning and locking mechanism.

While it would be possible to simply stall the motor by the detent, this is not desirable as the mechanism would be under load all the time and would have to withdraw under load. A second spool valve is therefore used to switch off the air supply to the motor. This could not be operated by a cam, as it would not then be possible to start the motor for the next revolution. A spring loaded ball mechanism, shown in Fig. 2.19, was therefore used, operating a roller valve with air pilot return. This valve is operated in conjunction with an air cylinder which withdraws the detent locking the vessel vertical.

When a button, midget spool valve is depressed, air is supplied to the cylinder, withdrawing the detent, and to the pilot side of the motor on-off valve. The spool of this valve moves, against the spring, and connects the air supply to the motor. This rotates the vessel with speed controlled, as described above. On releasing the operating valve the detent is extended by a spring but the motor valve remains in the 'on' position until the ball comes round and switches it to the 'off' position. Meanwhile the detent has operated and locked the vessel vertical. Thus, after depressing the button valve to start rotation, the system operates automatically.

As described in section 2.2.2, the viscometer must be rotated in different directions to select different sinkers for fall. The air motor has two ports and simply changing over inlet and exhaust reverses the direction of rotation. In the present system this changeover is carried out by a solenoid operated, five way, modular spool valve. Inlet is to the centre port on the three port side, while the other two ports are connected together and to the single port of the speed control valve. The two motor ports are connected to the two port side on the direction control valve. By operating the solenoid, rotation in either direction can be selected.

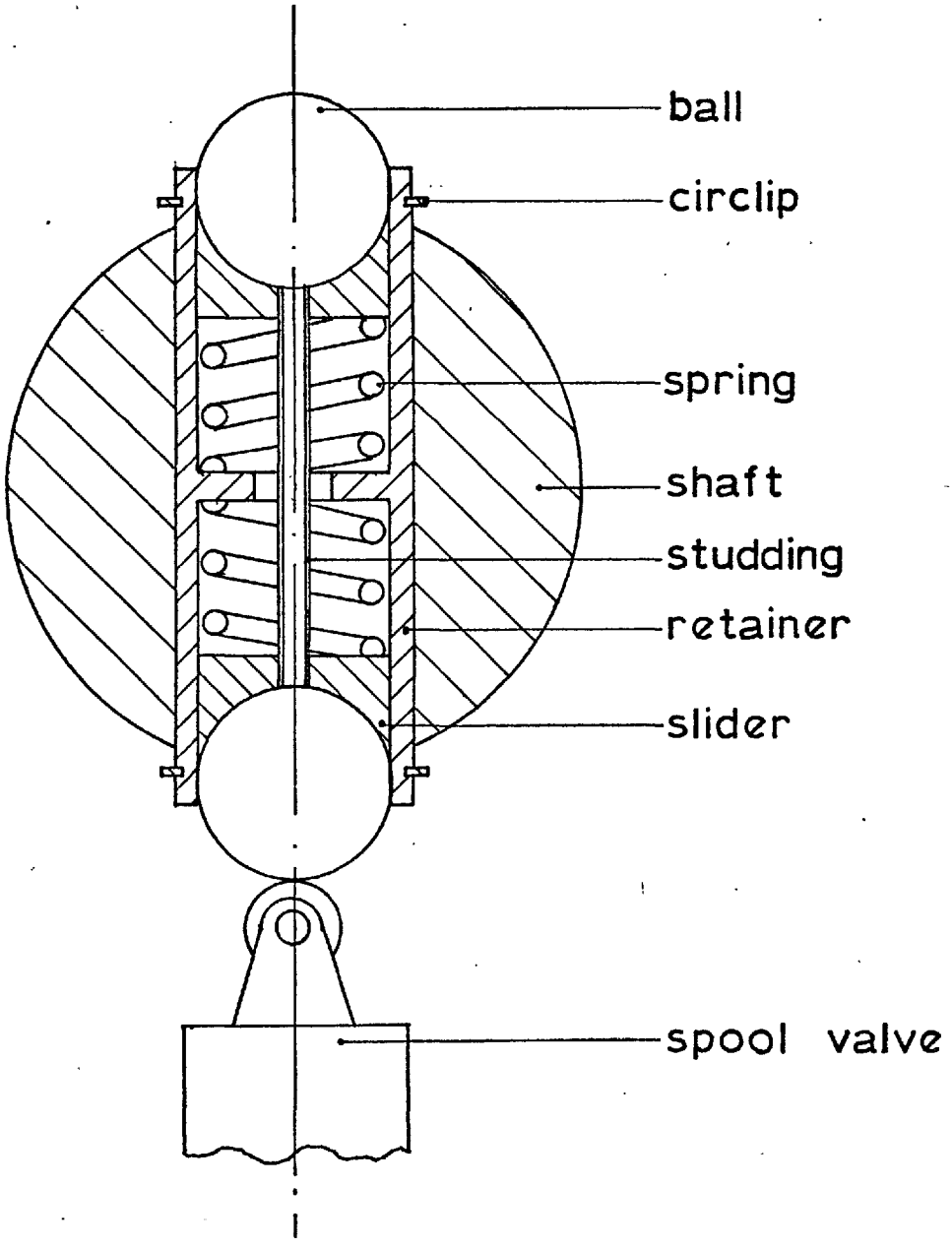

Fig. 2.19. Motor cut-off mechanism.

2.3.5 Electrical Leads

The method of taking leads from a high pressure environment which has found most use is that of a steel terminal insulated by a conical, ceramic insert. Unfortunately this method could not be used here as nine leads must be taken out of the vessel. Even if both pistons were used, it would still be necessary to have five leads through one punch and this would not be possible in a system expected to withstand 30 kbar.

A method suggested by Chandler (156) was first tried. This involves coating copper wires with an Araldite Lacquer and then cementing them in slots in a cone which is, in turn, cemented into a matching conical hole in the punch. There are a number of disadvantages, however; namely, painting the wire with lacquer is time consuming as each coat must be dried in an oven, the slots in the cone are difficult to machine accurately, the cone must be lapped into its seat and the final product has a limited fatigue life.

Another system, shown in Fig. 2.20 was therefore tried. It consists of a metal cone, for instance of silver steel, which is first coated with some compressible solid. Wires are then laid over the cone and coating is again applied until the outside surface is even. The assembly is then inserted in the conical hole in the plunger and held in place until the final coat is set.

For the first test P.V.C. was used as the elastic medium. It was dissolved in tetrahydrafuran and simply painted on with a brush. The wire used was piano wire, about 0.015 cm diameter, and thickness of P.V.C. was about 0.3 cm. The cone was about 2 cm long. This system worked well with Shell Tellus 27 as the fluid up to a pressure of 8 kbar. However, with a mixture of petrol and Univis as the fluid the initial seal was lost. Used with another elastic medium which makes a good bond with the metal this method should be satisfactory. It has the advantage of being very

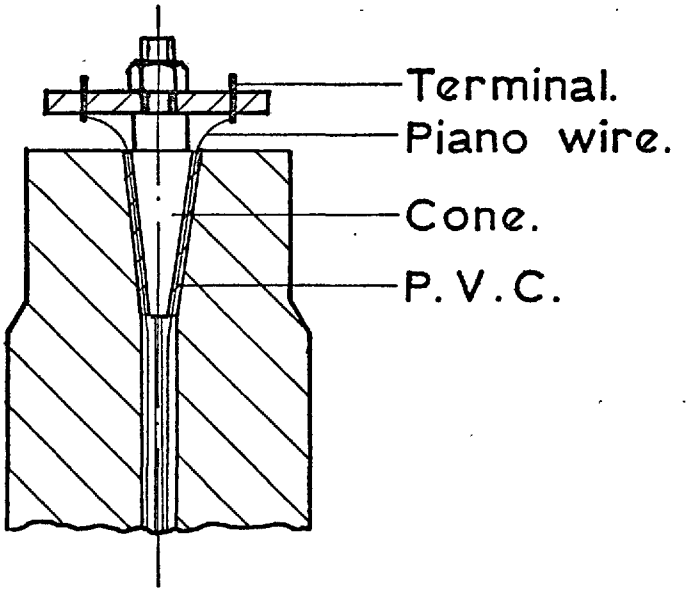

Fig. 2.20. New lead system.

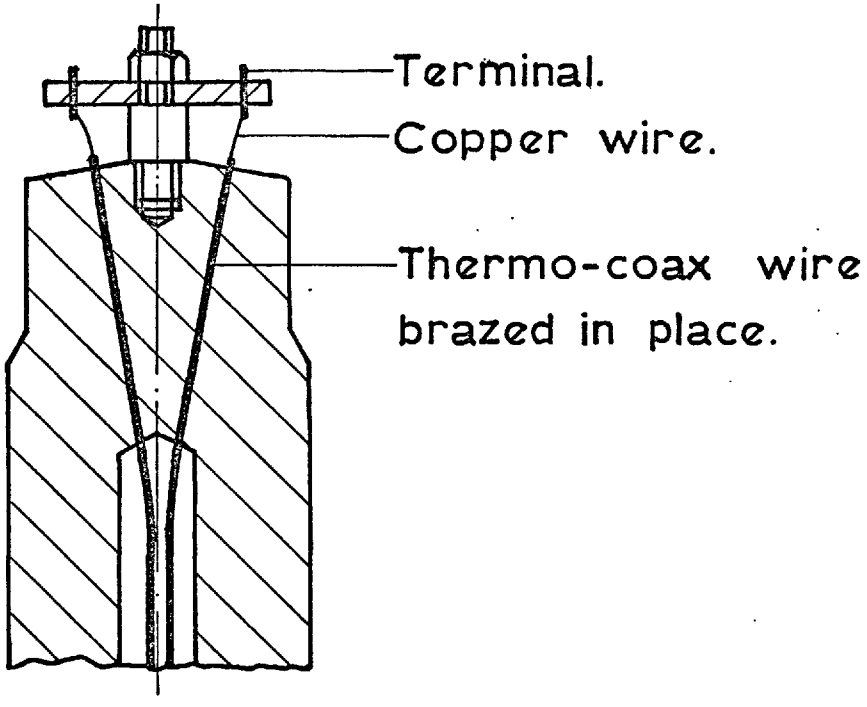

Fig. 2.21. Thermo-coax lead system.

easy to make and assemble as the exact cone angle and the surface finish of the cone and hole are not important.

In the end, the method detailed in Fig. 2.21 was used. While this method is much more difficult to manufacture then the previous one, it was thought to be more robust. Here, thermo-coax wires manufactured by Pye Unicam are vacuum brazed into holes in the punch using Johnson-Matthey Orobraze 950. This braze was chosen as it melts at 950°C and so the vacuum brazing could be carried out while the punch, of KEA180, was being hardened at 1040°C.

Two types of thermo-coax wires were used. Both had an 18/8 stainless steel sheath and magnesium oxide ceramic insulator. One of the types had two conductors one of chromel and one of alumel and the other had a single copper conductor with a very thin coating of stainless steel. Only one wire of the former type was used to form a thermocouple for temperature measurement. Seven wires of the other kind were inserted, two for the manganin coil and five for the viscometer. These wires have a thin stainless steel sheath to prevent migration of copper atoms into the ceramic during the brazing process; otherwise the insulation resistance would be reduced.

Holes to receive the wires were drilled 2.6 cm long with a clearance of 0.01 cm on the sheath to allow the braze to run. In fact, it did not penetrate the full length and it was not possible to find exactly how far it had penetrated. Later experience has shown that the braze will penetrate a hole 1.3 cm long and that this is sufficient to seal to at least 16 kbar. Higher pressures could not be generated in this test with the apparatus used.

2.3.6 Temperature Measurement

Temperature was measured by simply connecting the thermocouple, described in the previous section, to a Comark 'electronic thermometer'. The

calibration of this was checked at 0°C and 100°C, which completely covers the range of interest in these experiments. The temperature could be read to ±0.2°C by this method. This would have to be improved for more accurate work.

Ambient temperature was measured by a mercury-in-glass thermometer. The electronic thermometer contains a cold junction and the facility to correct for changes of ambient temperature.

2.3.7 Pressure Measurement

The change of resistance of a manganin coil is measured to monitor the change of pressure. A coil of 100 ohms of 42 S.W.G. diamel coated, manganin wire was wound and loosely tied to prevent it unwinding. After this the coil was stress relieved by heating to 140°C and holding for 10 hrs. This treatment was recommended by the manufacturers, Johnson-Matthey, who state that this is sufficient to stabilise the resistance without low temperature treatment.

As with all secondary gauges, the manganin coil must be calibrated by subjecting it to a known pressure and measuring the resistance of the coil. For the present purposes, an Harwood dead-weight tester, type DWT-1000, was used as the primary reference standard. This is of the controlled clearance type where the fall time of a piston, loaded with an accurately known weight, can be altered by altering the clearance between it and the cylinder with an external pressure on the cylinder.

Firstly, the piston itself must be calibrated with the fluid to be used. This is done by measuring the time for the piston to fall 0.25 cm at three different measured pressures and several different jacket (outside) pressures. For each measured pressure the jacket pressure is plotted against $1/\sqrt{[\text{Fall Time}]^3}$, this scale giving a straight line plot. By extrapolating back, the stall jacket pressure, that is the jacket

pressure to give an infinite fall time, can be found. Thus the stall curve of jacket pressure against measured pressure can be plotted.

The coil can now be calibrated by inserting it in the measured pressure side of the deadweight tester. The resistance is measured while the piston is falling with the jacket pressure not more than 0.3 kbar (4000 psi) below that to cause stall at that pressure. Pressure on the coil can then be calculated to 0.01% by accounting for the change in size of the piston due to temperature, measured and jacket pressure effects, air buoyancy on the weights and fluid buoyancy on the piston, the hydrostatic head between the coil and the piston and also the difference in gravity between Walpole, Massachussets, where the weights were measured, and Imperial College.

Of course, to justify this accuracy the resistance change must be measured to greater accuracy than 0.01% and great care must be taken to ensure that soldered joints, leads and insulation do not cause variations in resistance. In the present case the same leads and lengths of thermocoax were used in calibration as in use in the viscometry apparatus. Further the leads were first soldered together in the vessel and their resistance measured as they were subjected to a pressure of 12 kbar. No resistance change could be detected.

Resistance was measured by a Croprico Precision Wheatstone Bridge, manufactured by Croydon Precision Instrument Co. The accuracy claimed for the bridge was 0.01% on 100 ohms. In fact the bridge was calibrated in the electrical standards laboratory at Imperial College and found to be accurate to the limit of reading, or 0.001%, in the range 100 to 105 ohms at $20^{\circ}C$.

The major difficulty involved in the calibration was that of changes of ambient temperature. A change of temperature of $1^{\circ}C$ causes a change of resistance equivalent to a change of pressure of 0.043 kbar, at ambient pressure for the manganin used here. Unfortunately, the temperature

coefficient will change with pressure and using the value given above as a correction introduces an unknown error. Further calibration at different temperatures was not justified for the preliminary viscosity measurements to be described here as the temperature could neither be measured nor controlled with great accuracy in the present experiments.

As the upper limit of the deadweight tester described above is 15 kbar it would also be necessary to use one other point, such as the phase transition of bismuth at 22 kbar as a check on the extrapolated calibration in this region. For the present experiments the coil was calibrated at 25°C and pressures from 0 to 12 kbar. The graph of resistance change against pressure was found to be straight, within the accuracy of measurement, and so is not included here.

CHAPTER 3. THEORETICAL CONSIDERATIONS

3.1 Visioplasticity Approach

3.1.1 Introduction

The visioplasticity method was first suggested by Thomsen et al. (37,38,157) and the basis of the method described in section 1.1.3. As the numerical differentiations and integrations inherent in the method are extremely time consuming, if carried out by hand, the method lay in abeyance until the advent of digital computers.

The difficulties which are involved in computer application have been discussed by Shabaik et al. (39,40,158). They follow from the fact that when calculations are carried out by hand and a smooth curve is passed through the calculated velocities before strain rates are calculated, the results of the analysis are automatically smoothed. When the computations are carried out on a computer, the errors in reading the flow lines and in the numerical fitting methods can cause the higher order difference quotients to be both large and erratically varying. The methods of dealing with this problem and others which arise when applying visioplasticity to hydrostatic extrusion, will be described in sections 3.1.3 to 3.1.7, along with the program used.

Listings of the routines mentioned in these sections are given in Appendix III.

3.1.2 Visioplasticity Theory

As is usually the case in problems of large plastic deformation the elastic strains are ignored throughout the analysis and the material is assumed rigid-work hardening.

The method takes as its starting point flow lines which are defined by a steady state experiment. For each line a flow function is specified,

from the conditions in the rigid region, as

$$\psi_{\ell} = \pi R_{\ell}^2 |V_b| \tag{3.1}$$

This function is now constant along each line through the deformation region.

From the flow function, the axial and radial velocities, U and V respectively, are defined, as follows,

$$U = -\frac{1}{2\pi R} \cdot \frac{\partial \psi}{\partial R} \tag{3.2}$$

$$V = \frac{1}{2\pi R} \cdot \frac{\partial \psi}{\partial Z} \tag{3.3}$$

In turn, the strain rates are calculated from the velocity field according to the equations

$$\dot{\varepsilon}_{RR} = \frac{\partial V}{\partial R} \tag{3.4}$$

$$\dot{\varepsilon}_{\theta\theta} = \frac{V}{R} \tag{3.5}$$

$$\dot{\varepsilon}_{ZZ} = \frac{\partial U}{\partial Z} \tag{3.6}$$

$$\dot{\varepsilon}_{RZ} = \frac{\partial V}{\partial Z} + \frac{\partial U}{\partial R} \tag{3.7}$$

Assuming the flow to be incompressible, we have

$$\dot{\varepsilon}_{RR} + \dot{\varepsilon}_{\theta\theta} + \dot{\varepsilon}_{ZZ} = 0 \tag{3.8}$$

This condition is automatically satisfied by the system of equations 3.4, 3.5 and 3.6 with 3.2 and 3.3, viz.

$$\frac{\partial V}{\partial R} + \frac{V}{R} + \frac{\partial U}{\partial Z} =$$

$$\frac{\partial}{\partial R}\left(\frac{1}{2\pi R} \cdot \frac{\partial \psi}{\partial Z}\right) + \frac{1}{2\pi R^2} \cdot \frac{\partial \psi}{\partial Z} - \frac{\partial}{\partial Z}\left(\frac{1}{2\pi R} \cdot \frac{\partial \psi}{\partial R}\right) =$$

$$-\frac{1}{R^2} \cdot \frac{\partial \psi}{\partial Z} + \frac{1}{R}\frac{\partial^2 \psi}{\partial R \partial Z} + \frac{1}{R^2} \cdot \frac{\partial \psi}{\partial Z} - \frac{1}{R} \cdot \frac{\partial^2 \psi}{\partial R \partial Z} = 0$$

Once the values of the strain rates have been calculated in the three coordinate directions, along with the only non-zero shear strain rate, $\dot{\epsilon}_{RZ}$, the mean effective strain rate can be calculated from

$$\dot{\bar{\epsilon}} = \frac{1}{3}\sqrt{\left[2\left((\dot{\epsilon}_{ZZ} - \dot{\epsilon}_{RR})^2 + (\dot{\epsilon}_{RR} - \dot{\epsilon}_{\theta\theta})^2 + (\dot{\epsilon}_{\theta\theta} - \dot{\epsilon}_{ZZ})^2\right) + 3\dot{\epsilon}_{RZ}\right]} \qquad 3.9$$

Total strain values are next found by integrating the effective strain rate, with respect to time, along each flow line

$$\bar{\epsilon} = \int_0^{t_{\ell K}} \dot{\bar{\epsilon}}\, dt \qquad 3.10$$

The strain rate and total strain fields are now known for the whole deformation zone and can be used with the equilibrium equation, a constitutive equation and a yield criterion and associated flow rule to give the stress field.

The equations are as follows:-

$$\frac{\partial \sigma_{RR}}{\partial R} + \frac{\partial \sigma_{RZ}}{\partial Z} + \frac{\sigma_{RR} - \sigma_{\theta\theta}}{R} = 0 \qquad 3.11$$

$$\frac{\partial \sigma_{RZ}}{\partial R} + \frac{\partial \sigma_{ZZ}}{\partial Z} + \frac{\sigma_{RZ}}{R} = 0 \qquad 3.12$$

Yield Criterion and Flow Rule

$$\bar{\sigma}^2 = \frac{1}{2}\left[(\sigma_{RR} - \sigma_{\theta\theta})^2 + (\sigma_{\theta\theta} - \sigma_{ZZ})^2 + (\sigma_{ZZ} - \sigma_{RR})^2\right] + 3\sigma_{RZ}^2 \qquad 3.13$$

$$\dot{\lambda} = \frac{\dot{\epsilon}_{RR}}{\sigma_{RR} + p} = \frac{\dot{\epsilon}_{\theta\theta}}{\sigma_{\theta\theta} + p} = \frac{\dot{\epsilon}_{ZZ}}{\sigma_{ZZ} + p} = \frac{\dot{\epsilon}_{RZ}}{2\sigma_{RZ}} = \frac{3}{2}\frac{\dot{\bar{\epsilon}}}{\bar{\sigma}} \qquad 3.14$$

where $$p = -\frac{1}{3}(\sigma_{RR} + \sigma_{\theta\theta} + \sigma_{ZZ}) \qquad 3.15$$

Constitutive Equation

$$\bar{\sigma} = \bar{\sigma}(\bar{\epsilon}, \dot{\bar{\epsilon}}, T) \qquad 3.16$$

From eq's 3.14

$$\dot{\epsilon}_{RR} = \dot{\lambda}(\sigma_{RR} + p)$$

$$\dot{\epsilon}_{\theta\theta} = \dot{\lambda}(\sigma_{\theta\theta} + p)$$

$$\dot{\epsilon}_{ZZ} = \dot{\lambda}(\sigma_{ZZ} + p)$$

$$\therefore \quad \sigma_{RR} = \sigma_{ZZ} + \frac{\dot{\epsilon}_{RR} - \dot{\epsilon}_{ZZ}}{\dot{\lambda}} \qquad 3.17$$

$$\sigma_{\theta\theta} = \sigma_{ZZ} + \frac{\dot{\epsilon}_{\theta\theta} - \dot{\epsilon}_{ZZ}}{\dot{\lambda}} \qquad 3.18$$

Equation 3.12 can be integrated with respect to Z, to give the variation of σ_{ZZ} with Z for a constant value of R.

$$\sigma_{ZZ}(R,Z) = \int_{Z}^{a} \left[\frac{\partial}{\partial R} \left(\frac{\dot{\varepsilon}_{RZ}}{2\lambda} \right) + \frac{\dot{\varepsilon}_{RZ}}{2R\lambda} \right] dZ + \sigma_{ZZ}(R,a) \qquad 3.19$$

The variation of σ_{ZZ} with R must now be found by rearranging eq. 3.11 and integrating with respect to R, as follows

$$\frac{\partial}{\partial R} \left[\sigma_{ZZ} + \frac{\dot{\varepsilon}_{RR} - \dot{\varepsilon}_{ZZ}}{\lambda} \right] + \frac{\partial}{\partial Z} \left(\frac{\dot{\varepsilon}_{RZ}}{\lambda} \right) + \frac{\dot{\varepsilon}_{RR} - \dot{\varepsilon}_{\theta\theta}}{R\lambda} = 0$$

$$\sigma_{ZZ}(R,a) = \int_{0}^{R} \left[\frac{\partial}{\partial R} \left(\frac{\dot{\varepsilon}_{ZZ} - \dot{\varepsilon}_{RR}}{\lambda} \right) - \frac{\partial}{\partial Z} \left(\frac{\dot{\varepsilon}_{RZ}}{2\lambda} \right) - \frac{\dot{\varepsilon}_{RR} - \dot{\varepsilon}_{\theta\theta}}{R\lambda} \right]_{Z=a} dR$$

$$+ \sigma_{ZZ}(0,a) \qquad 3.20$$

Combining eqs. 3.19 and 3.20 gives

$$\sigma_{ZZ}(R,Z) = \int_{Z}^{a} \left[\frac{\partial}{\partial R} \left(\frac{\dot{\varepsilon}_{RZ}}{2\lambda} \right) + \frac{\dot{\varepsilon}_{RZ}}{2R\lambda} \right] dZ + \int_{0}^{R} \left[\frac{\partial}{\partial R} \left(\frac{\dot{\varepsilon}_{ZZ} - \dot{\varepsilon}_{RR}}{\lambda} \right) - \right.$$

$$\left. \frac{\partial}{\partial Z} \left(\frac{\dot{\varepsilon}_{RZ}}{2\lambda} \right) - \frac{\dot{\varepsilon}_{RR} - \dot{\varepsilon}_{\theta\theta}}{R\lambda} \right]_{Z=a} dR + \sigma_{ZZ}(0,a) \qquad 3.21$$

The constant $\sigma_{ZZ}(0,a)$ can be found as the integral of σ_{ZZ} over the exit from the deformation region must be equal to the applied drawing force, in this instance.

3.1.3 The Flow Function

Values of the function are found in the zone before deformation starts from eq. 3.1. This defines the function along each flow line. However, to carry out the numerical differentiations, the flow function must be evaluated at mesh points, which cover the field of deformation, by a numerical procedure which is now described.

3.1.31 Mesh for Computer Calculations

Previous applications of the visioplasticity method have used rectangular or square meshes for the calculations. This is standard procedure as the difference quotients, estimating the differentials, can be calculated using standard formulae. A number of difficulties are involved if the die half angle is much less than 45^{o}, which is usually the case in hydrostatic extrusion. Here, the choice of a rectangular mesh, such that mesh points lie on the die-workpiece interface, produces greater step length in the axial than in the radial direction. While this problem could easily be solved by decreasing the step length in the axial direction by a factor of 2 or 3 and not having the maximum radius at each section on the bounding flow line, there are still other problems.

In hydrostatic extrusion, it is well known that deformation can start before the billet reaches the die, by the build up of pressure due to the 'viscosity pump' effect. If the present method is to be successful in predicting the surface conditions then this effect cannot be overruled by enforcing a sharp change of slope on the surface of the billet at contact with the die. This is especially true if the conditions are favourable for the build up of hydrodynamic lubrication over the die surface.

Further, if the step length in the radial direction is chosen to give a reasonable number of steps in the billet, it is not usually possible to arrange for one of the mesh points to correspond with the product surface.

This is desirable as, in the stress program, the load on the exit deformation section must be equal to the drawing force. Thus the stress must be calculated up to the product surface to allow integration to find the drawing load.

For these reasons it was decided that a mesh with constant step length in the axial direction but variable step length in the radial direction would be used. This type of mesh is shown in Fig. 3.1. Input data to the program gives the number of mesh points in the radial direction both in the billet and the product. A mesh is then chosen with equal spacing up to the product diameter. After this radius has been reached another step length is chosen so that the mesh continues, with equal spacing, until the radius corresponds to the billet radius. The mesh is stopped if the radius at any K section exceeds that of the bounding flow line. The radius is then set equal to this value and the corresponding I value stored in an array IMAX.

One further array is used to characterise the mesh. This is the array KMIN, in which the minimum K value is stored, for each I section, for which R(I,K) = R(I, K + 1). The radial and axial coordinates of each mesh point (I,K) are stored in two arrays, R(I,K) and Z(I,K).

3.1.32 Subroutine XREAD

The calculations to give the four arrays R, Z,IMAX and KMIN, which define the mesh, can only be carried out after the input data has been transformed so that the radius of each flow line is known at each K section.

Data is first read in by XREAD giving material stress-strain points, pressure-viscosity data for the fluid used and the extrusion parameters, die angle, pressure,temperature and drawing stress. The coordinates of 20 to 25 points along each flow line are read in and are transformed by

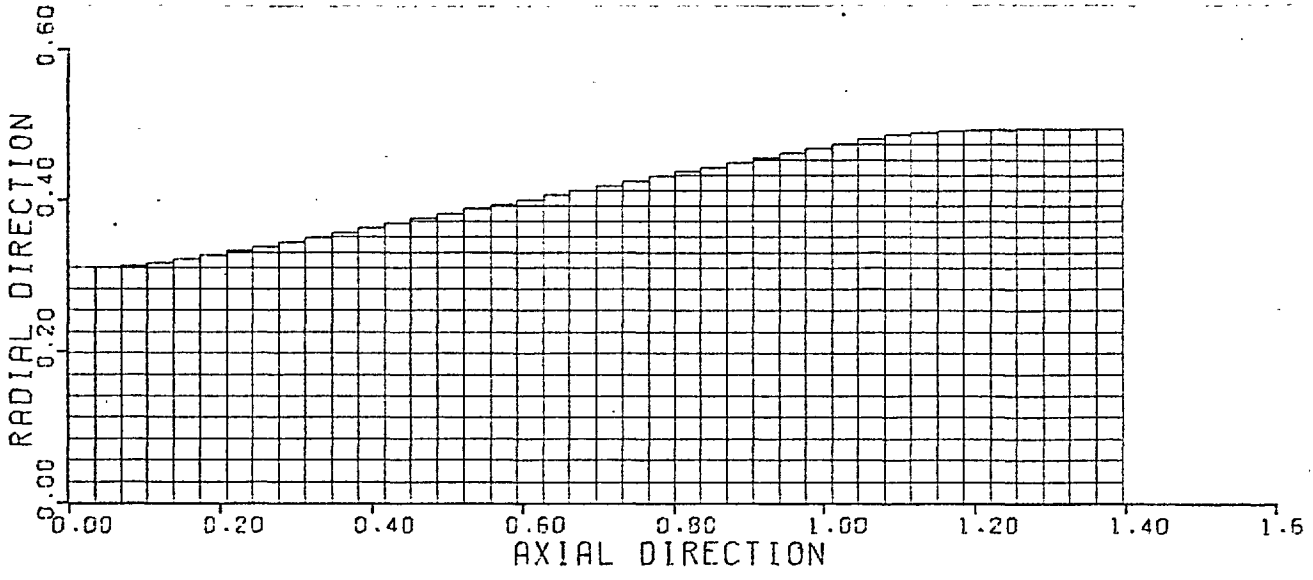

Fig. 3.1. Mesh for computations.

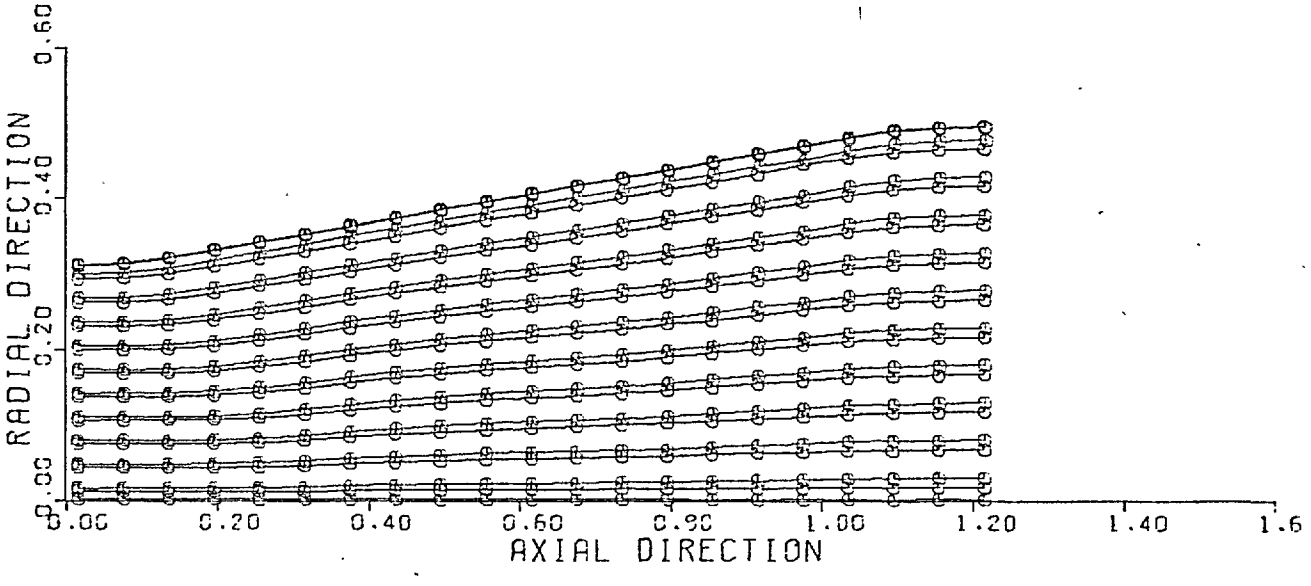

Fig. 3.2. Input data.

the equations

$$CR1(L,J) = |(CR(L,J)-RREF)\cos\theta - (ZREF-CZ(L,J))\sin\theta|$$

$$CZ1(L,J) = (ZREF-CZ(L,J))\cos\theta + (CR(L,J)-RREF)\sin\theta$$

so that the origin is then in the plane where deformation ends and so that all radial values are positive. Here, θ is the angle between the axis of the billet and the axis of the measuring machine when the co-ordinates were read. This transformation amounts to transferring all flow lines to one side of the axis. A computer plot of the input data in this form is given in Fig. 3.2.

The points are then sorted so that the lowest value of N in CZ(L,N) and CR(L,N) corresponds to the lowest value of CZ(L,N) and the lowest value of L is associated with the lowest value of CR(L,N).

Further data can be fed in giving the axial values at which deformation starts and stops for each flow line. This is transformed and sorted as above.

3.1.33 Subroutine MESH

Firstly, the radius of each flow line at each K section RPSI(L,K) must be found from the input data. The K sections are chosen so that the plane K = 2 coincides with the end of deformation and so that the step length is

$$XKDIV = 2(DBIL - DPROD)/3NK \tan\alpha.$$

Two different methods of finding the values of RPSI were tried. The first was to use linear interpolation and the second was to use a polynomial least mean squares fit to the experimental data. This was carried out by means of a library subroutine POLYFT. After some trials it was

found that a 10th order polynomial worked satisfactorily. None of the features of the lines were lost and there was no tendency to give a high frequency ripple to the line.

The flow lines were then smoothed using either the method of fives or the method of means. In the former method the smoothed value of RPSI(L,K) is estimated by (RPSI(L,K-2) + RPSI(L,K-1) + RPSI(L,K) + RPSI(L,K+1) + RPSI(L,K+2))/5. This method is rather severe, however, so the method of means, shown in Fig.3.3 was used instead. Smoothing the flow lines once in this way produced no measurable difference in the velocity and strain rates calculated later but it did make the total strain results smoother, as these were found by integration along each flow line. Using the two different methods of finding RPSI only produced changes of 0.5% in the effective strain and no changes in the shape of any curves. The polynomial fitting method was therefore used throughout, for the sake of consistency, although it was not markedly better. The flow lines tracked in this way are shown in Fig. 3.4 and can be compared with Fig. 3.2.

Once these calculations have been made the mesh coordinates, as described in section 3.1.21, can be found. The subroutine MESH also calls DLINE to find the slope of each line at each section.

3.1.34 Subroutine FLOW

At each K section, the value of the flow function is now known at the radii at which each line crosses that section. It must now be found at each mesh point defined by R(I,K), Z(I,K). To do this, three methods were tried, linear interpolation, polynomial interpolation and polynomial least mean squares curve fitting.

Linear interpolation was unsatisfactory as it could not adequately follow the curve in the region near the centre of the billet. If the

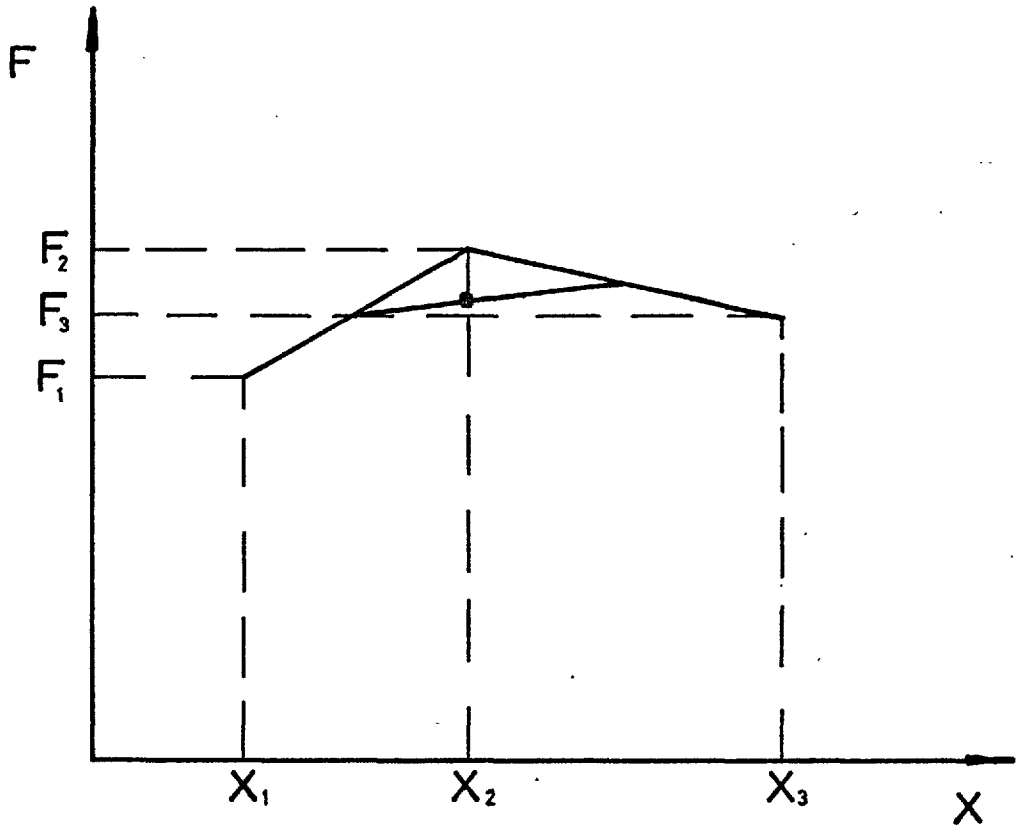

Smoothed value of F_2 is

$$\frac{F_1 + F_2}{2} + \left(\frac{F_3 - F_1}{2}\right)\left(\frac{X_2 - X_1}{2}\right) \Big/ \left(\frac{X_3 - X_1}{2}\right)$$

Fig. 3.3. Smoothing by method of means.

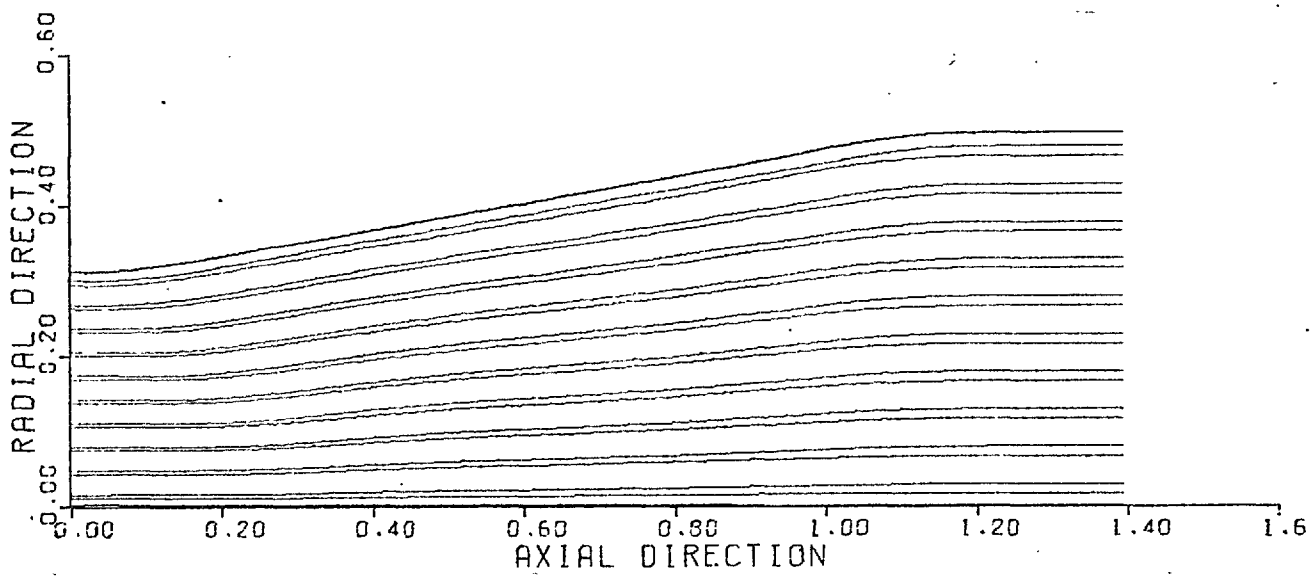

Fig. 3.4. Tracked flow lines.

billet were deforming uniformly, that is with plane sections remaining plane, then the curve of flow function against radius would be a quadratic. The change of slope is therefore greatest near the centre of the billet and linear interpolation consistently overestimates values here.

A second method, using a polynomial fit, with variable order of polynomial, was therefore tried in subroutine PPFIT. This worked satisfactorily in the majority of cases. However, when two lines were very close together, as sometimes occurs due to the method of transferring the lines to one side of the centre line, very large errors were produced. Quadratic and fourth order polynomials, requiring 3 or 5 points respectively, were tried and the problem arose in both cases.

The final method was to use a polynomial least squares fit again. For use in the radial direction it was found that a polynomial of the type

$$\psi = C_1 + C_2R^2 + C_3R^4 + C_4R^6 + C_5R^8$$

was most suitable. As the library routine could only deal with polynomials in which all the coefficients are defined a further routine, POLFYT, was written. The theory on which the coefficients are defined is given in Appendix IV. The linear simultaneous equations which are formulated are solved using the library subroutine SIMQ, which uses the matrix pivotal method of solution. This method was used throughout to define the flow function, CPSI(I,K), at each mesh point.

3.1.4 Smoothing Procedure

To ensure that the difference quotient estimates of the differentials are smooth, the flow function is smoothed and checked along the boundaries, where its value is known. While it would be simpler to smooth the velocities and then the strain rates, as they are calculated, this method could

not ensure that the compressibility condition is satisfied. The alternative procedure of building up a smooth flow function from a smoothed set of differences is therefore adopted.

3.1.41 Subroutine SMOTH

This subroutine firstly defines the zone in which deformation takes place. The input data has been read in, sorted and smoothed in XREAD. This data is obtained by estimating where the flow lines deviate from straight lines in the billet and product, either on the specimen itself under the microscope or on an enlarged plot of the data produced by the computer. The data is smoothed and a polynomial, in this case of order 5, is fitted. From this the value of Z, and hence of K, at which deformation starts and stops is found and stored in two arrays KB and KE. If no data is fed in then KB is set equal to (NK-2) and KE is set equal to 3.

In the regions where the material is rigid the flow function is known to be

$$\psi = \pi.R(I,K)^2.|VBIL| \qquad \text{before deformation}$$

and $$\psi = \pi.R(I,K)^2.|VPROD| \qquad \text{after deformation.}$$

The value of CPSI at the point immediately outside the deformation zone is compared with the correct value. If any error is found it is distributed linearly in the Z direction.

3.1.42 Subroutine SMOTHZ

The purpose of this routine is to smooth the differentials with respect to Z. As has been shown, the radial velocity depends on the difference quotient of the flow function with respect to Z. With the present coordinate system, this velocity must always be negative as it is

in the opposite direction to the radial coordinate, assuming there is no outward flow. After calling the routine which estimates the differentials DIFZ, the routine CHEC is called which ensures the differentials are all negative. The differentials are then smoothed twice in both the radial and axial directions by AVZ and AVR using the method of means described previously.

The flow function is then built up from the smoothed differentials using subroutine INGZAT. End values must be checked and then an error function is defined by subtracting the smoothed values from the original values. This is itself smoothed and added to the final values to bring them closer to the initial values.

Finally, the flow function is checked to ensure it is monotonically decreasing in the positive Z direction for constant values of R.

3.1.43 Subroutine SMOTHR

Unlike in the Z direction, in the R direction the second difference with respect to R is smoothed. For constant velocity flow at any section the second differential is a constant, whereas the first is not. Thus, if the smoothing is carried out on the second differential it is less likely to produce changes in the overall flow pattern, as its slope will be smaller than that of the first differential. The second differential can also be used to check that the axial velocity nowhere exceeds velocity at exit.

The second difference is smoothed by AVR, the condition of maximum axial velocity at exit is checked and then smoothing is again applied in the R and Z directions. Finally, the third differential is formed and smoothed in the R direction. The flow function is then built up from these smoothed differentials, using subroutine INGRAT, and its value at the surface is checked.

3.1.44 Subroutine STSM

Another, different type of smoothing was also attempted as an alternative to using routines SMOTHZ and SMOTHR. In this the strain rate in the radial direction was formed in the normal way, to be described in section 3.1.51, and then smoothed in the R and Z directions. From these smoothed values, new radial velocity and flow fields were built up by integration.

The strain rate in the Z direction was then formed and smoothed, as above, and integrated with respect to Z to give the axial velocity field. This was in turn integrated to give the flow field. Similarly, the differentials of the axial velocity with respect to R and the radial velocity with respect to Z were smoothed to give smooth values of the shear strain rate.

After smoothing in this way, the error function was formed as described in section 3.1.42, smoothed, and added to CPSI to bring it closer to the original values.

3.1.5 Calculation of Velocities and Strain Rates

From the flow function defined by experiment and the foregoing numerical procedure, the velocities at each mesh point can be calculated by eqs. 3.2 and 3.3. The strain rates are then evaluated, according to eqs. 3.4, 3.5, 3.6 and 3.7.

3.1.51 Subroutine STRATE

Difference quotient approximations to the differentials in equations 3.2 and 3.3 are calculated by subroutines DIFZ and DIFR by fitting a polynomial to 3 points, the point in question and one on either side. At the boundaries 2 points on one side must be used for the approximation.

Along the centre line, where R(1,K) = 0, the radial velocity is set to zero and the axial velocity is approximated by fitting a quadratic to points U(2,K) and U(3,K) such that the slope of U with respect to R is zero at the centre line. The equation used is

$$U(1,K) = (4U(2,K) - U(3,K))/3$$

Strain rates can now be calculated directly from the velocity field by forming the difference quotients as defined in the equations given above. Along the centre line

$$\dot{\varepsilon}_{\theta\theta} = \frac{\partial V}{\partial R} = \dot{\varepsilon}_{RR}$$

3.1.52 Subroutines DIFZ and DIFR

These routines were written in general form so that a polynomial could be fitted to any number of points to find the difference quotient. This method was used so the mesh could be defined with varying step length. The linear, simultaneous equations defining the coefficients of the polynomial were set up by routine FIT and solved by SIMQ.

Difficulties arose near the surface where, because of the mesh used, two points could be very close together. In this case, the point on the boundary streamline, at R(IMAX,K) and the points at R(IMAX-2,K), R(IMAX-3,K) and so on, as necessary, are used, the point at R(IMAX-1,K) being ignored. This method resulted in smoother difference quotients at the surface.

3.1.6 Equivalent Total Strain

3.1.61 Equivalent Strain Rate

The equivalent strain rate is calculated at each mesh point directly from its definition in eq. 3.9.

By linear interpolation, the value of equivalent strain rate on each flow line, at each K section, can be found. At the same time, the axial component of velocity at each section, UF(L,K),is also found for each flow line.

3.1.62 Total Equivalent Strain

From the axial component of velocity, UF(L,K), the time taken to reach each K section, along each flow line, can be found from

$$TIME(L,K) = TIME(L,K+1) + 2(Z(1,K+1) - Z(1,K)) / (UF(L,K+1) + UF(L,K))$$

The time is taken as zero at section NK.

Total effective strain along each line is now calculated from eq. 3.10. Finally, the total effective strain at each mesh point is calculated from values on the flow lines by linear interpolation.

3.1.7 Stresses

From the calculations detailed above the strain rate and total strain fields are known for the whole deformation zone. This can be used with the equilibrium equation, a constitutive equation and a yield criterion and associated flow rule to give the stress field, as described in section 3.1.2.

3.1.71 Subroutine STRESS

Firstly, if the deformation zone has not been specified as input data, it is formed here. The cut off points are arbitrary and chosen to give smooth boundaries, without altering their shape. Deformation is assumed to have started when the total effective strain is greater than

0.005 and to have ended when the effective strain rate is less than 0.01 sec^{-1}, these parameters being used for convenience in the program.

Next, the value of the equivalent stress is found from the equivalent strain, using the constitutive equation, by calling subroutine PROP. For the present experiments, which were carried out at slow speed, the change of flow stress with temperature and strain rate was not taken into account as it would have been negligible. Thus only the quasi-static stress-strain curve was needed as input data.

Variation of σ_{ZZ} in the R direction was found at a point just inside the deformation zone using eq. 3.20. The constant was assumed to be zero. From eq. 3.21 the variation of σ_{ZZ} from the reference point can be built up numerically. The actual values are then found by adjusting the calculated values so that the integral of σ_{ZZ} at the end of deformation is equal to the drawing force.

Once σ_{ZZ} is known throughout the deformation zone, σ_{RR} and $\sigma_{\theta\theta}$ can be calculated directly from eq.'s 3.17 and 3.18. The shear stress, σ_{RZ}, can also be calculated directly from eq. 3.14.

3.2 Surface Conditions

3.2.1 Normal and Shear Stresses on Boundary

The normal and shear stresses can be found from σ_{ZZ}, σ_{RR} and σ_{RZ}, calculated by the visioplasticity analysis, by the following transformation equations

$$\sigma_N = \sigma_{RR}\cos^2\alpha + \sigma_{ZZ}\sin^2\alpha - 2\sigma_{RZ}\sin\alpha.\cos\alpha \qquad 3.22$$

and

$$\sigma_S = \sigma_{RZ}(\cos^2\alpha - \sin^2\alpha) + (\sigma_{RR} - \sigma_{ZZ})\ \sin\alpha.\cos\alpha \qquad 3.23$$

Eq. 3.22 was given incorrectly by Shabaik and Thomsen (42) as

$$\sigma_N = \sigma_{ZZ}\cos^2\alpha + \sigma_{RR}\sin^2\alpha - 2\sigma_{RZ}\ \sin\alpha.\cos\alpha$$

In the present work, α cannot simply be taken as the die half-angle as deformation can start before the billet contacts the die due to hydrodynamic effects. The angle is therefore calculated from the velocity components, by

$$\alpha_K = \tan^{-1} (V(IM,K) / U(IM,K)) \qquad 3.24$$

where IM denotes the maximum I value at the section K.

From these two values, the local coefficient of friction can be defined simply as

$$\mu = \left| \frac{\sigma_S}{\sigma_N} \right| \qquad 3.25$$

3.2.2 Hydrodynamic Lubrication

In calculations to find the film thickness if hydrodynamic lubrication is assumed to be operative, the coordinate system shown in Fig. 3.5 is used.

The pressure build up in the film is governed by the equation

$$\frac{\partial p}{\partial x} = \eta \frac{\partial^2 U_f}{\partial y^2} \qquad 3.26$$

Two assumptions are now made: namely, that the pressure, p, and the viscosity, η, do not vary in the y direction. The former cannot be far from the truth, as the film is so thin. However, at high speeds where full film lubrication is most likely there will be large temperature differences between the deforming workpiece and the die, due to the heat generated during deformation. As viscosity is extremely sensitive to changes of temperature, considerable change is possible, even across the very thin film.

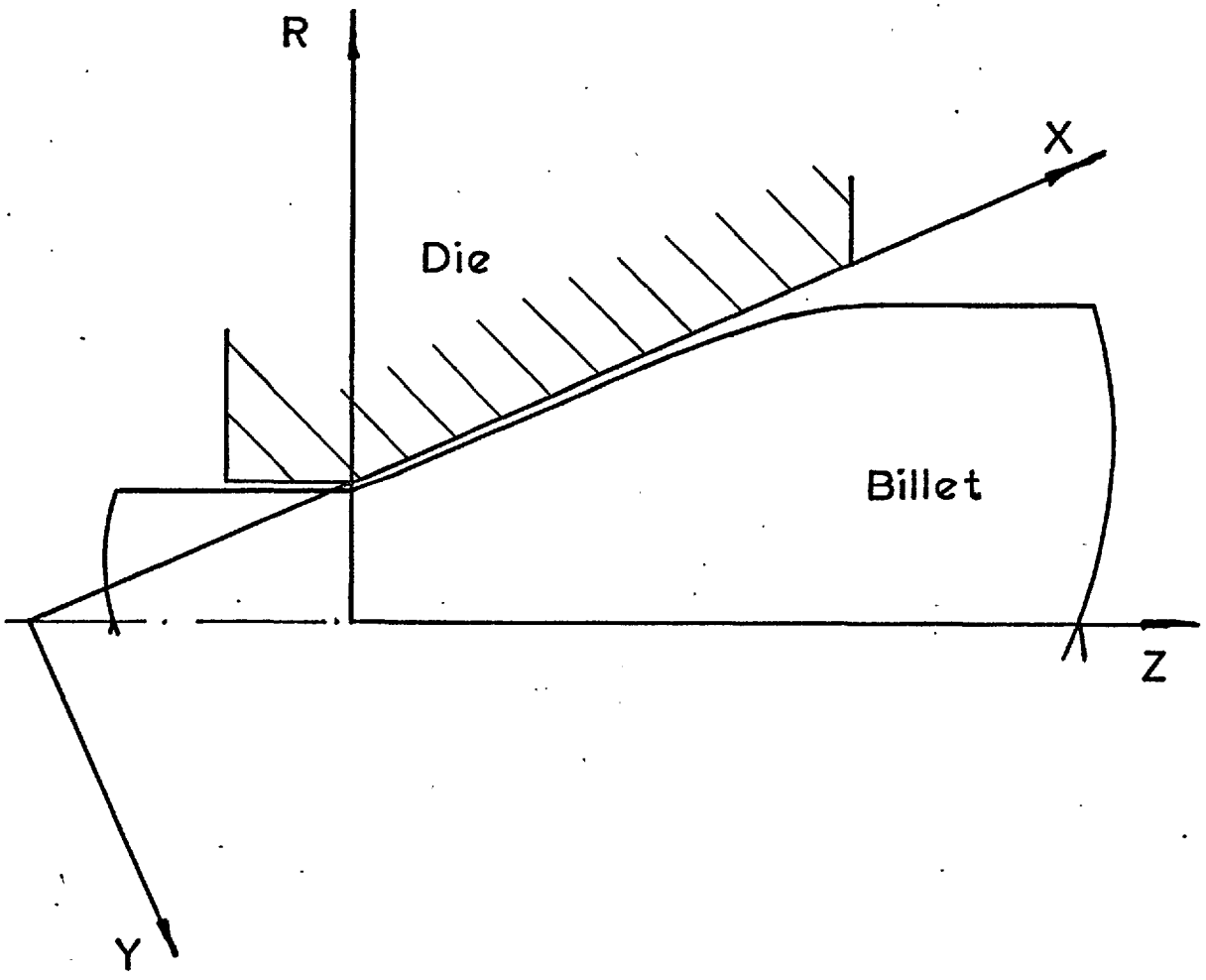

R,Z - coordinates for visioplasticity analysis.

X,Y - coordinates for fluid film analysis.

Fig.3.5. Coordinate system for hydrodynamic analysis.

In the present experiments, however, the speeds which can be achieved will be low. It is, therefore, acceptable to make the assumption of constant viscosity in the y direction in checking for hydrodynamic lubrication.

Integrating eq. 3.26, we get

$$\frac{\partial U_f}{\partial y} = \frac{1}{\eta} \frac{dp}{dx} \cdot y + C_1$$

$$U_f = \frac{1}{2\eta} \frac{dp}{dx} \cdot y^2 + C_1 y + C_2 \qquad 3.27$$

The boundary conditions are $U_f = 0$ when $y = 0$ and $U_f = U_S(x)$ when $y = h(x)$. Hence

$$U_f = \frac{y^2 - yh}{2\eta} \cdot \frac{dp}{dx} + U_S \frac{y}{h} \qquad 3.28$$

From the visioplasticity program, the shear stress along the surface of the workpiece is known as a function of x and can be calculated as in the previous section but in this case the angle is taken as the die half angle. This shear stress is related to the viscous shear in the fluid by

$$\tau = \eta \left(\frac{\partial U_f}{\partial y} \right)_{y=h} \qquad 3.29$$

From 3.28 and 3. 29

$$\tau = \eta \frac{U_S}{h} + \frac{h}{2} \frac{dp}{dx} \qquad 3.30$$

Rearranging and solving for h

$$h = \frac{\tau \pm \sqrt{\left[\tau^2 - 2\eta U_S \left(\frac{dp}{dx}\right)\right]}}{\frac{dp}{dx}} \qquad 3.31$$

All the quantities on the right hand side of eq. 3.31 can be found from the visioplasticity program with the exception of the viscosity. As viscosity is very sensitive to changes of pressure, a pressure-viscosity curve is fed in for the temperature of extrusion. The viscosity can then be found at each value of x from the known pressure. These calculations are carried out in subroutine SURF.

A further check that Reynold's equation is satisfied can be made by calculating the mass flow, $\dot{m}$, at each section. This is given by

$$\dot{m} = \int_0^h \rho \, U_f \, dy$$

Assuming the density is constant across each section and substituting eq. 3.28 we find

$$\frac{\dot{m}}{\rho} = -\frac{h^3}{12\eta} \cdot \frac{dp}{dx} + U_S \cdot \frac{h}{2} \qquad 3.32$$

3.3 Theories of the Viscometer

3.3.1 Relationship between Viscosity and the Viscometer Parameter.

In the ideal situation, where the flow past the sinker in the falling weight viscometer could be described exactly by an analytic solution, the viscometer would be an absolute instrument. Even in this situation, the instrument would only be accurate if the tube and sinkers could be made so that they were completely symmetric. The fall of the sinker would be at steady speed, exactly on the axis of the tube, guide pins

would be unnecessary and the flow would be laminar throughout.

However, assuming that these conditions could be achieved in practice, there would still be great difficulty in measuring the dimensions of the sinker and tube with sufficient accuracy for absolute measurements. Nevertheless, it is important to have a theory to predict the variation of viscosity with the viscometer characteristics so that this can be used for correcting the fall time for changes in geometry due to changes of temperature and pressure.

The viscometer constant is found by experiment and is given in the form

$$\left.\begin{aligned} \eta &= \frac{mg}{v} \cdot k_1' \\ \text{or} \quad \eta &= mg.t^* \cdot k' \end{aligned}\right\} \qquad 3.33$$

Before calculating the viscosity from the measured fall time, t, it must be corrected for:

1. The change in density of the fluid and the sinker due to change of temperature and pressure. The correction is

$$t_1^* = t. \frac{(\rho_{sp} - \rho_{fp})}{(\rho_{so} - \rho_{fo})} \cdot \frac{\rho_{so}}{\rho_{sp}}$$

2. The change in the length over which the fall is timed due to change of length of the viscometer tube. The correction is

$$t_2^* = t_1^* . (1 + p.G)(1 - \alpha(T - T_o))$$

3. The change in geometry of the flow due to the change in dimensions of the sinker and the tube. To do this a suitable theory must be evolved

so that the viscometer constant can be evaluated for the conditions of the calibration, k_o, and for the new dimensions at temperature and pressure, k_p. The correction is

$$t^* = t_2^* \cdot \frac{k_p}{k_o}$$

This corrected value of t* can now be used in 3.33 to give the viscosity, initial values being used for the other parameters.

Several theories of the falling cylinder viscometer have been suggested in the past, but these seem, without exception, to have analysed the flow past a plain cylindrical body with flat ends. Where sinkers with different shaped ends have been used, their effect has been ignored, as has the effect of guide pins. The type of situation analysed is shown in Fig. 3.6. In the following equations the clearance, C, is $(r_T - r_A)$.

The first theory is by Lawaczeck (159). This assumed that the flow could be represented by the flow between parallel surfaces. The calculation was carried out in two steps, firstly on the simple flow between stationary parallel surfaces and, secondly, on the relative movement of the surfaces with no flow. This results in

$$\eta = \frac{mg}{2\pi \ell_A v} \cdot \frac{C^3}{(3r_A^3 + 6r_A^2 C + 4r_A C^2)} \qquad 3.34$$

In the A.S.M.E. Pressure Viscosity Report (8) an expression is given, though not derived there, as,

$$\eta = \frac{mg}{6\pi \ell_A v} \cdot \left(\frac{r_T}{r_A}\right)^2 \cdot \left(\frac{C}{r_T}\right)^3 \cdot \left\{1 - \frac{1}{2}\left(\frac{C}{r_T}\right) - \frac{13}{20}\left(\frac{C}{r_T}\right)^2 - \frac{13}{40}\left(\frac{C}{r_T}\right)^3 + \ldots\right\} \qquad 3.35$$

A further study by Scott (160) produced the equation

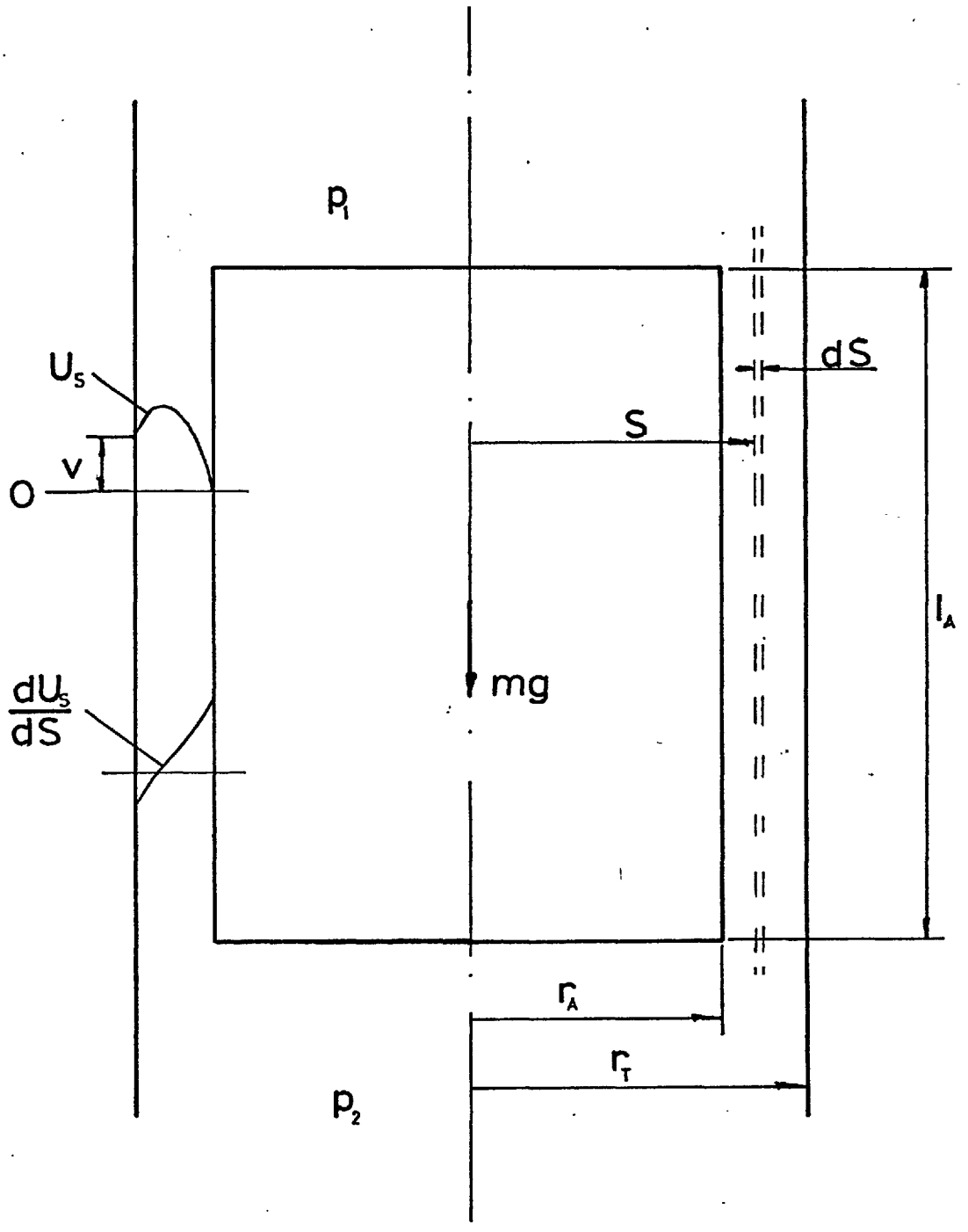

Fig.3.6. Sinker geometry used for simple theoretical analysis.

$$\eta = A(\rho_s - \rho_f)\, t^* - B.E.\, \frac{\rho_f}{t^*} \qquad 3.36$$

The constant A is given by

$$A = \frac{C^3 g}{6 \ell_T r_1 F}$$

where $$F = 1 + \frac{3C}{2r_A} + \frac{7C^2}{5r_A^2} + \frac{4C^3}{5r_A^3} + \ldots.$$

Thus the first term in eq. 3.36 is similar to eq.'s 3.34 and 3.35. The second term is a correction for the kinetic energy of the fluid leaving the annulus, which is assumed to be lost in turbulence, and for the development of flow in the annulus. The kinetic energy constant is

$$B = \frac{9 \ell_T C r_A}{280 F \ell_A} \left\{ 1 - \frac{C}{3r_A} + \frac{353}{540} \cdot \frac{C^2}{r_A^2} + \ldots \right\}$$

while that for flow development is

$$E = 1.056 \left(1 - 0.11 \frac{C}{r_A} + \ldots \right)$$

This last term is close to unity and, as Cappi (132) points out the whole of the second term is small and the dimensional changes due to change of temperature and pressure produce very little effect. Hence, its inclusion in the corrections for change of dimension is negligible.

Lohrenz and Kurata (161) in analysing the flow arrived at the equation

$$\eta = \frac{mgt^*}{2\pi \ell_A \ell_T} \cdot \left\{ \frac{(r_T^2 + r_A^2) \ln (r_T/r_A) - (r_T^2 - r_A^2)}{(r_T^2 + r_A^2)} \right\}$$

which was corrected by Cappi (132) to give

$$\eta = \frac{mgt^*}{2\pi \ell_A \ell_T} \left\{ \frac{(r_T^2 + r_A^2) \ln (r_T/r_A) - (r_T^2 - r_A^2)}{(3r_T^2 - r_A^2)} \right\} \qquad 3.37$$

He also derived the expression

$$\eta = \frac{mgt^*}{2\pi \ell_A \ell_T} \cdot \frac{C^3}{(3r_A^2 r_T + 3Cr_T^2 + 3Cr_A^2 + 4C^2 r_T)} \qquad 3.38$$

on the parallel surfaces approach and showed the difference between the two expressions was only ¼% for the range of interest.

In the present experiments, the fluids of interest are much more viscous than those in most of the studies above. Sinkers were therefore envisaged with central holes, as shown in Figs. 2.9 and 2.10. Thus, none of the theories above are applicable in this case.

In Appendix V, an expression is derived for a sinker with a central hole, on the same assumptions as for Lohrenz and Kurata's and Cappi's derivations. The final expression for the viscosity is

$$\eta = \frac{mgt^*}{2\pi \ell_A \ell_T} \left[\frac{(r_T^2 + r_A^2) \ln \frac{r_T}{r_A} - (r_T^2 - r_A^2) + \frac{\ell_A r_B^4 \ln \frac{r_T}{r_A}}{\ell_B (r_T^2 - r_A^2)}}{(3r_T^2 - r_A^2) + \frac{\ell_A r_B^4}{\ell_B (r_T^2 - r_B^2)}} \right] \qquad 3.39$$

Allowance has been made for the different lengths of the bore and the parallel portion of the annulus.

Although this theory is in error by as much as 20%, Lohrenz and Kurata have shown that theories of this type are capable of predicting changes of viscometer constant of up to 60% with an accuracy of 3%, by

comparison with experiment. As the changes in practice are much smaller than 60% this theory is perfectly adequate for correction purposes.

The more rigorous theory given in Appendix V can be used to show the flow pattern in the annulus. Referring to Fig. 3.7 the velocity distribution in the annulus is shown for a sinker with the same dimensions as the long stainless steel sinker but without the central hole and also for the long stainless and short duralumin sinkers.

The effect of the central hole in reducing the velocity gradient at the sinker surface, and thereby the shear stress on the surface, is immediately obvious. Thus the central hole is effective in reducing the fall time of the sinker without increasing the instability of the fall which occurs when large annular clearances are used. It can also be seen from Fig. 3.7 that recirculatory flow is developing for the short duralumin, which has a large bore hole.

A further advantage of sinkers with central holes is that the change of viscometer constant with pressure is much smaller when the sinker and tube are of different materials. Cappi had difficulty in getting accurate density measurements as the low density sinker he used had a correction of 22% at 15 kbar due to the change of viscometer constant. As the density measurements depend on small differences of relatively large quantities any error here is magnified.

With the present design of sinker, the corresponding correction would have been under 1%.

3.3.2 Calculation of Density

A method of determining the density of a fluid under pressure, suggested by Cappi (132), is to time the fall of two sinkers of different densities in the fluid. In the following the subscript h refers to the high density sinker, while ℓ refers to the one of low density. Subscripts o and p refer to zero and test pressure, respectively.

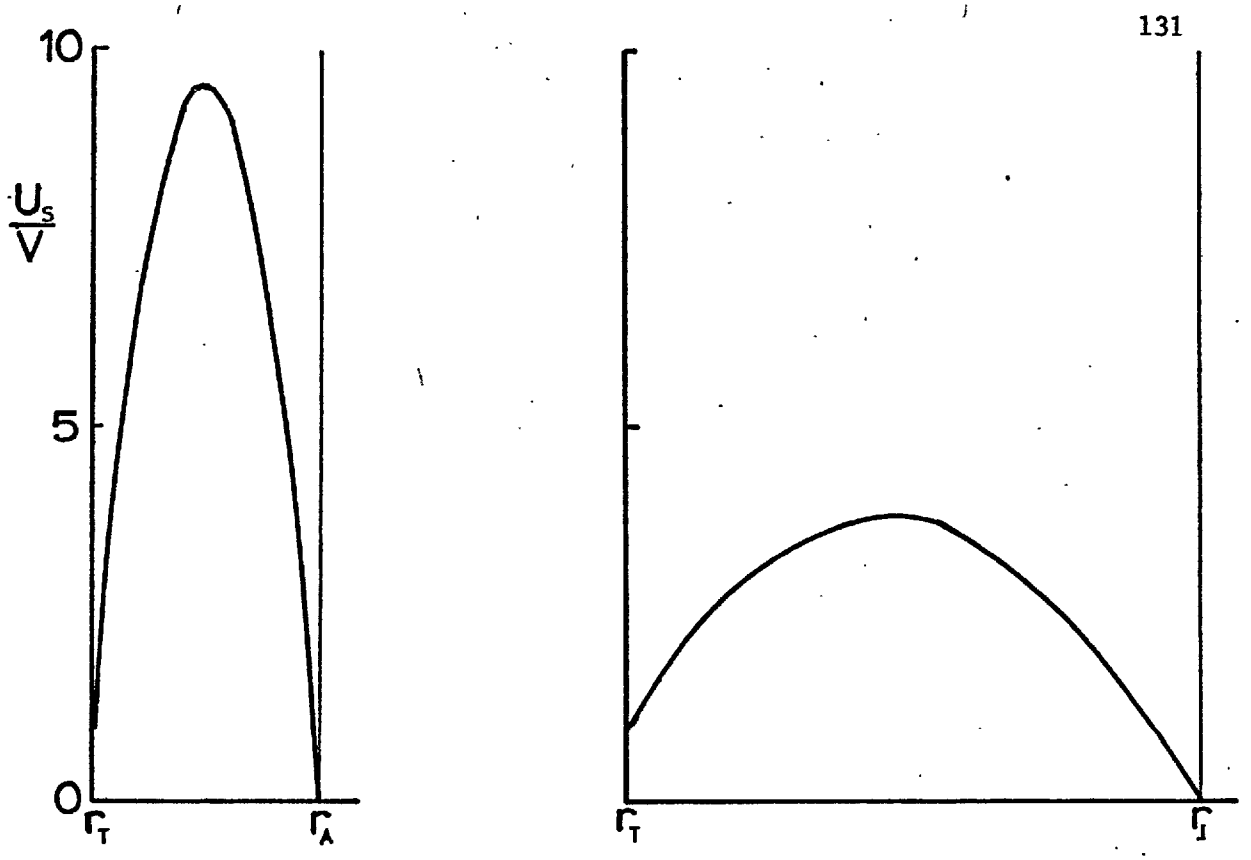

long stainless sinker
without bore hole

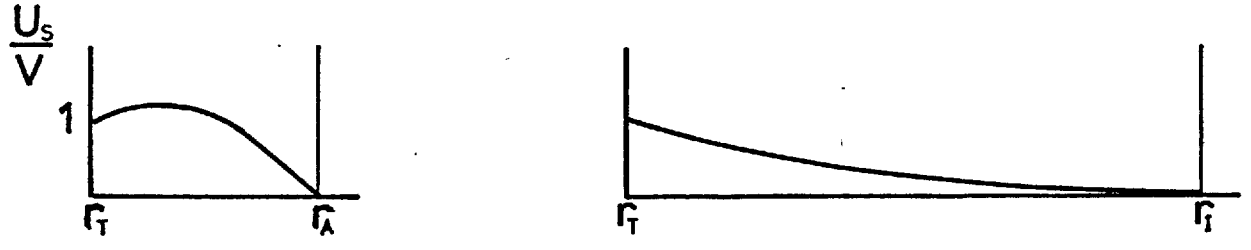

long stainless sinker

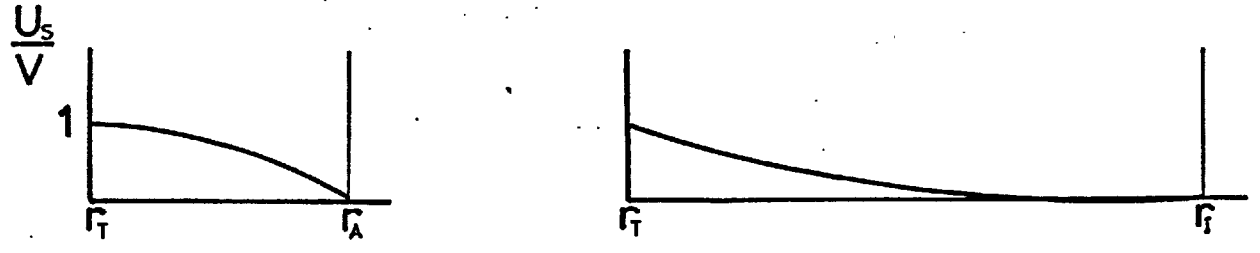

short dural sinker

Fig. 3.7. Flow patterns in the sinker annulus.

We may write

$$\eta_o = k_h\, t^*_{ho} \qquad 3.40$$

and $$\eta_o = k_\ell\, t^*_{\ell o}$$

and under pressure,

$$\eta_p = k_h\, t^*_{hp}\, \frac{(\rho_{hp} - \rho_{fp})}{(\rho_{ho} - \rho_{fo})} \cdot \frac{\rho_{ho}}{\rho_{hp}}$$

and $$\eta_p = k_\ell\, t^*_{\ell p}\, \frac{(\rho_{\ell p} - \rho_{fp})}{(\rho_{\ell o} - \rho_{fo})} \cdot \frac{\rho_{\ell o}}{\rho_{\ell p}}$$

where t^*_{hp} and $t^*_{\ell p}$ have been corrected for dimensional changes under pressure and are measured at the same temperature.

Then

$$\frac{\eta_p}{\eta_o} = \frac{t^*_{hp}}{t^*_{ho}} \cdot \frac{(\rho_{hp} - \rho_{fp})}{\rho_{hp}} \cdot C_h = \frac{t^*_{\ell p}}{t^*_{\ell o}} \cdot \frac{(\rho_{\ell p} - \ell_{fp})}{\rho_{\ell p}} \cdot C_\ell \qquad 3.41$$

where $$C_h = \frac{\rho_{ho}}{(\rho_{ho} - \rho_{fo})} \quad \text{and} \quad C_\ell = \frac{\rho_{\ell o}}{(\rho_{\ell o} - \rho_{fo})}$$

From 3.41

$$\rho_{fp} = \frac{(t^*_{\ell p}/t^*_{\ell o}) \cdot C_\ell - (t^*_{hp}/t^*_{ho}) \cdot C_h}{\left(\frac{t^*_{\ell p}}{t^*_{\ell o}}\right)\frac{C_\ell}{\rho_{\ell p}} - \left(\frac{t^*_{hp}}{t^*_{ho}}\right)\frac{C_h}{\rho_{hp}}} \qquad 3.42$$

Hence, from the atmospheric fall times and the fall times under pressure of two sinkers the density of the fluid can be calculated according to the equation above.

CHAPTER 4. EXPERIMENTAL PROCEDURE AND RESULTS

4.1 Experimental Results

4.1.1 Extrusion of Aluminium Billets

The first experiments on the extrusion-drawing apparatus were carried out with aluminium. This was of commercial, 99.9% purity, fully annealed for one hour at 350°C. Difficulties were encountered in that when the drawing force was applied the pressure reducing valve did not operate satisfactorily and pressure dropped off. As described in section 2.1.31, this pressure supply was replaced by an accumulator and from then onwards pressure was maintained satisfactorily; the pressure drop when load was applied being only around 0.1 kbar.

Other difficulties were experienced with aluminium as the extrusion material however. In the first place, the drawing stress which could be applied without fracturing the tag was very small. As the tag could not conveniently be formed by extrusion in the present apparatus, it was machined on the billet and hence was annealed along with the rest of the billet. Thus the extrusion pressure had to be carefully controlled.

A further difficulty is illustrated by Fig. 4.1. Fig. 4.1(a) shows a photograph of an extrusion of aluminium, ratio 2, die half angle 10° and fluid Shell Tellus 27, taken under oblique lighting. It can be clearly seen here that the surface of the split is no longer flat. This heterogeneous deformation is caused by the large grain size of the aluminium. Fig. 4.1(b) which shows the same billet under more direct lighting, illustrates that although the flow lines are still clearly visible, their path has, in places, been distorted by the cross flow on the meridian plane.

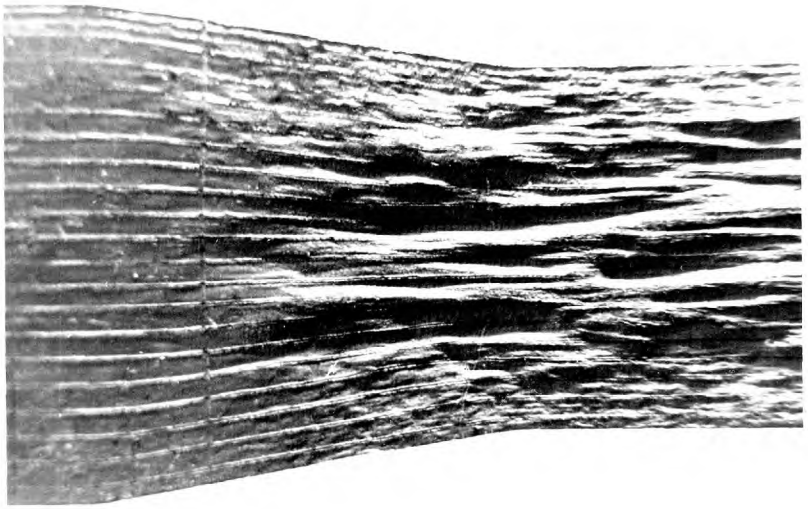

(a) under oblique lighting.

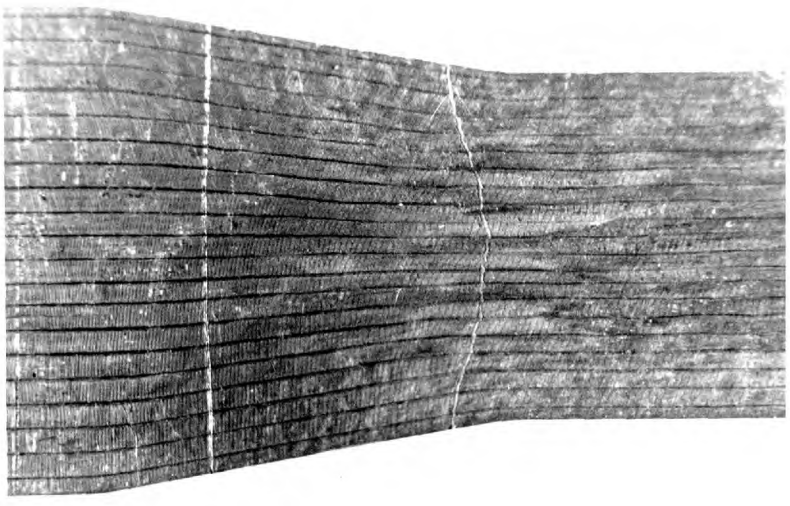

(b) under direct lighting.

Fig. 4.1. Aluminium billet.

At larger reductions, for instance 12, the mid-plane had become so heavily distorted that the grid was completely obliterated.

4.1.2 Extrusion of Copper Billets

The extrusion experiments on copper billets were limited to one geometry. This was a die half angle of 10^{o} and an extrusion ratio of 2.56. This geometry was used by Alexander and Kamyab (99) and its use here would facilitate comparison with their results for die pressure profile. Here, however, the billet size was limited to 1.27 cm in diameter whereas a billet of 2.54 cm had been used in the previous study.

The copper was electrolytic, tough pitch, high conductivity to B.S.1433 fully annealed for one hour at $600^{o}C$.

4.1.21 Experimental Procedure

Solid billets were first used to establish the extrusion pressure. Once this was known two split billets were extruded from Shell Tellus 27, two from castor oil and four from castor oil with molybdenum disulphide grease as lubricant, one of the latter group at higher speed. The experimental procedure used is given below.

1.) A split and gridded copper billet, of the type shown in Fig. 2.5, is taken, cleaned with carbon tetrachloride and then assembled in the guiding collar. The outside surface is then cleaned, by rubbing in a radial direction, with 600 grade emergy paper then degreased with carbon tetrachloride. If lubricant is to be used it is applied now.

2.) The billet is assembled into the die, which is in turn inserted into the high pressure subpress. This is filled up with a filtered sample of the extrusion fluid and time allowed for this to penetrate and fill the whole container.

3.) The high pressure subpress is next put into position, the high pressure plunger inserted and the low pressure intensifier assembled over it. The tag on the billet is connected to the pulling device.

4.) Connections are now made to the displacement transducer, load cell, thermocouple and manganin coil. The bridges are balanced and calibration marks put on the U.V. recorder paper, as necessary, with the stabilised voltage supply set at 6V.

5.) The pressure to be used during the experiment must be decided and the low pressure necessary to cause this can then be calculated. The nitrogen side of the intensifier is charged to approximately four-fifths of this pressure then oil is admitted to the other side to bring the system to the required pressure. During this procedure the low pressure intensifier is isolated by a stop valve.

6.) Next the recorder is started and pressure is admitted to the intensifier. Once the pressure has risen to the desired value the motor on the screw jack is started.

7.) Extrusion continues until the drawing head hits a stop, when the torque limiter operates, disconnecting the drive from the jack.

8.) Pressure is then released and the load removed from the jack. The recorder is left running until temperature returns to ambient so that the zero of the pressure coil can be rechecked.

9.) The rig is dismantled and the coordinates of the flow lines are measured on the universal measuring machine.

A typical U.V. recording made during this procedure is shown in Fig. 4.2. The only difficulty experienced was when a mixture of petrol and Univis was used as the extrusion fluid. This was tried as it is known to stay fluid to much higher pressures than either castor oil or Tellus 27. However, it could not be sealed successfully with the O- ring and

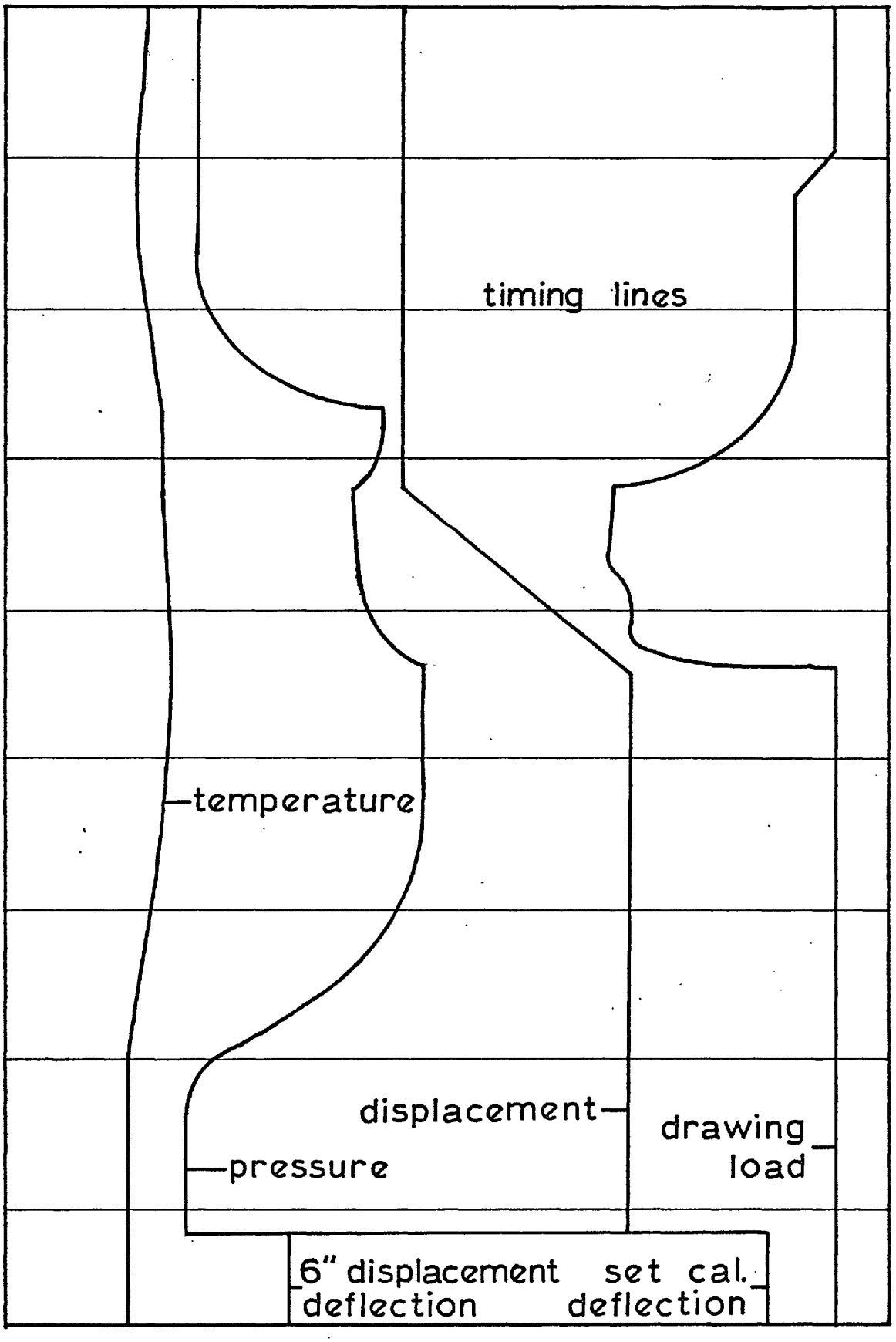

Fig.4.2. Typical U.V. recording of an extrusion experiment.

mitre ring on the high pressure plunger. On one occasion it did seal until the pressure was 4.2 kbar, and extrusion was still not taking place. This is about 20% higher than that necessary to cause extrusion with the other fluids and indicates the extremely poor lubrication properties of this fluid.

4.1.22 Measured Extrusion Pressures and Drawing Stresses

From the U.V. recordings the steady state extrusion pressure can be calculated, using the known pressure equivalent of the set calibration resistor. Also the drawing load can be read off by comparing the galvanometer deflection with the calibration graph. Product velocity is calculated from the displacement trace and temperature rise from the thermocouple trace. Ambient temperature is measured by a mercury-in-glass thermometer before the experiment.

A complete catalogue of these parameters is given in Table 4.1 for the ten extrusions carried out. The plot of extrusion stress against drawing stress is given in Fig. 4.3. Eleven points are available for this graph as extrusion number 7 had to be stopped and restarted. The second extrusion pressure was lower than the first giving another point on the graph.

Although eight experiments were performed on split billets, the flow lines could only be read for five extrusions. On the first split billet extrusion, number 3, the lines were too faint to be read. With number 5 the drawbench was allowed to overstroke so that the collar was in contact with the die on dismantling and, finally, extrusion number 7 was damaged in removal from the die. Thus only five sets of flow lines were usable after these had been rejected.

Referring again to Fig. 4.3, it can be seen that all the results except the one at higher speed lie within two lines ±4% from a mean line

TABLE 4.1 Extrusion Results

TEST NO.	1	2	3	4	5	6	7	8	9	10
EXTRUSION PRESSURE (kbar)	3.941	3.153	2.810	2.965	3.723	3.510	3.325 3.130	3.555	2.580	2.200
DRAWING LOAD (N)	0	3180	5470	5450	267	1468	3425 4410	2070	7030	6540
DRAWING STRESS (kbar)	0	0.506	0.869	0.865	0.042	0.232	0.543 0.698	0.378	1.391	1.294
TEMPERATURE ABOVE AMBIENT	0°C	0°C	0°C	0°C	0°C	3.5°C	4.5°C	1.0°C	4.0°C	5.3°C
SPEED (m/min)	-	0.0931	0.0931	0.0931	0.0927	0.0927	0.0927	0.0905	0.0889	0.825
BILLET DIAMETER	0.5014 in	0.4986 in	0.5002 in	0.5005 in	0.4992 in	0.4988 in	0.4999 in	0.4990 in	0.4996 in	0.4974 in
PRODUCT DIAMETER	0.3133 in	0.3131 in	0.3125 in	0.3125 in	0.3130 in	0.3131 in	0.3138 in	0.3128 in	0.3134 in	0.3128 in
FLUID	Tellus 27	Tellus 27	Tellus 27	Tellus 27	Castor Oil	Castor Oil	Castor Oil	Castor Oil	Castor Oil	Castor Oil
LUBRICANT	None	None	None	None	None	None	Molyslip	Molyslip	Molyslip	Molyslip
AMBIENT TEMPERATURE	21°C	20°C	20°C	20°C	21°C	19°C	21°C	22°C	22°C	21°C

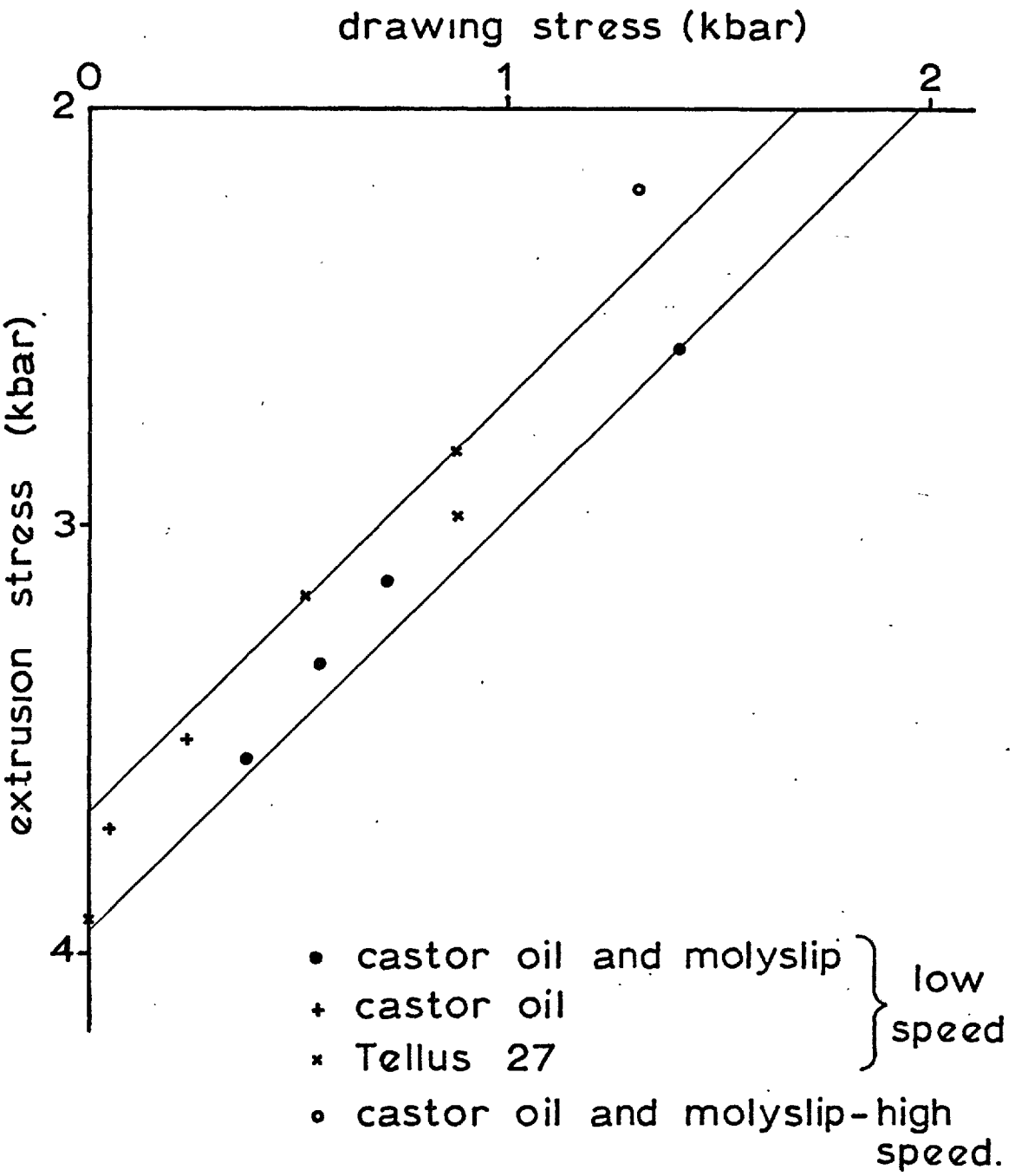

Fig.4.3. Plot of extrusion stress versus drawing stress.

through the results. Further, this mean line is at 45° to the axes, their being of the same scale, which indicates that the sum of the extrusion stress and the drawing stress is approximately constant. The single result at high speed, approximately nine times the speed for the other results where the product velocity was around 0.058 cm/sec, indicates that the sum of the extrusion stress and drawing stress is much lower in these conditions.

As all the other parameters were identical with the other extrusions from castor oil and molybdenum disulphide, the operative frictional force in this extrusion must have been lower than in the previous experiments. However, as only one result is available for higher speed, this conclusion must be regarded as tentative.

4.1.23 Surface Profile Measurements

After extrusion the surface profiles of both the billet and the product were plotted by a Talysurf machine. Fig. 4.4 shows the billet and product profile for extrusion number 4. This is typical of the four extrusions, nos. 1-4, which were from Tellus 27. Here the product had a highly polished surface, with only few scratch marks showing which had been on the billet. A similar result was found with the aluminium extrusion described previously and shown in Fig. 4.5. Here the product had a mirror finish although the billet had an extremely rough turned finish. The low frequency variation here on the product profile trace is due to the skid moving on the small diameter product and is not due to surface variations.

For extrusion from castor oil the product profiles given in Figs. 4.6 and 4.7 show that the surface is marginally rougher from those shown for Tellus 27. Further, the product profiles in these figures are very similar, although the billets had been very different. The billet for

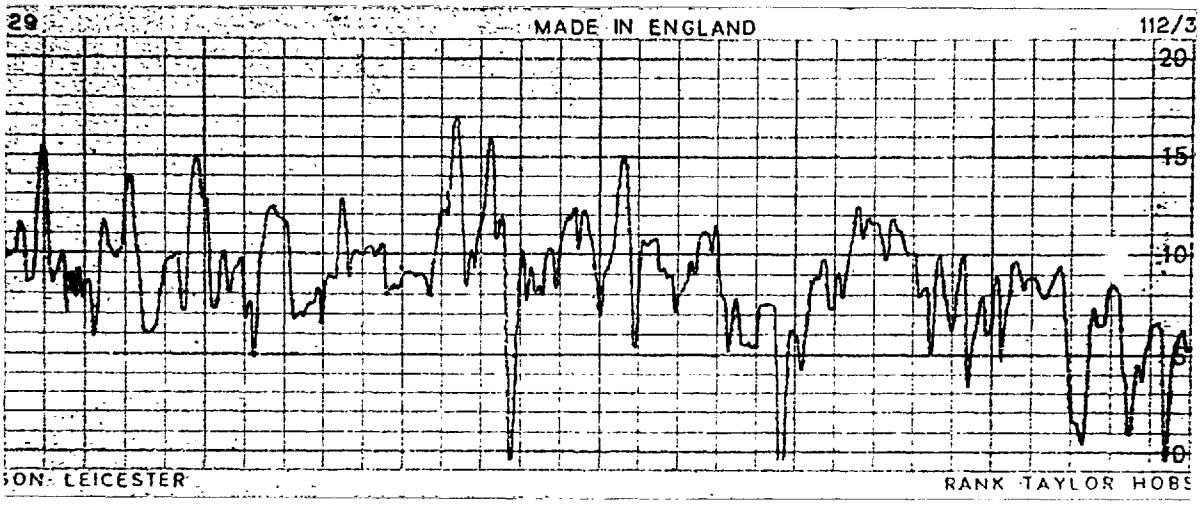

Billet profile

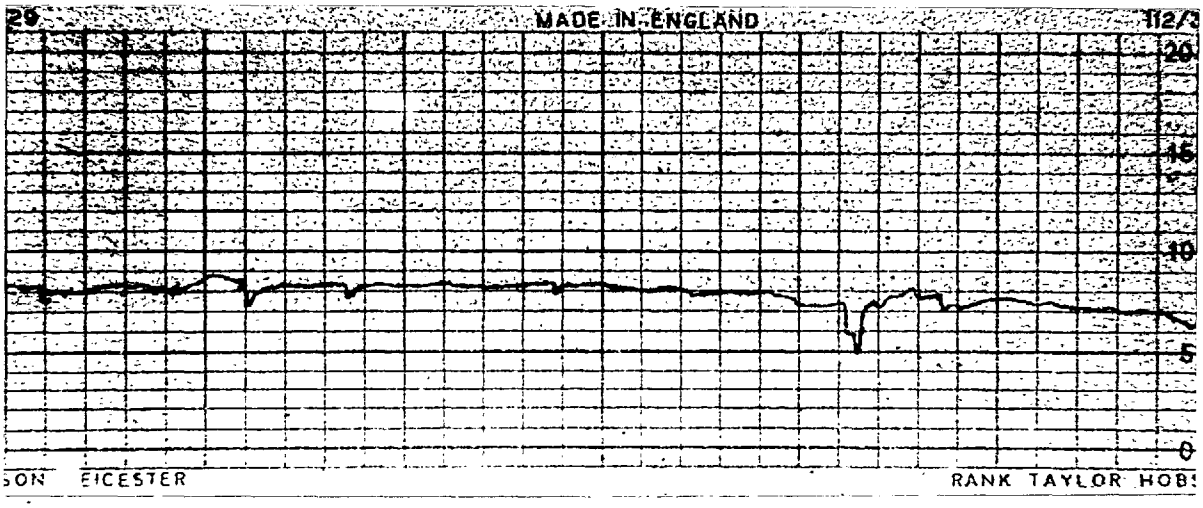

Product profile

In Figs. 4.4 - 4.9 the vertical magnification is 10,000 and the horizontal magnification 100, unless otherwise stated.

Fig. 4.4. Surface profile for extrusion no. 4.

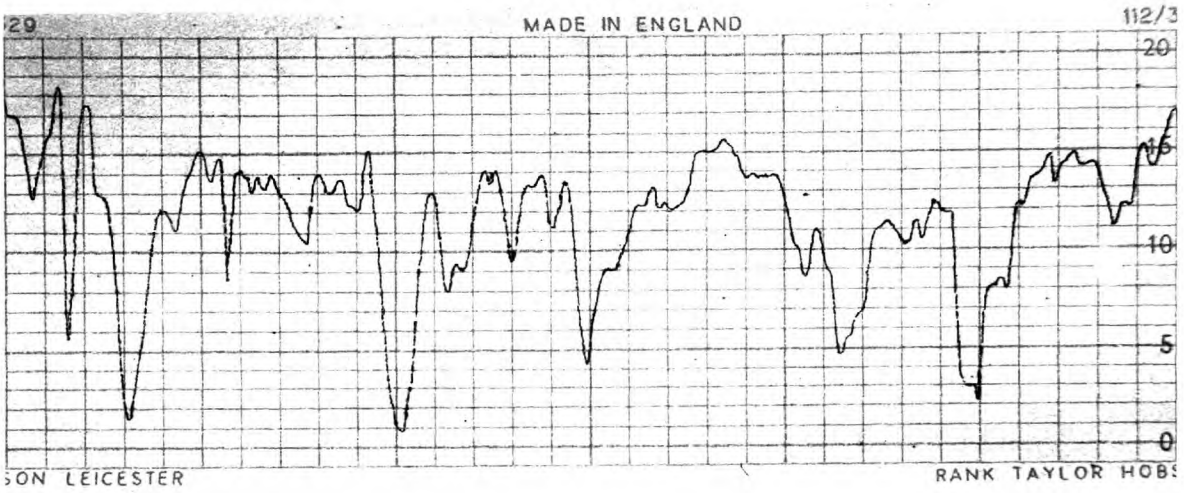

Billet profile

Vertical magnification 5,000

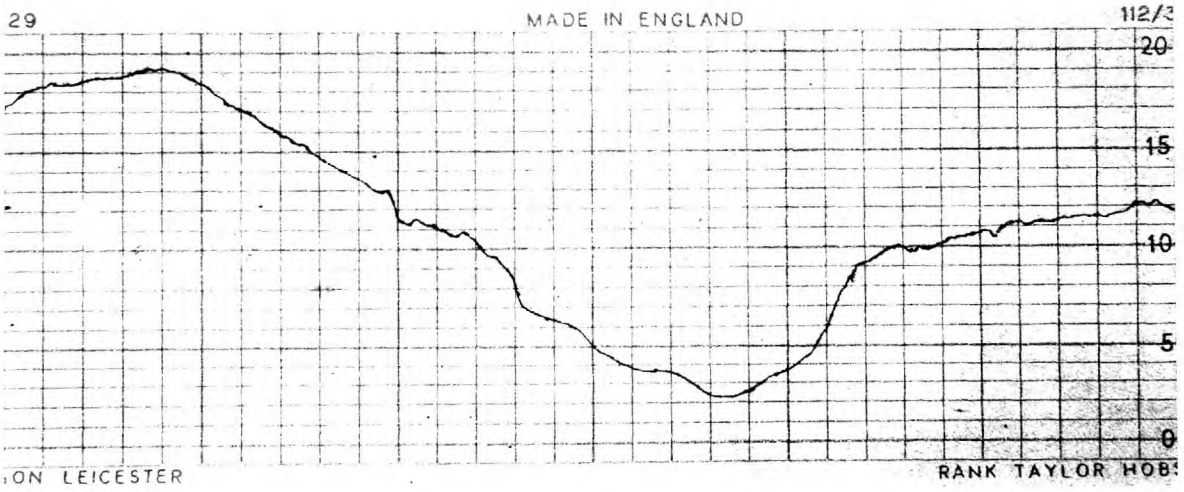

Product profile

Fig. 4.5 Surface profile for the aluminium extrusion.

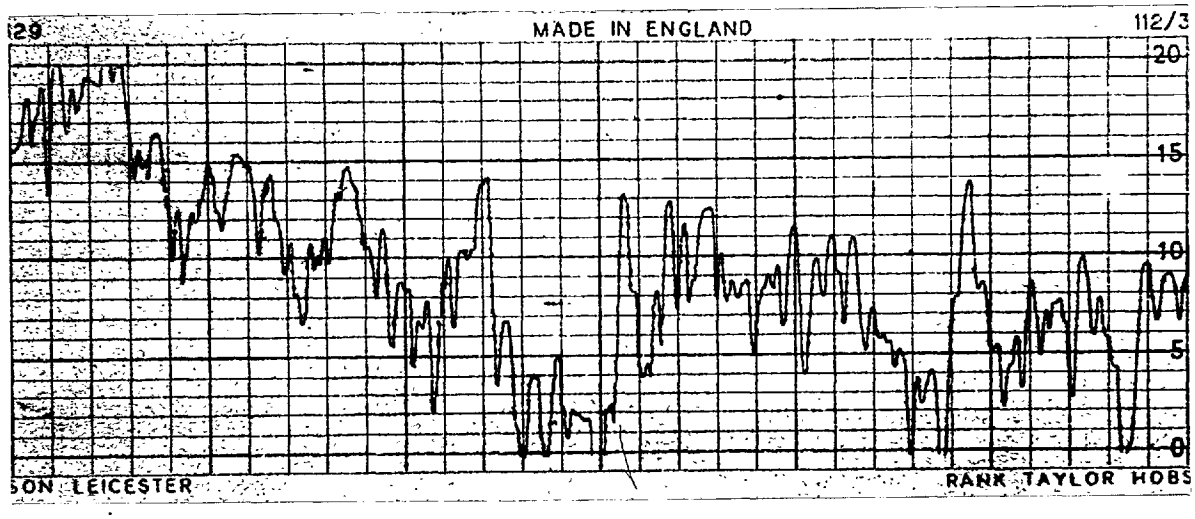

Billet profile

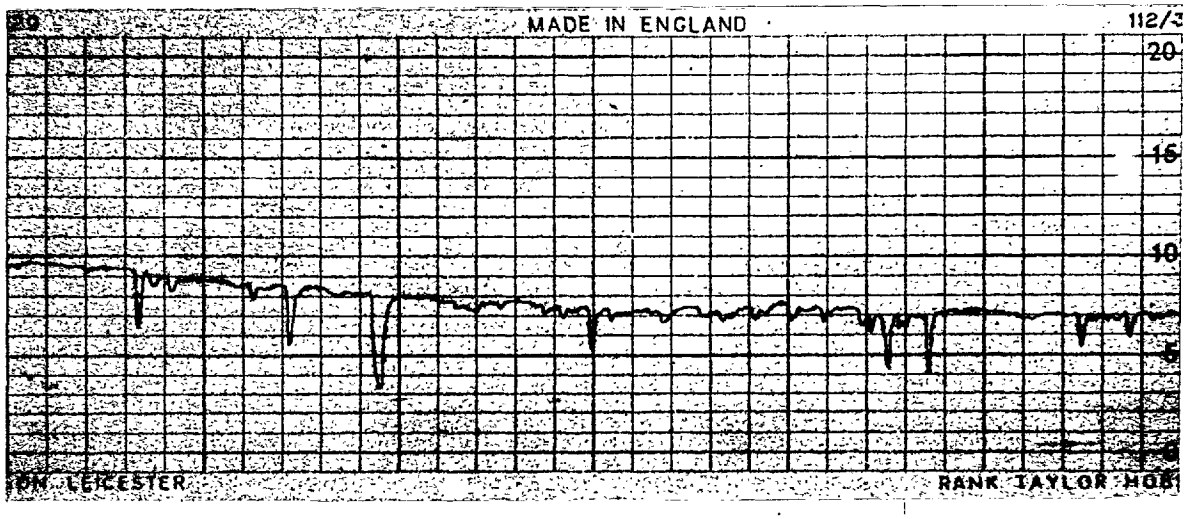

Product profile from castor oil

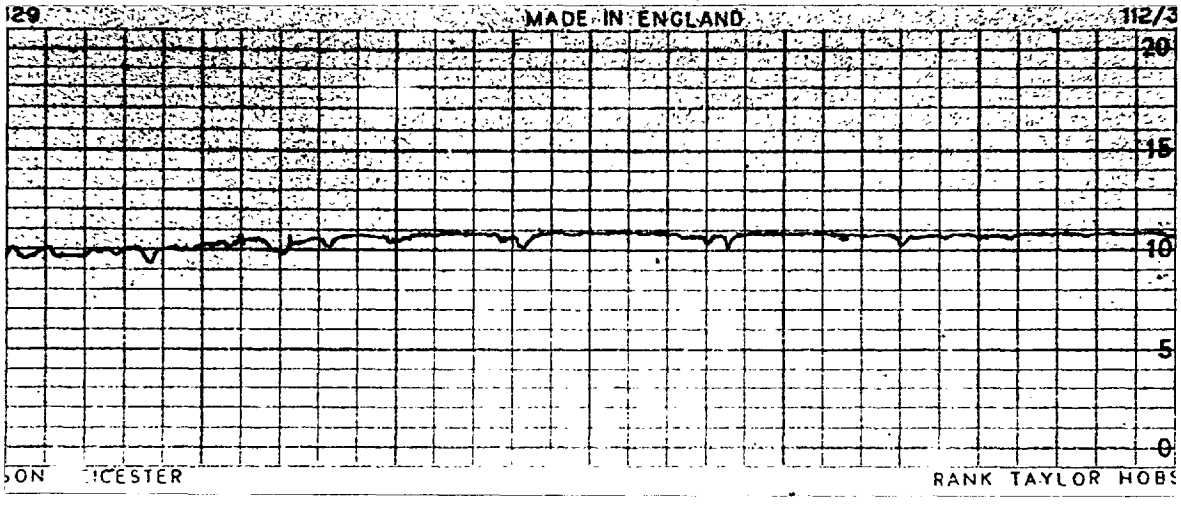

Product profile from petrol-univis

Fig.4.6. Surface profile for extrusion no. 5.

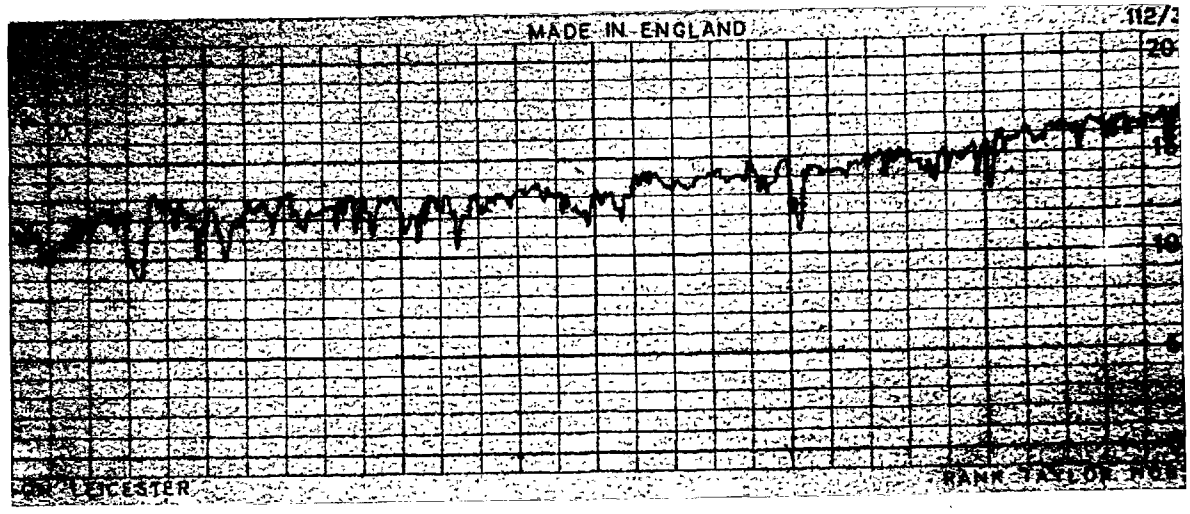

Billet profile

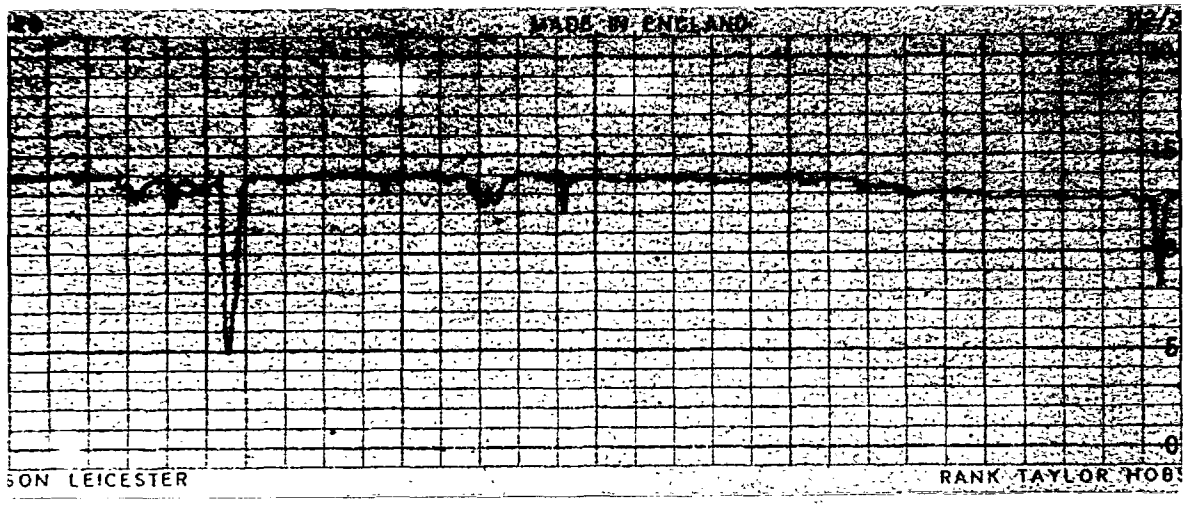

Product profile

Fig. 4.7. Surface profile for extrusion no. 6.

extrusion number 5 had not been polished, whereas that for number 6 had. Also shown in Fig. 4.6 is the profile for material which had been extruded from the petrol-univis fluid. This had only partially extruded and so this trace is from material which was initially in the nose region of the billet. Even so, the product surface was highly polished.

Extrusions nos. 7, 8 and 9 produced surface profiles which were very similar. That for number 9 is given in Fig. 4.8 as typical. However, as Fig. 4.9 shows, there was much less burnishing of the surface in extrusion number 10 than in the previous three extrusions at lower speed. This indicates that more pockets of molybdenum disulphide had been carried into the billet die interface at the higher speed. In turn, this could account for the lower driving stress described in the previous section.

4.1.24 Micro-Hardness Measurements

Micro-hardness measurements were taken across the product diameter. However, the random variations of hardness were much larger than any actual variations across the section. The average hardness was 120 H_v measured on a Vickers micro-hardness tester, for all the extrusions.

4.1.3 Pressure-Viscosity Results

Although the pressure-viscosity apparatus was designed to operate at pressures of up to 30 kbar, the preliminary results obtained here are solely for the two fluids and the pressure range of up to 3.5 kbar used in the extrusion drawing experiments. The pressure vessel and other high pressure equipment was also tested to a pressure of 18 kbar but viscosity measurements were not taken at higher pressures as the procedure is very time consuming and the data was not yet needed.

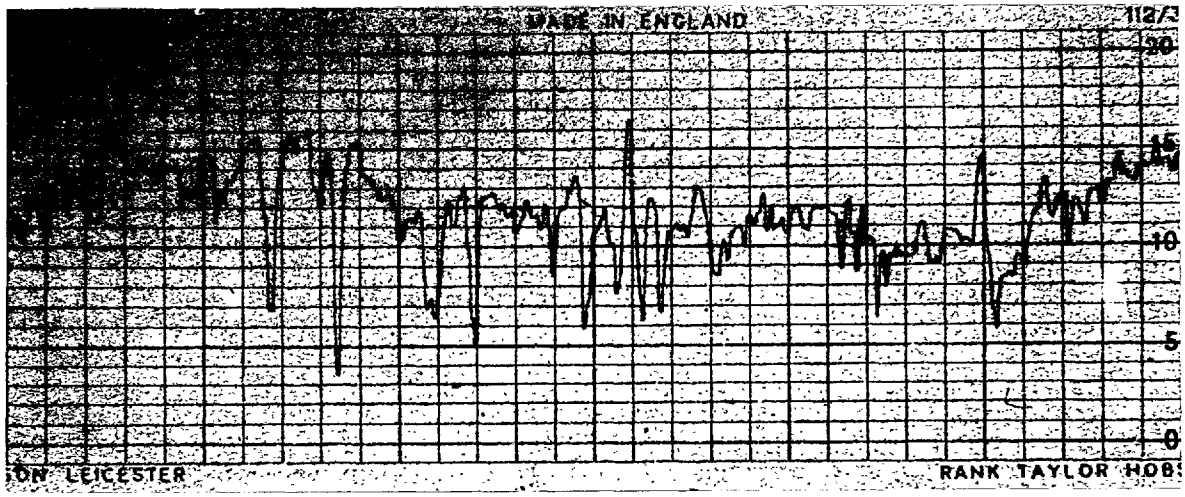

Billet profile

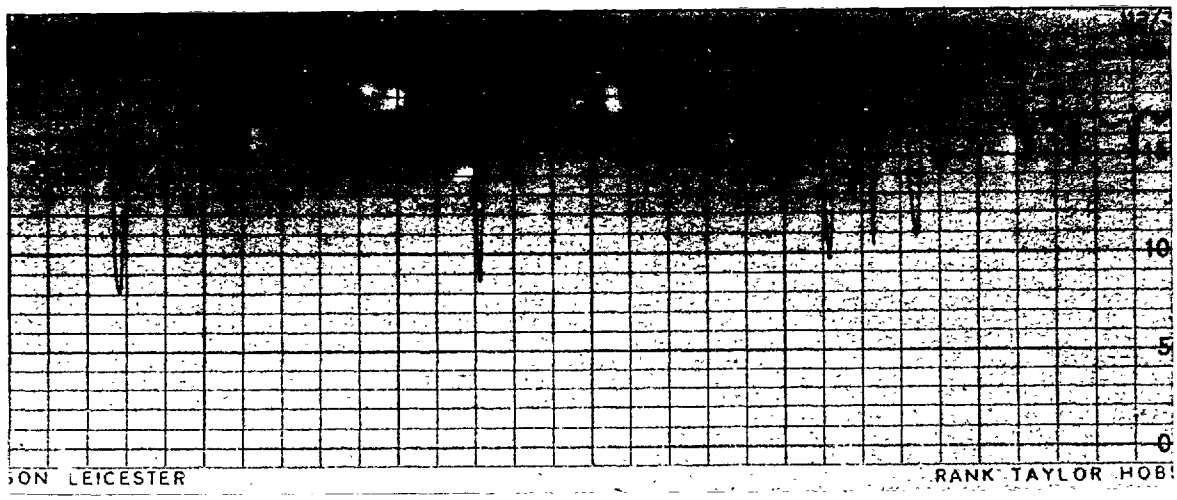

Product profile

Fig.4.8. Surface profile for extrusion no. 9.

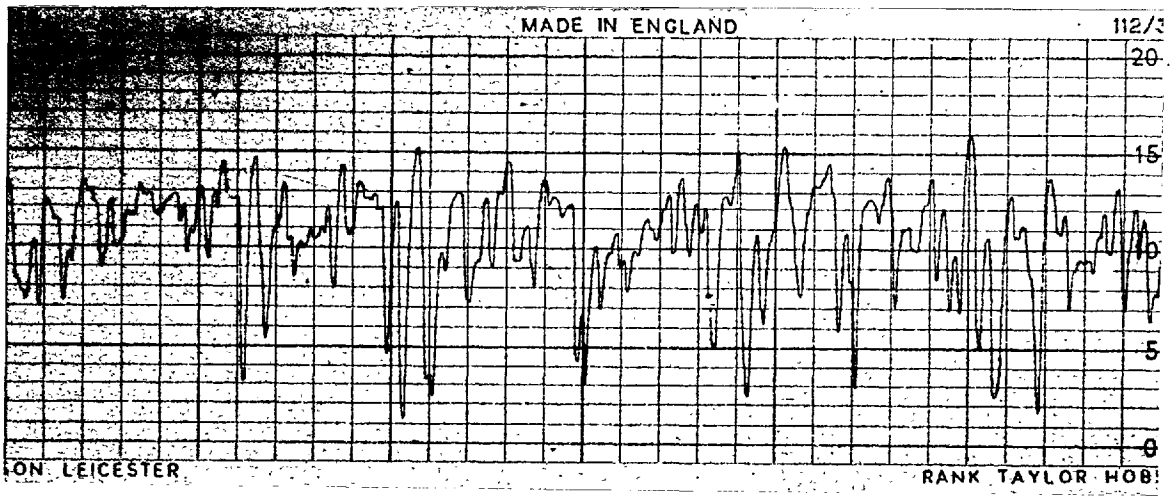

Billet profile

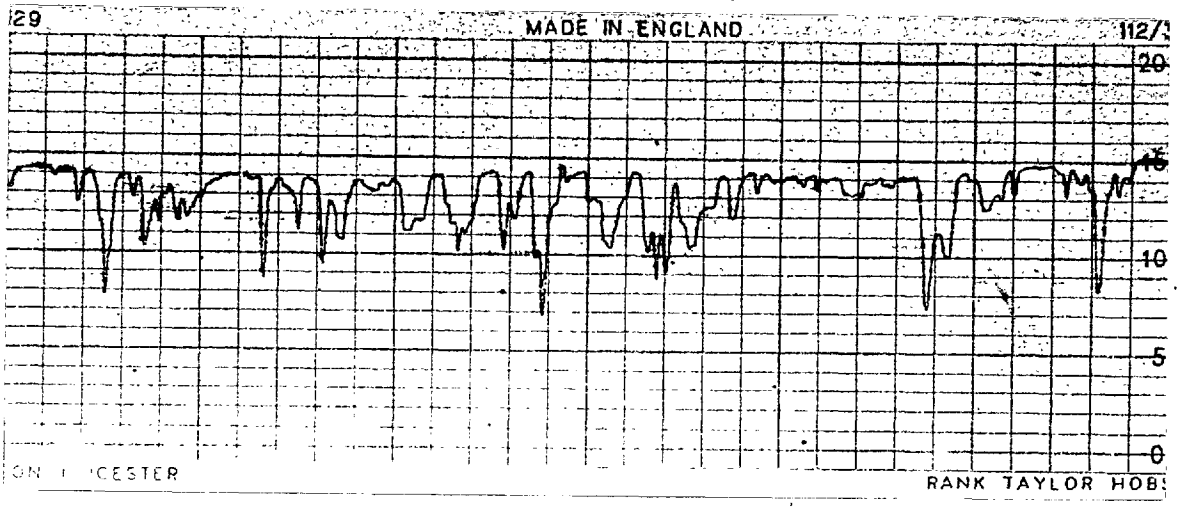

Product profile

Fig. 4.9. Surface profile for extrusion no. 10.

4.1.31 Experimental Procedure

1. The viscometer is cleaned and degreased then assembled containing the sinkers to be used in the test. The sinkers are always used in the same orientation in the tube.

2. A filtered sample of the fluid to be tested is used to fill the viscometer by the method described in section 2.2.5.

3. The viscometer is assembled into the high pressure apparatus and electrical leads connected to the punch. While the apparatus is being assembled, the leads are checked to ensure they do not short either to each other or earth.

4. Once all connections have been checked, the voltage supply to the timing system is switched on and the circuits left to warm up. The voltages from the amplifiers are measured and adjusted by adding resistance in parallel with the output until the two channels are balanced. This standing voltage, which is present as the viscometer coils are wound on metal, should have been constant from one assembly of the apparatus to the other. However, it did vary and, although the variations were decreased by using better connections and taking great care with soldered joints, they were not completely eliminated.

When the channels were balanced, the voltage from the oscillator was adjusted to standardise the output from the amplifiers for all tests.

5. The manganin coil was connected to the bridge and its resistance measured.

6. The thermocouple was connected to a direct reading Comark electronic thermometer and the ambient temperature measured and set on the thermometer. For later tests a Croprico thermocouple potentiometer was used but this did not produce markedly better results.

7. The fall time at atmospheric pressure is now measured several times. The number of measurements taken varied with the fall time from about 15 measurements at low fall times to a minimum of 2 measurements at high fall times. The trigger circuits and counter were reset immediately before the vessel was inverted, to reduce the risk of spurious triggering, but once the filter circuits were incorporated, this was not strictly necessary.

8. Pressure in the vessel was then raised by operating the air-hydro pump. At first it was intended that this should be stalled by adjusting the air pressure until the fluid pressure was at the requisite value. If there was a slight low pressure leak the pump would stroke forward maintaining pressure constant. This system proved insensitive, however, and the alternative of simply locking in pressure by a stop valve was adopted.

9. When the temperature had settled fall times were measured by resetting the timing system and inverting the vessel. After each fall, the direction of rotation was changed by means of the solenoid actuated valve and the direction switch on the timing system was operated.

The triggers were then reset and the vessel inverted. The resistance of the manganin coil and the output from the thermocouple were read immediately before timing started and immediately it finished. The reading on the counter was also read as soon as the stop trigger had been activated.

10. Testing was continued until either the pressure range of interest was covered or the fall times became too great. In the latter case the apparatus must be dismantled and another sinker inserted in the viscometer.

11. If a different fluid had been used outside the viscometer from that under test, the fall time at atmospheric pressure would be checked when pressure was released to ensure that the fluid under test had not been contaminated. A different fluid would be necessary if either the fluid under test were conductive or if it were likely to freeze under pressure, with the possibility of damage to the viscometer.

4.1.32 Operational Experience

Sinkers with guide pins were first tried. Some difficulty was experienced because O-rings had been substituted for the gasket seals for which the viscometer was originally designed, as the gaskets had failed to seal adequately. The sinkers would tend to stick at the gaps between the end caps and the main bore. This was overcome by machining the lead in angles on the pins which are shown in Fig. 2.9 and by increasing the clearance slightly between the pins and the tube. The diametral clearance was then approximately 0.03 mm.

Although the sinkers with guides were operating satisfactorily, it was decided that those without guides should be tried, as these are preferable if they give reproduceable fall times. They were first tried with guide tubes, to ensure concentricity at the start of fall, but the difficulty here was that they took too long to fall through the guides. These were therefore removed.

Without the guides, sinkers without guide pins have been used over a range of fall times of 200 in the determination of the pressure viscosity curves for Tellus 27 and castor oil. As this is approaching the limit of the range for sinkers with guide pins - the limit here being the maximum tolerable fall time - there seems to be no advantage in using sinkers with guide pins. All the tests detailed in the next section were carried out with sinkers without guide pins.

The only remaining problem with the sinkers used, which was also present with those with guide pins, was a large directional effect. In one direction the total spread of fall times would be typically less than 1% around the mean while in the other it would rise up as high as 10%. Further, in this direction the mean fall time was about 10% higher than that in the other direction. For these reasons the fall times could only

be taken in one direction, which doubles the time necessary for a series of experiments.

To demonstrate that the sinkers were responsible for the difference in times, they were also tried in the opposite orientation in the tube. When this was done they had erratic fall times when falling from the end of the tube which had previously given repeatable times. The most likely cause of asymmetry of the sinkers, which is responsible for this effect, is wandering of the bore hole in the sinkers. Although the final machining was carried out on a mandrel, it is possible that the hole at the end farther from the drill entry was significantly out of round. The other possibility is that the soft iron core was not exactly central after machining. This would mean that the centre of gravity was nearer one end of the sinker. When this end was downwards, the fall would be stable. Fall in the other direction would be less stable, however.

The rest of the high pressure apparatus worked satisfactorily, once the problem of high pressure leads had been solved, in the range of pressures used for testing. Attempts at sealing with a very thin fluid, n-propyl alcohol, were not successful and a leak developed at a pressure of 8 kbar. A similar problem had occurred in the extrusion apparatus with petrol-univis as the fluid. This could be overcome by redesigning the plunger, either for a static sealing arrangement if a plunger with a central hole for the electrical leads were strong enough, or for an unsupported area seal.

Also, it was realised that the temperature control was not adequate. With the coil calibrated as detailed, the change in temperature during a series of tests could become a major source of error. If the measured temperature is different from the nominal temperature, the fall time must be corrected using the atmospheric temperature coefficient of viscosity. As long as the temperature difference is small, the error introduced here is negligible.

A safety cubicle had been built for surrounding the apparatus when high pressure tests were started. This could easily be fitted with a temperature control unit to hold the ambient temperature constant within $0.1^{o}C$. As long as ambient conditions are maintained, the heaters could then be used to raise the temperature, without fluctuations. Further, for the most accurate work the resistance bridge should also be held at $20^{o}C$, the calibration temperature. Changes of bulk temperature produce negligible error in the bridge, but if gradients are allowed to develop large errors, of the order of 2%, can be introduced due to thermal effects.

Difficulties in the use of the timing system have already been mentioned.

4.1.33 Viscosity of Castor Oil

For the measurement of the change of viscosity with pressure of castor oil at $20.0^{o}C$, three sinkers were used, all without guide pins. One was of the long design shown in Fig. 2.10 of stainless steel, while the other two were of the short design, one each of stainless steel, EN58JM, and duralumin L65 alloy. The dimensions of these sinkers were measured on the universal measuring machine and are given in Appendix VI. The volume and the density of the sinkers is found by hydrostatic weighing.

The absolute viscosity of the castor oil was measured by measuring the transpiration time in a suspended level viscometer which had been previously calibrated. Density of the fluid was calculated by weighing a 2.54 cm diameter steel ball in air and the fluid. These results are also given in Appendix VI.

From the experimental readings the temperature was first calculated from the reading of the thermocouple potentiometer. The readings of resistance of the manganin coil were then corrected to the temperature at which it was calibrated, using the atmospheric pressure value of the temperature coefficient of resistance. The change of resistance per unit

resistance is then calculated and from this the pressure, using the slope of the calibration curve.

Next the average fall time at each pressure and temperature is calculated. This is then corrected for the change of viscometer constant due to change of pressure and temperature, the difference of temperature from the nominal temperature and the change of density of the fluid and sinker under pressure.

In previous work(132, 161) a correction for turbulence was also made by calibrating the sinkers against a range of fluids. The fall time, corrected for density and temperature, divided by the viscosity is plotted against the logarithm of fall time. If the flow becomes turbulent, this plot deviates from a straight horizontal line as shown in Fig. 4.10. In the present work, however, the viscosities are much higher and hence the radial clearance ratio is much higher to give reasonable fall times. Also sinkers with bore holes are used. This greatly reduces the Reynold's number of the flow, as the fluid velocity in the annulus is much lower. Further, no guides were used and these must cause turbulence to initiate at low fall times.

Fig. 4.11 shows the results for the three sinkers in castor oil. As these points lie on a smooth curve, it can be seen that the neglecting of turbulence is justified. In Fig. 4.12 the results are compared with those of Wilson (14) for castor oil found with his falling plate viscometer. The atmospheric values of density and viscosity were slightly different from the sample used in the present tests, density being 1% higher and viscosity 10% higher at 20°C. However, it can be seen that the limited results available here follow the same trend as the previous results.

4.1.34 Viscosity of Tellus 27

For this fluid only the long stainless steel sinker was used. The atmospheric values of viscosity and density were found as for castor oil and

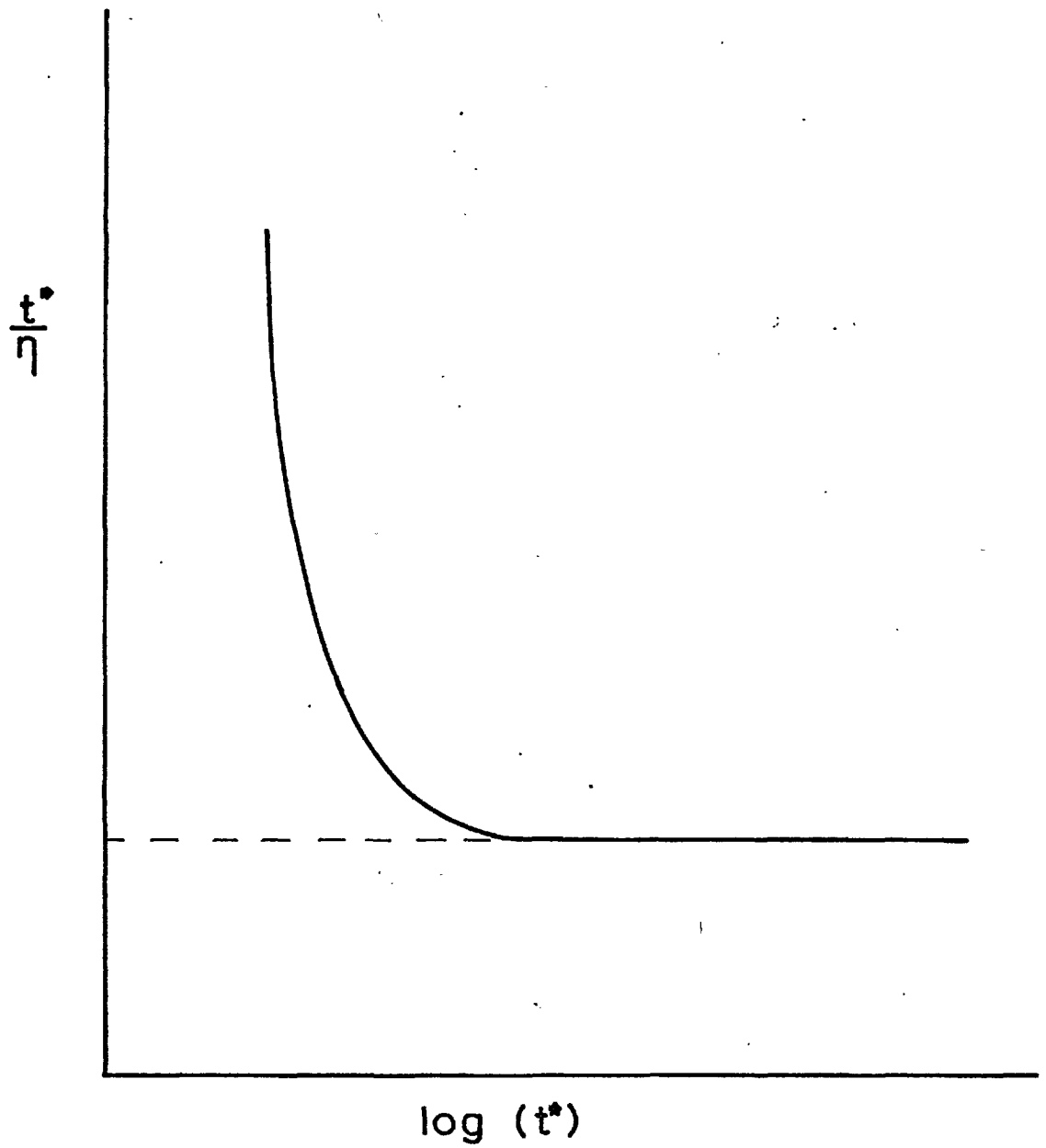

Fig. 4.10. Deviation from laminar flow at low fall times.

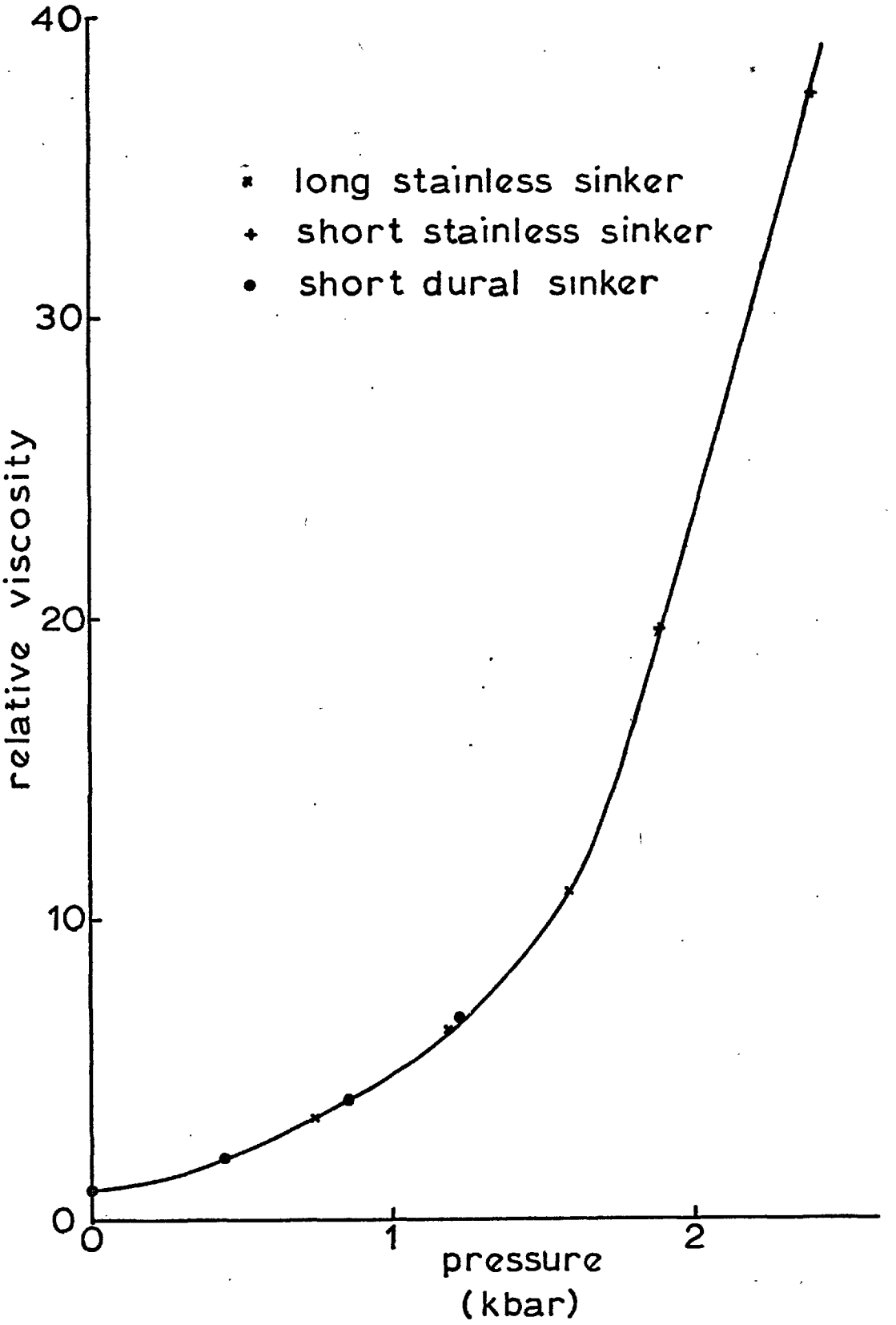

Fig. 4.11. Pressure - viscosity curve for castor oil at 20°.0 C

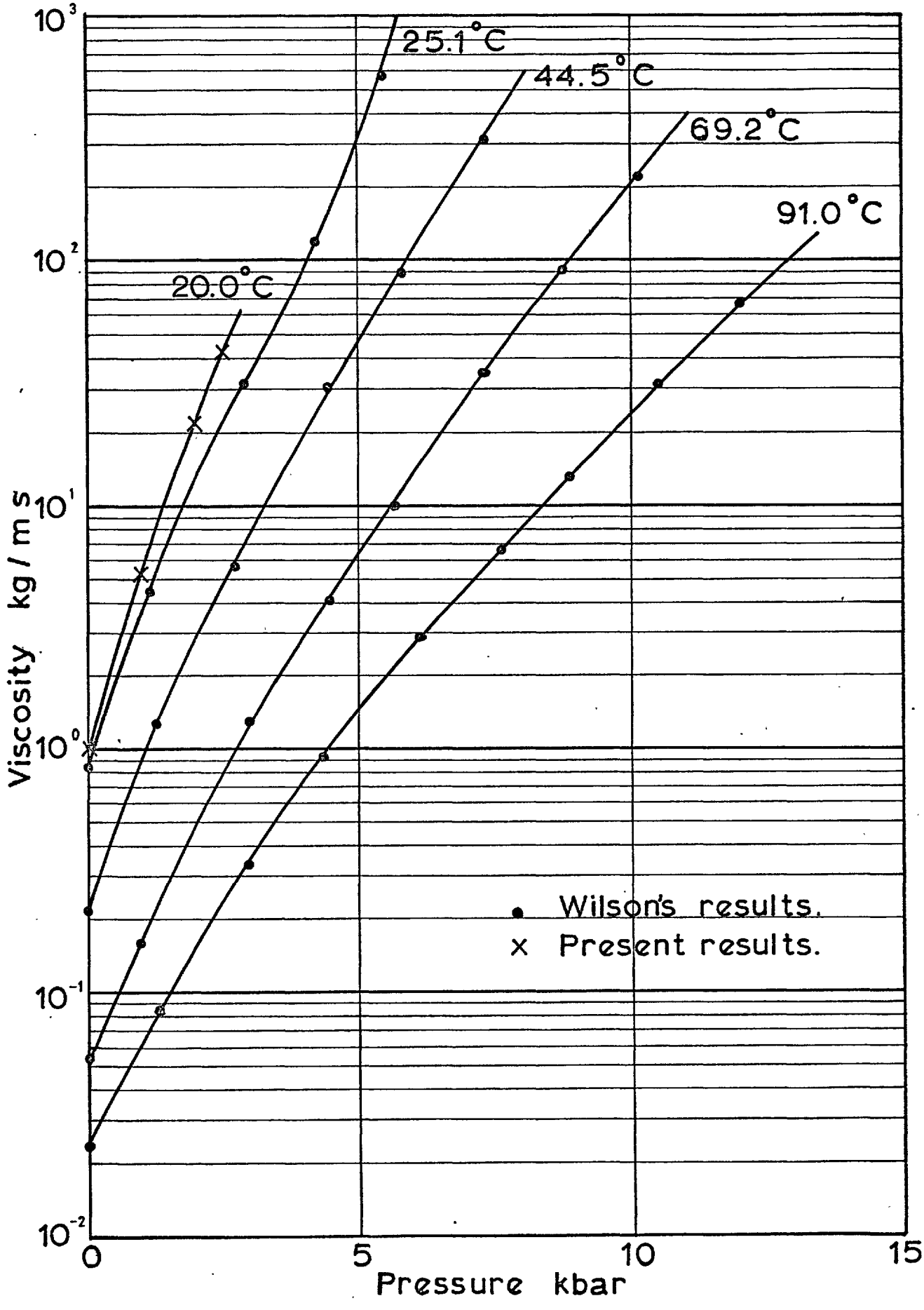

Fig. 4.12. Comparison with the results of Wilson (14).

are given in Appendix VI. Other calculations are as in the previous section, except that here the nominal temperature was 15°C. The results are plotted in Fig. 4.13. By comparison with Fig. 4.11 it can be seen that the pressure coefficient of viscosity is much higher than for castor oil.

4.1.35 Density of Castor Oil

Here, the results for fall time of the long stainless steel sinker and the short duralumin sinker are taken and corrected, as above, except that the density correction is not applied. The values found are plotted in Fig. 4.14 and no longer lie on the same line. From this figure values of $(t^*_{\ell p}/t^*_{\ell o})$ and (t^*_{hp}/t^*_{ho}) are read off at different pressures and fluid density calculated from eq. 4.42. These results are shown in Fig. 4.15 with the density measurements given by Wilson (114) at 25.1°C.

The scatter here is due to the difficulty in estimating accurately the difference between two curves, Fig. 4.14, which are close together. The two curves are beginning to diverge, however, and at higher pressures, where the change of density would be greater, this method would become more accurate.

4.2 Computed Results

4.2.1 Flow Lines

Once a billet has been extruded, it is extracted from the die and coordinates of 20-25 points along each line are measured. These coordinates, along with the extrusion pressure, drawing stress and other parameters then form the input data to the computer program.

Two billets, extrusions 8 and 10, are shown in Figs. 4.16 and 4.17. The tracked data for extrusion number 10 has already been given as an example in Fig. 3.4. From these figures it can be seen that there is no

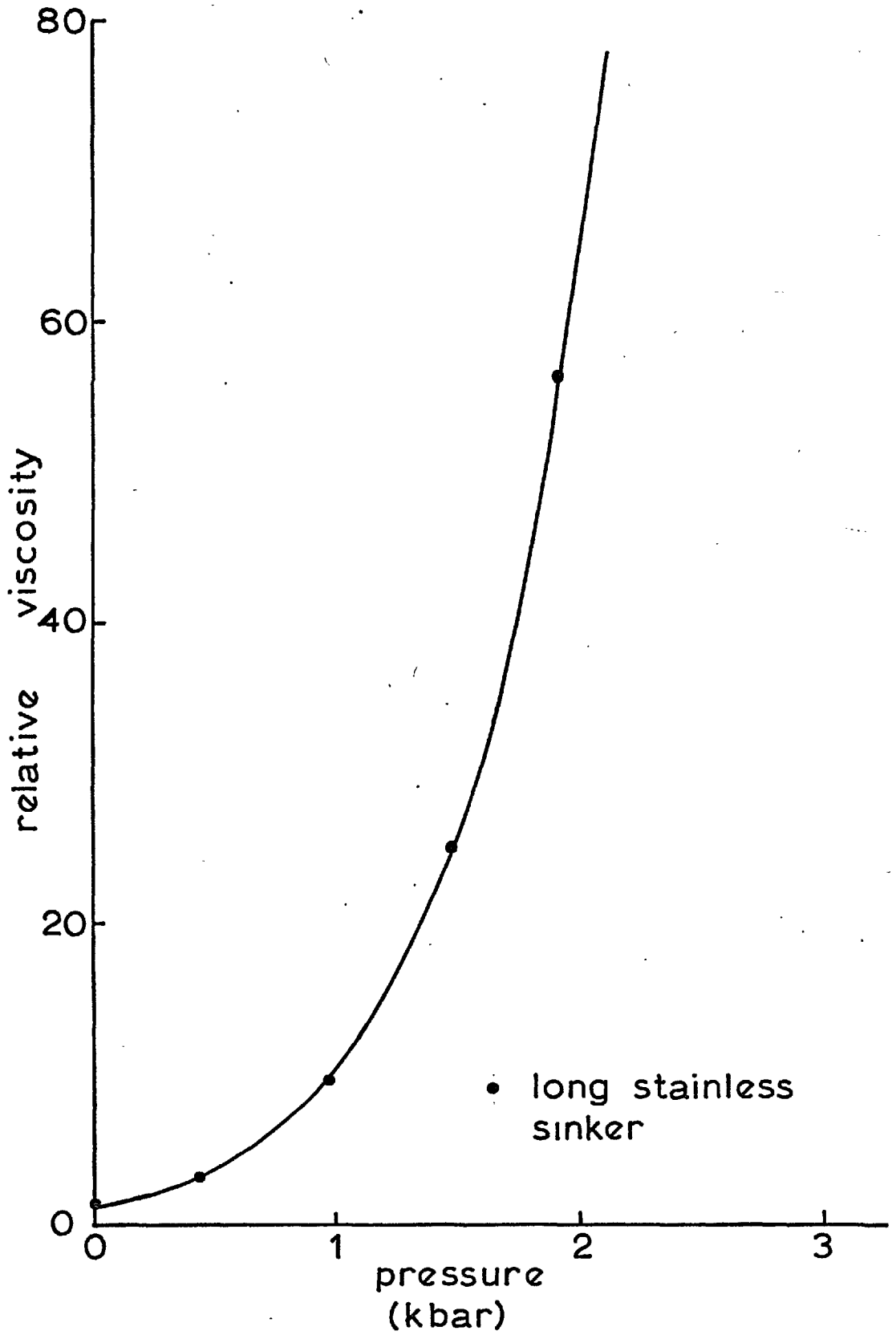

Fig. 4.13. Pressure-viscosity curve for Shell Tellus 27 at 15.0°C

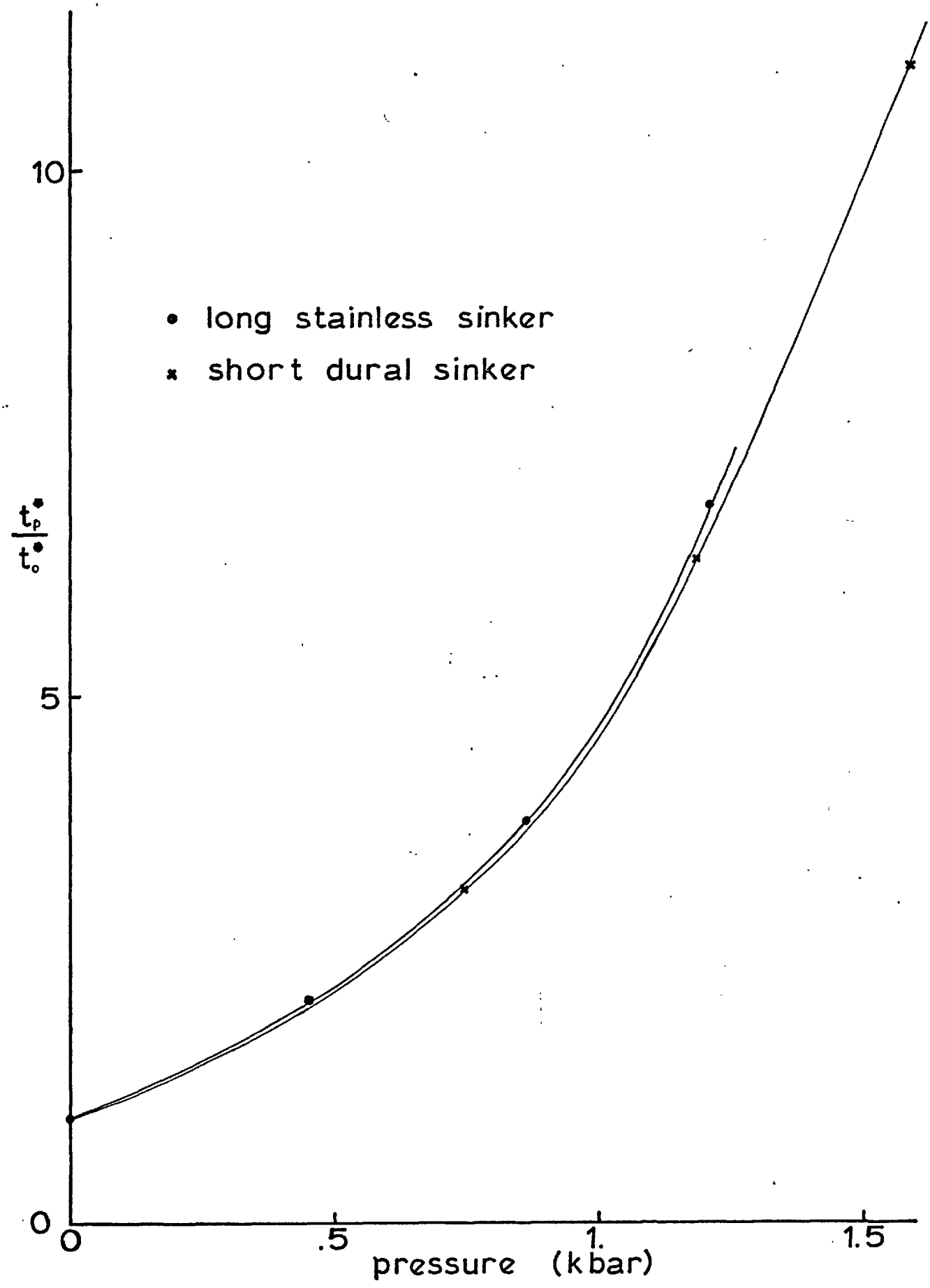

Fig. 4.14. Relative fall times without density correction.

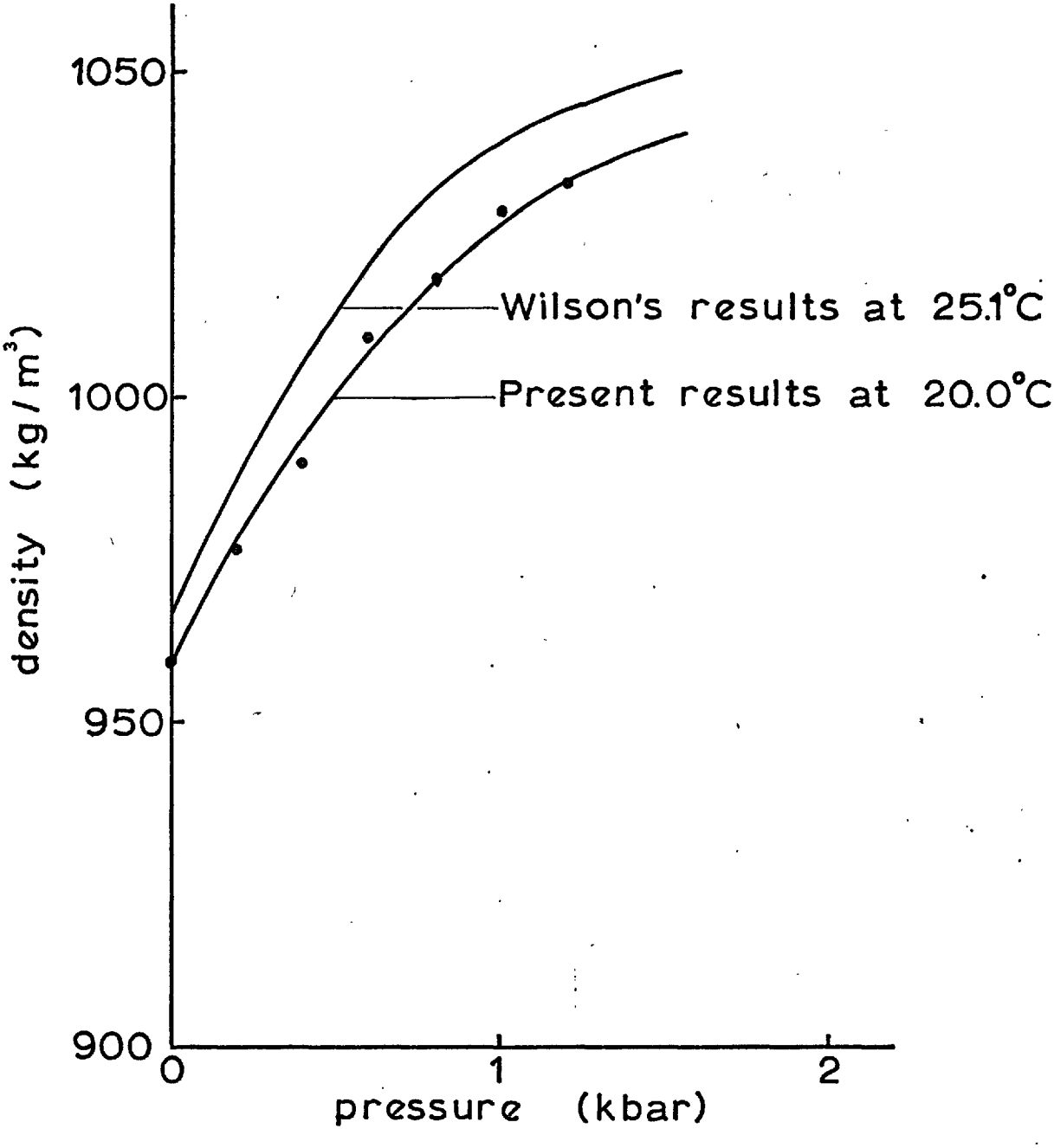

Fig. 4.15. Density of castor oil.

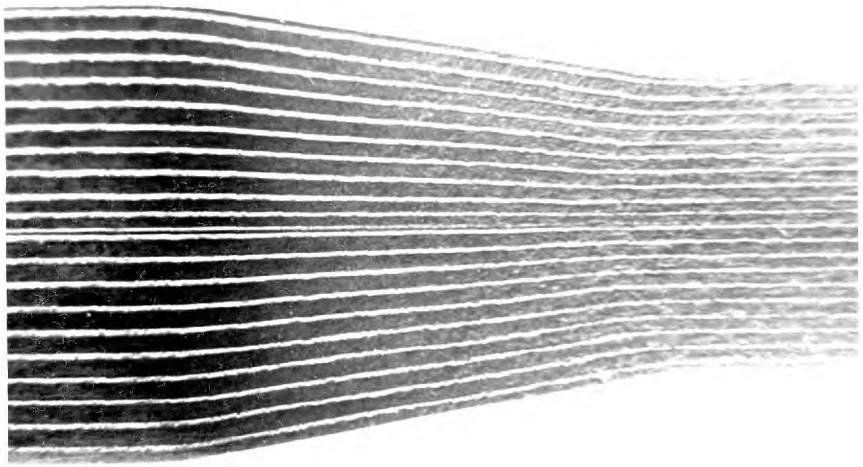

Fig. 4.16. Extrusion no. 8.

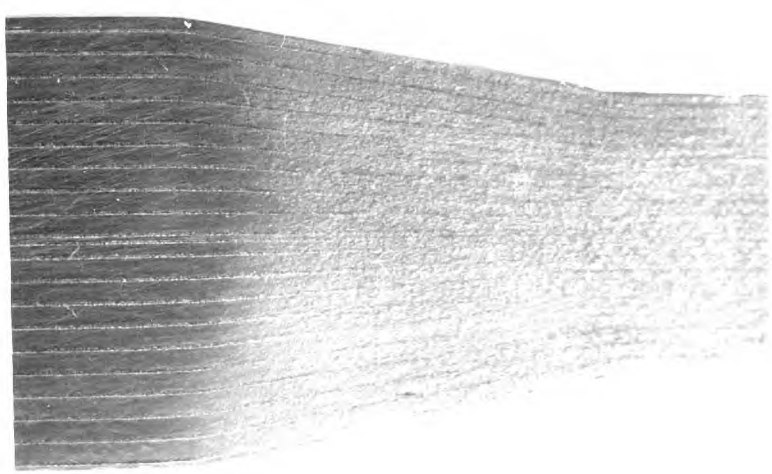

Fig. 4.17. Extrusion no. 10.

sharp change of slope at contact between the billet and the die. The deformation of the billet before the die is reached is not pronounced but is, nevertheless, present.

It is also apparent that flow in the deformation zone does not follow either the radial or parallel flow paths normally assumed in upper bound approaches. Taking as an example a line which is initially mid-way between the centre line and the surface, it deforms as follows. There is an initial region with a fairly sharp change of slope as the deformation zone is entered. Next there is a portion in which the line is nearly straight. However, the slope of the flow line then decreases slightly at a point about one third of the way along the die. The slope again increases and the line is once more approximately straight, until exit from the deformation region.

Fig. 4.17 clearly shows the boundary where the initial polished billet has deformed sufficiently for its surface to become roughened. This effect here is much smaller than in the case of the aluminium billet, Fig. 4.1 (a), as the grain size is much smaller. If it is assumed that this roughening takes place at a constant value of strain, it follows that the outer fibres of the billet are more heavily deformed than those near the centre line, contrary to the assumption often made in upper bound solutions of the type described in Chapter 1.

Further evidence that the deformation occurs in this manner can be gleaned from Fig. 4.1 (b). Here, a few lines were scribed perpendicular to the axis of flow. After extrusion these lines are iso-time lines and are an indication of the position reached along each flow line in a given time. It can be seen that the line just inside the deformation zone is curved so that the distance covered along a line near the surface is greater than along the centre line in the same time. This shows that the outer fibres are more heavily deformed.

Attempts were made to estimate the deformation region by following the lines from the billet and product until they deviated from straight lines parallel with the axis. It was very difficult to get reproducible results, especially near the centre where the change of curvature is smallest. As an example the field of deformation measured in this way is shown for extrusions 8 and 10 in Fig. 4.18.

When this data was used in the computer program, and smoothing was carried out between the deformation boundaries, the results near these boundaries were erratic. This was due to the inaccuracy of the boundary estimated as above forcing a deformation pattern on the flow which had not occurred in practice. It was found to be better to smooth the flow function between two K sections, one in the billet and one in the product. The strain rates then fell more smoothly to zero in the zones at the beginning and end of deformation. All the results detailed in the following sections were calculated in this way.

The smoothing procedure used in the results given was to call subroutines SMOTHZ and SMOTHR as, in practice, they were found preferable to STSM which greatly altered the flow pattern.

4.2.2 Velocity Fields

From the input data, the flow function, velocities, strain rates and total strains are calculated by the computer program. The results of this analysis are given in Figs. 4.19 to 4.23 for extrusions 4, 6, 8, 9 and 10. That differences existed in flow patterns in the various extrusions is evident directly from the velocity fields.

Extrusion number 10 shows the most marked deformation in the outer fibres although it is also pronounced on number 8. The effect is present on number 6 to a more limited extent but is not found at all for extrusions number 4 and 9. Under the microscope during measuring of the flow lines

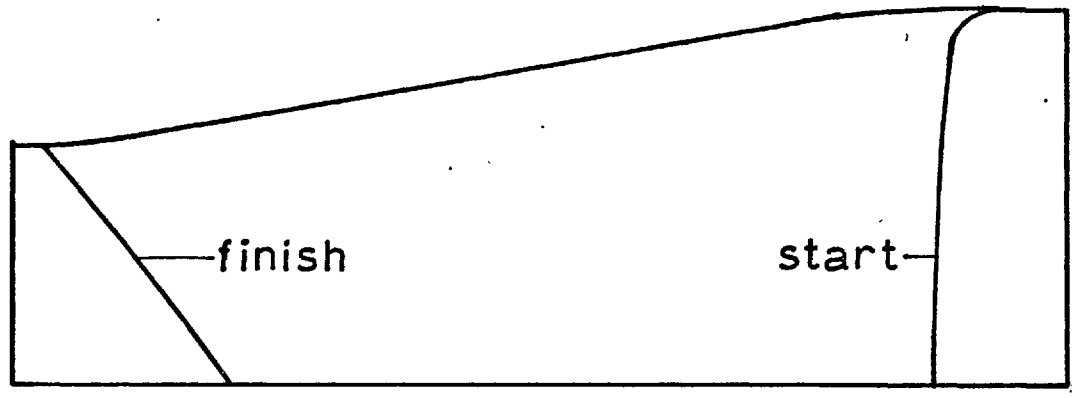

Extrusion no. 9.

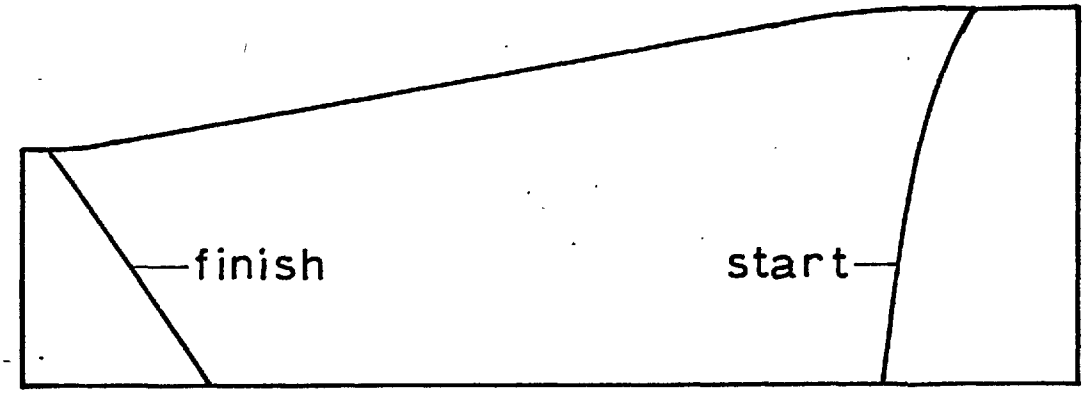

Extrusion no. 10

Fig. 4.18. Estimated deformation regions.

Table 4.2. Symbols used for stress and strain plots.

K section	Symbol
1	Y
6	Z
11	X
16	⏃
21	◇
26	X
31	+
36	△
41	⊙

Figs. 4.19.-4.23. Velocity, strain rate and strain fields for extrusions 4,6,8,9,10.

Figs. 4.24.-4.28. Stress fields for extrusions 4, 6, 8, 9, 10.

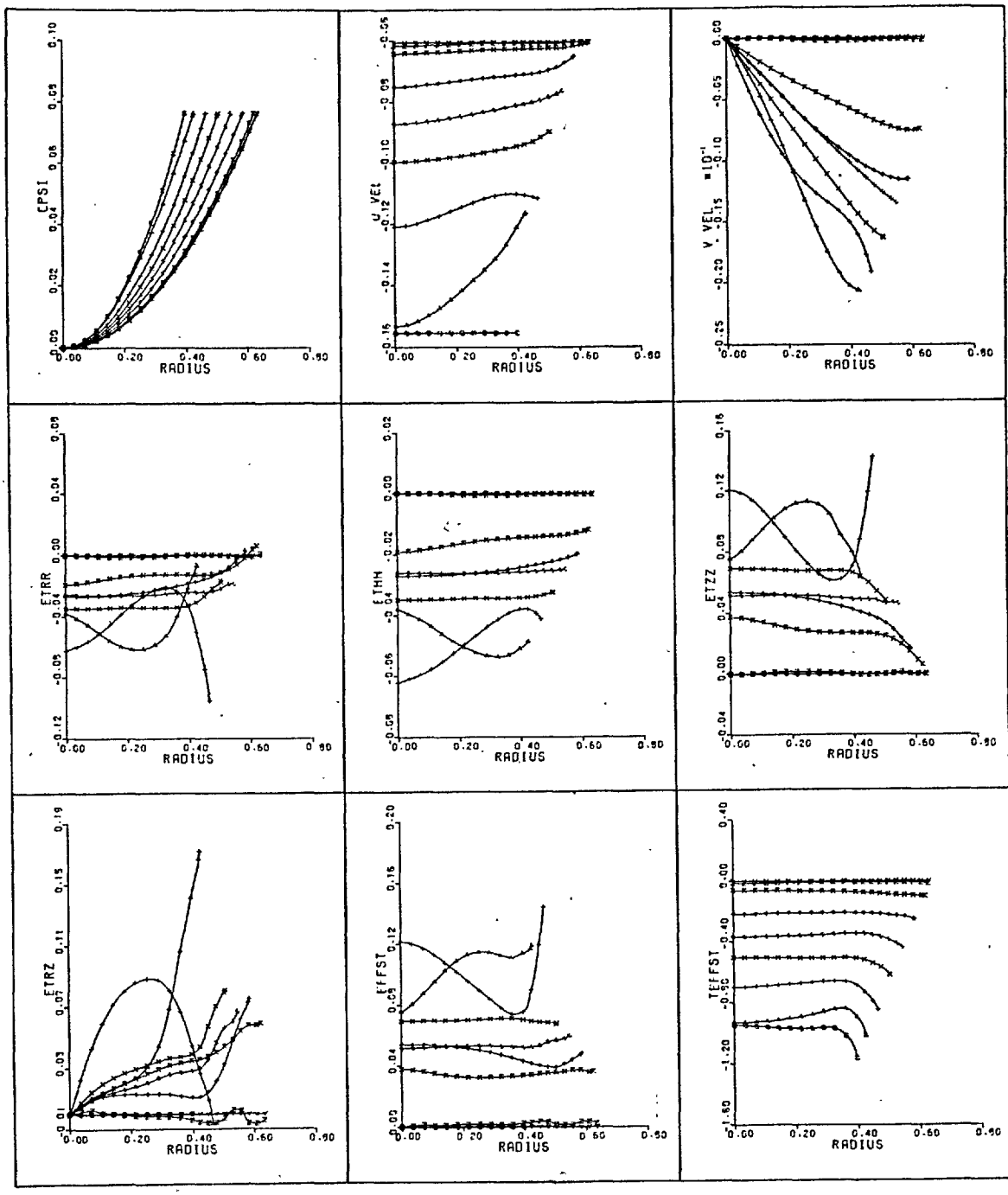

Fig.4.19. Extrusion no. 4.

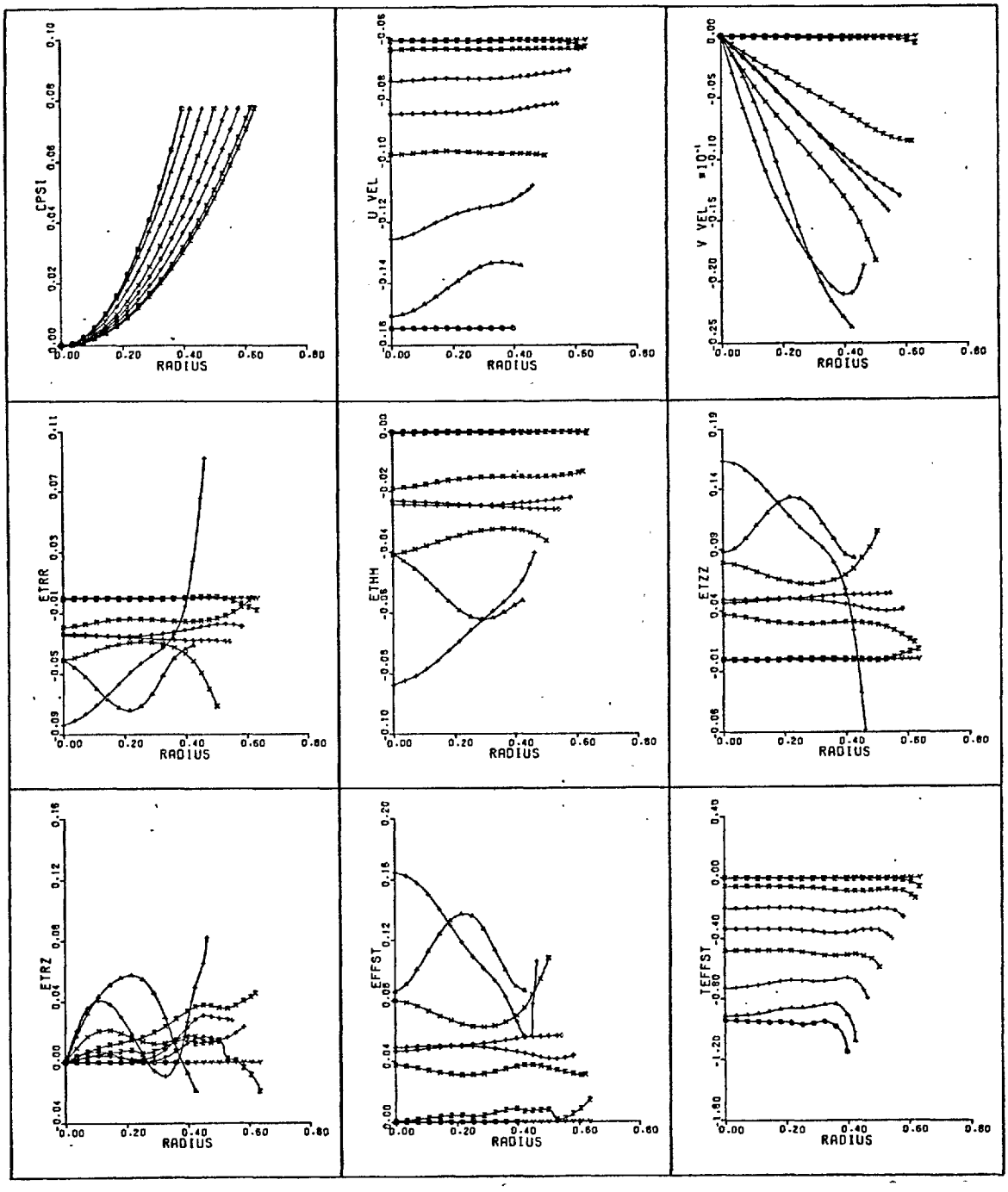

Fig. 4.20. Extrusion no. 6.

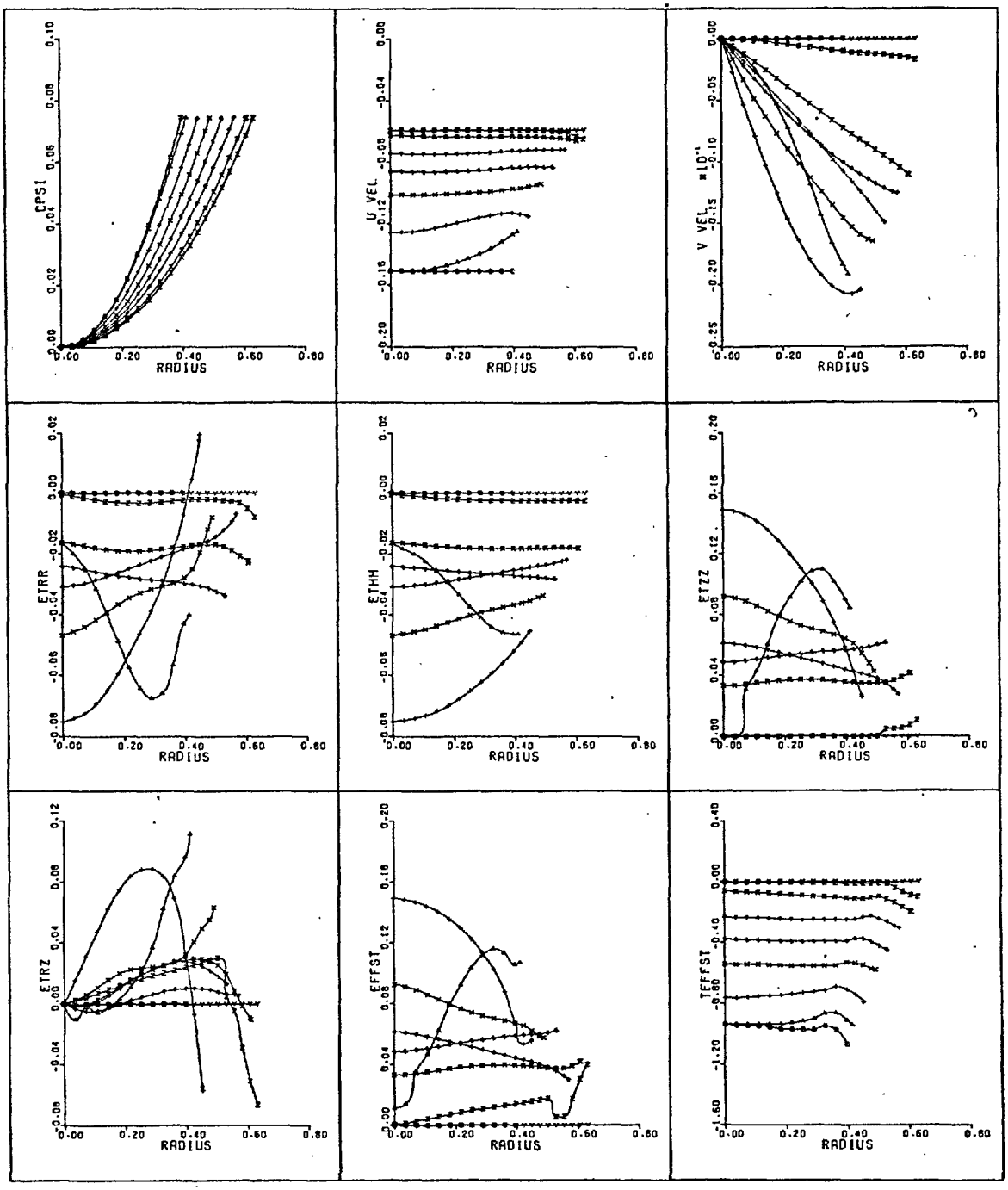

Fig.4.21. Extrusion no. 8.

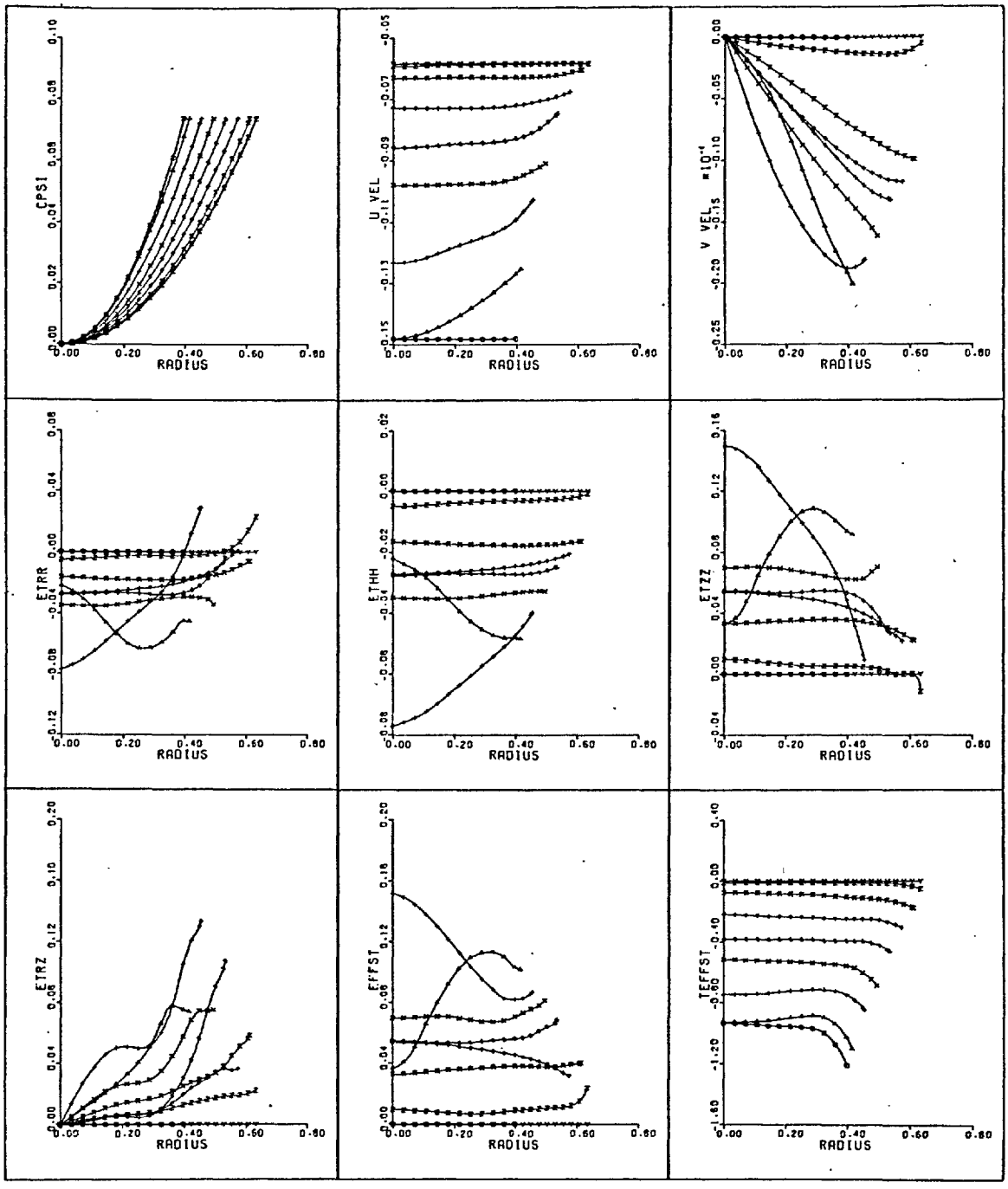

Fig.4.22. Extrusion no.9.

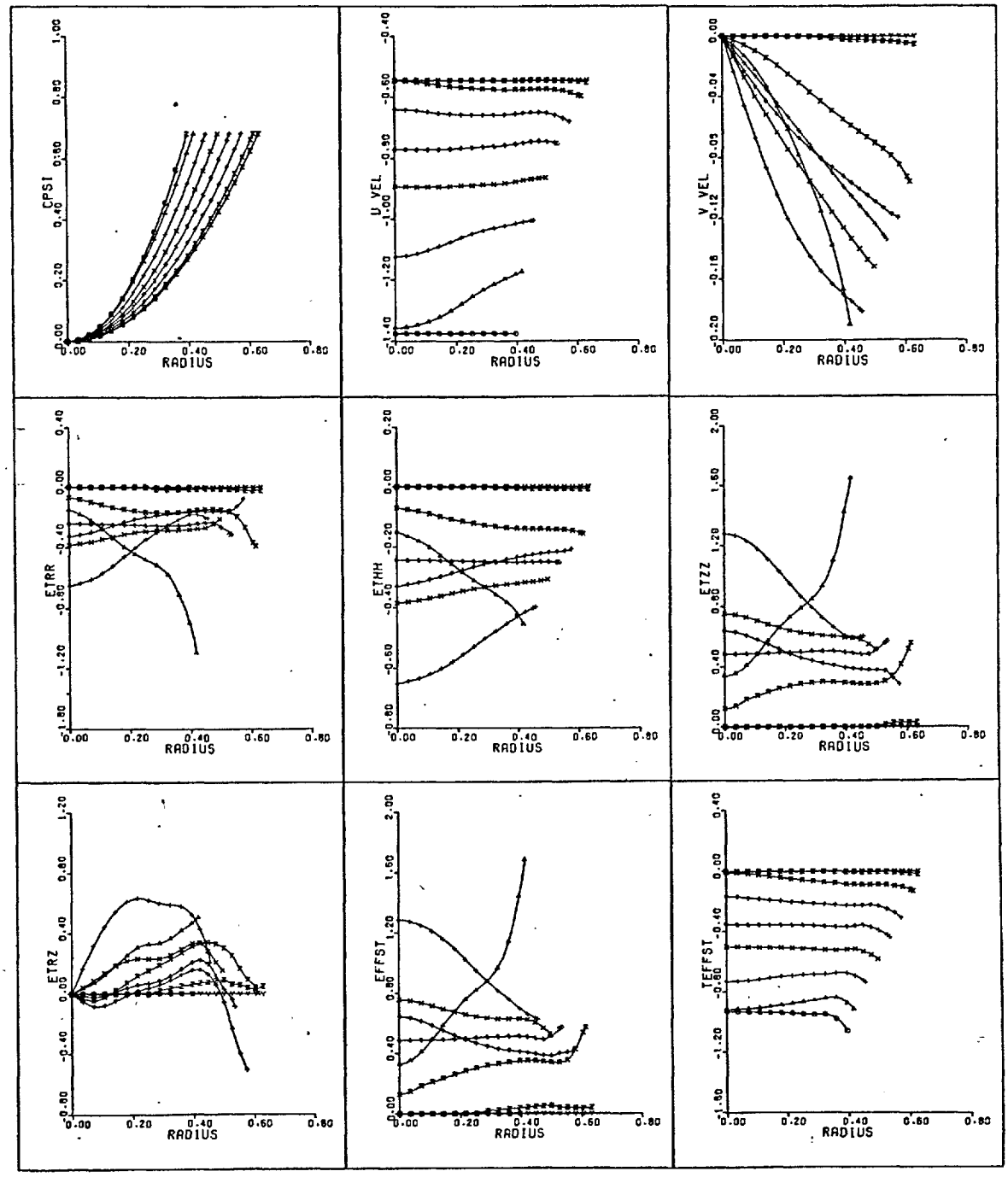

Fig.4.23. Extrusion no.10.

a very slight deformation before die contact was evident, but it was too small to be detected by the program. It can also be seen that the difference of axial velocity across the section is larger for 4 and 9 than for the other three extrusions.

Radial velocities are as expected given the axial velocity distributions described above. At each section where deformation is occurring, the radial velocity increases away from the centre line. In the entrance region where deformation is taking place, for example number 10, the rate of increase of velocity also rises. On the other hand, for number 9 the rate of increase falls in this region. In the figures the axial and radial velocities have negative values as flow is in the negative axis direction.

In the previous section, the change of slope of the flow lines was described. This explains the different shape of the radial velocity curve for K section 21 from that for K section 26. The sections referred to here are identified on Fig. 3.1. and the symbols on each line are shown in Table 4.2. along with the section to which they refer. Near the centre line the radial velocity is greater at K section 26 than at 21 for 10, say. As the radial velocity is calculated from the differential of the flow functions in the axial direction, this shows the flow is more nearly parallel at K section 21 than at K section 26.

4.2.3 Strain Rates and Total Strains

As eqs. 3.17 and 3.18 show, if the radial and hoop strain rates are the same at any point, then the radial and hoop stresses will also be the same. The assumption that the hoop stress is a principal stress and is equal to the radial stress is often made in analysing axisymmetric deformation problems. This is the Haar-von Kármán hypothesis. From the figures it can be seen that this is approximately true over the majority

of the deformation region but that large differences occur near the surface and near the exit region.

All three strain rates show a reduction near the centre line where the change of slope of the flow lines has occurred. Further they are all reasonably constant across the section except between sections 1 and 11. In this region the variations from the centre line, where deformation is ending, to the surface, which is still being heavily worked, are large.

The shear strain rate appears to be more sensitive to changing conditions than any of the other parameters, the shapes of the curves vary greatly from one extrusion to another. If we take as an example extrusion number 9 and extrusion number 10, the shear strain rate rises from the centre line to the surface, albeit with changes of slope for extrusion 9. For 10, however, the shear stress first becomes negative at several sections, then rises and falls again between centre line and surface.

Effective strain rate and total effective strain plots are very similar from one extrusion to another. The overall values are lower for, say, 10 than 9, taking into account the extrusion speed was higher for 10 than 9. Further, the difference in total effective strain across the product is smaller in 10 than 9 which indicates less work hardening has taken place at the surface in this case. In all the extrusions, the variation across the section is small, as would be expected for hydrostatic extrusion through a low die angle.

4.2.4 Stress Fields

The stress fields calculated from the strain rates and total strains described are given in Figs. 4.24 to 4.28. The first calculations were unsuccessful and produced erratic results. The shear strain rate was therefore smoothed in the R and Z directions. This did not alter the shape of the stress curves but it did reduce the range of stress across any section.

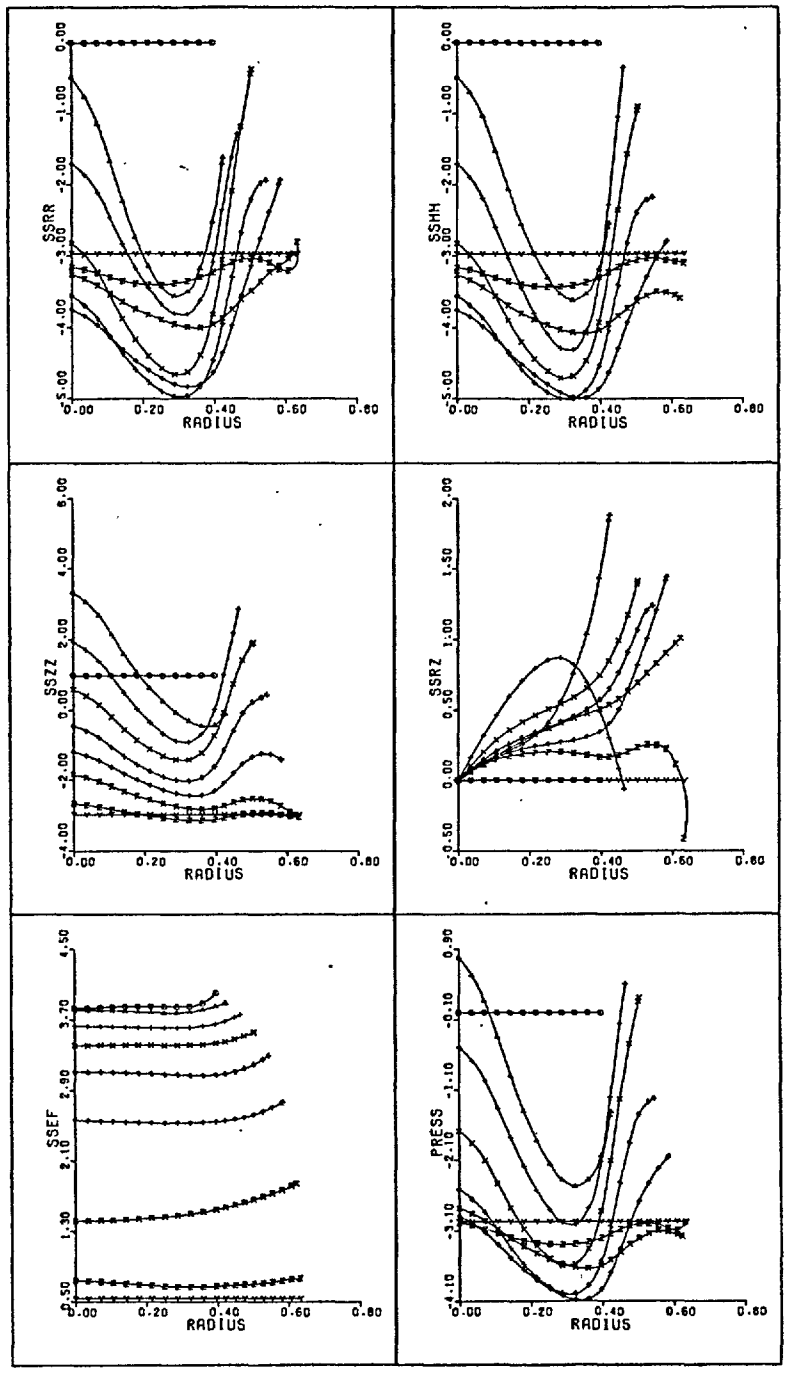

Fig.4.24. Extrusion no. 4.

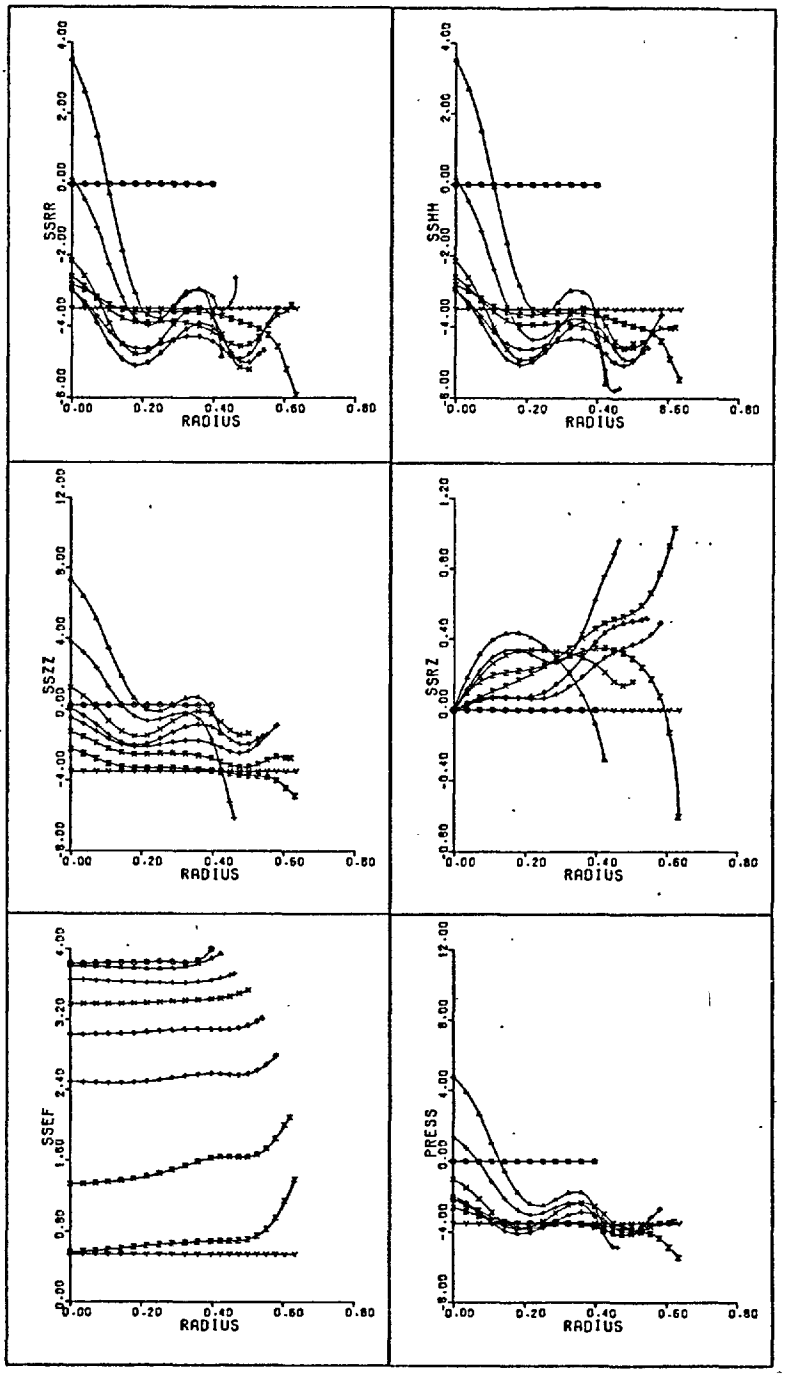

Fig.4.25. Extrusion no.6.

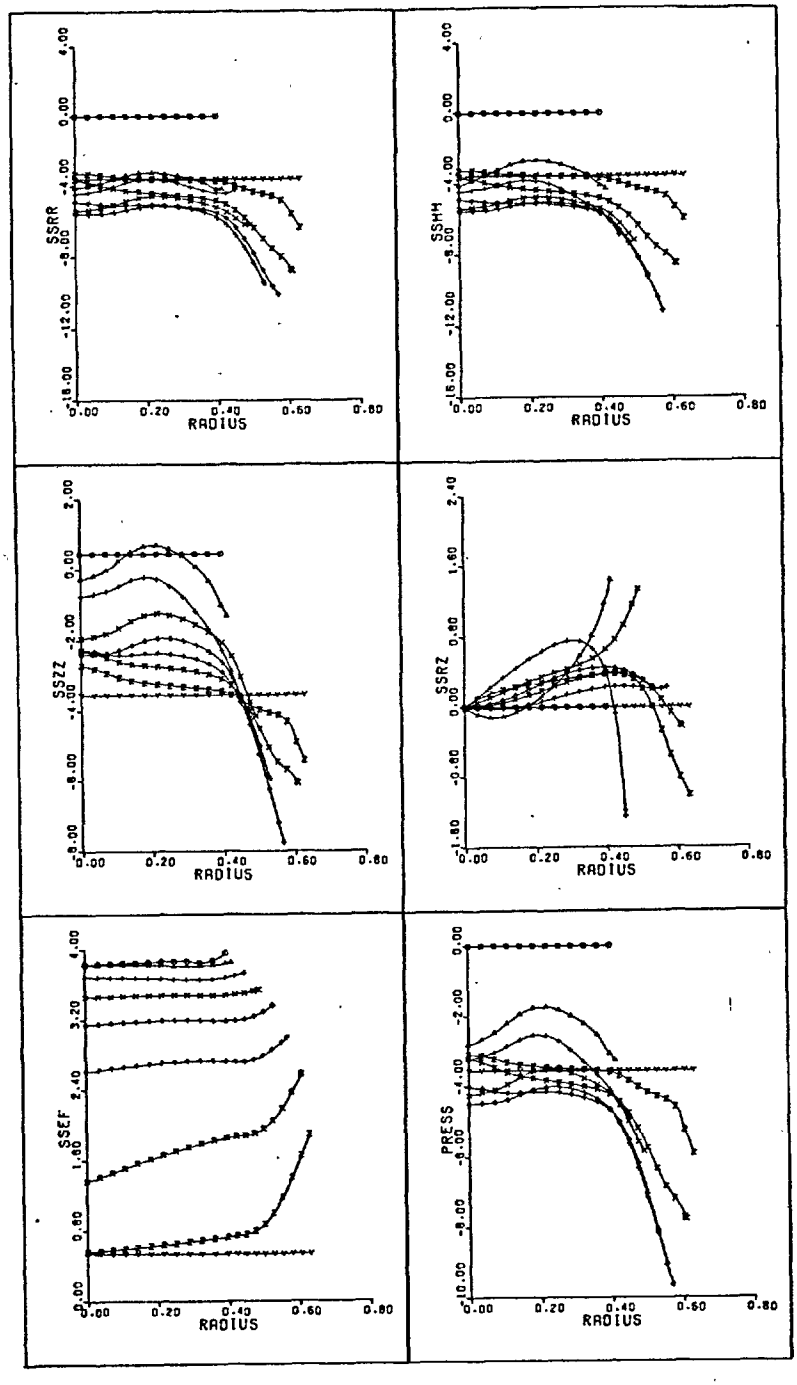

Fig.4.26. Extrusion no.8.

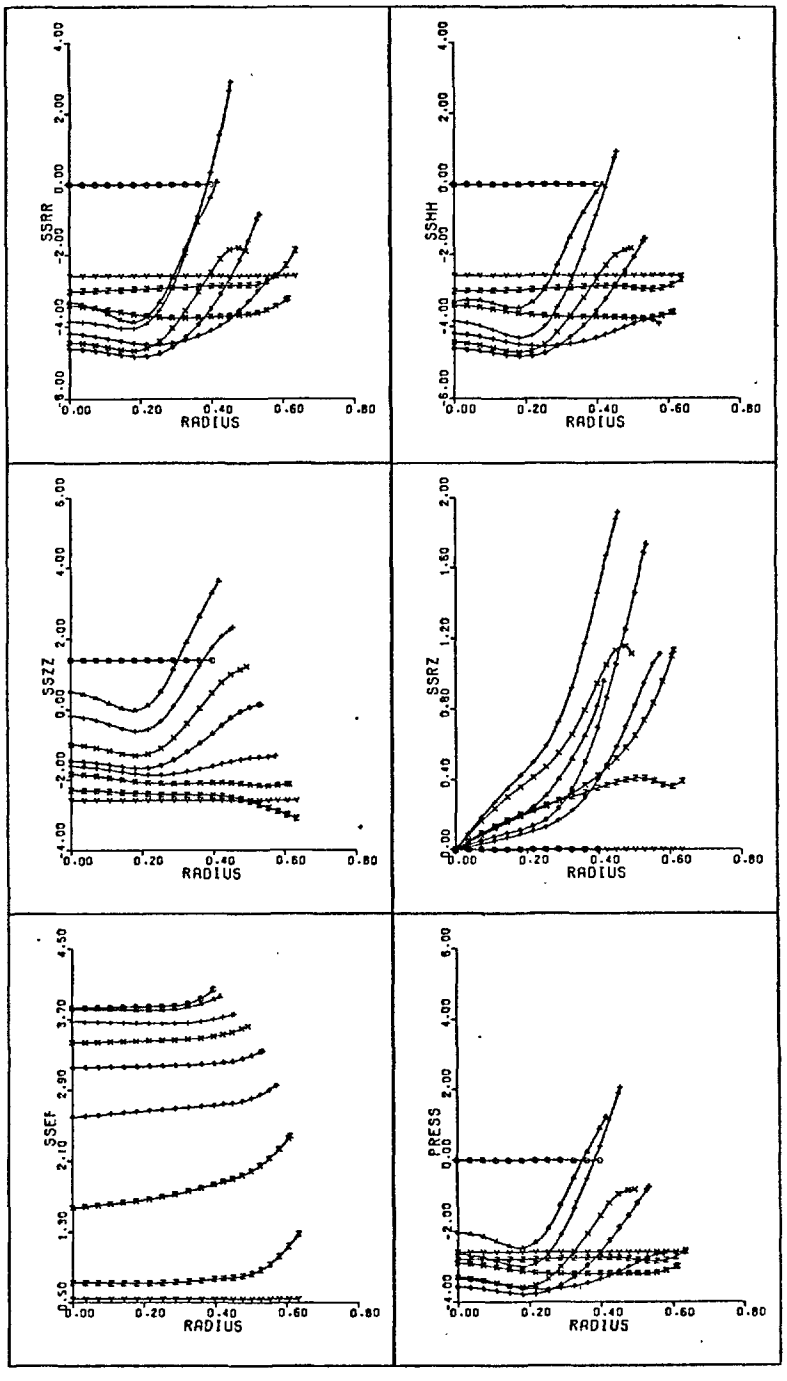

Fig. 4.27. Extrusion no. 9.

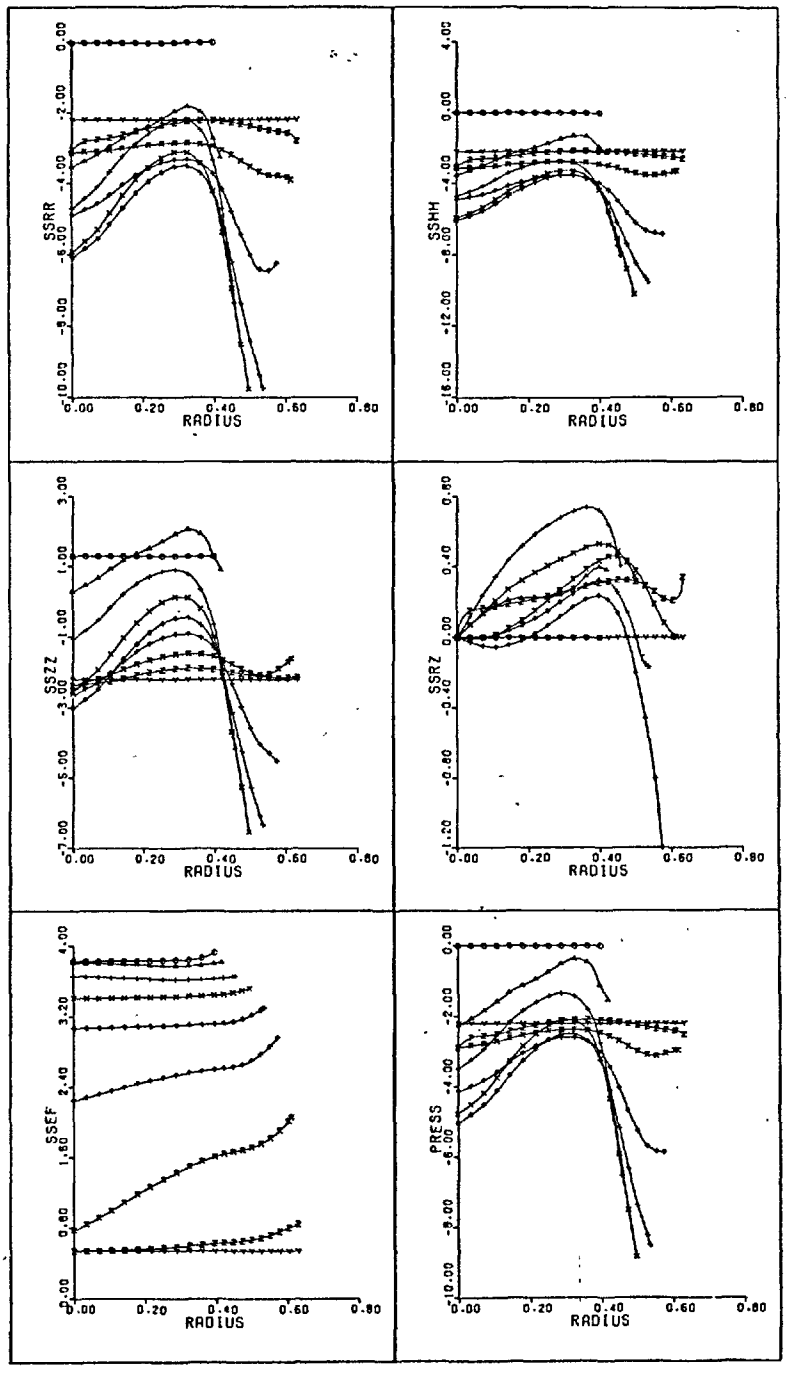

Fig. 4.28. Extrusion no. 10.

Values of the flow stress at the mesh points are found directly from the total effective strain and the stress-strain curve for the fully annealed copper used in the experiments, given in Fig. 4.29. It was found by the method of Cooke and Larke. For extrusions number 8 and 10, where the 'sinking in' effect before the die was reached was most prominent, there is considerable variation of flow stress across the section at entry to the die. As the material work hardens rapidly this is to be expected. By exit, the flow stress is quite uniform, as the stress-strain curve is very flat for natural strains of the order of 1.

With the flow stress and the known strain rates, the distribution of axial stress is calculated, and from this the actual values by equating the integrated axial stress at exit to the drawing load. It can be seen from the figures that this procedure gives a good estimate of the extrusion pressure as the values of radial, hoop and axial stresses are nowhere far from the experimental extrusion pressure, shown as a horizontal line in the region before deformation starts.

However, it is also apparent from the figures that the change of stress across each section is too large. This is due to inaccuracies in calculating the shear strain rate, which, according to eq. 3.20, is used to calculate the distribution of axial stress along lines of constant radius. As the shear strain rate is equal to the change of axial velocity in the radial direction plus the change of radial velocity in the axial direction, both small quantities, small errors in the velocity field will be magnified, after numerical differentiations, in the stress field. It is therefore necessary that the smoothing procedure be refined to give better values of the shear strain rate.

The inaccuracies in the stress fields meant that no useful values of local coefficient of friction could be found, nor could the hydrodynamic theory be used to calculate a hypothetical film thickness. As the previous

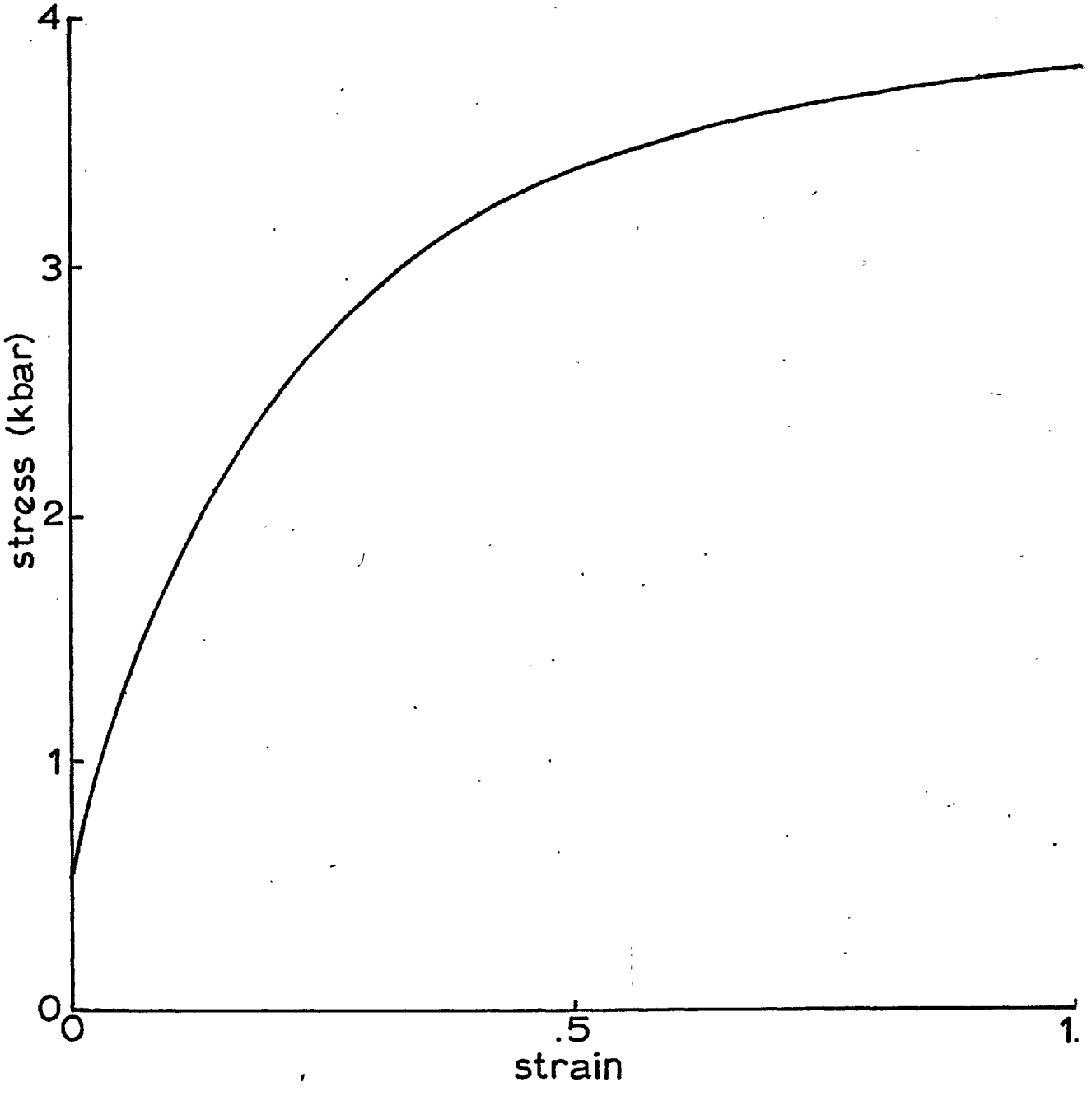

Fig. 4.29. Stress - strain curve for copper.

discussion has shown there was no fluid film over the die face, this is not important.

However, in all cases, the die pressure profile calculated is of the same shape. The profile for extrusion number 6 is given as typical in Fig. 4.30. This shows that the die pressure first rises as the billet starts to deform. After the initial sharp rise the die pressure falls then rises to a maximum of 5.78 kbar before falling to a value 4.18 kbar at exit. At this section the die pressure should be approximately the yield stress of the material minus the drawing stress applied, or, in this case about 3.8 kbar. Thus it would seem that the die pressure in this case is in error by about 8%.

For the other extrusions the scatter of points on the die pressure curve was larger, although, as stated above, they were the same shape. However, the results of Alexander and Kamyab (99) show a die pressure for a free hydrostatic extrusion, of the same geometry, in which the pressure is at first very flat and equal to the extrusion pressure plus the initial flow stress of the material and then falls smoothly to the exit pressure, which is equal to the final yield. They do not find the intermediate fall and rise of pressure found here.

Theoretical calculations of the die pressure distribution, such as that given by Duffill, Hooke and Mellor (163), suggest a die pressure falling from a maximum at the entry section, in the manner found by Alexander and Kamyab. The actual rate of fall would depend on the extrusion ratio and the work-hardening characteristics of the material.

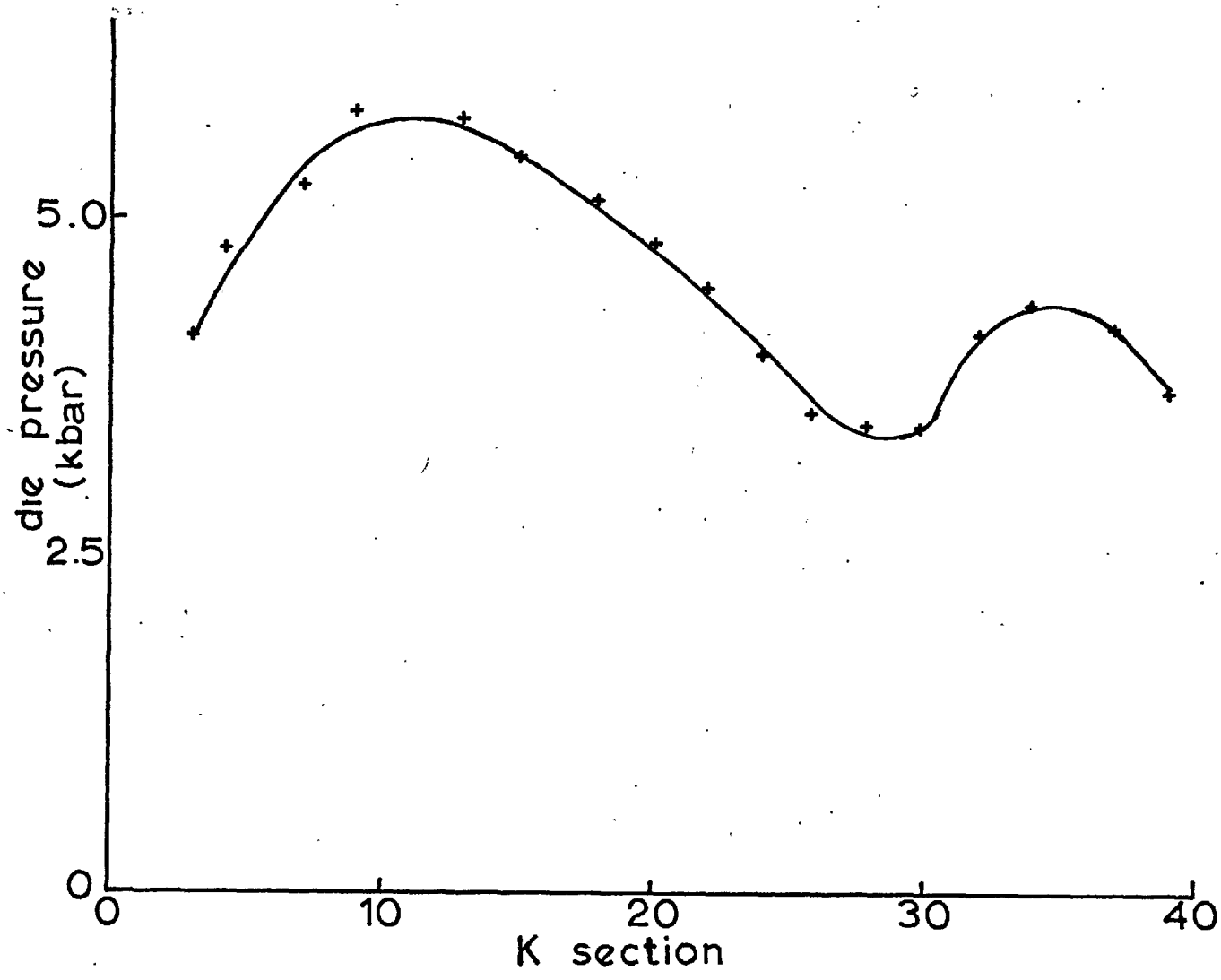

Fig.4.30. Die pressure profile for extrusion no.6.

Chapter 5. Discussion

5.1 Conclusions on the Present Work

As stated in Chapter 1 the basic aim of this work was to define a method by which lubricants could be evaluated for use in metal-working processes, with particular reference to hydrostatic extrusion. To be successful the method should be able to distinguish between small changes of frictional conditions. The various measurements which have been taken during the experiments will now be considered and their sensitivity to changes of friction discussed.

5.1.1 Driving Stress

The use of the extrusion pressure as a criterion to grade fluids and lubricants in hydrostatic extrusion was mentioned in section 1.1.5 and the results of Lowe and Goold (97) and Fiorentino, Sabroff and Boulger (94, 95) quoted. The difficulty here is that random variations, for instance in the material properties, can easily obscure the effect which is being considered.

In the present tests the high pressure which was applied when a petrol-univis mixture was used as the extrusion fluid was sufficient evidence that this fluid had very poor lubrication properties. Also, the single extrusion at higher speed showed a much lower combined driving stress than the other extrusions, which indicates lower friction.

On the whole, however, it is not possible to draw firm conclusions from the graph of extrusion stress versus drawing stress in Fig. 4.3. It can only be said that extrusions with molybdenum disulphide grease as lubricant required higher driving stresses than those from the castor oil or Tellus 27 without lubricant. The scatter of these results also casts doubt on the method of assuming an upper bound solution and then calculating the coefficient of friction to match an experimental pressure. In

any case, this would lead to low value of coefficient, due to the upper bound nature of the solution.

5.1.2 Surface Finish Measurements

It is well known that the surface of the product when hydrodynamic lubrication conditions exist is much worse than under boundary lubrication when no pick-up occurs. The 'bamboo effect' has been mentioned where the product has alternate portions of large diameter and bright surface finish followed by smaller diameter, rough portions.

Surface profiles in Figs. 4.4 to 4.9 show that the product is, without exception, smoother than the billet. Hence, full film lubrication is ruled out, although the possibility of a hydrodynamic component at die entry is not. However, the profiles also show that far less burnishing occurred when molybdenum disulphide grease was used.

There are two possible explanations for this phenomenon. Firstly, the highly viscous grease could have been entrained into the billet die interface in machining marks on the billet. Secondly, it is possible that the solid particles of molybdenum disulphide became embedded in the surface of the copper by the high normal pressure. The first explanation seems more likely and is borne out by the fact that the surface is rougher for the higher speed and by visual inspection, which showed the marks on the product were in the radial direction.

Thus the surface finish of the product can indicate whether boundary or full film lubrication has been operative, or if lubrication has broken down altogether. The variations within the region of boundary lubrication are not large enough to form a sensitive indication of the quality of the lubricant.

5.1.3 Hardness Measurements

As stated in section 4.1.24 no variation in hardness could be found across the section of the product. Referring to the mean effective stress

shown in Figs. 4.24 to 4.28 it is hardly surprising that no variation could be detected, as the variation of stress across the section is a maximum of 6% for number 9.

The results of Alexander and Kamyab where hardness was measured over the whole deformation zone are shown in Fig. 5.1. The contours, which are for a free extrusion of the same geometry and material as the experiments detailed here, again show that the material has work hardened more at the outer fibres at entrance to the die. However, the number of measurements necessary to get realistic contours is large and the procedure extremely time consuming. It was not carried out as a method of comparison therefore.

5.1.4 Strain Fields

Of all the parameters considered to judge the quality of different lubricants the velocity, strain rate and strain fields are by far the most sensitive to variations of frictional conditions. The fields obtained have been given in Figs. 4.19 to 4.23 and are described in sections 4.2.2 and 4.2.3. These results can be used to assess the dependence of the operative friction on the other conditions of extrusion.

5.4.41 Variation of Friction with Speed

The single high speed extrusion, number 10, may be compared directly with extrusion number 9 which was carried out in otherwise similar conditions. From the axial velocity and strain fields, the iso-time lines and constant strain contours are calculated and plotted in Figs. 5.2 and 5.3.

It can be seen immediately from these figures that the deformation pattern is very different in these two extrusions. The boundary at which extrusion starts is nearly plane transverse for number 9 whereas for number 10 it is curved in the opposite direction to that normally assumed for upper bound solutions. This finding is substantiated by the estimated

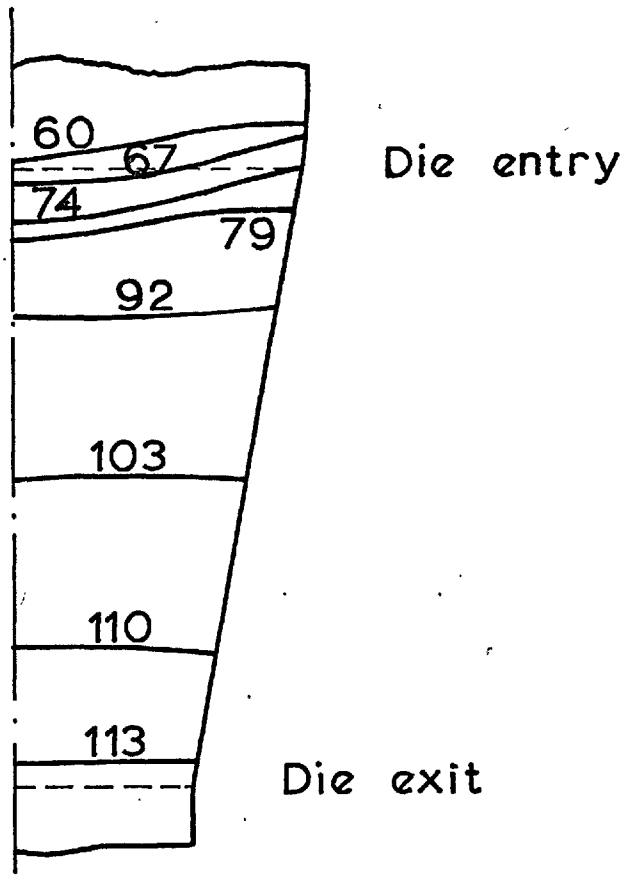

Fig. 5.1. Hardness contours in deformation zone.

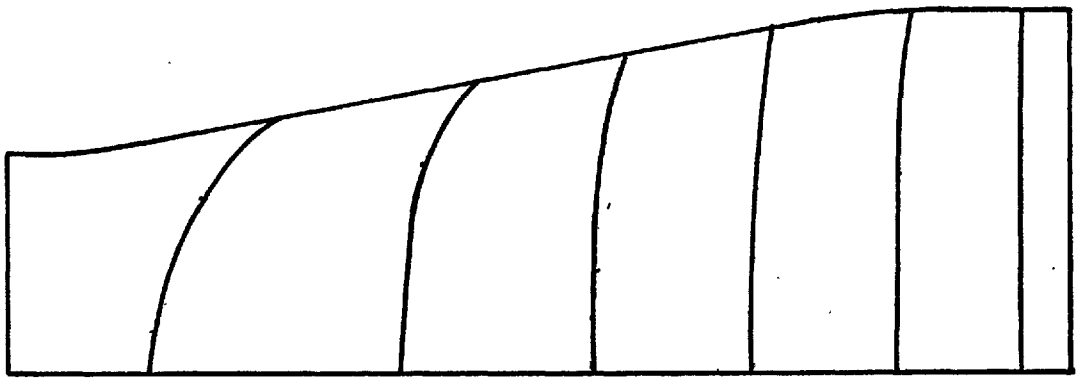

Extrusion no. 9.

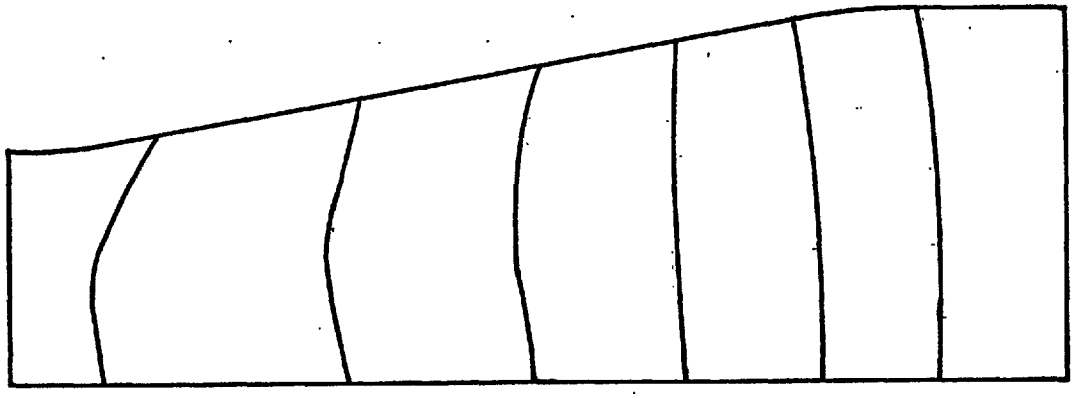

Extrusion no. 10.

Fig. 5.2. Iso-time contours.

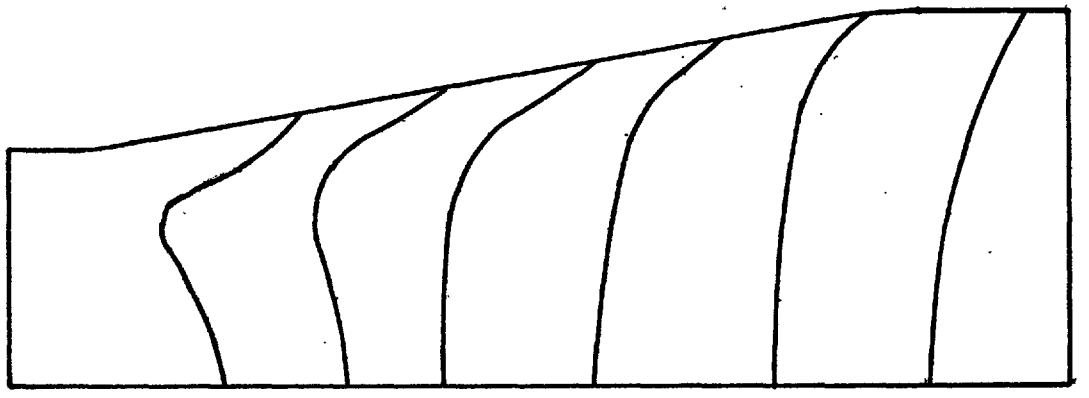

Extrusion no. 9.

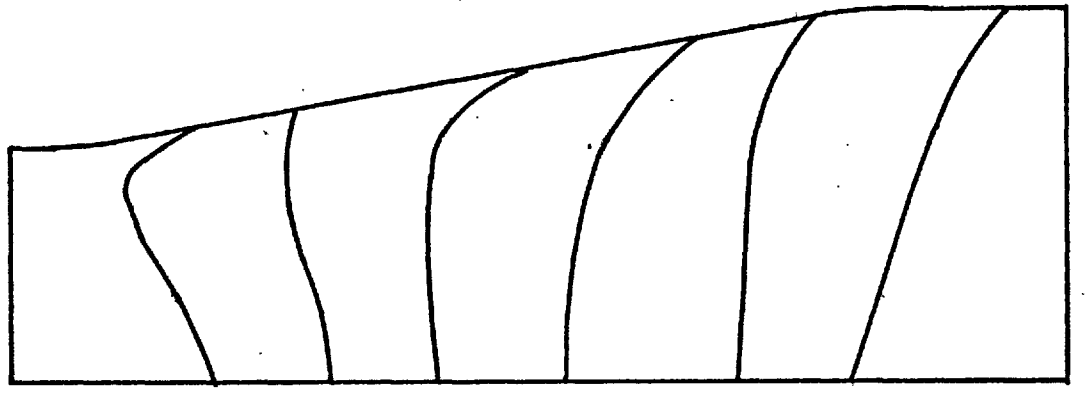

Extrusion no. 10

Fig. 5.3. Iso-strain lines.

boundaries, Fig. 4.18, the roughening of the plane of the split, Fig. 4.17 and the hardness results of Alexander and Kamyab, Fig. 5.1.

As the effect becomes much more pronounced at high speeds, this suggests that it is due to a hydrodynamic build up of pressure by the flow of fluid into the wedge formed by the billet and the die. Solving Reynold's equation for this geometry, assuming contact between the billet and the die with no flow of lubricant, yields the result that the pressure build up would be infinite. In fact a certain amount of lubricant is entrained and the material yields to relieve the pressure build up.

This explanation also agrees with the surface finish measurements, which indicated more pockets of lubricant on the product and hence a greater lubricant flow rate. To cause this, the pressure build up must have been larger than for the slower speed extrusion.

The velocity fields for extrusions 9 and 10 are replotted in Figs. 5.4 and 5.5 in a graphic manner. It can be seen from these distributions that for extrusion number 10 there is much less variation of axial velocity across the section. For the higher speed extrusion the region in which the surface velocity is greater than that at the centre, extends some way into the die zone. With extrusion number 9 however, the surface fibres are everywhere retarded, the frictional effect being much larger in this case. Even near the exit section, the axial velocity varies less across the section for extrusion number 10.

Figs. 5.6 and 5.7 show distributions of effective strain rate and total effective strain. Again it can be seen that there is smaller change of strain across the product in the higher speed extrusion. The strain rate plots show the effect of the change of slope of the flow lines in the deformation region described in section 4.2.1. It is more marked in number 10, where the strain rate along the centre rises at first, then falls and rises again until the exit is reached, where it falls to zero. The first fall in strain

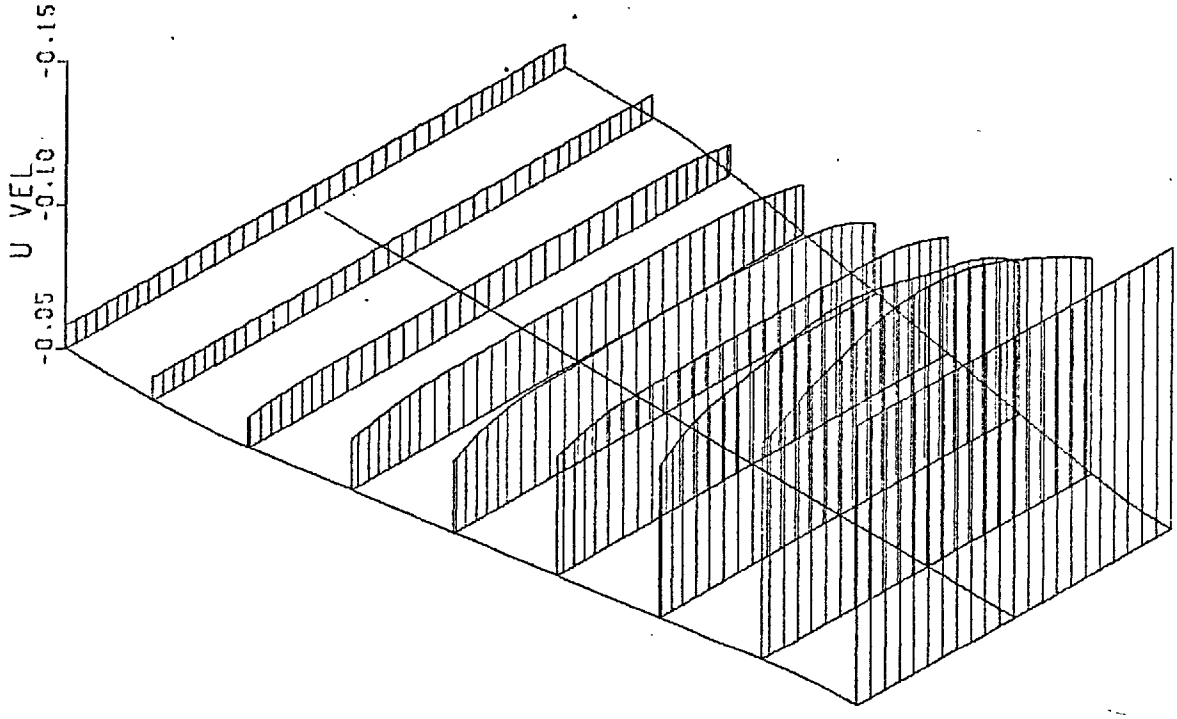

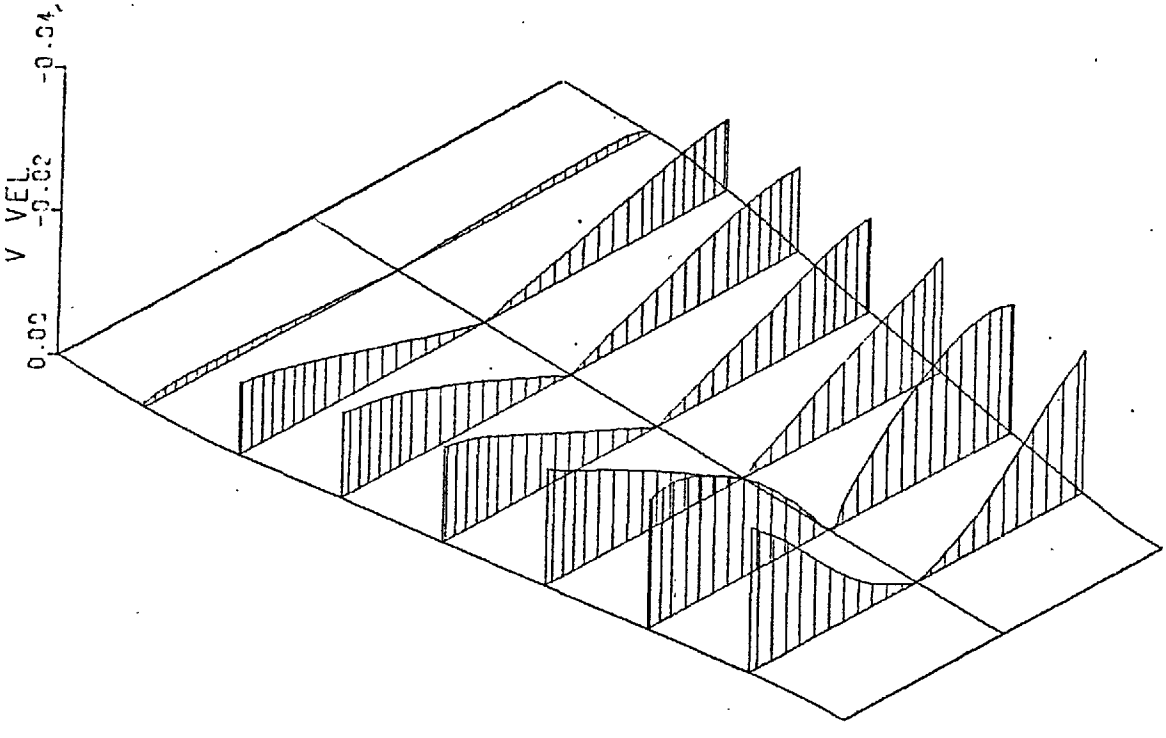

Fig. 5.4. Velocity fields for extrusion no. 9.

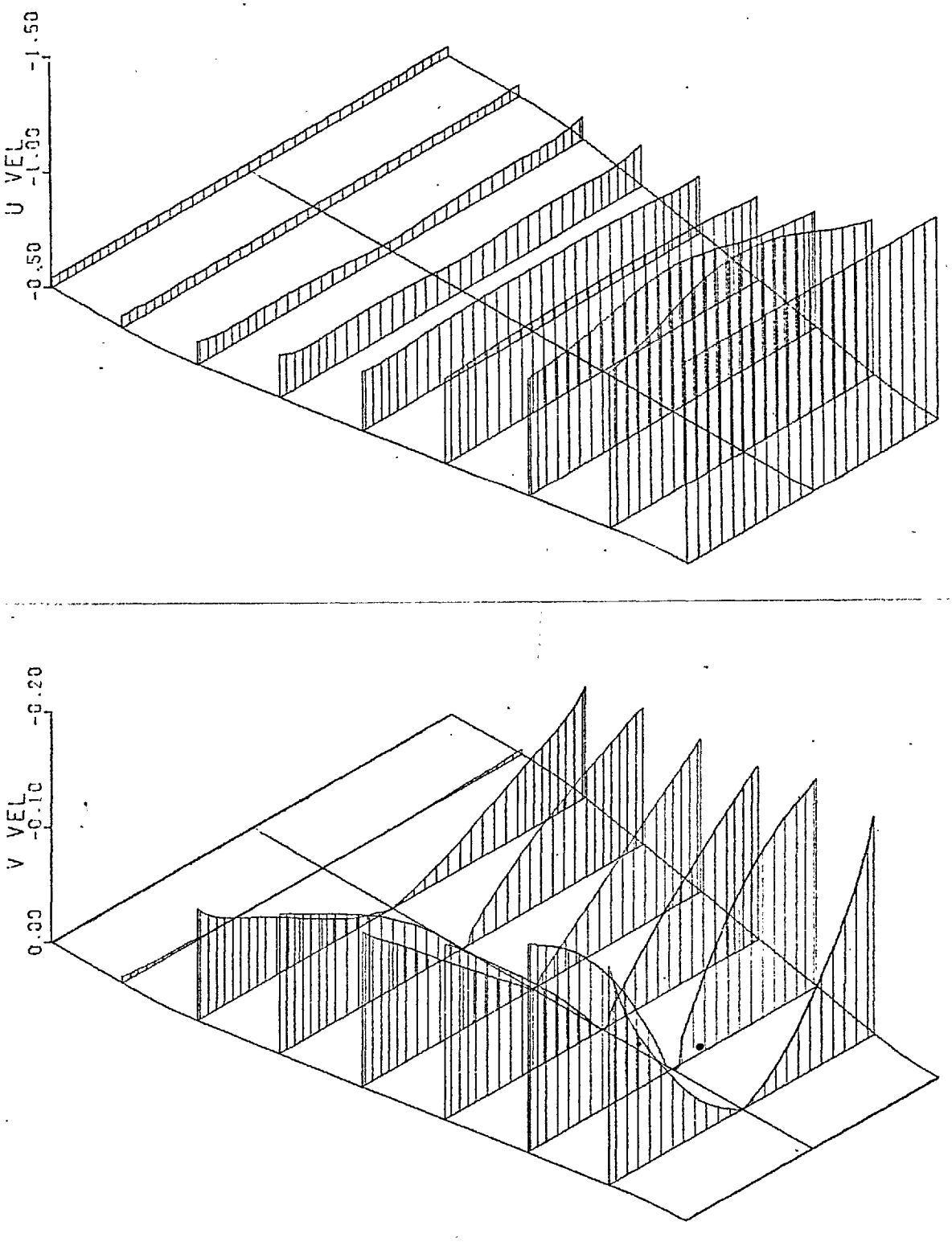

Fig. 5.5. Velocity fields for extrusion no. 10.

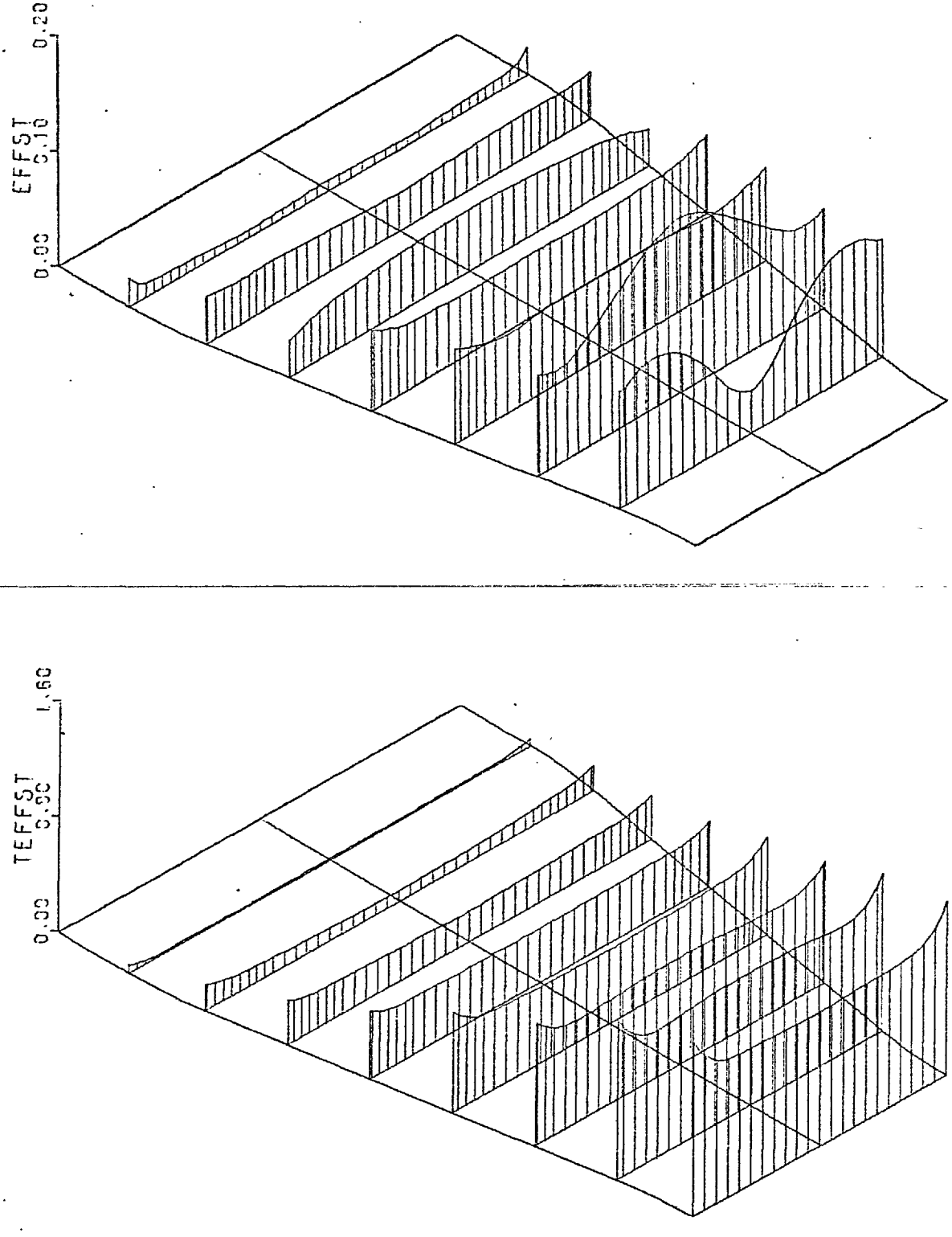

Fig. 5.6. Strain fields for extrusion no. 9.

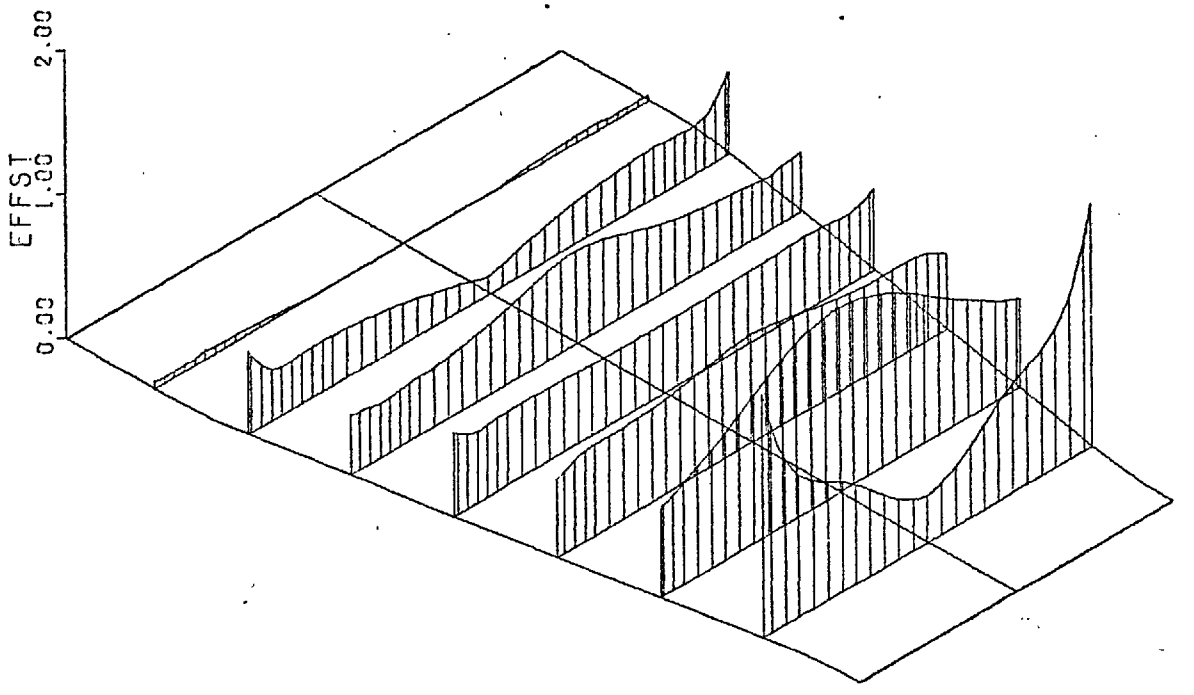

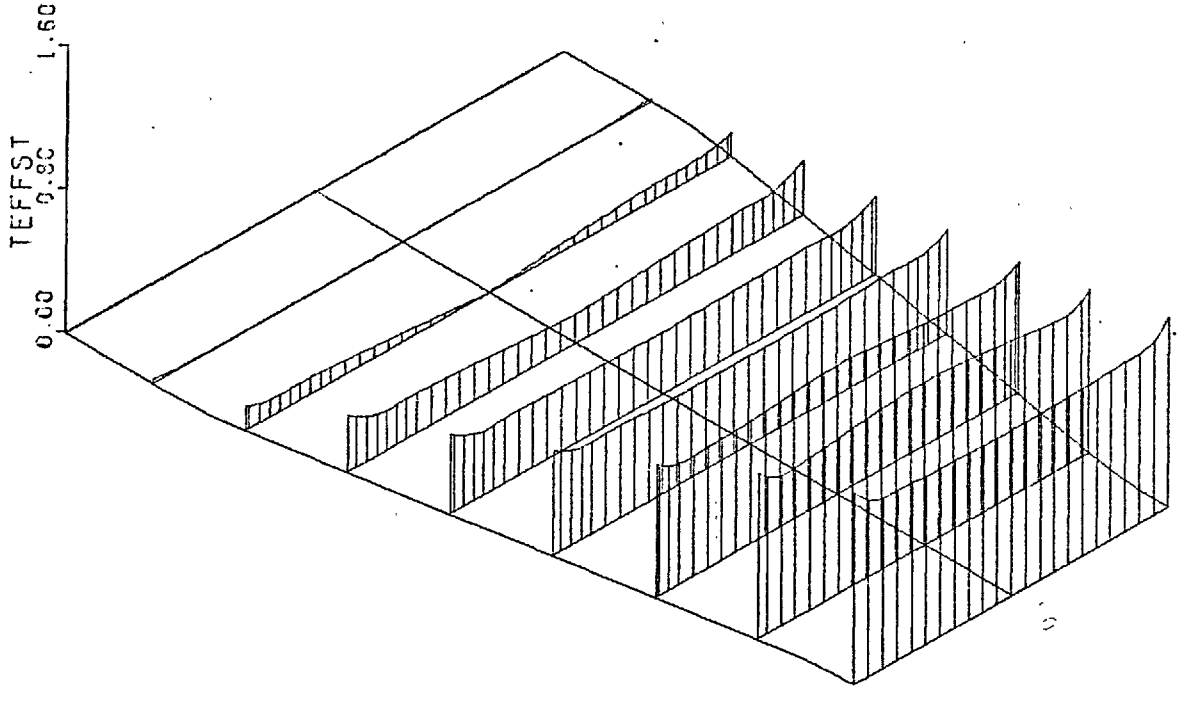

Fig. 5.7. Strain fields for extrusion no. 10.

rate corresponds with the position where the slope of the flow lines decreases.

Thus the visioplasticity analysis shows that the friction is lower over the whole die face for the higher speed extrusion. It also shows that the build up of pressure before the die causes deformation before the die. This explains the lower friction as there is a greater lubricant flow rate and this entrained lubricant is effective in reducing friction.

5.1.42 Variation of Friction with Extrusion Stress-Drawing Stress Ratio

To see the dependence of friction on extrusion stress-drawing stress ratio, we must consider two extrusions for which the other conditions were constant. In this case we may compare extrusions 8 and 9.

Here deformation before the die has again occurred for extrusion number 8 which was extrusion orientated, unlike number 9 which was at much higher drawing stress. When the drawing stress is high, the extrusion pressure is, of course, correspondingly lower. Thus to cause an initial yield before the die the build up of pressure by the hydrodynamic effect would have to be larger by, approximately, the amount of the drawing stress.

As in the previous section, the velocity and strain rates may be compared to show the variation of friction over the die surface. With the extrusion at lower drawing stress the build up of pressure is sufficient to cause yielding. This again reduces the friction coefficient, as is evidenced by Figs. 4.21 and 4.22, where the deformation is shown to be more uniform for extrusion number 8 than for number 9. Further the shear strain rate plots show that this parameter becomes negative at the points where the slope of the axial velocity curve is negative in extrusion number 8. This does not occur for extrusion number 9.

Considering the total strain distribution, it can be seen that there is less variation of total strain across the product for low drawing stress

extrusion, number 8. Also, the mean value of total strain and the total strain along the centre line are smaller for number 8 than number 9, which indicates that the redundant strain is smaller in this case. The smaller redundant strain must be attributable to lower coefficient of friction as other parameters were the same for the two extrusions. This is consistent with the distributions described above.

It should be stated that this result, namely that friction is lower in extrusion orientated processes, is at variance with the results of Parsons, Bretherton and Cole (50). Their results, plotted in Fig. 5.8, which were obtained with a strain gauged die, show that the mean coefficient increases with increasing extrusion stress.

5.1.43 Variation of Friction with Fluid and Lubricant

The comparison here is complicated by the fact that the single extrusion from Tellus 27 was at higher drawing stress than comparable ones from castor oil and castor oil with molybdenum disulphide grease. In view of the previous discussion the higher friction due to the higher drawing stress may be obscuring lower friction due to the fluid effect.

Comparing the velocity fields in Figs. 4.19, 4.20 and 4.21 shows that for the extrusion from Tellus 27, no deformation occurs before the die and that the central portion of the billet starts to deform first. As the Tellus 27 is less viscous than in the other two cases and the extrusion stress is lower, this is to be expected. Throughout the deformation region, the flow is more uniform for extrusions 6 and 8, than 4, as is evidenced by the shear strain rate plots, but the effect is not large.

Using the strain across the product to judge the effectiveness of the fluid in lubricating the deforming surface, shows there is less variation of strain across the section for extrusion number 8 than for 6 and 4, and that the mean strain for extrusion number 6 is marginally lower than for number 4. Thus, this method of grading shows that the molybdenum

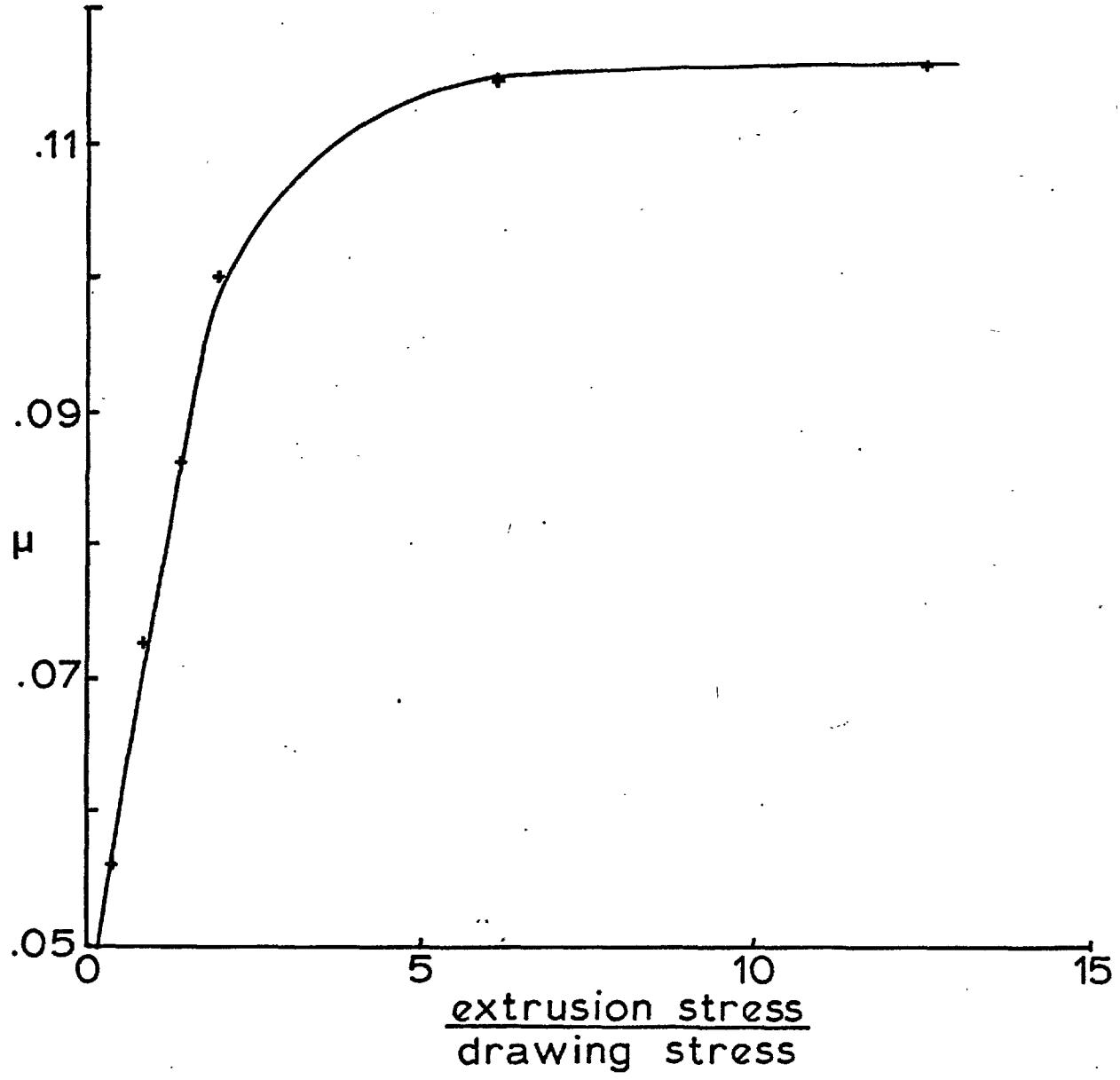

Fig.5.8. μ vs. extrusion stress - drawing stress ratio.

disulphide grease gives a lower coefficient of friction than castor oil, which in turn gives a lower value than Tellus 27.

The difference between the three conditions is, however, very small. It is therefore, hardly surprising that they could not be placed in this order simply by measuring the combined driving stress causing extrusion. The use of the visioplasticity analysis to compare the conditions is sufficiently sensitive to distinguish between the small changes of coefficient of friction, however.

5.1.5 Stress Fields

As stated in section 4.2.4 the change of stress across any K section, is too large, resulting in unreliable stress components near the surface. Nevertheless, the stress patterns show consistency with the results above. For the extrusions where friction was lowest, numbers 8 and 10, the axial stress across the section rises from the centre line, reaches a maximum and then falls off to the die surface. For those where friction is higher, for example number 4, the axial stress falls from the centre line value, then rises again.

These differences can be explained in terms of differences of the shear strain rate, which can in turn be related to the different velocity fields. Approaching the exit section the values of $\frac{\partial V}{\partial Z}$ become negative. Where the friction is low, the values of $\frac{\partial U}{\partial R}$ are also low and positive as there is less change of axial velocity across the section in this case. Thus the shear strain rate can become negative near the centre line sections near exit. This results in the variations of shear strain rates on which comment has been made. While it is not immediately obvious from these distributions and eq. 3.21, it is this effect which causes the different shapes of the axial stress curve across the section. Hence the stress curves could also be used to judge the suitability of a lubricant

but, in practice, they have no advantage over the velocity and total strain curves, where the effect of friction is easier to visualise.

Incidentally, the results above show the difficulty in using coefficients of friction in metalworking processes. It has been shown that in the present case the effect of a speed increase or an increase in drawing stress is much larger than the effect of using or not using molybdenum disulphide as a lubricant. Hence, a single coefficient cannot be defined for a given lubricant and materials and it would seem that a coefficient can only be defined by experiment on the actual geometry for which information is required.

5.1.6 Physical Properties

As the extrusions carried out were under predominantly boundary conditions, the physical properties measured do not help in assessing lubricant quality. Results of tests of this type are nonetheless useful in the design of apparatus and the selection of a fluid which does not freeze in the pressure range to be considered.

If the conditions are favourable for hydrodynamic lubrication, the pressure-viscosity-temperature characteristics of the fluid would then be essential for an analysis. In the present case it can be said that as the castor oil is more viscous than Tellus 27 at pressures below approximately 4.5 kbar, it will cause a greater 'sinking in' effect in this range. Above this pressure the Tellus 27 is more viscous, as it has a much higher pressure coefficient of viscosity.

5.2 Summary of Conclusions

1. The flow patterns found by experiment show that the flow is not radial towards the apex of the conical surface of the die, as the flow lines are not straight, even in the region removed from the deformation boundaries.

2. Visioplasticity analysis can be used to provide a more sensitive indication of changes of frictional conditions than has previously been possible.

3. In essence, the results of this analysis show:

a) friction forces decrease with increasing extrusion stress-drawing stress ratio.

b) frictional forces decrease with increasing speed.

c) molybdenum disulphide grease with castor oil gives the lowest friction followed by castor oil then Tellus 27. The difference between these is marginal, however. Petrol and univis mixture is unsuitable as an extrusion fluid.

4. The falling weight viscometer can be used to very high viscosities encountered with oils at high pressure.

5. Sinkers with central holes and no guide pins are usable over a larger range than those without central holes. They have the further advantage that when sinkers of materials different from the tube are used, the pressure change of viscometer constant is much smaller.

5.3 Suggestions for Future Work

As originally designed, the drawbench would have been used with the high pressure vessel built for the viscosity experiments. By combining these two pieces of apparatus, extrusion-drawing experiments could be performed under much higher driving stress and the forming of high strength materials investigated.

Further extrusion experiments could be carried out at high speed, preferably with product augmentation as this enables the speed to be controlled. The 'sinking in' effect and the conditions for full-film lubrication, could then be evaluated using the programs described.

New methods of smoothing could be tried in the computer programs to see if more accurate values of stresses can be calculated without losing the characteristics of the flow fields. These programs could also be extended to calculate the temperature distribution during the extrusion. For high speed extrusions, the effect of strain rate and temperature rise on the flow stress could easily be incorporated in the program as it stands.

The viscometer is operational and could be used to investigate the viscosity and compressibility of fluids over the range 0-30 kbar and 15-100^{o}C. Modifications which are necessary are the improvement of ambient temperature control and possibly the redesign of the plunger to take a different type of seal. To date the present sealing arrangement has been used to 22 kbar.

Finally, it may be necessary to know the thermal properties of the fluid, conductivity and specific heat, for use in high speed, hydrodynamic theory. It would also be interesting to investigate the properties of grease under pressure, as these can be important in producing hydrodynamic effects where the grease was only intended as a carrier for a solid lubricant. Both of these investigations would require the assembly of new apparatus.

APPENDIX I

A1.1 Stress Calculations for the First Cylinder Design

This design consists of a thick-walled tool steel liner with an auto-frettaged support ring of EN30B with an overall K ratio of 15. After a trial and error method, the optimum geometry was found to be a tool steel liner with a K ratio of 3, the support ring therefore having a ratio of 5.

Solving Lamé's equations for the liner, under load, with the boundary conditions $\sigma_{r1i} = -23$ kbar and $\sigma_{\theta 1i} = 0$ gives a radial stress at the external surface, σ_{r1O}, of -13 kbar. This is the pressure which must be carried by the outer ring.

To find the position of the elastic-plastic interface, the EN30B was assumed to be perfectly plastic with a shear yield stress of 6.95 kbar. Further the Tresca yield criterion was assumed to apply and the deformations assumed small, so the problem is statically determinate. On these assumptions, the diameter ratio of the elastic-plastic interface can be found from

$$\frac{p_{2i}}{k_2} = 2 \ln K_c + \left(1 - \left(\frac{K_c}{K_2}\right)^2\right) \qquad \text{A1.1}$$

This cannot be solved analytically but, for the known values of K_2 and k_2, values of p_{2i} corresponding to different values of K_c were calculated. From a graph the value of K_c corresponding to an internal pressure of 13 kbar was found to be 1.6.

The residual stresses are calculated on the assumption of elastic release of pressure. Franklin and Morrison (A.1) have shown that this leads to an overestimate of the residual stresses but, in view of the previous assumption of constant shear yield stress this is not important here.

The approximate radial, hoop and shear stresses, calculated on these assumptions, are given in Fig. 2.15.

Using eq. 2.2, section 2.3.23 and the following values of Young's Modulus and Poisson's Ratio, the relative interference was found to be 4.56×10^{-3} cm/cm.

$E_1 = 2280$ kbar, $\nu_1 = 0.31$ } For tool steel.

$E_2 = 2070$ kbar, $\nu_2 = 0.29$ } For EN30B.

If we further assume that the vessel will be assembled by push fit, on an included angle of 2^o, and that the sliding contact is well lubricated, so that the coefficient of friction is of the order of 0.1, we can calculate the assembly force.

$$F = \pi \ell D_{10} p_{r10} (\mu \cos \alpha + \sin \alpha) \qquad \text{A1.2}$$

where p_{r10} is the residual interface pressure. This gives, for the present case, F = 19.5 MN (1,960 tons).

A1.2 Stress Calculations for the Second Cylinder Design

Using the graphical optimisation technique described by Bett and Burns (A2) the optimum design of a four component system was with the two inner cylinders of high speed tool steel, both with diameter ratio 2, and the two outer cylinders of EN30B, both of diameter ratio 1.94. This gives the overall ratio of 15. Graphical representation of the stresses is given in Fig. A1.1 and, plotted against radius, in Fig. 2.16. The derivation of Fig. A1.1 is explained below.

In Fig. A1.1 the stresses are plotted against m^2, which is defined as $(D_{40}/D)^2$, as this produces straight line plots. Firstly, the design

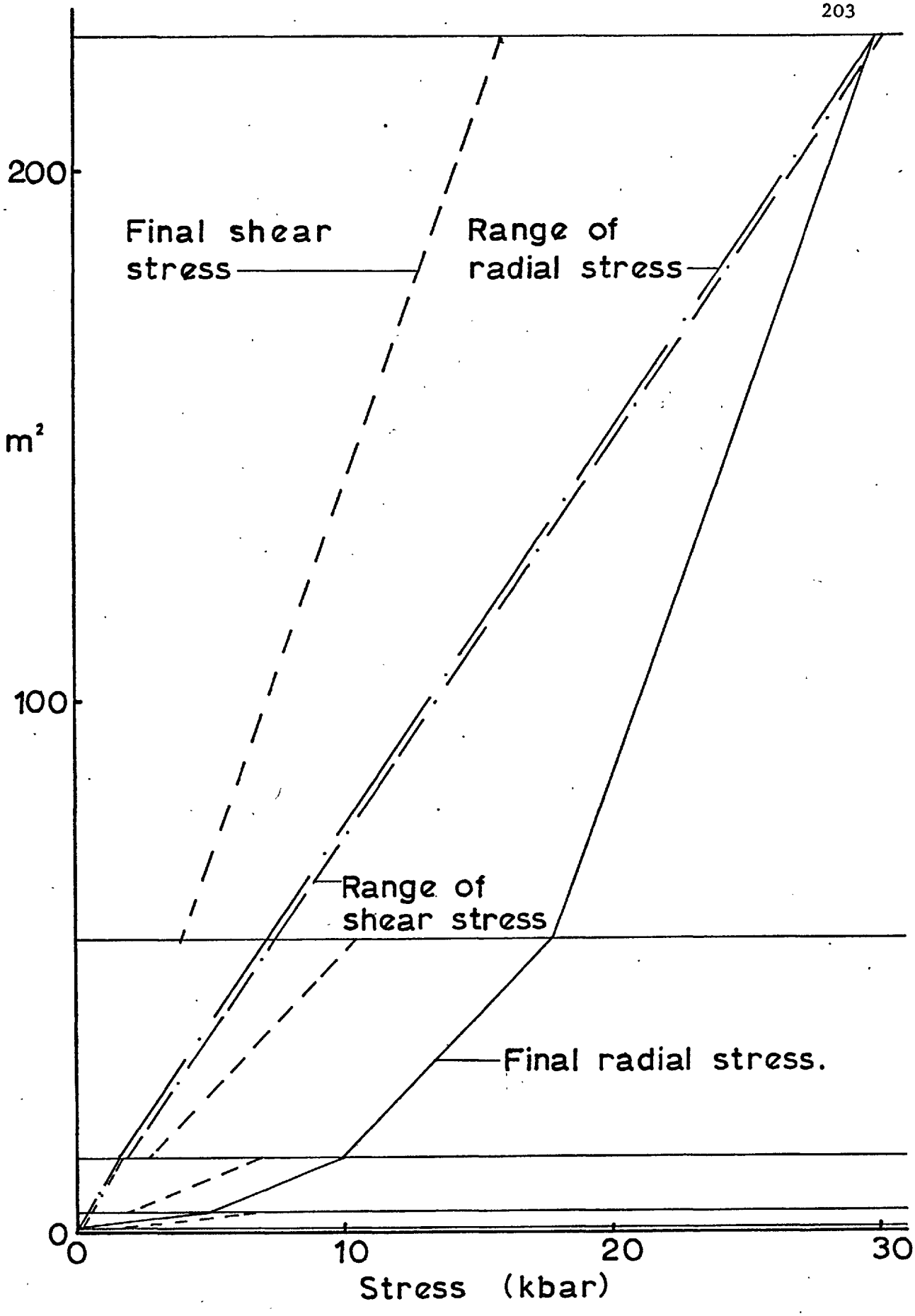

Fig. A1.1. Stress distribution for optimum four component design.

pressure for the bore, -30 kbar, is marked off, as this equals the final bore radial stress. Also the final shear stress at the bore, 16 kbar for the high speed steel, can be marked off as the maximum which the material can withstand. The final shear stress, τ, for any cylinder is given by

$$\tau = \frac{\sigma_\theta - \sigma_r}{2} = \left(\frac{p_i - p_o}{K^2 - 1}\right) \cdot m^2 \qquad \text{A1.3}$$

Therefore, when $m = 0$, $\tau = 0$ and the final shear stress distribution can be drawn, for the inner cylinder, from the point known at the bore such that when extrapolated back it would pass through the origin.

As the radial stress is given by

$$\sigma_r = \left(\frac{p_i - p_o}{K^2 - 1}\right) (K^2 - m^2) \qquad \text{A1.4}$$

then the final radial stress distribution must be parallel with the final shear stress distribution, found above.

A similar procedure is then carried out for the outer two components. The outside pressure is zero and both cylinders can withstand a shear stress of 6.9 kbar, hence the interface pressures p_{3i} and p_{4i}, are found to be -10.0 and -5.1 kbar, respectively. The final radial stress in component 2 is then found by joining p_{3i} and p_{2i}, and the shear stress by drawing a line parallel to the radial stress which, when extrapolated, would pass through the origin. The state of stress throughout the vessel under load is now known as the hoop stress can be found from

$$\sigma_\theta = \sigma_r + 2\tau \qquad \text{A1.5}$$

To find the residual stresses, the change of interference at the interface between the two materials must be taken into account. This is done by assuming a two component vessel, the inner of high speed steel with $K_1 = 4$ and the outer one of EN30B with $K_2 = 3.75$, assembled without interference. If this were to remain elastic under a pressure, p, of -30 kbar, we could then calculate the pressure at the interface on the assumption of strain compatibility. The equation is

$$p_{10} = \frac{2p}{E_1(K_1^2-1)\left\{\frac{1}{E_1}\left(\frac{K_1^2+1}{K_1^2-1} - \nu_1\right) + \frac{1}{E_2}\left(\frac{K_2^2+1}{K_2^2-1} - \nu_2\right)\right\}} \qquad \text{A1.6}$$

which gives $p_{10} = -1.61$ kbar for the present case with

$$\left.\begin{aligned} E_1 &= 2280 \text{ kbar} \\ \nu_1 &= 0.30 \end{aligned}\right\} \quad \text{For high speed steel}$$

$$\left.\begin{aligned} E_2 &= 2070 \text{ kbar} \\ \nu_2 &= 0.29 \end{aligned}\right\} \quad \text{For EN30B}$$

The range of radial stress can now be drawn in Fig. A1.1, using the value calculated at the interface, zero at the outer diameter and -30 at the bore. This curve now represents the change of radial stress at any section as the pressure is raised from zero to the design pressure. The range of shear stress must be parallel to the lines drawn above and must again pass through the origin, when extrapolated.

Thus the state of stress, both residual and under load, is now known at all sections. The stresses at the interfaces and external surfaces are tabulated in Table A1.1.

TABLE A1.1 Stresses in Four Component Cylinder Design

	UNDER LOAD			RESIDUAL		
D/D_i	Radial	Hoop	Shear	Radial	Hoop	Shear
1	-30.0	2.0	16.0	0.0	-28.4	-14.2
2	-17.8	-10.0	3.9	-10.7	-17.7	-3.5
2	-17.8	3.0	10.4	-10.7	-4.7	3.0
4	-10.0	-4.6	2.7	-8.4	-6.8	0.8
4	-10.0	3.8	6.9	-8.4	1.6	5.0
7.74	-5.1	-1.3	1.9	-4.8	-2.2	1.3
7.74	-5.1	8.7	6.9	-4.8	8.2	6.5
15	0.0	3.0	1.5	0.0	2.8	1.4

The free state interferences were calculated using eq. 2.2, section 2.3.23 and found to be 0.00570 cm/cm between cylinders 1 and 2, 0.00383 cm/cm between cylinders 2 and 3, and 0.00493 cm/cm between cylinders 3 and 4.

As the interference between cylinders 1 and 2 will not be affected by the application of external pressure, they will be assembled with the free state interference. The interface pressure after assembly, p_{1o}, is given by

$$\delta = \frac{1}{E}(\sigma_{\theta 2i} - \sigma_{\theta 1o}) \qquad \text{A1.7}$$

where $$\sigma_{\theta 2i} = p_{1o} \frac{1 + K_2^2}{K_2^2 - 1}$$

and $$\sigma_{\theta 1o} = - p_{1o} \frac{1 + K_1^2}{K_1^2 - 1}$$

Solving these for the interference and properties given previously gives an interface pressure of

$$p_{1o} = -3.90 \text{ kbar}$$

and $$\sigma_{\theta 1o} = -6.50 \text{ kbar}$$

$$\sigma_{\theta 2i} = 6.50 \text{ kbar.}$$

This demonstrates the interference is not changed by the application of internal or external pressure, as the difference $(\sigma_{\theta 2i} - \sigma_{\theta 1o})$ here is the same as for the vessel both under load and in the residual stress condition.

However, as the sleeve failed, during assembly, under the influence of the tensile hoop stress, $\sigma_{\theta 2i}$, the design procedure is not continued here.

A1.3 Stress Calculations for the Final Design

The final design consists of the outer two cylinders of the previous design with a thick-walled liner of maraging steel. They are assembled with minimal interference, simply to hold them together. In the calculations below it is assumed that they are a perfect sliding fit, that is with no interference, until an autofrettage pressure is applied.

It is first assumed that the elastic-plastic interface is within the liner; this will be shown to be the case later from the equations derived. As the EN30B has a lower yield point than the maraging steel, it must also be demonstrated that yield has not set in at the bore of the second cylinder.

An equation similar to A1.1 can be derived, on the same assumptions, but it is complicated here by the fact that the two cylinders have different elastic properties. The elastic stress distribution must be calculated with the assumption of strain compatibility at the interface. This gives

$$\frac{p_{1i}}{Y_1} = -\frac{2 \ln K_c}{\sqrt{3}} + \frac{p_e}{Y_1} \qquad \text{A1.8}$$

where p_e is the pressure to bring the bore of a compound cylinder, with K ratios K_{e1} (= K_1/K_c) and K_{e2} (= $K_2.K_3$), to the point of yield. This can be found assuming Tresca yield criterion, $k_1 = \sigma_\theta - \sigma_r$, to be

$$\frac{p_e}{k_1} = -\frac{(1 - K_{e1}^2)}{2K_{e1}^2} \left/ \left\{ \frac{2}{E_1(K_{e1}^2-1)\left[\frac{1}{E_1}\left(\frac{K_{e1}^2+1}{K_{e1}^2-1} - \nu_1\right) + \frac{1}{E_2}\left(\frac{K_{e2}^2+1}{K_{e2}^2-1} - \nu_2\right)\right]} \right\}^{-1}$$

A1.9

The value of K_c corresponding to a pressure of -30 kbar at the bore is found by assuming values of K_c and calculating the pressure to cause yield to this point. By interpolation the elastic-plastic interface corresponding to -30 kbar is found. In carrying out this calculation, the shear yield of the maraging steel was assumed to be $17/\sqrt{3}$ or 9.8 kbar. This amounts to modifying the Tresca yield criterion to give a better approximation to the more rigorous von Mises criterion, as first suggested by Hill (A3).

Calculated in this way the elastic-plastic interface was found to be at a ratio of 3.37. The pressure at the interface between the maraging and EN30B cylinders was also calculated and found to be -4.76 kbar. As

this is below the yield pressure for the outer two cylinders (-7.46 kbar) this shows that the assumption that the plastic region is confined to the liner is justified.

Estimating the residual stresses in the vessel is more difficult. In practice, the material will exhibit a Bauschinger effect. To obtain the most realistic solution to the problem, the method of Franklin and Morrison (A1) should be used. However, this entails knowing the shear stress-shear strain curve for the material for loading, unloading and re-loading. As this was not available here, unloading must be assumed to be elastic, except in the region at the bore, where $(\sigma_\theta - \sigma_r)$ is greater than $2k_1$. In this region the stresses are found from the yield criterion and by integrating the equilibrium equation, to give

$$\sigma_r = -2k_1 (\ln K + A)$$

The constant A = 0, as $\sigma_r = 0$ when K = 1

$$\therefore \quad \sigma_r = -2k_1 \ln K \qquad \text{A1.10}$$

$$\sigma_\theta = \sigma_r - 2k_1 \qquad \text{A1.11}$$

Stress distributions calculated on the assumptions given above are shown in Fig. 2.17. From this it can be seen that the K ratio up to which reversed yield takes place is 1.24.

Finally, using the Manning (155) method, the collapse pressure of the vessel was calculated and found to be -40.2 kbar. This gives an adequate safety factor on the working pressure of -30 kbar.

APPENDIX II

A2.1 To Show the Relative Interference of a Compound Vessel Changes with Pressure

From Lamé's equations, the stresses in an elastic cylinder under internal and external pressure are

$$\sigma_{r_i} = - p_i \qquad \text{A2.1}$$

$$\sigma_{\theta_i} = - p_i \left(\frac{1 + K^2}{1 - K^2} \right) + 2p_o \frac{K^2}{(1 - K^2)} \qquad \text{A2.2}$$

$$\sigma_{r_o} = - p_o$$

$$\sigma_{\theta_o} = - \frac{2p_i}{(1 - K^2)} + p_o \left(\frac{1 + K^2}{1 - K^2} \right) \qquad \text{A2.4}$$

Subscripts i and o refer to inside and outside diameters respectively.

Now consider two components, numbered 1 and 2, assembled together with interference. These are subjected to internal stress, p_{1i}, external stress, p_{2o}, and have an interference pressure of $p_{1o} = p_{2i}$.

The relative interference is given by

$$\delta = \varepsilon_{\theta_{2i}} - \varepsilon_{\theta_{1o}}$$

$$= \frac{1}{E_2} (\sigma_{\theta_{2i}} - \nu_2 \sigma_{r_{2i}}) - \frac{1}{E_1} (\sigma_{\theta_{1o}} - \nu_1 \sigma_{r_{1o}}) \qquad \text{A2.5}$$

Substituting the values of the stresses in A2.5 gives

$$\delta = \frac{1}{E_2}\left[-p_{2i}\left(\frac{1+K_2^2}{1-K_2^2}\right)+p_{2o}\ \frac{K_2^2}{(1-K_2{}^2)}-\nu_2 p_{2i}\right] -$$

$$\frac{1}{E_1}\left[-\frac{2p_{1i}}{(1-K_1{}^2)}+p_{1o}\left(\frac{1+K_1{}^2}{1-K_1{}^2}\right)-\nu_1 p_{1o}\right] \qquad \text{A2.6}$$

Consider now a change in the internal pressure of δp_{1i} with the external pressure held constant. The corresponding change in pressure (radial stress) at the interface can be found by strain compatibility.

$$\delta p_{1o} = \frac{2\delta p_{1i}}{E_1(K_1{}^2-1)\left\{\frac{1}{E_1}\left(\frac{K_1{}^2+1}{K_1{}^2-1}-\nu_1\right)+\frac{1}{E_2}\left(\frac{K_2{}^2+1}{K_2{}^2-1}-\nu_2\right)\right\}} \qquad \text{A2.7}$$

$$\delta p_{2o} = 0$$

From A2.6 we have

$$\delta_c = \frac{1}{E_2}\left[-\delta p_{1o}\left(\frac{1+K_2{}^2}{1-K_2{}^2}\right)-\nu_2\delta p_{1o}\right]-\frac{1}{E_1}\left[-\frac{2\delta p_{1i}}{(1-K_1{}^2)}\right.$$

$$\left.+\ \delta p_{1o}\left(\frac{1+K_1{}^2}{1-K_1{}^2}\right)-\nu_1\delta p_{1o}\right] \qquad \text{A2.8}$$

From A2.7 and A2.8

$$\delta_c = -\frac{2\delta p_{1i}\{(\nu_1E_2-\nu_2E_1)(1-K_1{}^2)(1-K_2{}^2)-E_1(1+K_2{}^2)(1-K_1{}^2)-}{E_1(K_1{}^2-1)\{E_2(K_2{}^2-1)(K_1{}^2+1-\nu_1(K_1{}^2-1))+E_1(K_1{}^2-1).}$$

$$\frac{E_2(1+K_1{}^2)(1-K_2{}^2)\}}{(K_2{}^2+1+\nu_2(K_2{}^2-1))\}}-\frac{2\delta p_{1i}}{E_1(1-K_1{}^2)} \qquad \text{A2.9}$$

If, and only if, $E_1 = E_2$ and $\nu_1 = \nu_2$ $\delta_c \equiv 0$. Otherwise, the change of internal pressure causes a change of interference.

A similar expression can be obtained for the change of interference due to a change of external pressure on the two component system.

APPENDIX III - Listing of Routines described in Chapter 3.

The routines POLYFT and SIMQ are library routines and are therefore omitted. Also listings of the routines which write out the results and plot them out with the CALCOMP plotter are omitted for the sake of brevity.

```
      SUBROUTINE XREAD
      COMMON /PAR/ PIE,ALPHA,ALPHAD,DBIL,DPROD,VBIL,NFL,NPFL(25),
     1CR(25,25),CZ(25,25)
      COMMON /PAR1/ TAMB,PRESS,DSTRS
      COMMON /MATP/ NPT,STRAI(50),STRES(50),NVP,PVD(50),VISC(50)
      COMMON /ZONE/ ZB(51),ZE(51),RB(51),RE(51)
      COMMON /DUM/ SAVE(100),SAVEZ(100),D(4761)
      COMMON /NAME/ NAM1(8),NAM2(8)
      DO 1000 L=1,25
      DO 1000 M=1,25
 1000 CR(L,M)=CZ(L,M)=0.0
      PIE=3.1415926536
C
C******READ IN VALUES FOR STRESS-STRAIN CURVE.
C******QUASI-STATIC CURVE IS USED FOR ONE TEMPERATURE ONLY.
C
      READ(5,550) NPT
      READ(5,551) ((STRAI(I),STRES(I)),I=1,NPT)
  550 FORMAT(I2)
  551 FORMAT(6F10.0)
      DO 7707 N=1,NPT
 7707 STRES(N)=STRES(N)*0.15445
C
C******READ IN PRESSURE-VISCOSITY DATA.
C
      READ(5,550) NVP
      READ(5,551) ((PVD(I),VISC(I)),I=1,NVP)
      READ(5,500) NAM1
      READ(5,500) NAM2
  500 FORMAT(8A10)
C
C******READ IN DIMENSIONS OF PROBLEM AND BILLET VELOCITY.
C******ALPHAD IS DIE HALF ANGLE.
C
      READ(5,501) TAMB,PRESS,DSTRS
  501 FORMAT(3F10.0)
      PRESS=PRESS*0.15445
      DSTRS=DSTRS*0.15445
      READ(5,51) ALPHAD,DBIL,DPROD,VPROD
   51 FORMAT(4F10.0)
      DBIL=DBIL*2.54
      DPROD=DPROD*2.54
      VPROD=VPROD*2.54
      VPROD=VPROD/60.0
      VBIL=VPROD*(DPROD/DBIL)**2
      ALPHA=ALPHAD*PIE/180.0
C
C******READ COORDINATES OF SEVERAL FLOW LINES.
C******POINT RREF,ZREF IS ON THE AXIS IN THE PLANE OF THE DIE EXIT.
C******NFL = NO. OF FLOW LINES.
C******NPFL(L) = NO. OF POINTS ON L TH. FLOW LINE.
C******ANGLE IS ANGLE IN DEGREES BETWEENAXIS + AXIS OF READINGS.
      READ(5,52) NFL,RREF,ZREF,ANGLE
   52 FORMAT(I2,3F10.0)
      RREF=RREF*2.54
      ZREF=ZREF*2.54
      ANGLE=ANGLE*PIE/180.0
      DO 1001 L=1,NFL
      READ(5,53) NPFL(L)
```

```
   53 FORMAT(I2)
      NPFLL=NPFL(L)
      READ(5,54) (CZ(L,J),CR(L,J),J=1,NPFLL)
   54 FORMAT(6F10.0)
      DO 1001 J=1,NPFLL
      CR(L,J)=CR(L,J)*2.54
      CZ(L,J)=CZ(L,J)*2.54
      IF (ZREF.LT.0.0) CZ(L,J)=-CZ(L,J)
      CR1=(CR(L,J)-RREF)
      CZ1=ZREF-CZ(L,J)
      CR(L,J)=ABS(CR1*COS(ANGLE)-CZ1*SIN(ANGLE))
 1001 CZ(L,J)=CZ1*COS(ANGLE)+CR1*SIN(ANGLE)
C
C******SORT LINES INTO ASCENDING VALUES.
C
      DO 1010 L=1,NFL
      NPFLL=NPFL(L)
      DO 1011 J=1,NPFLL
      SAVEZ(J)=CZ(L,J)
 1011 SAVE(J)=CR(L,J)
      DO 1012 M=1,NPFLL
      SMALL=1000.
      DO 1013 J=1,NPFLL
      IF (SAVEZ(J).LT.SMALL) N=J
      SMALL=SAVEZ(N)
 1013 CONTINUE
      CR(L,M)=SAVE(N)
      CZ(L,M)=SAVEZ(N)
 1012 SAVEZ(N)=2000.
 1010 CONTINUE
C
C******INTERCHANGE LINES.
C
      DO 1020 L=1,NFL
      NMAX=NFL-L+1
      BIG=-100.0
      DO 1021 M=1,NMAX
      IF (CR(M,1).GT.BIG) N=M
      BIG=CR(N,1)
      N1=NPFL(NMAX)
 1021 CONTINUE
      DO 1022 M=1,N1
      SAVE(M)=CR(NMAX,M)
 1022 SAVEZ(M)=CZ(NMAX,M)
      N2=NPFL(N)
      DO 1023 M=1,N2
      CR(NMAX,M)=CR(N,M)
 1023 CZ(NMAX,M)=CZ(N,M)
      DO 1024 M=1,N1
      CR(N,M)=SAVE(M)
 1024 CZ(N,M)=SAVEZ(M)
      NPFL(NMAX)=NPFL(N)
      NPFL(N)=N1
 1020 CONTINUE
      READ (5,5000) RREF1,ZREF1,ANGLE1
 5000 FORMAT(3F10.0)
      RREF1=RREF1*2.54
      ZREF1=ZREF1*2.54
       N     = N L   *P     8
```

```
      SIAN=SIN(ANGLE1)
      COAN=COS(ANGLE1)
      READ(5,5001) ((ZE(L),RE(L),ZB(L),RB(L)),L=1,NFL)
 5001 FORMAT(4F10.0)
      IF (ZE(1).EQ.0.0) RETURN
      DO 1100 L=1,NFL
      RB(L)=RB(L)*2.54
      RE(L)=RE(L)*2.54
      ZB(L)=ZB(L)*2.54
      ZE(L)=ZE(L)*2.54
      IF (ZREF1.LT.0.0) ZE(L)=-ZE(L)
      IF (ZREF1.LT.0.0) ZB(L)=-ZB(L)
      R1=RB(L)-RREF1
      R2=RE(L)-RREF1
      Z1=ZREF1-ZB(L)
      Z2=ZREF1-ZE(L)
      RB(L)=ABS(R1*COAN-Z1*SIAN)
      RE(L)=ABS(R2*COAN-Z2*SIAN)
      ZB(L)=Z1*COAN+R1*SIAN
 1100 ZE(L)=Z2*COAN+R2*SIAN
      NFL1=NFL-1
      DO 1200 L=1,NFL
      L1=NFL-L+1
      BIG1=BIG2=-100.0
      DO 1201 M=1,L1
      IF (RE(M).GT.BIG1) N1=M
      IF (RB(M).GT.BIG2) N2=M
      BIG1=RE(N1)
      BIG2=RB(N2)
 1201 CONTINUE
      SAVE1=RE(L1)
      SAVE2=RB(L1)
      SAVE3=ZE(L1)
      SAVE4=ZB(L1)
      RE(L1)=RE(N1)
      RB(L1)=RB(N2)
      ZE(L1)=ZE(N1)
      ZB(L1)=ZB(N2)
      RE(N1)=SAVE1
      RB(N2)=SAVE2
      ZE(N1)=SAVE3
      ZB(N2)=SAVE4
 1200 CONTINUE
      RE(NFL1)=(RE(NFL1)+RE(NFL))/2.0
      RB(NFL1)=(RB(NFL1)+RB(NFL))/2.0
      ZE(NFL1)=(ZE(NFL1)+ZE(NFL))/2.0
      ZB(NFL1)=(ZB(NFL1)+ZB(NFL))/2.0
      NFL2=NFL-2
      DO 1205 IT=1,3
      DO 1202 L=1,NFL2
      SAVE(L)=(RE(L)+RE(L+1))/2.0
 1202 SAVEZ(L)=(ZE(L)+ZE(L+1))/2.0
      DO 1203 L=2,NFL2
 1203 ZE(L)=SAVEZ(L-1)+(SAVEZ(L)-SAVEZ(L-1))*(RE(L)-SAVE(L-1))/(SAVE(L)
     1-SAVE(L-1))
      DO 1204 L=1,NFL2
      SAVE(L)=(RB(L)+RB(L+1))/2.0
 1204 SAVEZ(L)=(ZB(L)+ZB(L+1))/2.0
      DO 1205 L=2,NFL2
 1205 ZB(L)=SAVEZ(L-1)+(SAVEZ(L)-SAVEZ(L-1))*(RB(L)-SAVE(L-1))/(SAVE(L)
     1-SAVE(L-1))
      RETURN
      END
```

```
      SUBROUTINE MESH(NI,NK,IMAX,KMIN,R,Z,N1I,RPSI,SLOPE,IDENT,KOR,KOR2,
     1C,A,ISMRP)
      DIMENSION X(50),Y(50),C(KOR),A(KOR2)
      DIMENSION IMAX(NK),KMIN(NI),R(NI,NK),Z(NI,NK),RPSI(25,NK),
     1SLOPE(25,NK)
      COMMON /PAR/ PIE,ALPHA,ALPHAD,DBIL,DPROD,VBIL,NFL,NPFL(25),
     1CR(25,25),CZ(25,25)
C
C******CALCULATE COORDINATES OF MESH POINTS.
C******Z SECTIONS ARE EQUI-SPACED.
C******R SECTIONS ARE CHOSEN WITH N1I LINES IN PRODUCT AND NI LINES IN
C******BILLET.R(IMAX,K) IS CHOSEN SO IT LIES ON BOUNDING STREAMLINE.
C******IF IDENT=1 RPSI AT EACH K SECTION IS FOUND BY FITTING AN ORDER KO
C******POLYNOMIAL TO EACH FLOW LINE.
C******IF IDENT=2 LINEAR INTERPOLATION IS USED.
C
      DO 2000 I=1,NI
      DO 2000 K=1,NK
      R(I,K)=0.0
 2000 Z(I,K)=0.0
      N1K=3*NK/4
      XKDIV=(DBIL-DPROD)/(FLOAT(N1K)*TAN(ALPHA)*2.0)
      DO 2001 I=1,N1I
      DO 2001 K=1,NK
 2001 Z(I,K)=XKDIV*FLOAT(K-1)
C
C******TRANSFORM INPUT DATA TO MESH COORDINATES.
C
      DO 2002 L=1,NFL
      NPFLL=NPFL(L)
      DO 2002 J=1,NPFLL
 2002 CZ(L,J)=CZ(L,J)+XKDIV
      XIDIV=DPROD/(FLOAT(N1I-1)*2.0)
      CON=XIDIV*FLOAT(N1I-1)
      DO 2003 I=1,N1I
      DO 2003 K=1,NK
      R(I,K)=XIDIV*FLOAT(I-1)
 2003 KMIN(I)=1
      IMAX(1)=IMAX(2)=N1I
      N2I=NI-N1I
      XIDIV=(DBIL-DPROD)/(FLOAT(N2I)*2.0)
C
C******FIND R COORDINATES OF THE FLOW LINES AT EACH K SECTION USING
C******POLYNOMIAL FIT.
C
      IF (IDENT.EQ.2) GO TO 2100
      DO 2004 L=1,NFL
      NPFLL=NPFL(L)
      DO 2005 J=1,NPFLL
      X(J)=CZ(L,J)
 2005 Y(J)=CR(L,J)
      CALL POLYFT(X,Y,NPFLL,KOR,C,CO,A,-1)
      DO 2029 K=1,NK
      IF (Z(1,K).GT.CZ(L,NPFLL)) GO TO 2030
      IF (Z(1,K).LT.CZ(L,1)) GO TO 2430
      RPSI(L,K)=CO
      SLOPE(L,K)=0.0
      DO 2006 M=1,KOR
      IF (K.EQ.1) GO TO 2006
```

```
      SLOPE(L,K)=SLOPE(L,K)+C(M)*Z(1,K)**(M-1)*FLOAT(M)
 2006 RPSI(L,K)=RPSI(L,K)+C(M)*Z(1,K)**M
      GO TO 2029
 2030 RPSI(L,K)=CR(L,NPFLL)
      SLOPE(L,K)=0.0
      GO TO 2029
 2430 RPSI(L,K)=CR(L,1)
      SLOPE(L,K)=0.0
 2029 CONTINUE
 2004 CONTINUE
      IF (ISMRP.EQ.1.OR.ISMRP.EQ.2) CALL SMRPSI(NI,NK,Z,RPSI,2)
      IF (ISMRP.EQ.2) CALL SMRPSI(NI,NK,Z,RPSI,2)
      NFL=NFL-1
      DO 2440 K=1,NK
 2440 RPSI(NFL,K)=(RPSI(NFL,K)+RPSI(NFL+1,K))/2.0
C
C******FIND POSITION OF MESH POINTS.
C
      N3I=N1I+1
      DO 2007 K=3,NK
      M=0
      DO 2008 I=N3I,NI
      M=M+1
      R(I,K)=CON+FLOAT(M)*XIDIV
      IF (R(I,K).GE.RPSI(NFL,K)) GO TO 2009
 2008 CONTINUE
 2009 IMAX(K)=I
      IF (IMAX(K).GT.NI) IMAX(K)=NI
      IM=IMAX(K)
      R(IM,K)=RPSI(NFL,K)
      Z(IM,K)=Z(1,K)
 2007 CONTINUE
      DO 2201 I=N3I,NI
      DO 2011 K=1,NK
      IF (R(I,K).NE.0.0) GO TO 2012
 2011 CONTINUE
 2012 KMIN(I)=K
      KM=KMIN(I)
      DO 2010 K=KM,NK
      IF (R(I,K).EQ.R(I,K+1)) GO TO 2200
 2010 Z(I,K)=XKDIV*FLOAT(K-1)
 2200 KMIN(I)=K
      DO 2201 K=KM,NK
 2201 Z(I,K)=XKDIV*FLOAT(K-1)
      RETURN
C
C******FIND R COORDINATES OF THE FLOW LINES AT EACH K SECTION USING
C******LINEAR INTERPOLATION.
C
 2100 DO 2104 L=1,NFL
      NPFLL=NPFL(L)
      DO 2105 K=1,NK
      DO 2106 J=1,NPFLL
      IF (CZ(L,J).GT.Z(1,K)) GO TO 2107
 2106 CONTINUE
 2107 IF (Z(1,K).GT.CZ(L,NPFLL)) GO TO 2108
      IF (J.EQ.1) GO TO 2109
      RPSI(L,K)=CR(L,J-1)+(CR(L,J)-CR(L,J-1))*(Z(1,K)-CZ(L,J-1))/
     1(CZ(L,J)-CZ(L,J-1))
```

```
      GO TO 2105
 2109 RPSI(L,K)=CR(L,1)
      GO TO 2105
 2108 RPSI(L,K)=CR(L,NPFLL)
 2105 CONTINUE
 2104 CONTINUE
      IF (ISMRP.EQ.1.OR.ISMRP.EQ.2) CALL SMRPSI(NI,NK,Z,RPSI,2)
      IF (ISMRP.EQ.2) CALL SMRPSI(NI,NK,Z,RPSI,2)
      NFL=NFL-1
      DO 2441 K=1,NK
 2441 RPSI(NFL,K)=(RPSI(NFL,K)+RPSI(NFL+1,K))/2.0
C
      N2I=N1I+1
      DO 2110 K=3,NK
      M=0
      DO 2111 I=N2I,NI
      M=M+1
      R(I,K)=CON+FLOAT(M)*XIDIV
      IF (R(I,K).GE.RPSI(NFL,K)) GO TO 2112
 2111 CONTINUE
 2112 IMAX(K)=I
      IF (IMAX(K).GT.NI) IMAX(K)=NI
      IM=IMAX(K)
      R(IM,K)=RPSI(NFL,K)
      Z(IM,K)=Z(1,K)
 2110 CONTINUE
      NK1=NK-1
      DO 2301 I=N2I,NI
      DO 2121 K=1,NK
      IF (R(I,K).NE.0.0) GO TO 2122
 2121 CONTINUE
 2122 KMIN(I)=K
      KM=KMIN(I)
      DO 2120 K=KM,NK1
      IF (R(I,K).EQ.R(I,K+1)) GO TO 2300
 2120 Z(I,K)=XKDIV*FLOAT(K-1)
 2300 KMIN(I)=K
      DO 2301 K=KM,NK
 2301 Z(I,K)=XKDIV*FLOAT(K-1)
      NPT=5
      CALL DLINE(Z,NPT,NFL,NI,NK,RPSI,SLOPE)
      RETURN
      END
```

```
      SUBROUTINE DLINE(Z,NPT,NFL,NI,NK,RPSI,SLOPE)
      DIMENSION RPSI(25,NK),SLOPE(25,NK),Z(NI,NK)
      COMMON /DUM/ X(20),Y(20),A(20,20),B(20)
      DO 9000 K=1,NK
      DO 9000 L=1,25
 9000 SLOPE(L,K)=0.0
      NF=NPT/2
      KM3=NK-3
      DO 9001 K=3,KM3
      DO 9001 L=1,NFL
      DO 9002 M=1,NPT
      M1=K-NF+M-1
      X(M)=Z(1,M1)
 9002 Y(M)=RPSI(L,M1)
      CALL FIT(X,Y,NPT,A,B)
      DO 9003 M=2,NPT
 9003 SLOPE(L,K)=SLOPE(L,K)+B(M)*Z(1,K)**(M-2)*FLOAT(M-1)
 9001 CONTINUE
      RETURN
      END
```

```
      SUBROUTINE SMRPSI(NI,NK,Z,RPSI,ID)
      DIMENSION Z(NI,NK),RPSI(25,NK)
      COMMON /PAR/ PIE,ALPHA,ALPHAD,DBIL,DPROD,VBIL,NFL,NPFL(25),
     1CR(25,25),CZ(25,25)
      COMMON /DUM/ D(25,51)
      GO TO (9000,9001),ID
C
C******RPSI IS SMOOTHED USING METHOD OF FIVES.
C
 9000 NK2=NK-2
      DO 9002 L=1,NFL
      DO 9003 K=3,NK2
 9003 D(L,K)=(RPSI(L,K-2)+RPSI(L,K-1)+RPSI(L,K)+RPSI(L,K+1)+RPSI(L,K+2)
     1)/5.0
      DO 9002 K=3,NK2
 9002 RPSI(L,K)=D(L,K)
      RETURN
C
C******RPSI IS SMOOTHED USING MEANS
C
 9001 NK2=NK-2
      DO 9004 L=1,NFL
      DO 9005 K=3,NK2
 9005 D(L,K)=(RPSI(L,K-1)+2.*RPSI(L,K)+RPSI(L,K+1))/4.0
      DO 9004 K=3,NK2
 9004 RPSI(L,K)=D(L,K)
      RETURN
      END
```

```
      SUBROUTINE FLOW(NI,NK,IMAX,KMIN,NII,R,Z,RPSI,PSI,CPSI,
     1KC,KOR,NFIT,IDENT)
      DIMENSION IMAX(NK),KMIN(NI),R(NI,NK),Z(NI,NK),RPSI(25,NK),PSI(25),
     1CPSI(NI,NK),KC(KOR)
      COMMON /PAR/ PIE,ALPHA,ALPHAD,DBIL,DPROD,VBIL,NFL,NPFL(25),
     1CR(25,25),CZ(25,25)
      COMMON /DUM/ A(40,40),B(40),C(40),X(25),Y(25)
C
C******FIND VALUE OF FLOW FUNCTION AT EACH MESH POINT.
C******IF IDENT=1 LINEAR INTERPOLATION IS USED.
C******IF IDENT=2 POLYNOMIAL INTERPOLATION IS USED WITH NFIT POINTS
C******ON EITHER SIDE OF POINT (I.E. DEGREE OF POLYNOMIAL = 2*NFIT).
C******IF IDENT=3 A LEAST SQUARES POLYNOMIAL IS FITTED OF ORDER KOR
C******WITH NON-ZERO COEFFICIENTS DEFINED IN KC
C
      DO 3000 L=1,NFL
      NPFLL=NPFL(L)
 3000 PSI(L)=PIE*ABS(VBIL)*CR(L,NPFLL)**2
      GO TO (3001,3002,3003),IDENT
C
C******LINEAR INTERPOLATION VERSION.
C
 3001 DO 3004 K=1,NK
      IM=IMAX(K)
      IM1=IM-1
      DO 3005 I=2,IM1
      DO 3006 L=1,NFL
      IF (RPSI(L,K).GT.R(I,K)) GO TO 3007
 3006 CONTINUE
 3007 CPSI(I,K)=PSI(L-1)+(PSI(L)-PSI(L-1))*
     1(R(I,K)-RPSI(L-1,K))/(RPSI(L,K)-RPSI(L-1,K))
 3005 CONTINUE
      CPSI(1,K)=0.0
 3004 CPSI(IM,K)=PSI(NFL)
      RETURN
C
C******POLYNOMIAL INTERPOLATION VERSION.
C
 3002 DO 3008 K=1,NK
      IM=IMAX(K)
      IM1=IM-1
      DO 3009 I=2,IM1
      NC=NFIT*2+1
      CALL PPFIT(RPSI,PSI,NI,NK,NFL,IM,I,K,R,Z,NFIT,NC,A,B,ANS)
 3009 CPSI(I,K)=ANS
      CPSI(1,K)=0.0
 3008 CPSI(IM,K)=PSI(NFL)
      RETURN
C
C******POLYNOMIAL LEAST SQUARES FIT VERSION.
C
 3003 DO 3010 K=1,NK
      DO 3011 L=1,NFL
      X(L)=RPSI(L,K)
 3011 Y(L)=PSI(L)
      KTOT=0
      DO 3012 M=1,KOR
      IF (KC(M).EQ.0) GO TO 3012
      KTOT=KTOT+1
```

```
3012 CONTINUE
     KCOEF=KTOT+1
     CALL POLFYT(X,Y,NFL,KOR,KC,KTOT,CO,C,A,B,KCOEF)
     IM1=IMAX(K)-1
     DO 3013 I=2,IM1
     L=0
     CPSI(I,K)=CO
     DO 3013 M=1,KOR
     IF (KC(M).EQ.0) GO TO 3013
     L=L+1
     CPSI(I,K)=CPSI(I,K)+C(L)*R(I,K)**KC(M)
3013 CONTINUE
     IM=IMAX(K)
     CPSI(IM,K)=PSI(NFL)
3010 CPSI(1,K)=0.0
     RETURN
     END
```

```
     SUBROUTINE PPFIT(RPSI,PSI,NI,NK,NFL,IM,I,K,R,Z,NFIT,NC,A,B,ANS)
     DIMENSION RPSI(25,NK),PSI(25),A(NC,NC),B(NC),R(NI,NK),Z(NI,NK)
     IF (R(I,K).GE.RPSI(NFIT+1,K)) GO TO 6000
     DO 6001 KROW=1,NC
6001 A(KROW,1)=1.
     DO 6002 KROW=1,NC
     DO 6003 KCOL=2,NC
6003 A(KROW,KCOL)=RPSI(KROW,K)**(KCOL-1)
6002 B(KROW)=PSI(KROW)
     IDL=1
     CALL SIMQ(A,B,NC,KS)
     GO TO 6004
6000 NM=NFL-NFIT
     IF (R(I,K).LT.RPSI(NM,K)) GO TO 6005
     DO 6006 KROW=1,NC
     M=NFL-NC+KROW
     DO 6007 KCOL=2,NC
6007 A(KROW,KCOL)=RPSI(M,K)**(KCOL-1)
6006 B(KROW)=PSI(M)
     DO 6008 KROW=1,NC
6008 A(KROW,1)=1.
     IDL=NFL-NC
     CALL SIMQ(A,B,NC,KS)
     GO TO 6004
6005 DO 6009 KROW=1,NC
6009 A(KROW,1)=1.
     DO 6010 L=1,NFL
     IF (R(I,K).LE.RPSI(L,K)) GO TO 6011
6010 CONTINUE
6011 NL=L-NFIT
     IDL=NL
     DO 6012 KROW=1,NC
     DO 6013 KCOL=2,NC
6013 A(KROW,KCOL)=RPSI(NL,K)**(KCOL-1)
     B(KROW)=PSI(NL)
6012 NL=NL+1
     CALL SIMQ(A,B,NC,KS)
6004 ANS=B(1)
     DO 6014 M=2,NC
     ANS=ANS+B(M)*R(I,K)**(M-1)
6014 IDL=IDL+1
     RETURN
     END
```

```
      SUBROUTINE POLFYT(X,Y,N,KOR,KC,KTOT,CO,C,A,B,KCOEF)
      DIMENSION X(N),Y(N),KC(KOR),C(KTOT),A(KCOEF,KCOEF),B(KCOEF)
C
C******IF KC(I)=0, COEFFICIENT OF X**I = 0, OTHERWISE KC(I) EQUALS THE
C******POWER I.
C******KTOT = TOTAL NO. NON-ZERO TERMS.
C
      DIMENSION SUMX(200),SMYX(100)
C
C******INITIALIZATION.
      KTOR=2*KOR
      DO 1000 I=1,KOR
 1000 SMYX(I)=0.0
      DO 1001 I=1,KTOR
 1001 SUMX(I)=0.0
      SUMY=0.0
C
C******FORMULATION OF NORMAL EQUATIONS.
C
      DO 1005 J=1,KTOR
      DO 1005 I=1,N
 1005 SUMX(J)=SUMX(J)+X(I)**J
      DO 1006 I=1,N
 1006 SUMY=SUMY+Y(I)
      DO 1007 J =1,KOR
      DO 1007 I=1,N
 1007 SMYX(J)=SMYX(J)+Y(I)*X(I)**J
C
C******SET UP ARRAYS OF COEFFICIENTS AND CONSTANTS.
C******A(KTOT+1,KTOT+1) IS MATRIX OF COEFFICIENTS.
C******B(KTOT+1) IS MATRIX OF CONSTANTS.
C******POLYNOMIAL COEFFICIENTS ARE RETURNED IN B.
C
      B(1)=SUMY
      L=1
      DO 1008 I=1,KOR
      IF (KC(I)) 1019,1008,1019
 1019 L=L+1
      L1=KC(I)
      B(L)=SMYX(L1)
 1008 CONTINUE
      I1=1
      K=KOR+1
      DO 1009 I=1,K
      IF (I.EQ.1) GO TO 1012
      IF (KC(I-1)) 1011,1009,1011
 1011 I1=I1+1
 1012 L1=1
      DO 1009 L=1,K
      IF (I.EQ.1.AND.L.EQ.1) GO TO 1020
      IF (L.EQ.1) GO TO 1021
      IF (KC(L-1)) 1022,1009,1022
 1022 L1=L1+1
      A(I1,L1)=SUMX(I+L-2)
      GO TO 1009
 1021 A(I1,1)=SUMX(I-1)
      GO TO 1009
 1020 A(1,1)=N
 1009 CONTINUE
      K=KTOT+1
      CALL SIMQ(A,B,K,KS)
      CO=B(1)
      DO 1010 I=1,KTOT
 1010 C(I)=B(I+1)
      RETURN
      END
```

```
      SUBROUTINE STRATE(NI,NK,IMAX,KMIN,R,Z,NII,CPSI,U,V,ETRR,ETHH,
     1ETZZ,ETRZ,D)
      DIMENSION IMAX(NK),KMIN(NI),R(NI,NK),Z(NI,NK),CPSI(NI,NK),D(NI,NK)
     1,U(NI,NK),V(NI,NK),ETRR(NI,NK),ETHH(NI,NK),ETZZ(NI,NK),ETRZ(NI,NK)
      COMMON /PAR/ PIE,ALPHA,ALPHAD,DBIL,DPROD,VBIL,NFL,NPFL(25),
     1CR(25,25),CZ(25,25)
      COMMON /IZONE/ KB(51),KE(51)
C
C******FIND U + V VELOCITIES AT EACH MESH POINT.
C
      DO 7000 I=1,NI
      DO 7000 K=1,NK
 7000 ETRR(I,K)=ETHH(I,K)=ETZZ(I,K)=ETRZ(I,K)=U(I,K)=V(I,K)=D(I,K)=0.0
      CUT=1.0E-10
      CALL DIFR(R,Z,NI,NK,NII,IMAX,KMIN,CPSI,D,3,3,CUT)
      DO 7001 K=1,NK
      IM=IMAX(K)
      DO 7002 I=2,IM
      U(I,K)=-D(I,K)/(2.0*PIE*R(I,K))
 7002 CONTINUE
      U(1,K)=(4.*U(2,K)-U(3,K))/3.
 7001 CONTINUE
      CALL DIFZ(R,Z,NI,NK,NII,IMAX,KMIN,CPSI,D,3,3,CUT)
      DO 7004 K=1,NK
      IM=IMAX(K)
      DO 7004 I=1,IM
      IF (I.EQ.1) GO TO 7005
      V(I,K)=D(I,K)/(2.0*PIE*R(I,K))
      GO TO 7004
 7005 V(1,K)=0.0
 7004 CONTINUE
      DO 7006 I=1,NI
      IF (I.GT.NII) GO TO 7101
      U(I,1)=U(I,2)=-ABS(VBIL)*(DBIL/DPROD)**2
      V(I,1)=V(I,2)=0.0
 7101 U(I,NK)=U(I,NK-1)=-ABS(VBIL)
 7006 V(I,NK)=V(I,NK-1)=0.0
      VPROD=VBIL*(DBIL/DPROD)**2
      NK2=NK-2
      DO 7102 K=3,NK2
      IM=IMAX(K)
      DO 7102 I=1,IM
      IF (ABS(U(I,K)).GT.ABS(VPROD)) U(I,K)=-ABS(VPROD)
      IF (ABS(U(I,K)).LT.ABS(VBIL)) U(I,K)=-ABS(VBIL)
      IF (V(I,K).GT.0.0) V(I,K)=0.0
 7102 CONTINUE
      DO 7300 I=1,NII
      KEI=KE(I)-1
      DO 7300 K=1,KEI
      U(I,K)=-ABS(VBIL)*(DBIL/DPROD)**2
 7300 V(I,K)=0.0
      DO 7301 I=1,NI
      KBI=KB(I)+1
      DO 7301 K=KBI,NK
      U(I,K)=-ABS(VBIL)
 7301 V(I,K)=0.0
C
C******FIND STRAIN RATES.
```

```
      CALL DIFR(R,Z,NI,NK,N1I,IMAX,KMIN,V,ETRR,3,3,CUT)
      DO 7007 K=1,NK
      IM=IMAX(K)
      DO 7007 I=1,IM
      IF (I.EQ.1) GO TO 7008
      ETHH(I,K)=V(I,K)/R(I,K)
      GO TO 7007
 7008 ETHH(I,K)=ETRR(I,K)
 7007 CONTINUE
      CALL DIFZ(R,Z,NI,NK,N1I,IMAX,KMIN,U,ETZZ,3,3,CUT)
      CALL DIFR(R,Z,NI,NK,N1I,IMAX,KMIN,U,D   ,3,3,CUT)
      CALL DIFZ(R,Z,NI,NK,N1I,IMAX,KMIN,V,ETRZ,3,3,CUT)
      DO 7009 K=1,NK
      IM=IMAX(K)
      DO 7009 I=1,IM
      ETRZ(I,K)=ETRZ(I,K)+D(I,K)
 7009 D(I,K)=ETRR(I,K)+ETHH(I,K)+ETZZ(I,K)
      DO 7302 I=1,N1I
      KEI=KE(I)-1
      DO 7302 K=1,KEI
 7302 ETRR(I,K)=ETHH(I,K)=ETZZ(I,K)=ETRZ(I,K)=0.0
      DO 7303 I=1,NI
      KBI=KB(I)+1
      DO 7303 K=KBI,NK
 7303 ETRR(I,K)=ETHH(I,K)=ETZZ(I,K)=ETRZ(I,K)=0.0
      RETURN
      END
```

```
      SUBROUTINE EFTSTR(NI,NK,IMAX,KMIN,R,Z,RPSI,U,V,ETRR,ETHH,ETZZ,
     1ETRZ,EFFST,TEFFST,UF,TFEFST,TIME,FEFFST)
      DIMENSION IMAX(NK),KMIN(NI),R(NI,NK),Z(NI,NK),U(NI,NK),V(NI,NK),
     1ETRR(NI,NK),ETHH(NI,NK),ETZZ(NI,NK),ETRZ(NI,NK),EFFST(NI,NK),
     1TEFFST(NI,NK),RPSI(25,NK),UF(25,NK),TFEFST(25,NK),TIME(25,NK),
     1FEFFST(25,NK)
      COMMON /PAR/ PIE,ALPHA,ALPHAD,DBIL,DPROD,VBIL,NFL,NPFL(25),
     1CR(25,25),CZ(25,25)
      COMMON /IZONE/ KB(51),KE(51)
C
C******SUBROUTINE CALCULATES EFFECTIVE STRAIN RATE + TOTAL EFFECTIVE STRAI
C
      DO 7000 I=1,NI
      DO 7000 K=1,NK
      TEFFST(I,K)=0.0
 7000 EFFST(I,K)=0.0
      DO 7001 K=1,NK
      IM=IMAX(K)
      DO 7001 I=1,IM
 7001 EFFST(I,K)=(SQRT(2.0)/3.0)*SQRT((ETZZ(I,K)-ETRR(I,K))**2+(ETRR(I,K
     1)-ETHH(I,K))**2+(ETHH(I,K)-ETZZ(I,K))**2+1.5*ETRZ(I,K)**2)
      NII=IMAX(1)
      DO 7200 I=1,NII
      KEI=KE(I)-1
      DO 7200 K=1,KEI
 7200 EFFST(I,K)=0.0
      DO 7201 I=1,NI
      KBI=KB(I)+1
      DO 7201 K=KBI,NK
 7201 TEFFST(I,K)=0.0
      DO 7002 K=1,NK
      DO 7002 L=1,NFL
      DO 7003 I=1,NI
      IF (RPSI(L,K)-R(I,K)) 7004,7005,7003
 7003 CONTINUE
 7005 FEFFST(L,K)=EFFST(I,K)
      UF(L,K)=U(I,K)
      GO TO 7002
 7004 FEFFST(L,K)=EFFST(I-1,K)+(EFFST(I,K)-EFFST(I-1,K))*(RPSI(L,K)-
     1R(I-1,K))/(R(I,K)-R(I-1,K))
      UF(L,K)=U(I-1,K)+(U(I,K)-U(I-1,K))*(RPSI(L,K)-R(I-1,K))/(R(I,K)-
     1R(I-1,K))
 7002 CONTINUE
C
C******FIND TIME TO REACH EACH K SECTION ON EACH FLOW LINE.
C
      NK1=NK-1
      DO 7006 L=1,NFL
      TFEFST(L,NK)=0.0
      TIME(L,NK)=0.0
      DO 7006 KD=1,NK1
      K=NK-KD
 7006 TIME(L,K)=TIME(L,K+1)+2.0*(Z(1,K+1)-Z(1,K))/(UF(L,K+1)+UF(L,K))
      DO 7007 L=1,NFL
      DO 7007 KD=1,NK1
      K=NK-KD
 7007 TFEFST(L,K)=TFEFST(L,K+1)+(TIME(L,K)-TIME(L,K+1))*0.5*
     1(FEFFST(L,K)+FEFFST(L,K+1))
      DO 7008 K=1,NK
```

```
      IM=IMAX(K)
      TEFFST(IM,K)=TFEFST(NFL,K)
      IM1=IM-1
      TEFFST(1,K)=TFEFST(1,K)+RPSI(1,K)*(TFEFST(2,K)-TFEFST(1,K))/
     1(RPSI(2,K)-RPSI(1,K))
      DO 7008 I=2,IM1
      DO 7009 L=1,NFL
      IF (RPSI(L,K)-R(I,K)) 7009,7010,7011
7009  CONTINUE
      GO TO 7008
7010  TEFFST(I,K)=TFEFST(L,K)
      GO TO 7008
7011  TEFFST(I,K)=TFEFST(L-1,K)+(TFEFST(L,K)-TFEFST(L-1,K))*
     1(R(I,K)-RPSI(L-1,K))/(RPSI(L,K)-RPSI(L-1,K))
7008  CONTINUE
      DO 7202 I=1,N1I
      KEI=KE(I)
      KE1=KE(I)-1
      DO 7202 K=1,KE1
7202  TEFFST(I,K)=TEFFST(I,KEI)
      DO 7203 I=1,NI
      KBI=KB(I)+1
      DO 7203 K=KBI,NK
7203  TEFFST(I,K)=0.0
      RETURN
      END
```

```
      SUBROUTINE DIFZ(R,Z,NI,NK,NII,IMAX,KMIN,A,DAZ,IDC,IDB,CUT)
      DIMENSION R(NI,NK),Z(NI,NK),IMAX(NK),KMIN(NI),A(NI,NK),DAZ(NI,NK)
      COMMON /DUM/ X(20),Y(20),D(20,20),C(20),E(20)
C
C******DIFFERENTIATION OF ARRAY A W.R.T. Z IS CARRIED OUT.
C******IDC POINTS ARE USED IN THE CENTRE OF THE FIELD.
C******IDB POINTS ARE USED ALONG THE BOUNDARY.
C
      DO 3000 I=1,NI
      DO 3000 K=1,NK
 3000 DAZ(I,K)=0.0
      IF (IDC.NE.2) GO TO 3001
      DO 3002 I=1,NI
      KM=KMIN(I)
      DO 3002 K=KM,NK
      IF (K.EQ.KM) GO TO 3003
      DAZ(I,K)=(A(I,K)-A(I,K-1))/(Z(I,K)-Z(I,K-1))
      GO TO 3002
 3003 DAZ(I,K)=(A(I,K+1)-A(I,K))/(Z(I,K+1)-Z(I,K))
 3002 CONTINUE
      NK1=NK-1
      DO 3004 K=1,NK1
      IM=IMAX(K)
      DO 3005 M=1,NI
      IF (R(IM,K).EQ.R(M,K+1)) GO TO 3006
      IF (R(IM,K).LT.R(M,K+1)) GO TO 3007
 3005 CONTINUE
 3006 A1=A(M,K+1)
      GO TO 3008
 3007 A1=A(M-1,K+1)+(A(M,K+1)-A(M-1,K+1))*(R(IM,K)-R(M-1,K+1))/
     1(R(M,K+1)-R(M-1,K+1))
 3008 DAZ(IM,K)=(A1-A(IM,K))/(Z(1,K+1)-Z(IM,K))
 3004 CONTINUE
      IF (IDB.EQ.2) RETURN
      GO TO 3009
 3001 NF=IDC/2
      NK1=NK-1
      DO 3010 I=1,NI
      KM1=KMIN(I)+1
      NM1=KM1+NF-1
      NM2=NK-NF
      DO 3010 K=KM1,NK1
      IF (K.LT.NM1) GO TO 3011
      IF (K.GT.NM2) GO TO 3012
      DO 3013 M=1,IDC
      M1=K-NF+M-1
      X(M)=Z(I,M1)
 3013 Y(M)=A(I,M1)
      CALL FIT(X,Y,IDC,D,C)
      GO TO 3014
 3011 DO 3015 M=1,IDC
      M1=KM1+M-2
      X(M)=Z(I,M1)
 3015 Y(M)=A(I,M1)
      CALL FIT(X,Y,IDC,D,C)
      GO TO 3014
 3012 DO 3016 M=1,IDC
      M1=NK-IDC+M
      X(M =Z(I,M1
```

```
3016 Y(M)=A(I,M1)
     CALL FIT(X,Y,IDC,D,C)
3014 DAZ(I,K)=0.0
     IF (ABS(A(I,K)-A(I,K-1)).LT.CUT.OR.ABS(A(I,K)-A(I,K+1)).
    1LT.CUT) GO TO 3010
     DO 3017 M=2,IDC
3017 DAZ(I,K)=DAZ(I,K)+C(M)*Z(I,K)**(M-2)*FLOAT(M-1)
3010 CONTINUE
3009 DO 3018 I=1,NI
     DO 3019 M=1,IDB
     M1=NK-IDB+M
     X(M)=Z(I,M1)
3019 Y(M)=A(I,M1)
     CALL FIT(X,Y,IDB,D,C)
     IF (A(I,NK).EQ.A(I,NK1)) GO TO 3018
     DO 3020 M=2,IDB
3020 DAZ(I,NK)=DAZ(I,NK)+C(M)*Z(I,NK)**(M-2)*FLOAT(M-1)
3018 CONTINUE
     DO 3021 I=1,N1I
     KM=KMIN(I)
     DO 3022 M=1,IDB
     M1=KM+M-1
     X(M)=Z(I,M1)
3022 Y(M)=A(I,M1)
     CALL FIT(X,Y,IDB,D,C)
     DAZ(I,1)=C(2)
     IF (ABS(A(I,1)-A(I,2)).LT.CUT) DAZ(I,1)=DAZ(I,2)=0.0
3021 CONTINUE
     N2I=N1I+1
     NF=IDB/2
     NI1=NI-1
     DO 3023 I=N2I,NI1
     KM=KMIN(I)
     DO 3024 M=1,NF
     KSEC=KM-NF+M-1
     IMAXK=IMAX(KSEC)
     IMIN=IMAXK-IDB+1
     IMAXK1=IMAXK-1
     IMAXK2=IMAXK-2
     CON2=(R(IMAXK,KSEC)-R(IMAXK1,KSEC))/(R(IMAXK1,KSEC)-R(IMAXK2,
    1KSEC))
     IF (CON2.LT.0.75) IMIN=IMIN-1
     IMA=IMIN+IDB-1
     DO 3025 M1=IMIN,IMA
     M2=M1-IMIN+1
     X(M2)=R(M1,KSEC)
3025 Y(M2)=A(M1,KSEC)
     X(IDB)=R(IMAXK,KSEC)
     Y(IDB)=A(IMAXK,KSEC)
     CALL FIT(X,Y,IDB,D,C)
     E(M)=C(1)
     DO 3024 M1=2,IDB
3024 E(M)=E(M)+C(M1)*R(I,KM)**(M1-1)
     DO 3026 M1=1,NF
     KSEC=KM-NF+M-1
     X(M1)=Z(1,KSEC)
3026 Y(M1)=E(M1)
     X(NF+1)=Z(I,KM)
     Y(NF+1)=A(I,KM)
```

```
      M2=NF+2
      DO 3027 M1=M2,IDB
      M3=KM+M1-NF-1
      X(M1)=Z(I,M3)
 3027 Y(M1)=A(I,M3)
      CALL FIT(X,Y,IDB,D,C)
      DAZ(I,KM)=0.0
      IF (ABS(A(I,KM)-A(I,KM+1)).LT.CUT) GO TO 3023
      DO 3028 M=2,IDB
 3028 DAZ(I,KM)=DAZ(I,KM)+C(M)*Z(I,KM)**(M-2)*FLOAT(M-1)
 3023 CONTINUE
      KM=KMIN(NI)
      DAZ(NI,KM)=0.0
      KM=KM-1
      DO 3029 K=3,KM
      IM=IMAX(K)
      DO 3030 M=1,IDB
      KSEC=K-NF+M-1
      IMAXK=IMAX(KSEC)
      IMIN=IMAXK-IDB+1
      IMAXK1=IMAXK-1
      IMAXK2=IMAXK-2
      CON2=(R(IMAXK,KSEC)-R(IMAXK1,KSEC))/(R(IMAXK1,KSEC)-R(IMAXK2,
     1KSEC))
      IF (CON2.LT.0.75) IMIN=IMIN-1
      IMA=IMIN+IDB-1
      DO 3031 M1=IMIN,IMA
      M2=M1-IMIN+1
      X(M2)=R(M1,KSEC)
 3031 Y(M2)=A(M1,KSEC)
      X(IDB)=R(IMAXK,KSEC)
      Y(IDB)=A(IMAXK,KSEC)
      CALL FIT(X,Y,IDB,D,C)
      E(M)=C(1)
      DO 3030 M1=2,IDB
 3030 E(M)=E(M)+C(M1)*R(IM,K)**(M1-1)
      DO 3032 M=1,IDB
      M1=K-NF+M-1
      X(M)=Z(1,M1)
 3032 Y(M)=E(M)
      CALL FIT(X,Y,IDB,D,C)
      DAZ(IM,K)=0.0
      DO 3033 M=2,IDB
 3033 DAZ(IM,K)=DAZ(IM,K)+C(M)*Z(IM,K)**(M-2)*FLOAT(M-1)
 3029 CONTINUE
      RETURN
      END
```

```
      SUBROUTINE DIFR(R,Z,NI,NK,NII,IMAX,KMIN,A,DAR,IDC,IDB,CUT)
      DIMENSION R(NI,NK),Z(NI,NK),IMAX(NK),KMIN(NI),A(NI,NK),DAR(NI,NK)
      COMMON /DUM/ X(20),Y(20),D(20,20),C(20)
C
C******DIFFERENTIATION OF ARRAY A W.R.T. R IS CARRIED OUT.
C******IDC POINTS ARE USED IN CENTRE OF THE FIELD.
C******IDB POINTS ARE USED ALONG THE BOUNDARY.
C
      DO 4000 I=1,NI
      DO 4000 K=1,NK
 4000 DAR(I,K)=0.0
      IF (IDC.NE.2) GO TO 4001
      DO 4002 K=1,NK
      IM=IMAX(K)
      DO 4002 I=1,IM
      IF (I.EQ.1) GO TO 4003
      DAR(I,K)=(A(I,K)-A(I-1,K))/(R(I,K)-R(I-1,K))
      GO TO 4002
 4003 DAR(I,K)=(A(I+1,K)-A(I,K))/(R(I+1,K)-R(I,K))
 4002 CONTINUE
      IF (IDB.EQ.2) RETURN
      GO TO 4004
 4001 NF=IDC/2
      DO 4005 K=1,NK
      IM1=IMAX(K)-1
      NM=IM1-NF+1
      DO 4005 I=2,IM1
      IF (I.LT.NF) GO TO 4006
      IF (I.GT.NM) GO TO 4007
      DO 4008 M=1,IDC
      M1=I-NF+M-1
      X(M)=R(M1,K)
 4008 Y(M)=A(M1,K)
      CALL FIT(X,Y,IDC,D,C)
      GO TO 4009
 4006 DO 4010 M=1,IDC
      X(M)=R(M,K)
 4010 Y(M)=A(M,K)
      CALL FIT(X,Y,IDC,D,C)
      GO TO 4009
 4007 DO 4011 M=1,IDC
      M1=IM1-IDC+M+1
      X(M)=R(M1,K)
 4011 Y(M)=A(M1,K)
      CALL FIT(X,Y,IDC,D,C)
 4009 DAR(I,K)=0.0
      IF (ABS(A(I,K)-A(I-1,K)).LT.CUT.OR.ABS(A(I,K)-A(I+1,K)).LT.
     1CUT) GO TO 4005
      DO 4012 M=2,IDC
 4012 DAR(I,K)=DAR(I,K)+C(M)*R(I,K)**(M-2)*FLOAT(M-1)
      IF (I.EQ.2) GO TO 4005
      IF (ABS(A(I-1,K)-A(I-2,K)).GT.CUT) GO TO 4005
      DAR(I,K)=(A(I+1,K)-A(I,K))/(R(I+1,K)-R(I,K))
 4005 CONTINUE
 4004 DO 4013 K=1,NK
      DO 4014 M=1,IDB
      X(M)=R(M,K)
 4014 Y(M)=A(M,K)
      CALL FIT(X,Y,IDB,D,C)
```

```
      DAR(1,K)=C(2)
      IF (ABS(A(1,K)-A(2,K)).LT.CUT) DAR(1,K)=0.0
      IM=IMAX(K)
      IM1=IMAX(K)-1
      IM2=IMAX(K)-2
      CON1=(R(IM,K)-R(IM1,K))/(R(IM1,K)-R(IM2,K))
      IN=0
      IF (CON1.LT.0.75) IN=1
      IDB1=IDB-1
      DO 4015 M=1,IDB1
      M1=IM+M-IDB-IN
      X(M)=R(M1,K)
 4015 Y(M)=A(M1,K)
      X(IDB)=R(IM,K)
      Y(IDB)=A(IM,K)
      CALL FIT(X,Y,IDB,D,C)
      DAR(IM,K)=0.0
      DO 4016 M=2,IDB
 4016 DAR(IM,K)=DAR(IM,K)+C(M)*R(IM,K)**(M-2)*FLOAT(M-1)
      DO 4100 M=1,IDB
      M1=IM1+M-IDB-IN+1
      X(M)=R(M1,K)
 4100 Y(M)=A(M1,K)
      CALL FIT(X,Y,IDB,D,C)
      DAR(IM1,K)=0.0
      DO 4101 M=2,IDB
 4101 DAR(IM1,K)=DAR(IM1,K)+C(M)*R(IM1,K)**(M-2)*FLOAT(M-1)
 4013 CONTINUE
      RETURN
      END
```

```
      SUBROUTINE FIT(X,Y,NPT,A,B)
      DIMENSION X(NPT),Y(NPT),A(NPT,NPT),B(NPT)
      DO 5000 KROW=1,NPT
 5000 A(KROW,1)=1.0
      DO 5001 KROW=1,NPT
      DO 5002 KCOL=2,NPT
 5002 A(KROW,KCOL)=X(KROW)**(KCOL-1)
 5001 B(KROW)=Y(KROW)
      CALL SIMQ(A,B,NPT,KS)
      RETURN
      END
```

```
      SUBROUTINE SMOTH(NI,NK,IMAX,KMIN,NII,R,Z,CPSI,CHECK,ERR,IT)
      DIMENSION IMAX(NK),KMIN(NI),R(NI,NK),Z(NI,NK),CPSI(NI,NK),
     1CHECK(NI,NK),ERR(NI,NK)
      COMMON /PAR/ PIE,ALPHA,ALPHAD,DBIL,DPROD,VBIL,NFL,NPFL(25),
     1CR(25,25),CZ(25,25)
      COMMON /ZONE/ ZB(51),ZE(51),RB(51),RE(51)
      COMMON /IZONE/ KB(51),KE(51)
      COMMON /DUM/ X(51),Y(51),C(10),A(100)
      IF (IT.GT.1) GO TO 5500
C
C******FORM DEFORMATION ZONE.
C
      KF=5
      IF (ZB(1).NE.0.0) GO TO 5200
      DO 5210 I=1,NI
      KE(I)=KMIN(I)
      IF (KE(I).LT.3) KE(I)=3
 5210 KB(I)=NK-2
      GO TO 5220
 5200 DO 5600 L=1,NFL
      ZB(L)=ZB(L)+Z(1,2)
 5600 ZE(L)=ZE(L)+Z(1,2)
      DO 5230 L=1,NFL
      X(L)=RE(L)
 5230 Y(L)=ZE(L)
      CALL POLYFT(X,Y,NFL,KF,C,CO,A,-1)
      DO 5240 I=1,NII
      ZE(I)=CO
      DO 5250 M=1,KF
 5250 ZE(I)=ZE(I)+R(I,1)**M*C(M)
      DO 5260 K=1,NK
      IF (Z(I,K).GT.ZE(I)) GO TO 5270
 5260 CONTINUE
 5270 KE(I)=K
 5240 CONTINUE
      N2I=NII+1
      DO 5241 I=N2I,NI
 5241 KE(I)=KMIN(I)
      DO 5280 L=1,NFL
      X(L)=RB(L)
 5280 Y(L)=ZB(L)
      CALL POLYFT(X,Y,NFL,KF,C,CO,A,-1)
      DO 5290 I=1,NI
      ZB(I)=CO
      DO 5300 M=1,KF
 5300 ZB(I)=ZB(I)+R(I,NK)**M*C(M)
      DO 5310 K=1,NK
      IF (Z(I,K).GT.ZB(I)) GO TO 5320
 5310 CONTINUE
 5320 KB(I)=K-1
 5290 CONTINUE
 5220 CONTINUE
 5500 CONTINUE
C
C******CHECK CPSI IN ZONE BEFORE DEFORMATION.
C
      NI1=NI-1
      DO 5400 I=1,NI1
      CON=PIE*ABS(VBIL)*R(I,NK)**2
```

```
      K1=KB(I)+1
      DIF=CON-CPSI(I,K1)
      DO 5410 K=K1,NK
 5410 CPSI(I,K)=CON
      K1=KB(I)
      K2=KE(I)
      DO 5420 K=K2,K1
 5420 CPSI(I,K)=CPSI(I,K)+DIF*FLOAT(K-K2+1)/FLOAT(K1-K2+2)
 5400 CONTINUE
C
C******CHECK CPSI IN ZONE AFTER DEFORMATION.
C
      DO 5401 I=1,N1I
      CON=PIE*ABS(VBIL)*(R(I,1)*DBIL/DPROD)**2
      K1=KE(I)-1
      DIF=CON-CPSI(I,K1)
      DO 5402 K=1,K1
 5402 CPSI(I,K)=CON
      K1=KE(I)
      K2=KB(I)
      DO 5403 K=K1,K2
 5403 CPSI(I,K)=CPSI(I,K)+DIF*FLOAT(K2-K+1)/FLOAT(K2-K1+2)
 5401 CONTINUE
      RETURN
      END
```

```
      SUBROUTINE SMOTHZ(NI,NK,IMAX,KMIN,NII,R,Z,PSI,RPSI,CPSI,IT,
     1DPZ1,CHECK,ERRZ,DERZ)
      DIMENSION IMAX(NK),KMIN(NI),R(NI,NK),Z(NI,NK),PSI(25),RPSI(25,NK)
     1CPSI(NI,NK),DPZ1(NI,NK),CHECK(NI,NK),ERRZ(NI,NK),DERZ(NI,NK),X(50
      COMMON /PAR/ PIE,ALPHA,ALPHAD,DBIL,DPROD,VBIL,NFL,NPFL(25),
     1CR(25,25),CZ(25,25)
      COMMON /IZONE/ KB(51),KE(51)
      N2I=NII-1
      NK1=NK-1
      NK2=NK-2
      CUT=1.0E-10
      CALL DIFZ(R,Z,NI,NK,NII,IMAX,KMIN,CPSI,DPZ1,3,3,CUT)
C
C******CHECK DPZ1 LESS THAN OR EQUAL TO 0.0 THROUGHOUT ZONE.
C
      CALL CHEC(DPZ1,NI,NK,IMAX,KMIN,R,Z,NK,1)
C
C******SMOOTH DPZ1 IN Z DIRECTION BY AVERAGING.
C
      CALL AVZ(DPZ1,NI,NK,IMAX,KMIN,X)
      CALL AVR(DPZ1,R,NI,NK,IMAX,KMIN,X)
      CALL AVZ(DPZ1,NI,NK,IMAX,KMIN,X)
      CALL AVR(DPZ1,R,NI,NK,IMAX,KMIN,X)
C
      DO 5007 I=1,NII
      KM=KMIN(I)
 5007 CALL INGZAT(NI,NK,I,KM,CPSI,DPZ1,Z)
      DO 5400 I=1,NII
      CON=PIE*ABS(VBIL)*R(I,NK)**2
      K1=KB(I)+1
      DIF=CON-CPSI(I,K1)
      DO 5410 K=K1,NK
 5410 CPSI(I,K)=CON
      K1=KB(I)
      K2=KE(I)
      DO 5420 K=K2,K1
 5420 CPSI(I,K)=CPSI(I,K)+DIF*FLOAT(K-K2+1)/FLOAT(K1-K2+2)
 5400 CONTINUE
      DO 5008 K=1,NK
      IM=IMAX(K)
      CPSI(IM,K)=PSI(NFL)
      DO 5008 I=1,IM
 5008 ERRZ(I,K)=CHECK(I,K)-CPSI(I,K)
C
C******AVERAGE ERRZ IN Z DIRECTION.
C
      CALL AVZ(ERRZ,NI,NK,IMAX,KMIN,X)
      CALL AVR(ERRZ,R,NI,NK,IMAX,KMIN,X)
      CALL AVZ(ERRZ,NI,NK,IMAX,KMIN,X)
      DO 5009 I=1,NI
      KM=KMIN(I)
      DO 5009 K=KM,NK
 5009 CPSI(I,K)=CPSI(I,K)+ERRZ(I,K)
      CALL DIFZ(R,Z,NI,NK,NII,IMAX,KMIN,CPSI,DPZ1,3,3,CUT)
 5004 CONTINUE
C
C******CHECK CPSI(I,K) LESS THAN CPSI(I,K-1) FOR ALL I + K.
C
      0  000 ITER=1,40
```

```
      DO 5000 I=1,NI
      KEI=KE(I)
      KBI=KB(I)
      KE1=KE(I)+1
      DO 5001 K=KE1,KBI
      IF (CPSI(I,K).GT.CPSI(I,K-1)) GO TO 5002
 5001 CONTINUE
      GO TO 5000
 5002 KK=K-1
      IF (KK.EQ.KEI) GO TO 5003
      IF (CPSI(I,KK+1).GT.CPSI(I,KK-1)) GO TO 5003
      CPSI(I,KK)=(CPSI(I,KK-1)+CPSI(I,KK+1))/2.0
      GO TO 5000
 5003 CPSI(I,KK+1)=(CPSI(I,KK)+CPSI(I,KK+2))/2.0
 5000 CONTINUE
      RETURN
      END
```

```
      SUBROUTINE INGZAT(NI,NK,I,KM,A,DAZ,Z)
      DIMENSION A(NI,NK),DAZ(NI,NK),Z(NI,NK)
      KM1=KM+1
      DO 2000 K=KM1,NK
      CC=(DAZ(I,K)-DAZ(I,K-1))/(2.*(Z(I,K)-Z(I,K-1)))
      CB=DAZ(I,K)-2.*CC*Z(I,K)
      CA=A(I,K-1)-CB*Z(I,K-1)-CC*Z(I,K-1)**2
 2000 A(I,K)=CA+CB*Z(I,K)+CC*Z(I,K)**2
      RETURN
      END
```

```
      SUBROUTINE INGRAT(NI,NK,K,IM,A,DAR,R)
      DIMENSION A(NI,NK),DAR(NI,NK),R(NI,NK)
      DO 1000 I=2,IM
      CC=(DAR(I,K)-DAR(I-1,K))/(2.*(R(I,K)-R(I-1,K)))
      CB=DAR(I,K)-2.*CC*R(I,K)
      CA=A(I-1,K)-CB*R(I-1,K)-CC*R(I-1,K)**2
 1000 A(I,K)=CA+CB*R(I,K)+CC*R(I,K)**2
      RETURN
      END
```

```
      SUBROUTINE CHEC(X,NI,NK,IMAX,KMIN,R,Z,IT,IDENT)
      DIMENSION X(NI,NK),IMAX(NK),KMIN(NI),R(NI,NK),Z(NI,NK)
      DO 4000 I=1,NI
      DO 4000 ITER=1,IT
      IF (IDENT.EQ.1) GO TO 4001
      KM=KMIN(I)
      DO 4010 K=KM,NK
      IF (X(I,K).LT.0.0) GO TO 4011
 4010 CONTINUE
      GO TO 4000
 4011 K1=K
      K1P1=K1+1
      K1M1=K1-1
      DO 4012 K=K1P1,NK
      IF (X(I,K).GT.0.0) GO TO 4005
 4012 CONTINUE
      GO TO 4000
 4001 KM=KMIN(I)
      DO 4002 K=KM,NK
      IF (X(I,K).GT.0.0) GO TO 4003
 4002 CONTINUE
      GO TO 4000
 4003 K1=K
      K1P1=K1+1
      K1M1=K1-1
      DO 4004 K=K1P1,NK
      IF (X(I,K).LE.0.0) GO TO 4005
 4004 CONTINUE
      GO TO 4000
 4005 K2=K
      K2M1=K2-1
      IF (K1.EQ.1) GO TO 4007
      KINT=K2-K1+1
      DEL=(X(I,K2)-X(I,K1M1))/FLOAT(KINT)
      DO 4006 K=K1,K2M1
 4006 X(I,K)=X(I,K-1)+DEL
      GO TO 4000
 4007 IF (K2.EQ.2) GO TO 4008
      DEL=X(I,K2)/FLOAT(K2-1)
      X(I,1)=0.0
      DO 4009 K=2,K2M1
 4009 X(I,K)=X(I,K-1)+DEL
      GO TO 4000
 4008 X(I,1)=0.0
 4000 CONTINUE
      RETURN
      END
```

```
      SUBROUTINE SMOTHR(NI,NK,IMAX,KMIN,N1I,R,Z,PSI,RPSI,CPSI,DPR1,
     1CHECK,ERRR,DERR,DPR2,DPR3,CH1,CH2)
      DIMENSION IMAX(NK),KMIN(NI),R(NI,NK),Z(NI,NK),PSI(25),RPSI(25,NK)
     1CPSI(NI,NK),DPR1(NI,NK),DPR2(NI,NK),DPR3(NI,NK),CH1(NI,NK),
     1CH2(NI,NK),CHECK(NI,NK),ERRR(NI,NK),DERR(NI,NK),X(50)
      COMMON /PAR/ PIE,ALPHA,ALPHAD,DBIL,DPROD,VBIL,NFL,NPFL(25),
     1CR(25,25),CZ(25,25)
      COMMON /IZONE/ KB(51),KE(51)
C
C******FIND FIRST + SECOND DIFFERENCES OF CPSI W.R.T. R.
C
      CUT=1.0E-10
      CALL DIFR(R,Z,NI,NK,N1I,IMAX,KMIN,CPSI,DPR1,3,3,CUT)
      CALL DIFR(R,Z,NI,NK,N1I,IMAX,KMIN,DPR1,DPR2,3,3,CUT)
C
C******SMOOTH DPR2 IN Z + R DIRECTIONS.
C
      IT=2
      DO 9002 ITER=1,IT
      CALL AVR(DPR2,R,NI,NK,IMAX,KMIN,X)
 9002 CONTINUE
      DO 9100 K=1,NK
      IM=IMAX(K)
      DO 9100 I=1,IM
      IF (DPR2(I,K).GT.DPR2(1,1)) DPR2(I,K)=DPR2(1,1)
 9100 CONTINUE
      CALL AVR(DPR2,R,NI,NK,IMAX,KMIN,X)
      CALL AVR(DPR2,R,NI,NK,IMAX,KMIN,X)
      CALL AVZ(DPR2,NI,NK,IMAX,KMIN,X)
      CALL AVZ(DPR2,NI,NK,IMAX,KMIN,X)
      DO 9010 K=1,NK
      IM=IMAX(K)
      CH1(1,K)=0.0
      DPR1(1,K)=0.0
      CALL INGRAT(NI,NK,K,IM,DPR1,DPR2,R)
 9010 CALL INGRAT(NI,NK,K,IM,CH1 ,DPR1,R)
C
C******SMOOTHING DPR3 IN R DIRECTION.
C
      CALL DIFR(R,Z,NI,NK,N1I,IMAX,KMIN,DPR2,DPR3,3,3,CUT)
      DO 9011 K=1,NK
 9011 DPR3(1,K)=0.0
      CALL AVR(DPR3,R,NI,NK,IMAX,KMIN,X)
      DO 9019 K=1,NK
      IM=IMAX(K)
      CPSI(1,K)=0.0
      DPR1(1,K)=0.0
      CALL INGRAT(NI,NK,K,IM,DPR2,DPR3,R)
      CALL INGRAT(NI,NK,K,IM,DPR1,DPR2,R)
      CALL INGRAT(NI,NK,K,IM,CPSI,DPR1,R)
      IF (CPSI(IM,K).EQ.PSI(NFL)) GO TO 9019
      DIF=(PSI(NFL)-CPSI(IM,K))/R(IM,K)**2
      DO 9020 I=2,IM
 9020 CPSI(I,K)=CPSI(I,K)+DIF*R(I,K)**2
 9019 CONTINUE
      RETURN
      END
```

```
      SUBROUTINE AVZ(X,NI,NK,IMAX,KMIN,XM)
      DIMENSION X(NI,NK),IMAX(NK),KMIN(NI),XM(NK)
      COMMON /IZONE/ KB(51),KE(51)
C
C******SUBROUTINE SMOOTHS ARRAY X IN Z DIRECTION BY AVERAGING.
C
      NI1=NI-1
      DO 2000 I=1,NI1
      KBI=KB(I)
      KEI=KE(I)
      KB1=KB(I)+1
      IF (KEI.EQ.KMIN(I)) KEI=KEI+1
      DO 2001 K=KEI,KB1
 2001 XM(K)=(X(I,K-1)+X(I,K))/2.0
      DO 2002 K=KEI,KBI
 2002 X(I,K)=(XM(K)+XM(K+1))/2.0
 2000 CONTINUE
      RETURN
      END
```

```
      SUBROUTINE AVR(X,R,NI,NK,IMAX,KMIN,XM)
      DIMENSION X(NI,NK),R(NI,NK),IMAX(NK),KMIN(NI),XM(NI),RM(50)
      COMMON /IZONE/ KB(51),KE(51)
C
C******SUBROUTINE SMOOTHS ARRAY X IN R DIRECTION BY AVERAGING.
C
      DO 8000 K=1,NK
      IM=IMAX(K)
      DO 8001 I=1,IM
      IF (K.GE.KE(I).AND.K.LE.KB(I)) GO TO 8002
 8001 CONTINUE
      GO TO 8000
 8002 IST=I
      DO 8003 I=IST,IM
      IF (K.GT.KB(I)) GO TO 8004
 8003 CONTINUE
      IFI=IM-1
      GO TO 8005
 8004 IFI=I
 8005 IF (IST.GT.1) IST=IST-1
      IST1=IST+1
      DO 8006 I=IST,IFI
      RM(I)=(R(I,K)+R(I+1,K))/2.0
 8006 XM(I)=(X(I,K)+X(I+1,K))/2.0
      DO 8007 I=IST1,IFI
 8007 X(I,K)=XM(I-1)+(XM(I)-XM(I-1))*(R(I,K)-RM(I-1))/(RM(I)-RM(I-1))
 8000 CONTINUE
      RETURN
      END
```

```
      SUBROUTINE STRESS(NI,NK,NII,IMAX,KMIN,R,Z,ETRR,ETHH,ETZZ,ETRZ,
     1EFFST,TEFFST,SSEF,SSRR,SSHH,SSZZ,SSRZ,HYD,TEMP,LAM,AC,BC,DCDR,
     2ID,IT)
      DIMENSION IMAX(NK),KMIN(NI),R(NI,NK),Z(NI,NK),ETRR(NI,NK),
     1ETHH(NI,NK),ETZZ(NI,NK),ETRZ(NI,NK),EFFST(NI,NK),TEFFST(NI,NK)
      DIMENSION SSEF(NI,NK),SSRR(NI,NK),SSHH(NI,NK),SSZZ(NI,NK),
     1SSRZ(NI,NK),HYD(NI,NK),LAM(NI,NK),AC(NI,NK),BC(NI,NK)
      DIMENSION TEMP(NI,NK),DCDR(NI,NK)
      COMMON /DUM/                A(51),B(51),DACDZ(51),AE(51),E(51),
     1IST(51),XL(51),YL(51),X(51),DUMMY(2464)
      COMMON /PAR/PIE,ALPHA,ALPHAD,DBIL,DPROD,VBIL,NFL,NPFL(25),
     1CR(25,25),CZ(25,25)
      COMMON /PAR1/ TAMB,PRESS,DSTRS
      COMMON /IZONE/ KB(51),KE(51)
      REAL LAM
      WRITE (6,60)
   60 FORMAT(1H1)
      NK2=NK-2
      IF (KE(1).NE.3.AND.KB(1).NE.NK2) GO TO 8800
      DO 8801 I=1,NI
      KM=KMIN(I)
      DO 8802 K=KM,NK
      IF (EFFST(I,K).GT.0.01) GO TO 8803
 8802 CONTINUE
 8803 KE(I)=K
      KEI=KE(I)
      DO 8804 K=KEI,NK
      IF (ABS(TEFFST(I,K)).LT.0.005) GO TO 8805
 8804 CONTINUE
 8805 KB(I)=K-1
 8801 CONTINUE
 8800 CONTINUE
      IF (ID.NE.1) GO TO 7001
      DO 7000I=1,NI
      DO 7000K=1,NK
 7000 SSEF(I,K)=SSRR(I,K)=SSHH(I,K)=SSZZ(I,K)=SSRZ(I,K)=HYD(I,K)=
     1LAM(I,K)=AC(I,K)=BC(I,K)=TEMP(I,K)=0.0
      DO 7002 K=1,NK
      IM=IMAX(K)
      DO 7002 I=1,IM
 7002 TEMP(I,K)=TAMB
C
C******FIND VALUES OF EFFECTIVE STRESS AT MESH POINTS.
C
 7001 DO 7003 K=1,NK
      IM=IMAX(K)
      DO 7003 I=1,IM
 7003 CALL PROP(TEFFST(I,K),EFFST(I,K),TEMP(I,K),SSEF(I,K))
      NII=NI-1
      DO 7009 K=1,NK
      IM=IMAX(K)
      DO 7009 I=1,IM
      IF (KE(I).GT.K.AND.I.LE.NII) GO TO 7100
      IF (KB(I).LT.K) GO TO 7100
      LAM(I,K)=EFFST(I,K)/SSEF(I,K)
      AC(I,K)=ETRZ(I,K)/LAM(I,K)
      IF (I.EQ.1) GO TO 7009
      BC(I,K)=AC(I,K)/R(I,K)
      GO TO 7009
```

```
 7100 LAM(I,K)=AC(I,K)=BC(I,K)=0.0
 7009 CONTINUE
C
C******INTEGRATION ALONG K = KB(1)
C
      K=KB(1)
      IM=IMAX(K)
      DO 7010 I=1,IM
      A(I)=(ETZZ(I,K)-ETRR(I,K))/LAM(I,K)
      IF (I.EQ.1) GO TO 7011
      B(I)=(ETRR(I,K)-ETHH(I,K))/(R(I,K)*LAM(I,K))
      GO TO 7010
 7011 B(I)=(ETRR(2,K)-ETHH(2,K)-ETRR(I,K)+ETHH(I,K))/(R(2,K)*LAM(I,K))
 7010 CONTINUE
      K1=K-1
      DO 7012 I=1,IM
      IF (AC(I,K).EQ.0.0) GO TO 7040
      IF (AC(I,K1).EQ.0.0) GO TO 7041
      DACDZ(I)=(AC(I,K)-AC(I,K1))/(Z(I,K)-Z(I,K1))
      GO TO 7012
 7040 DACDZ(I)=0.0
      GO TO 7012
 7041 IF (AC(I,K+1).EQ.0.0) GO TO 7042
      DACDZ(I)=(AC(I,K+1)-AC(I,K))/(Z(I,K+1)-Z(I,K))
      GO TO 7012
 7042 DACDZ(I)=DACDZ(I-1)+(DACDZ(I-1)-DACDZ(I-2))*(R(I,K)-R(I-1,K))/
     1(R(I-1,K)-R(I-2,K))
 7012 E(I)=-B(I)-DACDZ(I)/2.0
      AE(1)=0.0
      DO 7013 I=2,IM
 7013 AE(I)=AE(I-1)+(E(I-1)+E(I))*(R(I,K)-R(I-1,K))/2.0
      DO 7014 I=1,IM
 7014 AE(I)=AE(I)+A(I)-A(1)
C
C******INTEGRATION ALONG K = KB(1) IS FINISHED.
C
      NK2=NK-2
      CUT=1.0E-10
      CALL DIFR(R,Z,NI,NK,N11,IMAX,KMIN,AC,DCDR,3,3,CUT)
      KEI=KE(1)
      KBI=KB(1)
      DO 7700 K=KEI,KBI
 7700 BC(1,K)=DCDR(1,K)
      DO 7020 I=1,NI1
      KBI=KB(I)
      KEI=KE(I)
      DO 7022 K=KEI,KBI
      IF (I.EQ.1) GO TO 7021
      XL(K)=DCDR(I,K)+BC(I,K)
      GO TO 7022
 7021 XL(K)=2.0*DCDR(I,K)
 7022 CONTINUE
      K1=KB(1)-1
      YL(K1)=0.0
      K1M1=K1-1
      DO 7023 KS=KEI,K1M1
      K=K1M1-KS+KEI
 7023 YL(K)=YL(K+1)+(XL(K+1)+XL(K))*(Z(1,K+1)-Z(1,K))/2.0
      K1P1=K1+1
```

```
      DO 7123 K=K1P1,KBI
7123  YL(K)=YL(K-1)+(XL(K)+XL(K+1))*(Z(1,K)-Z(1,K-1))/2.0
      DO 7024 K=KEI,KBI
7024  SSZZ(I,K)=2.0*AE(I)/3.0+YL(K)/3.
7020  CONTINUE
      NK3=NK-3
      DO 7200 K1=3,NK3
      IM=IMAX(K1)
7200  SSZZ(IM,K1)=SSZZ(IM-1,K1)+(R(IM,K1)-R(IM-1,K1))*(SSZZ(IM-1,K1)
     1-SSZZ(IM-2,K1))/(R(IM-1,K1)-R(IM-2,K1))
      KEI=KE(1)
      X(1)=PIE*R(2,1)**2*SSZZ(1,KEI)/4.0
      N2=N1I-1
      DO 7025 I=2,N2
      KEI=KE(I)
7025  X(I)=X(I-1)+PIE*SSZZ(I,KEI)*((R(I,KEI)+R(I+1,KEI))**2/4.0-
     1(R(I,KEI)+R(I-1,KEI))**2/4.0)
      KEI=KE(N1I)
      X(N1I)=X(N2)+PIE*SSZZ(N1I,KEI)*(R(N1I,KEI)**2-(R(N1I,KEI)+
     1R(N2,KEI))**2/4.0)
      SAV=X(N1I)/(PIE*R(N1I,KEI)**2)
      DO 7026 K=1,NK
      IM=IMAX(K)
      DO 7026 I=1,IM
7026  SSZZ(I,K)=SSZZ(I,K)-SAV+DSTRS
      DO 7027 I=1,N1I
      KEI=KE(I)
      KBI=KB(I)
      DO 7030 K=KEI,KBI
      SSRR(I,K)=SSZZ(I,K)+2.0*(ETRR(I,K)-ETZZ(I,K))/(3.*LAM(I,K))
      SSHH(I,K)=SSZZ(I,K)+2.0*(ETHH(I,K)-ETZZ(I,K))/(3.*LAM(I,K))
      SSRZ(I,K)=ETRZ(I,K)/(3.0*LAM(I,K))
7030  HYD(I,K)=(SSRR(I,K)+SSHH(I,K)+SSZZ(I,K))/3.0
      KBI=KBI+1
      DO 7027 K=KBI,NK
      SSRR(I,K)=PRESS
      SSHH(I,K)=PRESS
      SSZZ(I,K)=PRESS
      HYD(I,K)=PRESS
      SSRZ(I,K)=0.0
7027  CONTINUE
      DO 7031 K=3,NK
      N2I=N1I+1
      IM=IMAX(K)
      DO 7031 I=N2I,IM
      IF (K.GT.KB(I)) GO TO 7032
      SSRR(I,K)=SSZZ(I,K)+2.0*(ETRR(I,K)-ETZZ(I,K))/(3.*LAM(I,K))
      SSHH(I,K)=SSZZ(I,K)+2.0*(ETHH(I,K)-ETZZ(I,K))/(3.*LAM(I,K))
      SSRZ(I,K)=ETRZ(I,K)/(3.0*LAM(I,K))
      HYD(I,K)=(SSRR(I,K)+SSHH(I,K)+SSZZ(I,K))/3.0
      GO TO 7031
7032  K1=KB(I)
      SSRR(I,K)=PRESS
      SSHH(I,K)=PRESS
      SSZZ(I,K)=PRESS
      HYD(I,K)=PRESS
      SSRZ(I,K)=0.0
7031  CONTINUE
      DO 7444 I=1,N1I
```

```
      K1=KE(I)
      DO 7444 K=1,K1
      SSRR(I,K)=0.0
      SSHH(I,K)=0.0
      HYD(I,K)=0.0
      SSRZ(I,K)=0.0
7444  SSZZ(I,K)=DSTRS
      RETURN
      END
```

```
      SUBROUTINE PROP(TST,STRA,TEMP,STRS)
      COMMON /MATP/ NPT,STRAI(50),STRES(50),NVP,PVD(50),VISC(50)
      DO 1000 N=1,NPT
      IF (STRAI(N).GT.ABS(TST)) GO TO 1001
1000  CONTINUE
      IF (N.GT.NPT) N=NPT
1001  STRS=STRES(N-1)+(STRES(N)-STRES(N-1))*(ABS(TST)-STRAI(N-1))/
     1(STRAI(N)-STRAI(N-1))
      RETURN
      END
```

```
      SUBROUTINE SURF(NI,NK,NII,IMAX,KMIN,U,V,SSRR,SSZZ,SSRZ,R,Z,ID)
      DIMENSION IMAX(NK),KMIN(NI),U(NI,NK),V(NI,NK),SSRR(NI,NK),
     1SSZZ(NI,NK),SSRZ(NI,NK),R(NI,NK),Z(NI,NK)
      COMMON /IZONE/ KB(51),KE(51)
      COMMON /MATP/ NPT,STRAI(50),STRES(50),NVP,PVD(50),VISC(50)
      COMMON /DUM/ SVEL(51),ANGLE(51),SNORS(51),SSHES(51),SMU(51),X(51)
     1PD(51),SD(51),DPDDX(51),H(51),VD(51)
      DO 9000 K=1,NK
      IM=IMAX(K)
      SVEL(K)=SQRT(U(IM,K)**2+V(IM,K)**2)
      ANGLE(K)=ATAN(V(IM,K)/U(IM,K))
      SNORS(K)=SSRR(IM,K)*COS(ANGLE(K))**2+SSZZ(IM,K)*SIN(ANGLE(K))**2
     1-2.*SSRZ(IM,K)*SIN(ANGLE(K))*COS(ANGLE(K))
      SSHES(K)=SSRZ(IM,K)*(COS(ANGLE(K))**2-SIN(ANGLE(K))**2)+
     1(SSRR(IM,K)-SSZZ(IM,K))*SIN(ANGLE(K))*COS(ANGLE(K))
 9000 SMU(K)=SSHES(K)/SNORS(K)
      WRITE(6,60)
   60 FORMAT(1H1)
      WRITE(6,61)
   61 FORMAT(1X,70H K SECTION  NORMAL PRESSURE  SHEAR STRESS  FRICTION
     1OEFFICIENT                //)
      KBI=KB(NI)
      WRITE(6,62) ((K,SNORS(K),SSHES(K),SMU(K)),K=3,KBI)
   62 FORMAT(6X,I2,8X,F7.4,9X,F7.4,12X,F6.4)
      IF (ID.EQ.1) RETURN
C
C******SET UP COORDINATE SYSTEM FOR FLUID FILM CALCULATIONS.
C
      SIAN=SIN(ALPHA)
      COAN=COS(ALPHA)
      TAAN=TAN(ALPHA)
      CON=DPROD/(2.0*SIAN)
      DIF=(Z(1,2)-Z(1,1))/(2.0*COAN)
      KBI=KB(NI)
      DO 9001 K=3,KBI
      IM=IMAX(K)
      R1=(CON+Z(1,K)-Z(3,K))/TAAN-R(IM,K)
      X(K)=(CON+Z(1,K)-Z(3,K))/SIAN-R1*COAN
      PD(K)=SSZZ(IM,K)*COAN**2+SSRR(IM,K)*SIAN**2-2.*SSRZ(IM,K)*SIAN*
     1COAN
      SD(K)=SSRZ(IM,K)*(COAN**2-SIAN**2)+(SSRR(IM,K)-SSZZ(IM,K))*SIAN*
     1COAN
      IF (K.EQ.3) GO TO 9002
      IF (K.EQ.KBI) GO TO 9003
      DPDDX(K)=(PD(K)-PD(K-1))/(X(K)-X(K-1))+(X(K)-X(K-1))*((PD(K+1)-PD
     1(K))/(X(K+1)-X(K))-(PD(K)-PD(K-1))/(X(K)-X(K-1)))/(X(K+1)+X(K-1))
      GO TO 9001
 9002 DPDDX(3)=(PD(4)-PD(3))/(X(4)-X(3))
      GO TO 9001
 9003 DPDDX(KBI)=(PD(KBI)-PD(KBI-1))/(X(KBI)-X(KBI-1))
 9001 CONTINUE
      DO 9004 K=3,KBI
      DO 9005 L=1,NVP
      IF (PD(K).GT.PVD(L)) GO TO 9006
 9005 CONTINUE
 9006 VD(K)=VISC(L-1)+(VISC(L)-VISC(L-1))*(PD(K)-PVD(L-1))/(PVD(L)-
     1PVD(L-1))
 9004 H(K)=(SSHES(K)+SQRT(SSHES(K)**2-2.*VD(K)*SVEL(K)*DPDDX(K)))/
     1DPDDX(K)
```

```
      KBI=KB(NI)
      WRITE(6,60)
      WRITE(6,63)
   63 FORMAT(1X,40H K SECTION  VISCOSITY  FILM THICKNESS          //)
      WRITE(6,64) ((K,VD(K),H(K)),K=3,KBI)
   64 FORMAT(6X,I2,6X,F7.4,6X,F8.6)
      RETURN
      END
```

APPENDIX IV - Least Mean Square Polynomial Fit

The least mean square fitting is used to fit a polynomial, $y = f(x)$, to a series of experimental points (x_i, y_i) where $i = 1, N$. The program to calculate the values of the coefficients of the polynomial, POLYFT, is written so that any coefficients, specified in an array, KC, can be set to zero. The polynomial is given by

$$y = C_1 + C_2 x^{KC(1)} + C_2 x^{KC(2)} + \ldots + C_{n+1} x^{KC(N)}$$

If KC(1) = 0, then the coefficient is set to zero, otherwise KC(I) is set equal to the power, I. In all cases the coefficients are numbered consecutively. For instance, in the routine FLOW, the optimum form for finding the flow function at the mesh points from the known values along the flow lines was found to be

$$y = C_1 + C_2 x^2 + C_3 x^4 + C_4 x^6 + C_5 x^8$$

In calculating the coefficients, the sum of the squared deviations must be minimised.

$$S = \sum_{i=1}^{N} [y_i - (C_1 + C_2 x_i^{KC(I)} \ \ldots \ C_{n+1} x^{KC(N)})]^2$$

The condition that S should be a minimum, with respect to the coefficients, results in

$$\frac{\partial S}{\partial C_1} = \frac{\partial S}{\partial C_2} = \ldots. = \frac{\partial S}{\partial C_{n+1}} = 0$$

Carrying out the partial derivatives gives

$$NC_1 + \sum_1^N x_i C_2 + \cdots\cdots + \sum_1^N x_i^{KC(n)} C_{n+1} = \sum_1^N y_i$$

$$\sum_1^N x_i C_1 + \sum_1^N x_i^2 C_2 + \cdots\cdots + \sum_1^N x_i^{KC(n)+1} C_{n+1} = \sum_1^N y_i x_i$$

$$\vdots$$

$$\sum_1^N x_i^{KC(n)} C_1 + \sum_1^N x_i^{KC(n)+1} C_2 + \cdots\cdots \sum_1^N x_i^{2KC(n)} C_{n+1} = \sum_1^N y_i x_i^{KC(n)}$$

This system of simultaneous linear equations is solved digitally by SIMQ. The total number of unknowns is the number of non-zero elements in KC plus one. This corresponds to the number of equations above, as one equation is lost for each zero coefficient.

APPENDIX V Derivation of the Viscometer Relationship

A5.1 Extension of Simple Theory

The dimensions referred to in the following analysis are detailed in Fig. A5.1. For convenience, the sinker is assumed to be at rest and the tube moving upwards at constant velocity, V.

The total mass flow rate past the sinker is given by

$$Q = Q_A + Q_B = \pi r_T^2 V \qquad \text{A5.1}$$

where Q_A is the flow rate through the annulus and Q_B is that through the bore.

In this theory the change of pressure in the inlet and outlet regions is ignored, that is $p_3 = p_2$ and $p_4 = p_1$.

The buoyancy corrected weight of the sinker is balanced by a viscous shear force, S_S composed of two parts, S_A on the sinker surface and S_B in the bore, and by the pressure difference across its ends.

$$-mg + S_S + (p_2 - p_1)(r_A^2 - r_B^2) = 0 \qquad \text{A5.2}$$

where $$S_S = S_A + S_B \qquad \text{A5.3}$$

Considering the bore first, the flow pattern and distribution of velocity gradient are given in Fig. A5.2.

By equilibrium

$$S_B = -2\pi r_B \ell_B \eta \left(\frac{dU_S}{dS}\right)_{r_B} = (p_2 - p_1)\, \pi r_B^2 \qquad \text{A5.4}$$

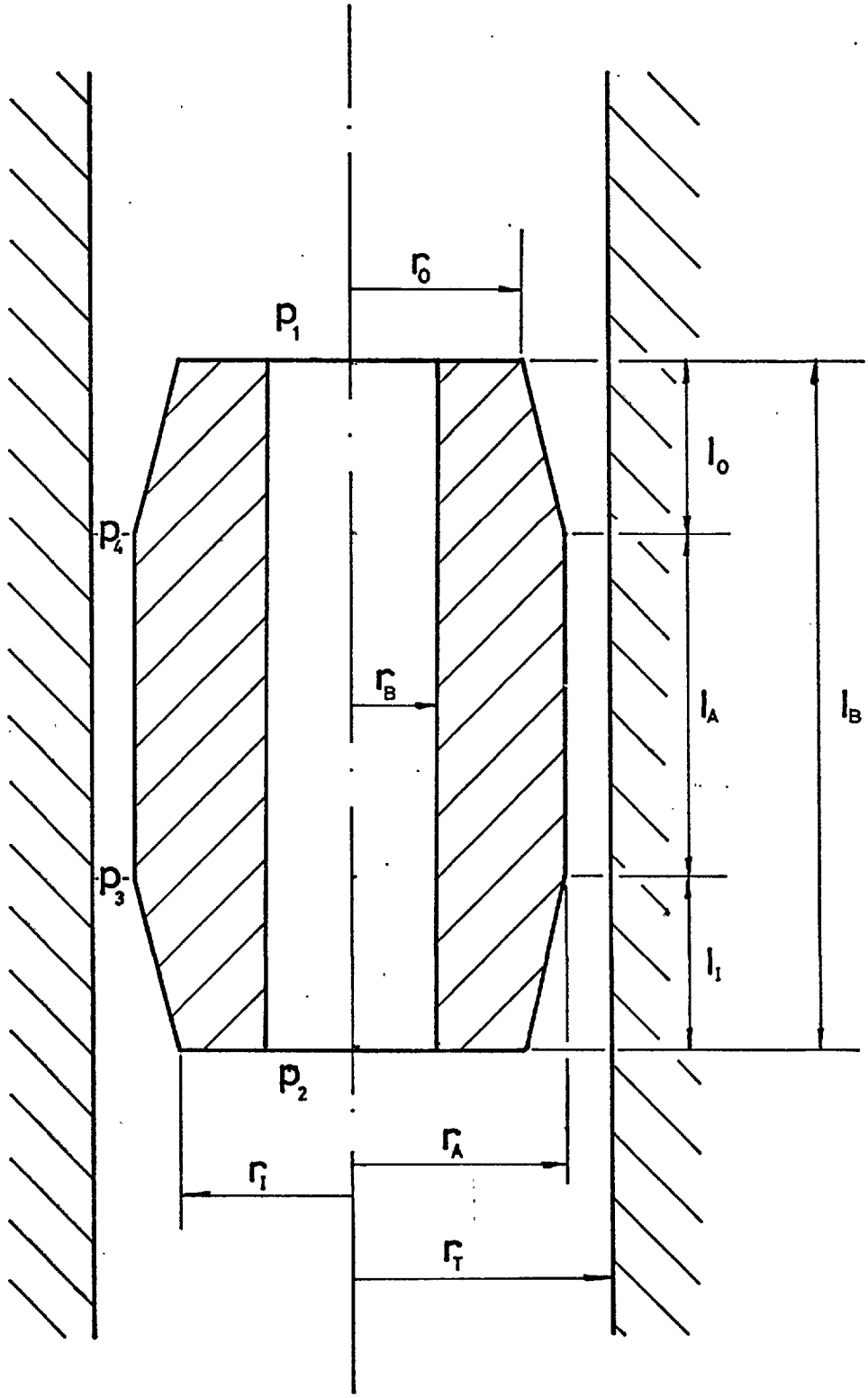

Fig. A5.1. Sinker geometry.

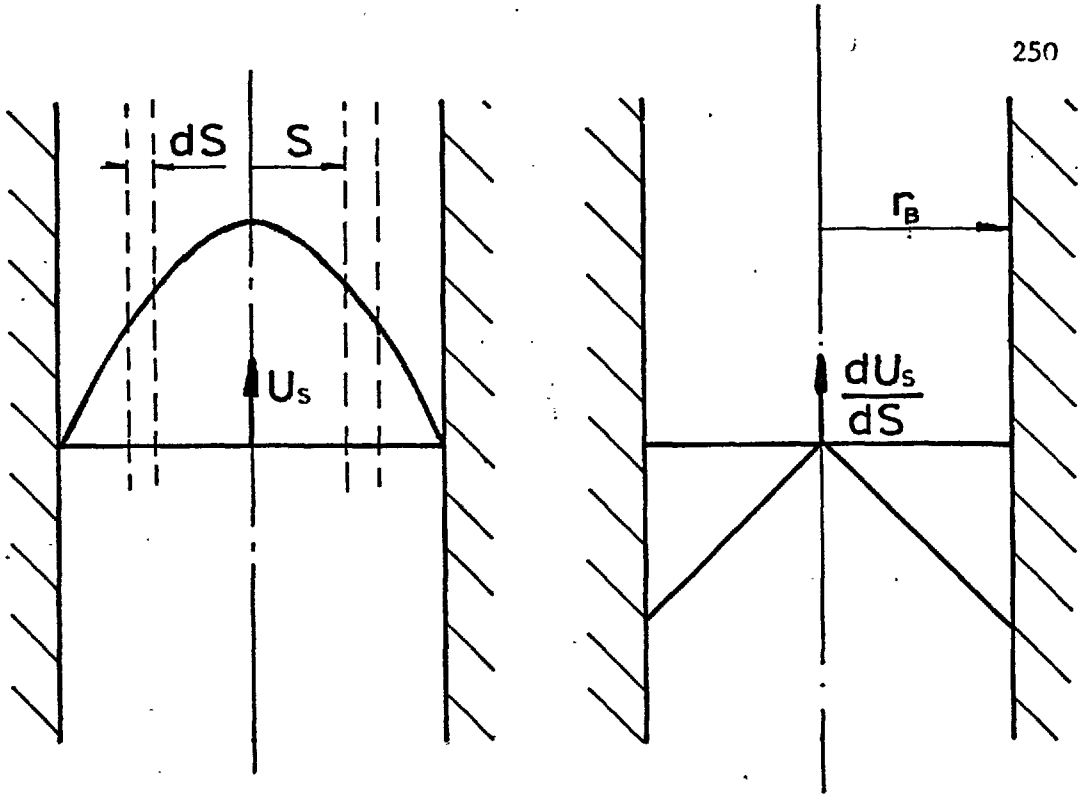

Fig.A5.2. Velocity and velocity gradient distribution in bore.

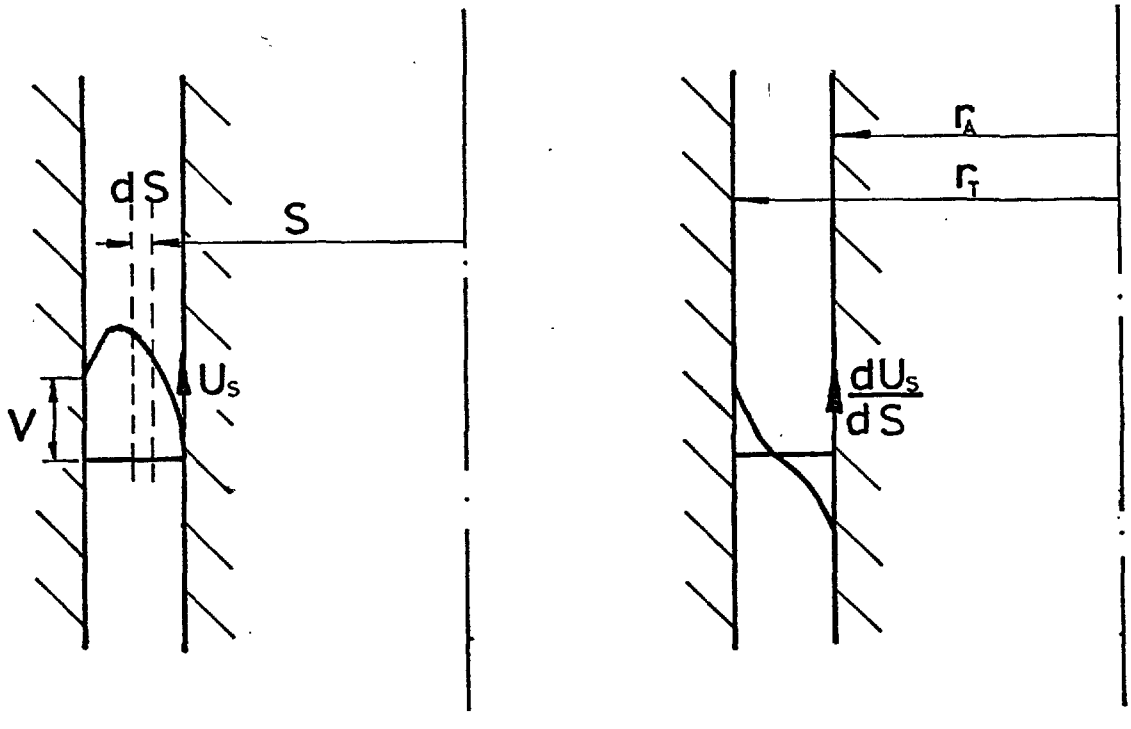

Fig.A5.3. Velocity and velocity gradient distribution in the annulus.

and $$(p_2 - p_1)\ \pi S^2 + 2\pi S \ell_B \eta \left(\frac{dU_S}{dS}\right) = 0$$

Integrating the last equation and substituting the boundary conditions $U_S = 0$ at $S = r_B$ gives

$$2\ell_B \eta U_S = \frac{1}{2}(p_2 - p_1)(r_B^2 - S^2)$$

The flow through the bore is given by

$$Q_B = 2\pi \int_0^{r_B} S.U_S.dS$$

Hence $$Q_B = \frac{\pi(p_2 - p_1) r_B^4}{8\ell_B \eta} \qquad \text{A5.5}$$

From eqs. A5.1 and A5.5 we may now write

$$Q_A = \pi r_T^2 V - \frac{\pi(p_2 - p_1) r_B^4}{8\ell_B \eta} \qquad \text{A5.6}$$

and from A5.2, A5.3 and A5.4

$$-mg + S_A + (p_2 - p_1)\ \pi r_A^2 = 0 \qquad \text{A5.7}$$

Now considering the flow in the annulus, with velocity and velocity gradient distributions as shown in Fig. A5.3, we may write, by equilibrium

$$\pi(p_2 - p_1)(S^2 - r_A^2) - S_A + 2\pi S \ell_A \eta \frac{dU_S}{dS} = 0 \qquad \text{A5.8}$$

Adding A5.7 and A5.8, rearranging and integrating gives

$$U_S = \frac{mg \ln S}{2\pi \ell_A \eta} - \frac{(p_2 - p_1)S^2}{4\ell_A \eta} + C$$

The boundary conditions are $U_S = 0$ when $S = r_A$ and $U_S = V$ when $S = r_T$.

$$\therefore \quad p_2 - p_1 = \frac{2mg \ln (r_T/r_A)}{\pi(r_T^2 - r_A^2)} - \frac{4\ell_A V\eta}{(r_T^2 - r_A^2)} \qquad \text{A5.9}$$

and $$C = \frac{- mg \ln r_A}{2\pi \ell_A \eta} + \frac{(p_2 - p_1) r_A^2}{4\ell_A \eta} - V$$

$$\therefore \quad U_S = \frac{mg \ln(S/r_A)}{2\pi \ell_A \eta} - \frac{mg(S^2 - r_A^2) \ln(r_T/r_A)}{2\pi \ell_A \eta (r_T^2 - r_A^2)} + V \frac{(S^2 - r_T^2)}{(r_T^2 - r_A^2)} \qquad \text{A5.10}$$

The flow through the annulus, Q_A, is given by

$$Q_A = 2\pi \int_{r_A}^{r_T} S.U_S.dS$$

Substituting A5.10 and integrating gives

$$Q_A = \frac{mg}{4\ell_A \eta} \left[(r_T^2 + r_A^2) \ln \frac{r_T}{r_A} - (r_T^2 - r_A^2) \right] - \frac{\pi V}{2} (r_T^2 - r_A^2) \qquad \text{A5.11}$$

The volume flow rate through the annulus is also given by A5.6. Therefore, equating A5.6 and A5.11, we get on substituting $(p_2 - p_1)$ from A5.9 and $V = \frac{\ell_T}{t^*}$

$$\eta = \frac{mgt^*}{2\pi\ell_A\ell_T} \left[\frac{(r_T^2 + r_A^2) \ln \frac{r_T}{r_A} - (r_T^2 - r_A^2) + \frac{\ell_A r_B^4 \ln \frac{r_T}{r_A}}{\ell_B(r_T^2 - r_A^2)}}{(3r_T^2 - r_A^2) + \frac{\ell_A r_B^4}{\ell_B(r_T^2 - r_A^2)}} \right] \qquad \text{A5.12}$$

A5.2 Theory including Inlet and Outlet Flow

The analysis is exactly as in the previous section as far as eq. A5.7.

Considering the inlet region first, the pressure change is governed by the equilibrium equation in polar coordinates

$$\frac{dp}{dx} = \frac{d\tau}{dS} + \frac{\tau}{S} \qquad \text{A5.13}$$

Assuming a Newtonian fluid

$$\tau = \eta \frac{dU_S}{dS}$$

Substituting in A5.13 gives

$$\frac{dp}{dx} = \eta \frac{d^2U_S}{dS^2} + \frac{\eta}{S} \frac{dU_S}{dS}$$

$$S. \frac{dp}{dx} = \eta \frac{d}{dS} \left(S \frac{dU_S}{dS}\right)$$

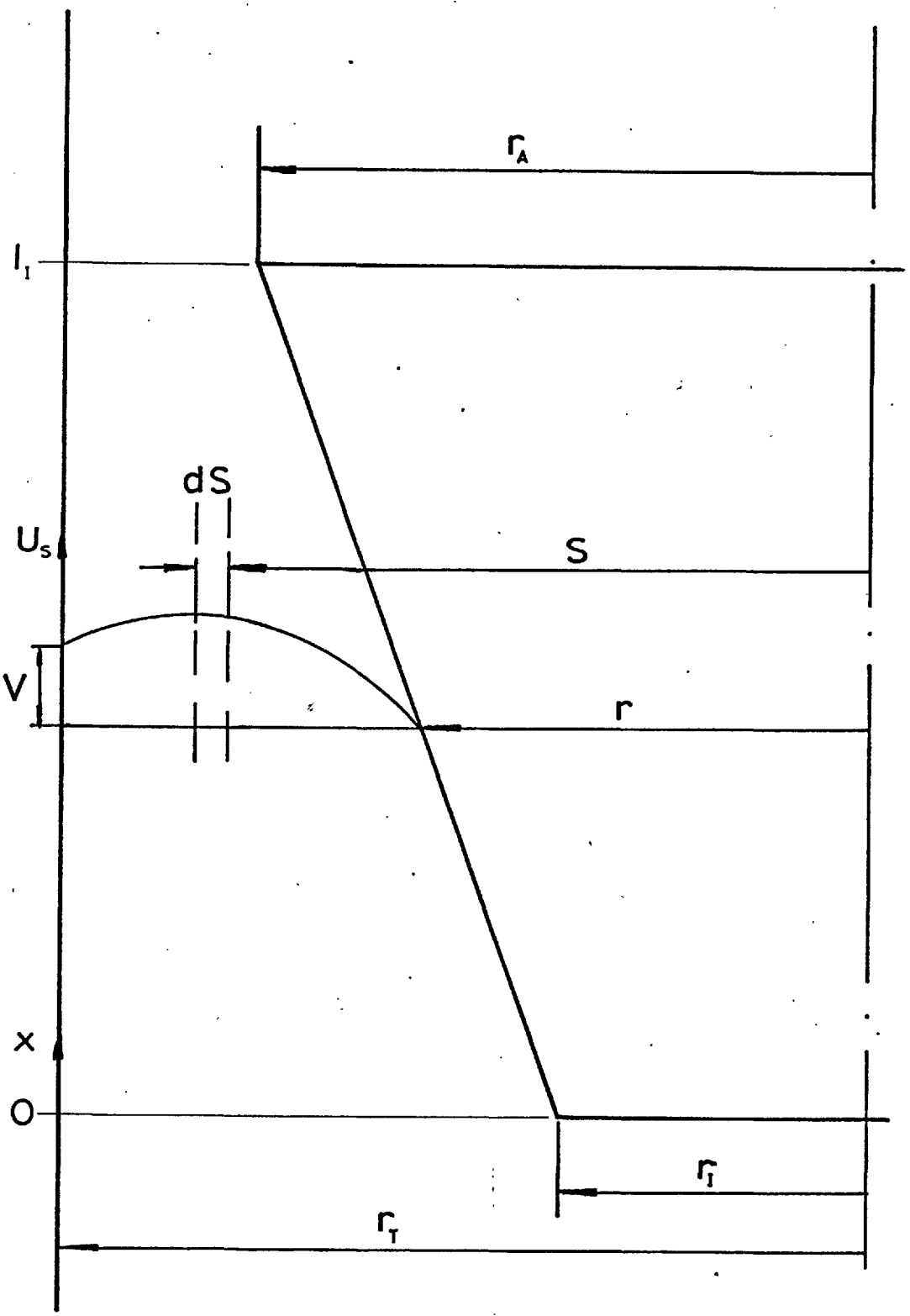

Fig.A5.4. Velocity distribution in the inlet region.

Finally $$U_S = \frac{S^2}{4\eta}\frac{dp}{dx} + A.S + B$$

When $S = r$, $U_S = 0$ and when $S = r_T$, $U_S = V$ therefore

$$U_S = \frac{S^2 - r^2}{4\eta} \cdot \frac{dp}{dx} + \left[\frac{V}{r_T - r} - \frac{r_T + r}{4\eta} \cdot \frac{dp}{dx}\right] (S - r)$$

The flow through the annulus is given by

$$Q_A = 2\pi \int_r^{r_T} S.U_S.dS$$

Substituting for U_S, integrating and solving for $\frac{dp}{dx}$ gives

$$\frac{dp}{dx} = \frac{8\eta(3Q_A(r-r_T) + V\pi(2r_T^3 - 3r_T^2\, r + r^3))}{\pi(r_T-r)(r_T^4 - 2r_T^3\, r + 2r_T r^3 - r^4)} \qquad \text{A5.14}$$

Taking S_{AI} as the vertical component of the shear stress on the annulus, we have

$$\frac{dS_{AI}}{dx} = 2\pi r\eta \left(\frac{dU_S}{dS}\right)_r$$

Substituting for U_S we get

$$\frac{dS_{AI}}{dx} = 2\pi r\eta \left(\frac{V}{r_T - r} + \frac{r - r_T}{4\eta} \cdot \frac{dp}{dx}\right) \qquad \text{A5.15}$$

Also, from geometry

$$r = r_I + \frac{x(r_A - r_I)}{\ell_I} \qquad \text{A5.16}$$

In the parallel portion of the annulus the derivation is exactly as above with r replaced by r_A. As the right hand side of eq. A5.14 is then a constant, it can be integrated to give

$$(p_4 - p_3) = 8\eta\ell_A \frac{(3Q_A(r_A - r_T) + V\pi(2r_T^2 - 3r_T^2 r_A + r_A^3))}{\pi(r_T - r_A)(r_T^4 - 2r_T^3 r_A + 2r_T r_A^3 - r_A^4)} \qquad \text{A5.17}$$

Similarly, the shear stress equation can be integrated to give

$$S_{AA} = 2\pi r_A \eta \ell_A \left(\frac{V}{r_T - r_A} + \frac{r_A - r_T}{4\eta} \frac{(p_4 - p_3)}{\ell_A} \right) \qquad \text{A5.18}$$

In the outlet portion the derivation is the same as for the inlet and eqs. A5.14 and A5.15 stand. Eq. A5.16 is replaced by

$$r = r_A - \frac{x(r_A - r_0)}{\ell_0} \qquad \text{A5.19}$$

As equations A5.15 and A5.16 cannot be integrated directly, they are integrated numerically by Simpson's Rule. The equations may be written as follows:

$$\begin{aligned}
&\text{Inlet} && p_3 - p_2 = (A_1 Q_A + B_1 V)\eta \\
&\text{Parallel} && p_4 - p_3 = (A_2 Q_A + B_2 V)\eta \\
&\text{Outlet} && p_1 - p_4 = (A_3 Q_A + B_3 V)\eta \\
&\text{and} && p_1 - p_2 = (A_4 Q_A + B_4 V)\eta
\end{aligned} \qquad \text{A5.20}$$

Substituting in A5.6 gives

$$Q_A = \pi r_T^2 V + \frac{\pi(A_4 Q_A + B_4 V) r_1^4}{8\ell_B}$$

$$Q_A = \frac{\pi r_T^2 8\ell_B V + \pi r_B^4 B_4 V}{8\ell_B - \pi A_4 r_B^4} = D.V \qquad \text{A5.21}$$

Once Q_A is known, the values of S_{AI}, S_{AA} and S_{AO} can be found. Three expressions are formed

$$S_{AI} = C_1 \eta V$$

$$S_{AA} = C_2 \eta V$$

$$S_{AO} = C_3 \eta V$$

Therefore

$$S_A = C_4 \eta V \quad \text{where } C_4 = C_1 + C_2 + C_3$$

Substituting in eq. A5.7 gives

$$-mg + C_4 \eta V - (A_4 D + B_4) \eta V \pi r_A^2 = 0$$

on the assumption that $r_I = r_0$. If this is not the case the absolute magnitude of the pressure becomes important.

Writing $V = \frac{\ell_T}{t^*}$ and rearranging, we get

$$\eta = \frac{mgt^*}{\ell_T} \quad \frac{1}{(C_4 - (A_4 D + B_4)\pi r_A^2)} \qquad \text{A5.22}$$

or $\eta = mg.t^* k$

APPENDIX VI - Atmospheric Measurements

A6.1 Viscometer Measurements

As the universal measuring machine used for the measurements read in inches, these units are used here. Conversion to S.I. units was carried out by the computer programs in which the values were used.

A6.1.1 Tube Dimensions

The tube diameter was measured and found to be 0.31725 in.

To find the distance between the triggering points a sinker was lowered through the coils by a depth micrometer. The average distance over which fall was timed was found to be 7.206 in, the difference between the two directions being only 0.004 ins.

A6.1.2 Sinker Dimensions

	L.EN58	S.EN58	S.L65
D_B	0.09488	0.13160	0.13449
D_A	0.28789	0.28260	0.28359
D_I	0.24113	0.23435	0.24295
D_O	0.25746	0.23246	0.24212
ℓ_I	0.18835	0.17150	0.14448
ℓ_A	0.40682	0.35529	0.40662
ℓ_O	0.18487	0.17363	0.14815
ℓ_B	0.78004	0.70042	0.69925

Here L.EN58 refers to the long stainless steel sinker,

S.EN58 refers to the short stainless steel sinker,

and S.L65 refers to the short duralumin sinker.

By hydrostatic weighing the densities of the long stainless, short stainless and short dural sinkers were found to be 7640, 7750 and 4070 kg/m^3 respectively.

For stainless steel the coefficient of thermal expansion is $1.6 \times 10^{-5}/^{o}C$ and the volume compressibility is 2.123×10^{-4}/kbar. The corresponding values for the L65 alloy are $2.2 \times 10^{-5}/^{o}C$ and 4.43×10^{-4}/kbar.

A6.2 Fluid Properties

To measure the viscosity at atmospheric pressure, suspended level viscometers complying with specifications by BS/IP/SL were used. A size 2A capillary was used for castor oil and a size 2 for Tellus 27. At $21.7^{o}C$ the kinematic viscosity of the castor oil was found to be 9.232×10^{-4} m^2/s while that of the Tellus 27 was 0.7474×10^{-4} m^2/s.

Density values were found by weighing a precision 2.54 cm diameter ball in the two fluids and in air. After correction for the density of air, the densities of castor oil and Tellus 27 were found to be 957.7 kg/m^3 and 843.5 kg/m^3 respectively, at $21.7^{o}C$. Thus the absolute viscosities can be calculated as 0.8841 kg/ms for castor oil and 0.06304 kg/ms for Tellus 27, both at $21.7^{o}C$.

REFERENCES

1. Feldman, H.D. 'Cold Forging of Steel'. Hutchinson, London, 1961.
2. Ling, F.F., Whitely, R.L., Ku, P.H. and Peterson, M.B. (Eds.) 'Friction and Lubrication in Metal Processing', A.S.M.E. 1966.
3. Schey, J.A. (Ed.). 'Metal Deformation Processes - Friction and Lubrication', Marcel Dekker, 1970.
4. Krönberger, H., 'Hydrostatic Extrusion'. Proc. Roy. Soc. 1968.
5. Hornmark, N. 'Design of the ASEA Hydrostatic Extrusion Equipment'. Lecture 21. Post-Experience Course - Hydrostatic Extrusion. Imperial College, 1969.
6. Bowden, F.P. and Tabor, D. 'The Friction and Lubrication of Solids'. Clarendon Press, 1950.
7. Cameron, A. 'Principles of Lubrication'. Longmans, 1966.
8. 1953 A.S.M.E. Pressure-Viscosity Report.
9. Chu, P.S.Y. and Cameron, A. 'Pressure-Viscosity Characteristics of Lubricating Oils'. J. Inst. Petrol. 48, (461), pp 147-155, 1962.
10. Bridgman, P.W. 'The Effect of Pressure on the Viscosity of 43 Pure Liquids'. Proc. Am. Acad. Arts Sci. 61, pp 57-99, 1926.
11. Bridgman, P.W. 'Viscosities to 30,000 kg/cm^2'. Ibid. 77, pp 117-128, 1949.
12. Hersey, M.D. and Hopkins, R.E. 'Viscosity of Lubricants under Pressure'. A.S.M.E. New York, 1954.
13. Hersey, M.D. 'Theory and Research in Lubrication', Wiley, New York, 1966.
14. Wilson, W.R.D. 'The Viscometry of Lubricants Under High Pressures and Temperatures'. Ph.D. Thesis, Queens Univ. Belfast, 1967.
15. MacLellan, G.D.S. and Cameron, A. British Patent No. 566,434, 1944.

16. Christopherson, D.G. and Naylor, H. 'Promotion of Fluid Lubrication in Wire Drawing'. Proc. Inst. Mech. Engrs., 169, pp 643-53, 1955.

17. Dromgold, L.D. and Rodman, S. 'Effects of Rolling Lubricant Viscosity on the Reduction of Aluminium during Cold Rolling'. Jour. ASLE, pp 26-31, 1970.

18. Schroeder, W. and Webster, D.A. 'Press-Forging Thin Sections: Effect of Friction, Area and Thickness on Pressures Required'. ASME J. Appl. Mechs. pp 289-294, 1949.

19. van Rooyen, G.T. and Backofen, W.A. 'A Study of Interface Friction in Plastic Compression'. Int. J. Mech. Sci. 1, pp 1-27, 1960.

20. Kunogi, M. J. Sci. Research Inst. (Tokyo) 50, p 215, 1956.

21. Male, A.T. and Cockcroft, M.G. 'A Method for the Determination of the Coefficient of Friction of Metals under Conditions of Bulk Plastic Deformation'. J. Int. Metals, 93, p 38, 1964-5.

22. Kobayashi, S. 'Upper Bound Solutions of Axi-Symmetric Forming Problems'. ASME, J. Eng. Ind. 86, p 326, 1964.

23. Kudo, H. 'Some Analytical and Experimental Studies of Axi-Symmetric Cold Forging and Extrusion - I', Int. J. Mech. Sci., 2, pp 102-7, 1961 and Part II, Int. J. Mech. Sci., 3, pp 91-117, 1962.

24. Avitzur, B. 'Forging of Hollow Discs'. Israel J. Tech., 2, pp 295-304, 1964.

25. Male, A.T. 'Variations in Friction Coefficients of Metals during Compressive Deformation'. J. Inst. Metals, 94, p 121, 1966.

26. Guminski, R.D. and Willis, J. J. Inst. Metals, 88, p 481, 1960.

27. Watts, A.B.and Ford, H. Proc. Inst. Mech. Engrs. 169, p 123, 1955.

28. Alexander, J.M. 'The Effects of Coulomb Friction in the Plane-Strain Compression of a Plastic-Rigid Material '. J. Mech. Phys. Solids, 3, pp 233-45, 1955.

29. Takahashi, H. and Alexander, J.M. 'Friction in the Plane-Strain Compression Test'. J. Inst. Metals 90, pp 72-79, 1962.

30. Shaw, M.S., Stableford, W.H. and Sansome, D.H. 'Critical Review of Drawing with Particular Reference to Lubrication'. Int. J. Mech. Tool Des. Res. 10, pp 203-212, 1970.

31. Wistreich, J.G. 'Investigation of the Mechanics of Wire Drawing'. Proc. Inst. Mech. Engrs. 169, p 654, 1955.

32. MacLellan, G.D.S. 'A Critical Survey of Wire Drawing Theory'. J. Iron Steel Inst. 158, p 347, 1948.

33. Yang, C.T. 'On the Mechanics of Wire Drawing'. J. Eng. Ind. A.S.M.E. 83, p 523, 1956.

34. Majors, H. 'Studies in Cold Drawing.Part 3 - Determination of Coefficient of Friction'. A.S.M.E. 78, p 79, 1956.

35. Blazynski, T.Z. and Cole, I.M. 'An Investigation of the Plug Drawing Process'. Proc. Inst. Mech. Engrs. 174, p 797, 1960.

36. Lancaster, P.R. and Rowe, G.W. 'Experimental Study of the Influence Of Lubrication upon Cold Drawing under Approximately Plane-Strain Conditions'. Ibid. 178, p 69, 1964.

37. Thomsen, E.G. and Lapsley, J.T. 'Experimental Stress Determination within a Metal during Plastic Flow'. Proc. Soc. Exp. Stress Anal. 11, p 59, 1954.

38. Thomsen, E.G., Yang, C.T. and Bierbower, J.B. 'An Experimental Investigation of the Mechanics of Plastic Deformation of Metals'. Univ. of California ~~Press~~ Publications in engineering. Vol 5 no 4, pp 89-144, 1954.

39. Shabaik, A., Lee, C.H., and Kobayashi, S. 'Application of the Visioplasticity Method to Extrusion through a Conical Die'. 7th M.T.D.R. conf. Birmingham 1966. Pergamon, p 633.

40. Shabaik, A. and Kobayashi, S. 'Computer Application to the Visioplasticity Method'. A.S.M.E., J. Eng. Ind. 89, p 339, 1967.

41. Altan, T. and Kobayashi, S. 'A Numerical Method for Estimating the Temperature Distributions in Extrusion through Conical Dies'. Ibid. 90, p 107, 1968.

42. Shabaik, A. and Thomsen, E.G. 'Friction Studies by the Visioplasticity Method'. 9th M.T.D.R. conf. Birmingham 1968. Pergamon.

43. Pomp, A., Siebel, E. and Houdrement, E. Mitt K.W. Inst. Eisenforsch, 22, p 395, 1940.

44. Siebel, E. 'Der Derzeitige Stand der Erkenntrisse über die Mechanischen Vorgänge biem Drahtziehen'. Stahl and Eisen, 66-67, p 171, 1947.

45. Shield, R.T. 'Plastic Flow in a Converging Conical Channel'. J. Mech. Phys. Solids, 3, p 246, 1955.

46. Hill, R. and Tupper S.J. 'A New Theory of Plastic Deformation in Wire Drawing'. J.I.S.I. 159, p 353, 1948.

47. Duffill, A.W. and Mellor, P.B. 'A Comparison of Wire Drawing and Hydrostatic Extrusion through Straight Conical Dies'. 9th M.T.D.R. conf. Birmingham 1968. Pergamon.

48. Sachs, G. and van Horn, K.R. 'Practical Metallurgy'. Ann. Soc. Metals, Cleveland, Ohio, 1949.

49. Green, A.P. 'Plane Strain Theories of Drawing'. Proc. Inst. Mech. Engrs. 174, p 847, 1960.

50. Parsons, B., Bretherton, D. and Cole, B.N. 'A Preliminary Investigation of the Combined Hydrostatic Extrusion and Drawing Process'. 9th M.T.D.R. conf. Birmingham 1968, Pergamon.

51. Sachs, G. 'Zur Theorie des Zeitworgangs'. Z. angew Math. und Mech. 7, p 235, 1927.

52. Hill, R. 'On the State of Stress in a Plastic-Rigid Body at the Yield Point'. Phil. Mag. 42, p 868, 1951.

53. Drucker, D.C., Greenberg, H.J. and Prager, W. 'The Safety Factor of an Elastic-Plastic Body in Plane Strain'. J. Appl. Mech. 18, p 371, 1951.

54. Pugh, H. Ll. D. 'Redundant Work and Friction in the Hydrostatic Extrusion of Pure Aluminium and an Aluminium Alloy'. J. Mech. Eng. Sci. 6, p 362, 1964.

55. Eichinger, A. and Lueg, W. Archiv Eisenhuttenwesen 14, p 47, 1940-41; Walziw-Ausschen 157.

56. Avitzur, B. 'Analysis of Wire Drawing and Extrusion through Conical Dies of Small Cone Angle'. A.S.M.E. J. Eng. Ind. 85, p 89, 1963.

57. Avitzur, B. 'Analysis of Wire Drawing and Extrusion through Dies of Large Cone Angle'. Ibid. 86, p 385, 1964.

58. Avitzur, B. 'Hydrostatic Extrusion'. Ibid, 87, p 487, 1965.

59. Avitzur, B. 'Flow Characteristics through Conical Converging Dies'. Ibid. 88, p 410, 1966.

60. Avitzur, B. 'Analysis of Central Bursting Defects in Extrusion and Wire Drawing'. Paper 67-Prod 5, A.S.M.E. conf. Cleveland, Ohio, 1967.

61. Evans, W.M. and Avitzur, B. 'Die Design for Drawing and Extrusion'. Paper MF67-582, A.S.T.M.E. conf. 1967.

62. Evans, W.M. and Avitzur, B. 'Measurement of Friction in Drawing, Extrusion and Rolling'. J. Lub. Tech. A.S.M.E., 89, 1967.

63. Zimerman, Z. and Avitzur, B. 'Metal Flow through Conical Converging Dies - A Lower Upper Bound Approach using Generalised Boundaries of the Plastic Zone'. J. Eng. Ind., A.S.M.E., 92, p 115, 1970.

64. Lambert, E.R. and Kobayashi, S. 'A Theory on the Mechanics of Axisymmetric Extrusion through Conical Dies'. J. Mech. Eng. Sci. 5, p 367, 1968.

65. Lambert, E.R. and Kobayashi, S. 'An Approximate Solution for the Mechanics of Axisymmetric Extrusion'. 9th Int. M.T.D.R. conf. Birmingham 1968 Pergamon.

66. Kobayashi, S. 'Upper Bound Solutions of Axisymmetric Forming Problems - II'. J. Eng. Ind., A.S.M.E., 86, p 326, 1964.

67. Halling, J. and Mitchell, L.A. 'Upper-Bound Solution for Axi-symmetric Extrusion'. Int. J. Mech. Sci. 7, p 277, 1965.

68. Pierce, C.M. 'Forces Involved in Axisymmetric Extrusion of Metals through Conical Dies'. Ph.D. Dissertation, Ohio State Univ. 1966.

69. Richmond, O. and Devenpeck, M.L. 'A Die Profile for Maximum Efficiency in Strip Drawing'. Proc. IVA U.S. Nat. Congress Appl. Mech. 2, p 1053, 1962.

70. Devenpeck, M.L. and Richmond, O. 'Strip Drawing Experiments with a Sigmoidal Die Profile'. J. Eng. Ind., A.S.M.E., 87, p 425, 1965.

71. Richmond,O. and Morrison, H.L. 'Streamlined Wire Drawing Dies of Minimum Length'. J. Mech. Phys. Solids, 15, p 195, 1967.

72. Hill, R. 'Ideal Forming Operations for Perfectly Plastic Solids'. J. Mech. Phys. Solids, 15, p 223, 1967.

73. Sortais, H.C. and Kobayashi, S. 'An Optimum Die Profile for Axi-symmetric Extrusion'. Int. J. Mach. Tool Des. Res., 8, p 61, 1968.

74. Tattersall, G.H. 'Hydrodynamic Lubrication in Wire Drawing'. J. Mech. Eng. Sci. 3, p 378, 1961.

75. Osterle, J.F. and Dixon, J.R. 'Viscous Lubrication in Wire Drawing'. Trans. A.S.L.E., 5, p 233, 1962.

76. Rozner, A. and Faupel, J.H. 'Some Considerations of the Mechanics of Hydrostatic Extrusion'. J. Franklin Inst. 277, p 217, 1964.

77. Hillier, M.J. 'A Hydrodynamic Model of Hydrostatic Extrusion'. Int. J. Prod. Res. 5, p 171, 1966.

78. Iyengar, H.S.R. and Rice, W.B. 'Fluid Film Lubrication in Hydro-static Extrusion'. Annals C.I.R.P., 17, p 117, 1969.

79. Rice, W.B. and Iyengar, H.S.R. 'An Experimental Investigation of Fluid-Film Lubrication in Hydrostatic Extrusion using Wax to Simulate Metals'. Annals C.I.R.P., 18, p 193, 1970.

80. Wilson, W.R.D. and Walowit, J.A. 'An Isothermal Hydrodynamic Lubrication Theory for Hydrostatic Extrusion and Drawing Processes with Conical Dies'. Battelle Memorial Institute, 1969.

81. Thiruvarudchelvan, S. and Alexander, J.M. 'Hydrodynamic Lubrication in Hydrostatic Extrusion using a Double Reduction Die'. 11th M.T.D.R. conf. Birmingham, 1970, Pergamon.

82. Robertson, J. 'Improvements in the Manufacture of Metal Tubes, Tubular and Hollow Articles, Plates, Rods, Bars, Wires and the Like, and in Means and Apparatus Therefor'. British Patent Spec. No. 19356, 1893.

83. Bridgman, P.W. 'Studies in Large Plastic Flow and Fracture'. McGraw-Hill, New York and London, 1952.

84. Beresnev,B.I., Vereshchagin, L.F., Riabinen, Yu. N., and Livshits, L.D. 'Some Problems of Large Plastic Deformation of Metals at High Pressure'. 1963, Pergamon Press.

85. Pugh, H. Ll. D. 'Recent Developments in Cold Forming' Bulleid Memorial Lectures, 1965, Vol. IIIB, Lecture 3. Univ. of Nottingham.

86. Pugh, H. Ll. D. 'Hydrostatic Extrusion'. Paper 18, 9th Commonwealth Mining and Metallurgical Conf. 1969.

87. Pugh, H. Ll. D. (Ed.) 'Mechanical Behaviour of Materials under Pressure'. Elsevier Materials Science Series, 1970.

88. Randall, R.N., Davies, D.M., Sievgiej, J.M. and Lowestein, P. 'Experimental Hydrostatic Extrusion Points to New Production Techniques'. Modern Metals, 17 (7), p 68, 1962.

89. Fiorentino, R.J., Sabroff, A.M. and Boulger, F.W. 'Hydrostatic Extrusion of Metals at Battelle'. Machinery Lloyd (European Edit.) 17, p 18, 1963.

90. Anon. Pressure Technology Corporation of America Progress Report 1964 (1). Navy Bureau of Naval Weapons Contract, NOW 64-D 180-C.

91. Green, D. 'An Experimental High Speed Machine for the Practical Exploitation of Hydrostatic Extrusion'. J. Inst. Metals, 93 (3), p 65, 1964-5.

92. Alexander, J.M. and Lengyel, B. 'Semi-Continuous Hydrostatic Extrusion of Wire'. Proc. Inst. Mech. Engrs. 180, p 317, 1965-6.

93. Lengyel, B. and Ashford, P.G. 'An Experimental Pre-Production Unit for Semi-Continuous Hydrostatic Extrusion'. 8th M.T.D.R. Conf. Birmingham, 1967, Pergamon.

94. Fiorentino, R.J., Sabroff, A.M. and Boulger, F.W. Interim Report. Battelle Memorial Institute, Project 8-198, Contract AF33(615)-1390, 1965.

95. Fiorentino, R.J., Sabroff, A.M. and Boulger, F.W. Final Report, Battelle, Contract AF33(600)-43, 328, 1965.

96. Bobrowsky, A. and Stack, E.A. 'Final Report on an Investigation of Fluid Extrusion of Metals'. NASA Contract NASW-742, 1965.

97. Lowe, B.W.H. and Goold, D. 'An Account of Some Recent Experimental Work on the Hydrostatic Extrusion of Non-Ferrous Metals'. High Pressure Engineering Conf. Proc. Inst. Mech. Engrs. 182 part 3C, p 197, 1967-8.

98. Parsons, B., Bretherton, D. and Cole, B.N. 'Further Studies of the Combined Hydrostatic Extrusion and Drawing Process'. 11th M.T.D.R. conf. Manchester, 1970, Pergamon.

99. Alexander, J.M. and Kamyab, S. 'On the Pressure Distribution in Hydrostatic Extrusion Dies'. To be published.

100. Warburg, E. and Babo, L.V. 'Uber den Zusammenhang zwischen Viscosität und Dichtigkeit bei flüssigen, insbesondere gasförmig flussigen Körperen'. Wied. Ann. 17, p 390, 1882.

101. Roentgen, W.C. 'Uber den Einfluss des Druckes auf die Viscosität der Flüssigkeiten, speciell dess Wassers'. Wied. Ann. 22, p 510, 1884.

102. Warburg, E. and Sachs, J. 'Uber den Einfluss der Dichtigkeit auf die Viscosität tropfborer Flüssigkeiten'. Wied. Ann. 22, p. 518, 1884.

103. Cohen, R. 'Uber den Einfluss des Druckes auf die Viscosität von Flussigkeiten'. Ann. Phys. 45, p 666, 1892.

104. Hanser, L. 'Uber den Einfluss des Druckes auf die Viscosität des Wassers'. Ann. Phys. Folge 4, Band 5, p 597, 1901.

105. Rankine, A.O. 'On a Method of Determining the Viscosity of Gases, especially those Available only in Small Quantities'. Proc. Roy. Soc. 83A, p 266, 1910.

106. Phillips, P. 'The Viscosity of Carbon Dioxide'. Proc. Roy. Soc. 87A, p 48, 1912.

107. Nasini, A.G. and Pastonesi, G. G. Gazz. Chim. Ital. 63, p 821, 1933.

108. Comings, E.W. and Egly, R.S. 'Viscosity of Gases and Vapours at High Pressures'. Ind. Eng. Chem. 32, p. 714, 1940.

109. Comings, E.W. and Egly, R.S. 'Viscosity of Ethylene and Carbon Dioxide under Pressure'. Ind. Eng. Chem. 33, p.1224, 1941.

110. Hyde, J.H. 'On the Viscosities and Compressibilities of Liquids at High Pressures'. Proc. Roy. Soc. 97A, p 240, 1920.

111. Eakin, B.E. and Ellington, R.T. 'Improved High Pressure Capillary Tube Viscometer'. J. Petrol. Technol. 11, p 71, 1959.

112. Parisot, P.E. and Johnson, E.F. 'Liquid Viscosity above the Normal Boiling Point'. J. Chem. Eng. Data, 6, p. 263, 1961.

113. Michels, A. and Gibson, R.O. 'The Measurement of the Viscosities of Gases at High Pressures - The Viscosity of Nitrogen to 1000 Atms.' Proc. Roy. Soc. 134A, p 288, 1932.

114. Swearingen, J.S. and Redding, E.D. 'Viscosity Characteristics of Lubricating Oils Saturated with Natural Gases at High Pressures'. Ind. Eng. Chem. 34, p 1496, 1942.

115. Dane, E.B. and Birch, F. 'The Effect of Pressure on the Viscosity of Boric Anhydride Glass'. J. Appl. Phys. 9, p 669, 1938.

116. Mayinger, F. 'Messumgen der Viskosität von Wasser und Wasserdampf bis zu 700°C und 800 At.' Int. J. Heat Mass Trans. 5, p 807, 1962.

117. Novak, J.D. and Winer, W.O. 'Some Measurements of High Pressure Lubricant Rheology'. A.S.M.E. J. Lub. Tech. 90, p 580, 1968.

118. Barnett, J.D. and Bosco, C.D. 'Viscosity Measurements on Liquids to Pressures of 60 kbar'. J. Appl. Phys. 40, p 3144, 1969.

119. Flowers, A.E. 'Viscosity Measurement and a New Viscosimeter'. Proc. Am. Soc. Test. Mat. 14, p 565, 1914.

120. Hersey, M.D. 'Theory of the Torsion and Rolling Ball Viscosimeters, and the Effect of Pressure on Viscosity'. J. Wash. Acad. 6, p 525, 1916.

121. Hersey, M.D. and Shore, H. 'Viscosity of Lubricants under Pressure'. Mech. Eng. 50, p 221, 1928.

122. Dow, R.B. 'Viscosity of Liquids at High Hydrostatic Pressures'. Phil. Mag. 28, Series 7, p 403, 1939.

123. Dow, R.B. 'The Effects of Pressure and Temperature on the Viscosity of Lubricating Oils'. J. Appl. Physics, 8, p 367, 1937.

124. Sage, B.H., Lacey, W.N. and Yale, W.D. 'Effect of Pressure on Viscosity of n-Butane and Isobutane'. Ind. Eng. Chem. 31, p 223, 1939.

125. Biche, L.B. and Katz, D.L. 'Viscosities of the Methane-Propane System'. Ind. Eng. Chem. 35, p 754, 1943.

126. Hubbard, R.M. and Brown, G.B. 'Viscosity of n-Pentane'. Ind. Eng. Chem. 35, p 1276, 1943.

127. Webb, W., Griest, E.M. and Schiessler, R.W. 'The Effect of Pressure on the Viscosity of Higher Hydrocarbons and their Mixtures'. Phys. Rev. 86, p 612, 1952.

128. Carmichael, L.T. and Sage, B.H. 'Viscosity of Liquid Ammonia at High Pressures'. Ind. Eng. Chem. 44, p 2728, 1952.

129. Kleinschmidt, R.V. 'Discussion - Progress in Lubrication Research'. Mech. Eng. 50, p 682, 1928.

130. Dow, R.B. Physics, 6, p 71, 1935.

131. Mason, C. 'Apparatus for Measuring the Viscosity of Liquids at High Pressures'. Proc. Phys. Soc. 47, p 519, 1935.

132. Cappi, J.B. 'The Viscosity of Water at High Pressure'. Ph.D. Thesis, Univ. of London, 1964.

133. Hawkins, G.A., Solberg, H.L. and Potter, A.A. 'The Viscosity of Water and Superheated Steam'. Trans. A.S.M.E. 57, p 395, 1935.

134. Von Wijk, W.R., Van der Veen, J.H., Brinkman, H.C. and Seeder, W.A. 'The Influence of Temperature and the Specific Volume on the Viscosity of Liquids - III'. Physica, 7, p 45, 1940.

135. Boelhouwer, J.W.M. and Toneman, L.H. I. Mech. E. conf. on Lub. and Wear, Oct. 1957.

136. Jobling, A. and Lawrence, A.S.C. 'Viscosities of Liquids at Constant Volume'. Proc. Roy. Soc. 206A, p 257, 1951.

137. Suge, Y. 'Physical Properties of Lubricants'. Gen. Discussion on Lubrication, 2, Group IV, p 412, I. Mech. E. 1937.

138. Rowe, G.W. 'Measurement of Boundary Lubricant Viscosity at Metal-Deformation Pressures (3000 Atmospheres, 20 tons/sq in)'. Trans. A.S.M.E., J. Lub. Tech., 89, p 272, 1967.

139. Nadai, A. 'Theory of Flow and Fracture of Solids'. McGraw-Hill, 1950.

140. Thomas, B.W., Horn, W.R. and Dow, R.B. 'Viscosity-Pressure Characteristics of Lubricating Oils'. Ind. Eng. Chem. 31, p 1267, 1939.

141. Maxwell, C. Phil. Trans. Roy. Soc. 156, p 349, 1866.

142. Mason, J.G. and Maass, O. 'Measurement of Viscosity in the Critical Region - Ethylene'. Can. J. Res. 18B, p 128, 1940.

143. Gonikberg, M.G. and Vereshchagin, L.F. Compt. Rend. Acad. Sci. U.S.S.R. 55, p 801, 1947.

144. Moszynski, J.R. 'The Viscosity of Steam and Water at Moderate Pressures and Temperatures'. Trans. A.S.M.E., J. Heat Trans., 85, p 111, 1963.

145. Litowitz, T.A. and Carnevale,E.H. 'Effect of Pressure on Sound Propagation in Water'. J. App. Physics, 26, p 816, 1955.

146. Tait, R.I. 'An apparatus for the Study of Ultrasonic Propagation in Liquids under Pressure'. Acustica, 7, p 193, 1957.

147. Richardson, E.B. and Tait, R.I. 'Ratios of Specific Heat and High-Frequency Viscosities in Organic Liquids under Pressure derived from Ultrasonic Propagation'. Phil. Mag. 8th Series, 2, p 441, 1957.

148. Eden, H.F. and Richardson, E.G. 'Propagation of Ultrasonics in Organic Liquids under Pressure. Variation of Specific Heat Ratio and Viscosity with Pressure'. Acustica, 10, p 309, 1960.

149. Barlow, A.J., Harrison, C., Richter, J., Sequin, H. and Lamb, J. 'Electrical Methods for the Viscoelastic Behaviour of Liquids under Cyclic Shearing Stress'. Lab. Practice, 10, p 786, 1961.

150. Lengyel, B., Burns, D.J., and Prasad, L.V. 'Design of Containers for a Semi-Continuous Hydrostatic Extrusion Production Machine'. Proc. 7th Int. M.T.D.R. conf., p 319, Pergamon, 1967.

151. Hornmark, N. 'Design of the A.S.E.A. Hydrostatic Extrusion Equipment'. Lecture 21, Post Experience Course in Hydrostatic Extrusion, Imperial College, 1969.

152. Pennell, J.A. 'Design and Development of High-Pressure Equipment at Vickers'. Lecture 15, Ibid.

153. Heiks, J.R. and Orban, E. J. Phys. Chem. 60, p 1025, 1956.

154. Becker, S.J. and Mollick, L. 'The Theory of the Ideal Design of a Compound Cylinder'. A.S.M.E. J. Eng. Ind., 82B, p 136, 1960.

155. Manning, W.R.D. 'The Overstrain of Tubes by Internal Pressure'. Engineering, London, 159, 101, 183.

156. Chandler, E.F. 'Tensile Properties of a Number of Materials under Hydrostatic Pressure'. N.E.L. Report No. 306, August, 1967.

157. Thomsen, E.G. and Frisch, J. 'Stresses and Strains in Cold-Extruding 2S-O Aluminium'. Trans. A.S.M.E. 76, p 599, 1954.

158. Shabaik, A.H. and Thomsen, E.G. 'Some Additional Studies of the Mechanics of Axisymmetric Extrusions by the Visioplasticity Method'. C.I.R.P. conf. Ann Arbor, Michigan, 1967.

159. Lawaczeck, F. Z. Ver. Deut. Ing. 63, p 677, 1919.

160. Scott, R. 'Viscosity of Argon'. Ph.D. Thesis, 1959, London.

161. Lohrenz, J. and Kurata, F. 'Design and Evaluation of a New Body for Falling Cylinder Viscometers'. A.I.Ch.E. Journal, 8, p 190, 1962.

162. Lohrenz, J., Swift, G.W. and Kurata, F. 'An Experimentally Verified Theoretical Study of the Falling Cylinder Viscometer'. Ibid, 6, p 547, 1960.

163. Duffill, A.W., Hooke, C. J. and Mellor, P.B. 'Design of Straight Conical Dies for Hydrostatic Extrusion'. 9th M.T.D.R. conf. Birmingham, 1968, Pergamon.

A.1 Franklin, G.J. and Morrison, J.L.M. 'Autofrettage of Cylinders: Prediction of Pressure/External Expansion Curves and Calculation of Residual Stresses'. Proc. I. Mech. E. 174, No.35, p 947, 1960.

A.2 Bett, K.E. and Burns, D.J. 'Design of Elastic Multi-Component Compound Cylinders'. High Pressure Engineering Conf. Proc. I. Mech. E. 182, part 3C, 1967-8.

A.3 Hill, R. 'The Mathematical Theory of Plasticity'. Oxford, Clarendon Press, 1950.